Successive formation of a gel network and a lyotropic liquid crystal: does the chronology play a role?

Von der Fakultät Chemie der Universität Stuttgart
zur Erlangung der Würde einer
Doktorin der Chemie (Dr. rer. nat.)
genehmigte Abhandlung

Vorgelegt von
Katja Steck
aus Weißenhorn

Hauptberichterin: Prof. Dr. Cosima Stubenrauch
Mitberichter: Prof. Dr. Thomas Hellweg
Prüfungsvorsitz: Prof. Dr. Peer Fischer

Tag der mündlichen Prüfung: 04.03.2020

Institut für Physikalische Chemie
der Universität Stuttgart
2019

Acknowledgements

First of all, I wish to thank *Prof. Dr. Cosima Stubenrauch* for giving me the opportunity to do my PhD thesis in her group. Thank you very much for your encouragement, support and guidance and for the opportunity to attend national and international conferences.

Further, I would like to thank *Prof. Dr. Thomas Hellweg* for being the second examiner for my thesis and *Prof. Dr. Peer Fischer* for taking over the chair during the defense.

Special thanks goes to all co-authors of my publications: *Prof. Dr. Claudia Schmidt, Prof. Dr. Jan H. van Esch, Prof. Dr. David K. Smith, Dr. Natalie Preisig* and *Prof. Dr. Cosima Stubenrauch*. I learned a lot from all their contributions. Additional thanks goes to *Prof. Dr. Claudia Schmidt* for giving me the opportunity of conducting deuterium NMR studies in her group in Paderborn and *Dr. Natalie Preisig* for taking the amazing FFEM pictures.

Furthermore, I would like to thank all members of the "Gelled Lyotropic Liquid Crystals" project: *Prof. Dr. Cosima Stubenrauch, Prof. Dr. Frank Gießelmann,* who I also wish to thank for being my mentor during my PhD, *Apl. Prof. Dr. Thomas Sottmann, Dr. Natalie Preisig, Birgit Feucht,* especially for her help regarding the visual phase studies, and *Sonja Dieterich* for fruitful discussions and her help with the SAXS measurements. In addition, special thanks goes to Marco Grunwald and David Moser who worked with me during a research internship and a Bachelor thesis, respectively. Moreover, I wish to thank *Prof. Dr. Michael Hunger* for the possibility of performing NMR measurements in Stuttgart. Further thanks goes to *Diana Zauser, Gabriele Bräuning,* and the *mechanical* and *electrical workshops* for their support in the laboratories.

A very big thank you goes to all members of the *Stubenrauch* and the *Sottmann group*. Thank you for the nice atmosphere and the laughter we had during lunch and coffee breaks. A special thank goes to *Miriam Dabrowski*, *Yaseen Qawasmi* and *Julian Fischer* for their moral support and friendship. At this point I want to thank *Dr. Natalie Preisig* for the nice atmosphere in our office. I enjoyed our talks and laughter a lot. I am very happy that I shared the office with her. Further thanks goes to all my other friends, especially *Dr. Nittaya Hansupo*.

Finally, I wish to thank my family. I am grateful to my parents *Ede* and *Cille*, my brother *Andreas* and my sister *Ramona* for their support and love.

Abstract

In this work lyotropic liquid crystals are gelled with low molecular weight gelators (LMWG). The focus is thereby on two fundamental questions. (1) Does the chronology of LLC and gel formation influence the size and orientation of the LLC domains and the alignment of the gel fibers? (2) Do the gel network and the LLC form simultaneously but independently, i.e. are gelled LLC orthogonal self-assembled systems?

In order to answer these questions, the hexagonal H_1 and the lamellar L_α phase of the system H_2O – $C_{12}E_7$ (heptaethylene glycol monododecyl ether) are gelled with the organogelator 1,3:2,4-dibenzylidene-D-sorbitol (DBS) and studied by complementary methods. The gelator DBS was carefully chosen to avoid interactions of the gelator and the surfactant layer. The characteristic properties of the gelled lyotropic liquid crystals (gelled LLCs) are compared to those of the binary counterparts, i.e. the binary system H_2O – $C_{12}E_7$ and the binary gel ethylene glycol – DBS. Visual Phase Studies and rheology showed that DBS gels the L_α phase and the H_1 phase of the system H_2O – $C_{12}E_7$ system without affecting the phase boundaries. In addition, varying the DBS mass fraction η, it is possible to form the gelled LLCs via two ways such that (a) the LLCs are formed first, followed by gel formation at $\eta = 0.0075$ and (b) the gel is formed first in the isotropic phase, which subsequently transforms into an LLC at $\eta = 0.015$. Decoupling the gel and the LLC formation, the influence of the LLC on the formation of the gel network and vice versa, can be examined by small angle X-ray scattering (SAXS), dynamic light scattering (DLS) and freeze fracture electron microscopy (FFEM). In both the gelled L_α phases and the gelled H_1 phases the two structures, i.e. the LLC and the gel network, form via self-assembly independent on which structure is formed first. Moreover, they show only marginal structural differences to the binary counterparts. In a nutshell, this study proves that gelled H_1 and gelled L_α phases of the system H_2O – $C_{12}E_7$ at DBS mass fractions of $\eta = 0.0075$ and $\eta = 0.015$ are orthogonal self-assembled systems, in which a surfactant and a gelator self-assemble to form two coexisting structures, namely an LLC and a gel network.

Kurzzusammenfassung

In dieser Arbeit wurden lyotrope Flüssigkristalle mit niedermolekularen Gelatoren geliert. Der Fokus dieser Arbeit lag dabei auf zwei fundamentalen Fragen. (1) Hat die Reihenfolge der Gelbildung und der lyotropen Flüssigkristallbildung einen Einfluss auf die Domänengröße und Orientierung des lyotropen Flüssigkristalls und/oder die Struktur des Gelnetzwerks? (2) Sind gelierte lyotrope Flüssigkristalle orthogonal selbst-organisierte Systeme? In anderen Worten, bilden sich das Gelnetzwerk und der lyotrope Flüssigkristall gleichzeitig, aber unabhängig voneinander?

Um diese Fragen zu beantworten, werden die hexagonale H_1 Phase und die lamellare L_α Phase des Systems H_2O – $C_{12}E_7$ (Heptaethylenglykol Monododecylether) mit dem Organogelator 1,3:2,4-Dibenzyliden-D-Sorbitol (DBS) geliert und mit verschiedenen Methoden untersucht. Der Gelator DBS wurde sorgfältig ausgewählt, um Wechselwirkungen zwischen Gelator und Tensidschicht zu vermeiden. Visuelle Phasenstudien in Kombination mit Rheologie zeigen, dass DBS die H_1 Phase und die L_α Phase des Systems H_2O – $C_{12}E_7$ geliert, ohne die Phasengrenzen zu verändern. Außerdem ist es durch Variation der DBS Konzentration η möglich, die gelierten lyotropen Flüssigkristalle auf zwei verschiedenen Wegen herzustellen. (a) Bei $\eta = 0.0075$ wird zuerst der lyotrope Flüssigkristall und dann das Gelnetzwerk gebildet. (b) Bei $\eta = 0.015$ wird zuerst das Gel in der isotropen Phase gebildet, welche anschließend in einen lyotropen Flüssigkristall umgewandelt wird. Durch die Entkopplung der Gelbildung und der lyotropen Flüssigkristallbildung ist es möglich, den Einfluss des lyotropen Flüssigkristall auf die Gelbildung, und umgekehrt, mittels Röntgenkleinwinkelstreuung, dynamischer Lichtstreuung und Gefrierbruchelektronenmikroskopie zu untersuchen. Sowohl in der gelierten L_α Phase als auch in der gelierten H_1 Phase bilden sich beide Strukturen, nämlich der lyotrope Flüssigkristall und das Gelnetzwerk, durch Selbstorganisation, unabhängig davon, welche Struktur zuerst geformt wird. Des Weiteren weisen beide gelierten lyotropen Flüssigkristalle nur geringfügige strukturelle Unterschiede zu den binären Systemen auf. Kurz zusammengefasst, die gelierten H_1 Phasen und die gelierten L_α Phasen des Systems H_2O – $C_{12}E_7$ bei DBS Konzentrationen von $\eta = 0.0075$ und $\eta = 0.015$ sind orthogonal selbstorganisierte Systeme, in welchen das Tensid und der Gelator zu zwei koexistierenden Phasen, nämlich einem lyotropen Flüssigkristall und einem Gelnetzwerk, selbstaggregieren.

List of Papers

I. **The Twofold Role of 12-Hydroxyoctadecanoic Acid (12-HOA) in a Ternary Water – Surfactant – 12-HOA System: Gelator and Co-surfactant.**
Katja Steck, Claudia Schmidt, and Cosima Stubenrauch,
Gels **2018**, *4*, 78. (DOI: 10.3390/gels4030078)
Reproduced from [Ste18] with permission from MDPI, open access journal.

II. **Tuning gelled lyotropic liquid crystals (LLCs) – probing the influence of different low molecular weight gelators on the phase diagram of the system H_2O/NaCl – Genapol LA070.**
Katja Steck, Jan H. van Esch, David K. Smith, and Cosima Stubenrauch,
Soft Matter **2019**, *15*, 3111-3121. (DOI: 10.1039/c8sm02330a)
Reproduced from [Ste19a] with permission from The Royal Society of Chemistry.

III. **Gelling Lyotropic Liquid Crystals with the Organogelator 1,3:2,4-Dibenzylidene-D-sorbitol Part I: Phase Studies and Sol-Gel Transitions.**
Katja Steck and Cosima Stubenrauch,
Langmuir **2019**, *35*, 17132-17141. (DOI: 10.1021/acs.langmuir.9b01688)
Reproduced with permission from [Ste19b]. Copyright (2019) American Chemical Society.

IV. **Gelling Lyotropic Liquid Crystals with the Organogelator 1,3:2,4-Dibenzylidene-D-sorbitol Part II: Microstructure.**
Katja Steck, Natalie Preisig, Cosima Stubenrauch,
Langmuir **2019**, *35*, 17142-17149. (DOI: 10.1021/acs.langmuir.9b03346)
Reproduced with permission from [Ste19c]. Copyright (2019) American Chemical Society.

Contribution Report

I. Responsible for writing the manuscript and for all experimental work. The co-authors revised the first version of the manuscript.

II. Responsible for writing the manuscript and for all experimental work. The co-authors revised the first version of the manuscript.

III. Responsible for writing the manuscript and for all experimental work. The co-authors revised the first version of the manuscript.

IV. Responsible for writing the manuscript and for all experimental work except freeze fracture electron microscopy (done by Dr. Natalie Preisig). The co-authors revised the first version of the manuscript.

Contents

1 Introduction

1.1 Motivation

Gelled Complex Fluids are interesting candidates in (trans-)dermal drug delivery and tissue healing applications since they combine the microstructure of a complex fluid and the mechancal stability of a gel. They can be obtained by either adding a gelator to a complex fluid or by replacing the solvent of a gel by a complex fluid. If the two structures, i.e. the complex fluid and the gel network, form simultaneously but independently, gelled complex fluids can be assigned orthogonal self-assembled systems [Stu16]. The term orthogonal self-assembly was introduced by Laibinis et al. in 1979 for alkanethiols and alkane carboxylic acids on gold and alumina, respectively [Lai79]. However, it is not restricted to surface chemistry because orthogonal self-assembled structures have been studied in bulk systems as well [Hu14, Kum14, Li12, Sah13]. In a recent review article, Stubenrauch and Gießelmann present examples of gelled complex fluids and their applications and classified them with regard to orthogonal self-assembly [Stu16]. In fact, the group of van Esch was the first that combined the ideas of orthogonal self-assembly and gelled complex fluids [Hee03]. They studied surfactant micelles [Hee03], worm-like micelles [Bri08], liposomes [Bri09] and phospholipids [Boe16] entrapped in gel networks of low molecular weight gelators (LMWG) [Hee03]. The latter self-assemble into fibers to form so called self-assembled fibrillar networks (SAFiNs) [Wei05]. Another example of an orthogonal self-assembled gelled complex fluid was introduced by Laupheimer et al. who studied the bicontinuous microemulsion of the system H_2O – *n*-decane – $C_{10}E_4$ (tetraethylene glycol monodecyl ether) gelled by the organogelator 12-HOA (12-hydroxyoctadecanoic acid) [Lau13a, Lau13b, Lau14]. Xu *et al*. also gelled the lamellar (L_α) phase of the very same system with the organogelator 12-HOA which was to the best of our knowledge the first example of a gelled lyotropic liquid crystal (gelled LLC) formed by the addition of an LMWG [Xu15].

Gelled lyotropic liquid crystals are a special case of gelled complex fluids. They combine the anisotropic properties of lyotropic liquid crystals (LLCs) with the mechanical stability of a gel [Stu16]. In literature, various examples of gelled LLCs, more specifically gelled lamellar (L_α) phases, are known: the cell [Kel09], lamellar biogels [War96], lamellar hydrogels [Ily17, Mit17] and the gelled L_α phases of synthetic surfactants and a low molecular weight gelator [Xu15, Koi17] (Figure 1.1).

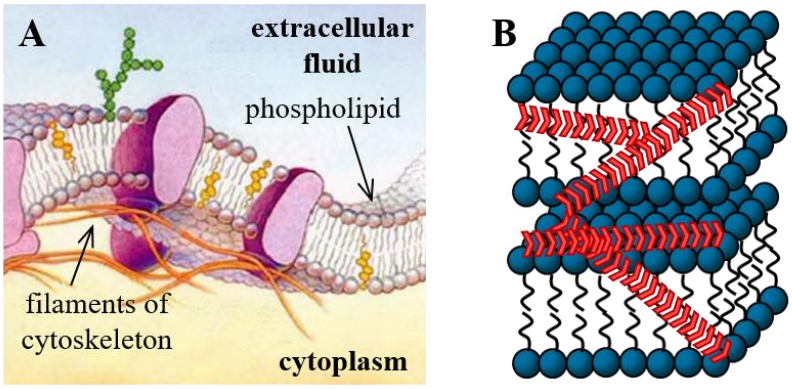

Figure 1.1: Examples of gelled lyotropic liquid crystals (gelled LLCs). **A** Orthogonal self-assembly in the cell [Kel09]. Adapted from [Lau13a] with permission from Springer. **B** Gelled lamellar L_α phase of synthetic surfactants and a low molecular weight gelator.

The cell surely is the most prominent example of an orthogonal self-assembled gelled LLC (Figure 1.1 A) [Kel09]. Phospholipids self-assemble to form the cell membrane, a phospholipid bilayer, which coexist independently with the filaments. The latter are, in turn, formed by self-assembled proteins and provide the mechanical stability of the cell. In contrast, lamellar biogels [War96] and lamellar hydrogels [Ily17, Mit17] can be seen as an example of a non-orthogonal self-assembled gelled LLC. Lamellar biogels, introduced by Warriner *et al*., consist of a lipid bilayer formed by dimyristoyl phosphatidyl choline (DMPC), the co-surfactant pentanol and tiny amounts of poly(ethylene glycol)-derived polymer lipids (PEG-lipids). The latter is attached to the bilayers but can diffuse freely within the lamellar layers which are separated by water. The lamellar biogels are formed out of a fluid lamellar phase by either increasing the volume fraction of water or the PEG-lipid concentration. Due to their ability to diffuse freely within the bilayers, the PEG-lipids accumulate in regions of high curvature. These are caused by defects which are, in turn, stabilized by the segregation of the PEG-lipids. Lamellar hydrogels [Ily17, Mit17], introduced by Gong e*t al*., consist of alternating stacks of anisotropic bilayers of poly(dodecyl glyceryl itaconate) (PDGI) with soft hydrogel layers of hydrophilic polyacrylamide (PAAm) in between. In this case, the thickness of the hydrogel layers and the thickness of the bilayers is directly correlated. For the fourth example, i.e. gelled L_α phases formed by low molecular weight gelators (Figure 1.1 B), the question whether or not they are orthogonal self-assembled systems, still needs to be answered. The first examples are L_α phases gelled with the organogelator 12-HOA (12-hydroxyoctadecanoic acid), namely the gelled L_α phases of the systems H_2O – *n*-decane – $C_{10}E_4$ – 12-HOA [Xu15] and H_2O – $2C_{12}$DAB (didodecyldimethylammonium bromide) – 12-HOA [Koi17]. In the former case, Xu et al. called

into question whether gelled L_α phases are truly orthogonal self-assembled systems. They found that the gel network and the L_α phase influence one another such that (a) the gel network increases the order of the L_α phase and (b) the gel fiber structure is changed from being twisted to not being twisted in the presence of the L_α phase (instead of *n*-decane). The second case, i.e. the gelled L_α phase of the system H_2O – $2C_{12}$DAB – 12-HOA, was reported to be formed via orthogonal self-assembly. Koitani *et al*. showed that solely the interlayer spacing of the L_α phase is slightly increased in the gelled state compared to the pure L_α phase, but other than this no change in the structure of both the L_α phase and the gel fibers was detected. Altogether, these observations revealed that the interactions of the gelator and the L_α phase need to be better understood in order to answer the question under which conditions gelled L_α phases are orthogonal self-assembled systems. In fact, they raised another fundamental question, namely: Does the chronology of gel and LLC formation influence the microstructure of the gelled LLC?

A first experimental evidence that the chronology may indeed play a role was reported by Kato *et al* [Miz99, Kat02, Miz03, Kat07]. They studied gelled thermotropic liquid crystals (nematic phases) with a focus on the influence of the chronology of gel and thermotropic LC formation on the final microstructure of the gelled thermotropic LCs. The starting point of this study was an isotropic solution of a gelator and a mesogen that forms a nematic phase in a specific temperature range. Using two gelators with different sol-gel transition temperatures, they investigated the microstructure of the gelled thermotropic LCs formed via two different routes. (1) In the first route, the sol-gel transition temperature $T_{\text{sol-gel}}$ of the gelator was above the transition temperature of the thermotropic LC ($T_{\text{sol-gel}} > T_{\text{LC-iso}}$). In this case the thermotropic LC is formed within the gel network that consists of randomly distributed gel fibers. (2) Following the second route ($T_{\text{sol-gel}} < T_{\text{LC-iso}}$), one induces gel formation in the thermotropic LC, which leads to aligned gelator fibers. In the thesis at hand, this concept was to be transferred to gelled LLCs (Figure 1.2) with the aim to better understand the influence of the gel network and the LLC on the structure of each other and finally to answer the question whether gelled LLCs are orthogonal self-assembled systems.

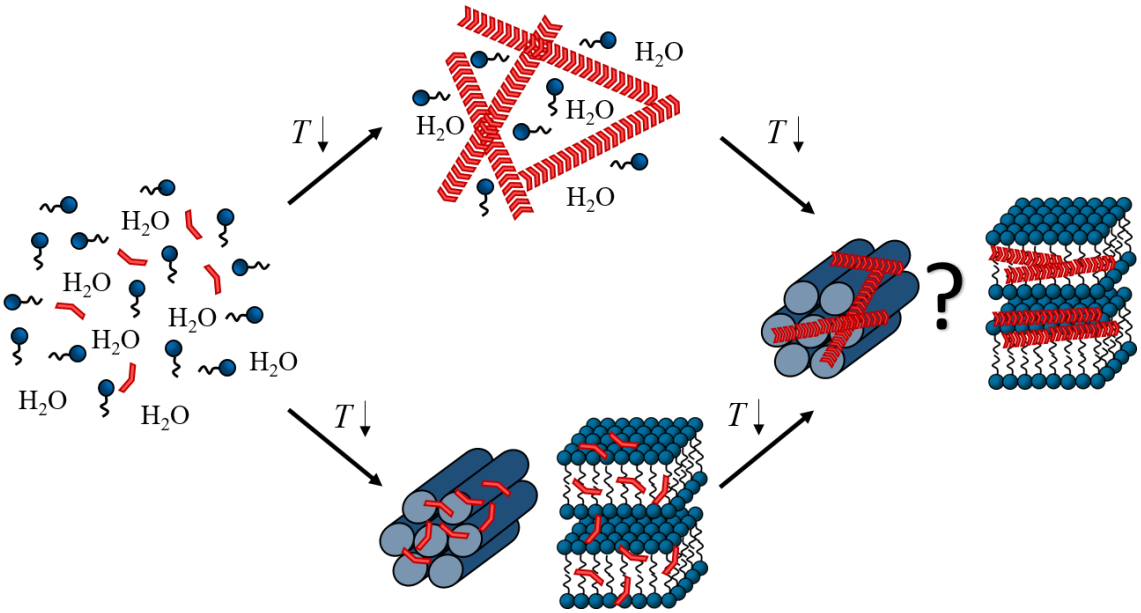

Figure 1.2: Gelling Lyotropic Liquid Crystals (LLCs) via two routes. (1) The gel network (red) is formed in the isotropic phase which is transformed into an LLC on cooling down (upper route). (2) The LLCs are formed first, and the gel network subsequently grows in the LLC (lower route). Adapted with permission from [Ste19b]. Copyright (2019) American Chemical Society.

1.2 Task Description

In order to study the gelation of lyotropic liquid crystals, we chose the binary system water – heptaethylene glycol monododecyl ether ($C_{12}E_7$) [Ino01] for the following reasons. Firstly, it gives access to a broad range of lyotropic liquid crystals since it forms three LLCs, namely the lamellar phase (L_α), the bicontinuous cubic phase (V_1), and the hexagonal phase (H_1) in specific temperature and composition ranges. Secondly, the occurring liquid crystalline phases melt at moderate temperatures ($T \approx 50$ °C), which allows easy handling (Figure 1.3).

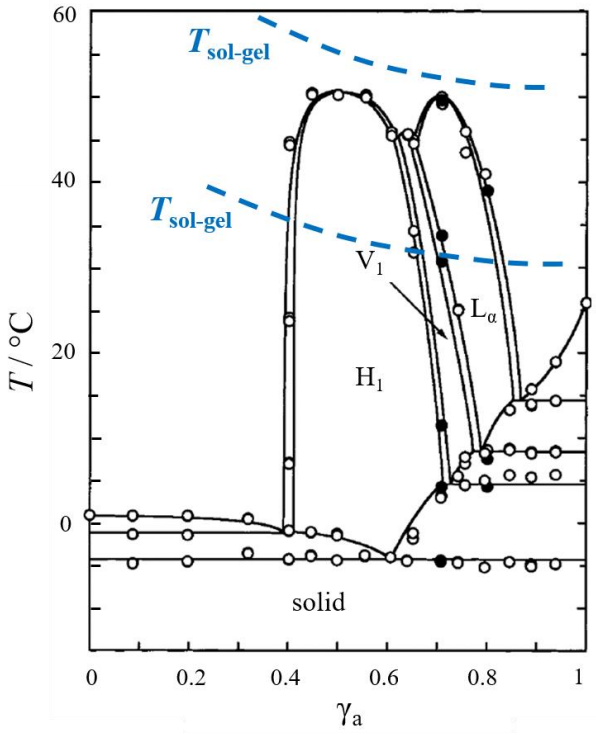

Figure 1.3: Temperature (T) – surfactant mass fraction (γ_a) phase diagram of the binary system H_2O – $C_{12}E_7$ with two theoretical sol-gel transition temperature ($T_{sol\text{-}gel}$) lines. Three lyotropic liquid crystals are formed, i.e. the hexagonal H_1 phase, the bicontinuous cubic V_1 phase and the lamellar L_α phase. Adapted with permission from [Ino01]. Copyright (2001) American Chemical Society.

From a fundamental point of view two questions needed to be answered: (1) Does the chronology of gel and lyotropic liquid crystal formation influence the microstructure of gelled lyotropic liquid crystals? (2) Are gelled lyotropic liquid crystals orthogonal self-assembled systems? The task was thus to investigate (a) whether the LLC phases serve as template for the gelator network leading to well-aligned gelator fibers and (b) whether the gel network does influence the structure of the LLC phase. For this purpose, two sol-gel transition lines had to be adjusted such that (a) the sol-gel transition temperature of the gelator is lower than the phase transition temperature of the LLC to the isotropic phase ($T_{sol\text{-}gel} < T_{LLC\text{-}iso}$) and (b) the sol-gel transition temperature is higher than the phase transition temperature of the LLC to the isotropic phase, i.e. $T_{sol\text{-}gel} > T_{LLC\text{-}iso}$ (Figure 1.3).

In order to address these issues, the study was divided into three work packages, i.e. (a) sample formulation including the choice of the low molecular weight gelator (LMWG), (b) measuring the phase behaviour and the sol-gel transitions, and (c) studying the microstructure of the system of choice. First and foremost, it was to be investigated how the addition of a LMWG influences the phase boundaries of the LLCs of the system H_2O – $C_{12}E_7$ and whether

gelled LLCs are formed. To do so, the system H_2O – $C_{12}E_7$ was to be studied at selected surfactant mass fractions γ_a in the presence of a gelator by visual observation of birefringence in thermostatted water basins. At the same time, it was to be qualitatively determined whether (a) gelled LLCs are formed and (b) whether it was possible to adjust $T_{sol\text{-}gel}$ as required. After finding a suitable gelator and careful optimization of the preparation of gelled LLCs, the temperature (T) – surfactant mass fraction (γ_a) phase diagram of the system of choice was to be mapped out systematically by visual observation. The visual observations were to be supplemented by deuterium (^2H) NMR if necessary. The second and the third step were the investigation of the rheological behaviour and the microstructure of the system of choice. For these investigations, the gelled LLCs were to be formed via two ways as mentioned above, i.e. the samples were to be gelled either before ($T_{sol\text{-}gel} > T_{LLC\text{-}iso}$) or after LLC formation ($T_{sol\text{-}gel} < T_{LLC\text{-}iso}$). In addition, two parent systems were to be defined, i.e. the pure LLCs of the system H_2O – $C_{12}E_7$ on the one hand and a binary gel on the other. Both systems were to be studied by the very same methods for comparison. The rheological behaviour was to be studied via oscillation shear frequency sweeps, in which the storage (G') and the loss modulus (G'') of the gelled LLCs were measured. Moreover, performing oscillation shear temperature sweeps, the sol-gel transition temperatures of the gelled LLCs were to be detected. Finally, the microstructure of the gelled LLCs formed via the two routes was to be studied. Small angle X-ray scattering (SAXS) measurements were to be performed in order to investigate whether the gel network influences the microstructure of the lyotropic liquid crystals such as the layer spacing of the L_α phase and the lattice parameters of the H_1 phase. In order to quantify characteristic length scales of the gel networks such as mesh size, dynamic light scattering (DLS) was to be conducted. Last, FFEM pictures were to be taken in order to complement the scattering techniques and thus confirm the length scales of both the LLCs and the gel networks. All in all, these investigations aimed to create a better understanding of the interactions of gel networks and LLCs by having a close look on the influence of the chronology of gel and LLC formation on the final microstructure of the gelled LLCs.

2 Theoretical Background

In the following Sections, the two base systems of gelled lyotropic liquid crystals will be introduced, namely **lyotropic liquid crystals** and **gels**. The starting point, however, is a general overview of **liquid crystals** and **gels** (Section 2.1). In Section 2.2 and 2.3 the focus is then on **lyotropic liquid crystals** and **molecular gels**, i.e. gels formed by low molecular weight gelators (LMWG). The basic theory of liquid crystals and gels is described in numerous textbooks and articles. Unless otherwise stated, the relevant theory of **liquid crystals** was taken from [Ste99, Col97, Lau94, Tid80, Eva99], and that of **gels** from [Wei06, Nis09, Alm93, Ter97] and in both cases of references therein.

2.1 Liquid Crystals and Gels

Liquid Crystals. In 1888, Friedrich Reinitzer studied melts of cholesterol esters and discovered that they change from a crystalline solid state to an opaque liquid state at higher temperatures which, in turn, transforms to an optically clear liquid on heating up. The opaque liquid state was further analyzed by Otto Lehmann who observed that the latter is characterized by optical birefringence similar to solid crystals. Lehmann also was the one who named these phases *"Liquid Crystals"*.

Liquid Crystals are a state of matter between solid crystals and conventional liquids. Crystals are characterized by both a positional order as well as an orientational order due to which they have direction-dependent, i.e. anisotropic physical properties. Liquids, in contrast, possess neither a positional nor a orientational order. The molecules are randomly distributed which is why they have isotropic (direction-independent) physical properties. Liquid Crystals, in turn, possess properties of both, i.e. the anisotropy of a crystal and the fluidity of a conventional liquid. They are defined as mesophases without the long-range positional order of crystals but with 1- or 2-dimensional long-range orientational order of their building blocks, i.e. they possess less orientational and positional order than a crystal but more than a liquid. In other words, although still flowing, the building blocks of liquid crystals possess a preferred direction, which is indicated by the director $\hat{n}$. On the microscopic level, liquid crystals are highly dynamic systems whose building blocks exhibit thermal motion with fluctuations along their preferred directional order (Figure 2.1). For liquid crystals with only one preferred directional order, the order parameter S quantifies the orientational order. It holds

$$S = \frac{1}{2} \langle 3\cos^2 \theta - 1 \rangle, \tag{2.1}$$

with θ being the angle of the molecular axis of the building blocks with respect to the director n̂.

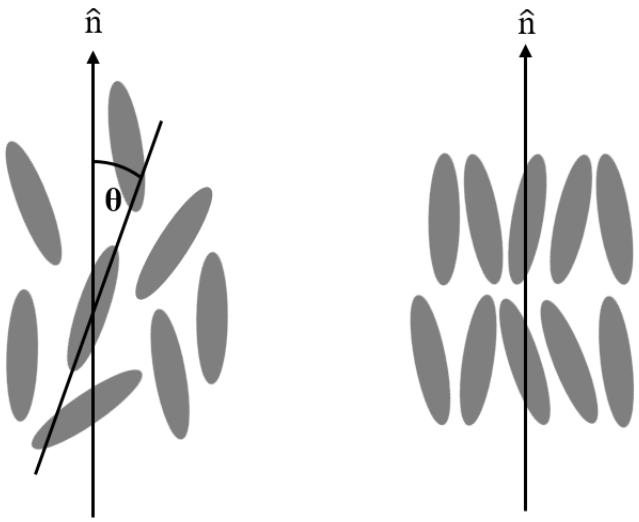

Figure 2.1: Molecular orders in two different liquid crystals. (left) Nematic liquid crystal liquid with orientational order in one direction, given by the director n̂. (right) Smectic A liquid crystal with additional positional order.

Liquid crystals can be divided into two classes, namely thermotropic and lyotropic liquid crystals. What they have in common is that their building blocks are anisometric, i.e. their shape is different from a spherical shape. In the case of thermotropic liquid crystals, the building blocks, also referred to as mesogens, can be rod-shaped or disc-like molecules whose molecular axes differ in their length. The term thermotropic is derived from the temperature-induced phase transitions of the pure mesogens or of mixtures of mesogens. The building blocks of lyotropic liquid crystals, however, are anisometric micelles formed by the self-aggregation of surfactants in polar solvents, mostly water. Dependent on the concentration of the surfactant in the solvent, micelles of different anisometric shape may be formed such as cylindrical micelles or bilayers, which then arrange to form lyotropic liquid crystals. The fact that a change in the surfactant concentration induces the phase transition lead to the term lyotropic liquid crystals. However, the phase transitions of lyotropic liquid crystals are temperature dependent as well. Note that lyotropic liquid crystals were firstly observed in a mixture of myelin and water in 1850, i.e. they were even discovered before thermotropic liquid crystals, though they were recognized as such only later by Otto Lehmann. To summarize, the building blocks of

both thermotropic and lyotropic liquid crystals need to be anisometric. In the former case, the anisometric building blocks are single molecules. In the latter case, the building blocks are anisometric aggregates of surfactants (Figure 2.2).

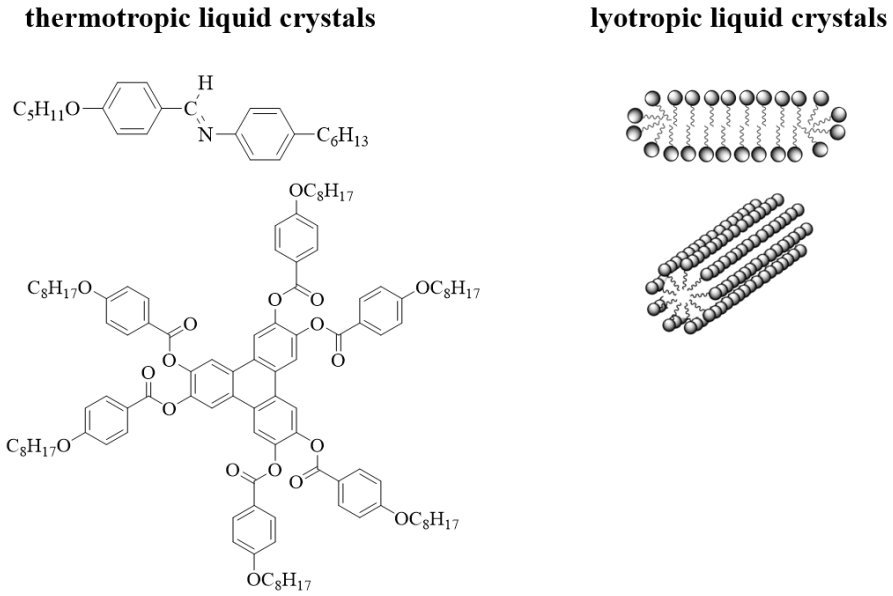

Figure 2.2: Building blocks of thermotropic and lyotropic liquid crystals.

Gels. Over the years, many definitions of the term "gel" have been proposed from a phenomenological point of view as well as based on structural characteristics. However, none of them cover the whole variety and entity of gels or systems which are recognized as gel-like. Hence, a statement given by Nijenhuis best describes the ambiguity of the term gel: "A gel is a gel, as long as one cannot prove that it is not a gel." [Nij97]. Generally, gels can be defined as 3-dimensional cross-linked and dilute systems that do not flow in the steady state, though this is a very wide description. More precisely, gels can be distinguished by the nature of the cross-links, the solvent and the type of gelator. In literature, the terms chemical and physical gels, as well as hydro- and organogels have been widely introduced (Figure 2.3). In chemical gels the cross-links are covalent bonds such as in polyacrylamide gels. Physical gels, in contrast, are formed due to non-covalent interactions between molecules, such as hydrogen bonding or hydrophobic interactions like π-π-stacking. The latter are either formed by polymeric networks, i.e. gelatine- or agar-based gels, or by so-called low molecular weight gelators (LMWG). These LMWG self-aggregate via non-covalent interactions in suitable solvents to form self-assembled fibrillar networks (SAFINs) which, in turn, are referred to as molecular gels. Gels are further classified into hydro- and organogels dependent on whether the solvent is an organic solvent or

a hydrophilic solvent, respectively. Accordingly, the gelling component is called hydro- or organogelator. Other classifications include the optical, thermal and mechanical properties of gels, of which the latter will be further discussed within Section 3.2.

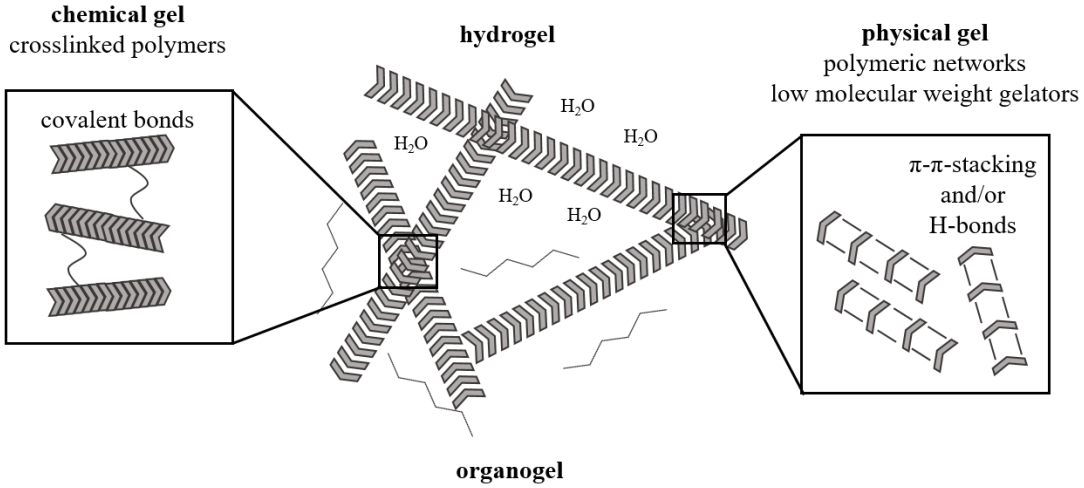

Figure 2.3: Classification of gels according to the type of cross-links and the type of solvent.

2.2 Lyotropic Liquid Crystals

Lyotropic liquid crystals occur in binary systems of water and surfactants as well as in ternary systems of water, surfactant and co-surfactant or water, oil, surfactant, respectively. Dependent on its concentration, the surfactant self-aggregates into spherical or non-spherical micelles, of which the latter are the building blocks of the lyotropic liquid crystalline phases. Since the focus of this study is on the lyotropic liquid crystals of the binary system $H_2O - C_{12}E_7$, the emphasis of this section is on the behaviour of surfactants in water.

Surfactants are amphiphilic molecules, i.e. they have polar and non-polar structural units and are thus soluble in both oil and water. Generally, surfactants consist of a hydrophobic alkyl chain and a hydrophilic head group (Figure 2.4). They can be categorized dependent on the charge of their head group or their structure of their alkyl chain. Anionic surfactants possess a negatively charged head group such as carboxylates, sulfonates or phosphates. The most common one is sodium dodecyl sulfate (SDS), which is widely used in household products. The head group of cationic surfactants is consequently positively charged. Typical examples are quaternary ammonium salts, such as didodecyl dimethylammonium bromide ($2C_{12}$DAB). Zwitterionic surfactants possess head groups with both negative and positive charges, i.e.

dependent on the solvent and the pH they can be either anionic or cationic. Betaines, for instance cocamidopropyl betaine (CAPB), are typical examples of this class of surfactants. In the case of non-ionic surfactants, sugar surfactants and polyethylene oxides such as heptaethylene glycol monododecyl ether ($C_{12}E_7$) are common examples. Furthermore, surfactants with fluorinated alkyl chains, with two head groups (bolaamphiphiles), and polymeric amphiphiles (block copolymers) are known.

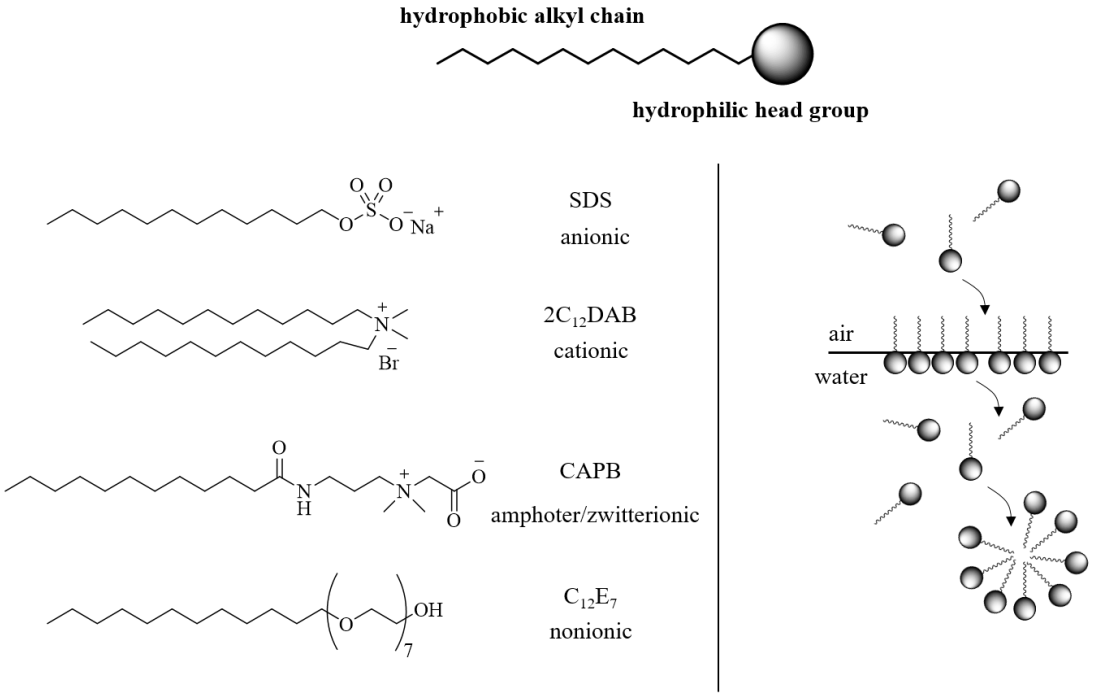

Figure 2.4: (top) Schematic drawing of a surfactant. (left) Classification of surfactants according to the hydrophilic head group with typical examples: sodium dodecyl sulfate (SDS) for anionic surfactants, didodecyl dimethyl ammonium bromide ($2C_{12}DAB$) for cationic surfactants, cocamidopropyl betaine (CAPB) for zwitterionic surfactants and heptaethylene glycol monododecyl ether ($C_{12}E_7$) for non-ionic surfactants. (right) Micelle formation in a binary system of water and surfactant.

The term surfactant is an acronym for surface active agents. If added to water at low concentrations, surfactants accumulate at the air/water surface with the hydrophilic head groups toward the water and the hydrophobic alkyl chains toward the gas phase, respectively. Further increasing the surfactant concentration, the interface becomes saturated and surfactant molecules are monomerically solubilized in the water phase. However, at a certain concentration, i.e. the critical micelle concentration (cmc), the surfactants spontaneously aggregate into micelles, in which the hydrophobic alkyl chains are located in the core and the hydrophilic head groups point outward in the water phase (Figure 2.4). Micelle formation is

one example of the hydrophobic effect, i.e. the aggregation of non-polar compounds in water. The driving force is an increase of the total entropy of the system and thus a minimization of the change of the free energy of the system. Note that micelles can only be formed at temperatures at which the monomeric solubility of the surfactant at least equals the cmc, i.e. at the so-called Krafft point.

The shape of micelles can be predicted by taking the molecular structure and the shape of the surfactants into account (Figure 2.5). In 1976, Israelachvili *et al*. introduced the Packing parameter *P*

$$P = \frac{V_c}{a_0 \cdot l_c} = \frac{a_{chain}}{a_0} \tag{2.2}$$

with the volume of the hydrocarbon chain V_c, the effective head group area a_0 and the length of the hydrocarbon chain l_c [Isr76]. Generally speaking, *P* is the ratio of the area of the hydrocarbon chain a_{chain} and the effective head group area a_0. With this, not only the space of the surfactants themselves is described, but also the hydration shell of the head group is considered. For a Packing parameter of $P \leq 1/3$, i.e. for cone-shaped surfactants, spherical micelles with the hydrocarbon chains in the inner of the micelles are formed. At values of $1/3 \leq P \leq 1/2$, obtained for surfactants with a shape of a truncated cone, cylindrical micelles are formed. In the case of cylindrical-shaped surfactants, such as surfactants with two alkyl chains, bilayers are obtained ($P = 1$). Moreover, inverse structures with the hydrophilic head groups pointing inward and the hydrophobic alkyl chains outward occur for surfactants with a shape of an inverted cone, i.e. $P > 1$.

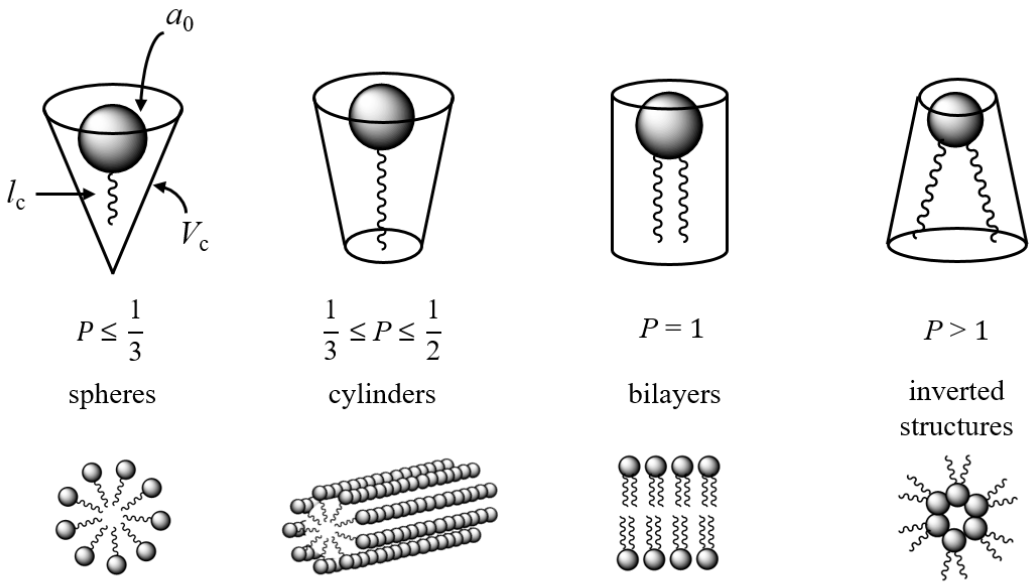

Figure 2.5: Packing parameters P of different shaped surfactant molecules and the resulting shape of the micelles. The packing parameter is the ratio of the area of the hydrophobic chain and the effective head group area a_0. V_c is the volume of the hydrophobic chain, l_c its length.

The occurrence of lyotropic liquid crystals, however, is not only dependent on the shape of the surfactant but also on its concentration in water. In Figure 2.6, a schematic phase sequence of lyotropic liquid crystals in a binary system water – surfactant system is shown. At medium and high surfactant concentrations, i.e. above the cmc, a variety of different structures may be formed such as the cubic I_1 phase, the hexagonal H_1 phase, the bicontinuous cubic V_1 phase, the lamellar L_α phase and the inverse structures of the latter. All of these phases except the cubic I_1 phase are lyotropic liquid crystals. The cubic I_1 phase is referred to as plastic crystal, which will be explained further below. In between the phases, there are two-phase regions. At higher temperatures, the lyotropic liquid crystals melt and transform into miscellaneous, isotropic phases (L_1) via two-phase regions. Note that the index 1 for the I_1, H_1 and the V_1 phase indicates water as outer, i.e. continuous medium, whereas the index 2 is used for inverse structures.

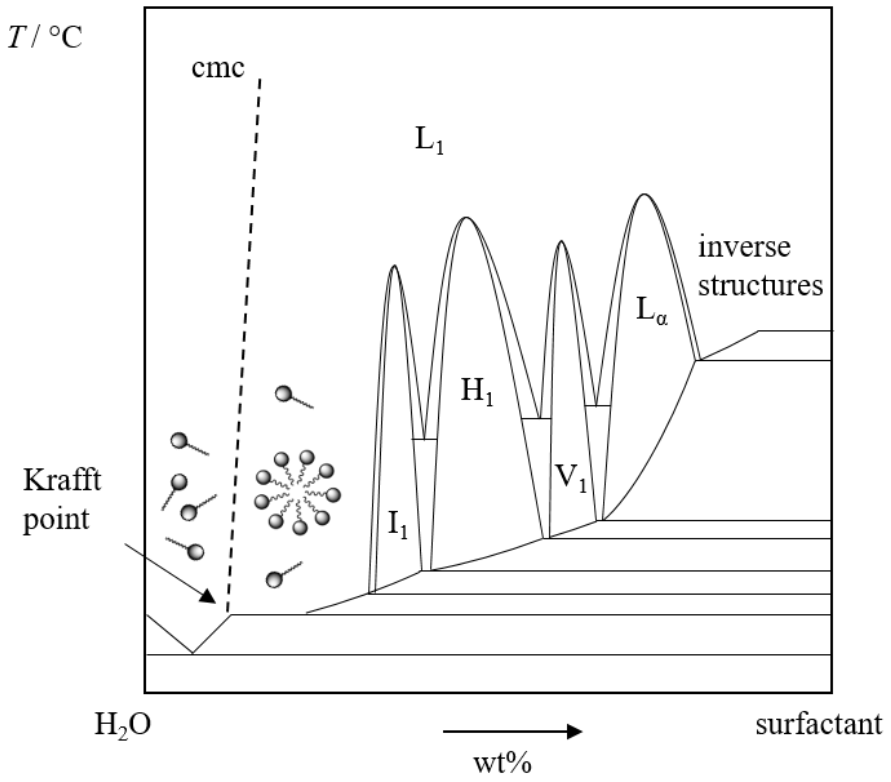

Figure 2.6: Schematic phase diagram of a binary system water – surfactant with possible lyotropic liquid crystalline phases dependent on the surfactant mass fraction: hexagonal H_1 phase, bicontinuous cubic V_1 phase, lamellar L_α phase, inverse structures. The cubic I_1 phase is referred to as plastic crystal. Micelles and lyotropic liquid crystals are formed above the critical micelle concentration (cmc) and at temperatures above which the monomeric surfactant solubility equals the cmc (Krafft point). At low temperatures heterogeneous mixtures with solid, crystalline fractions are present. In between the phases, two-phase regions occur. At high temperatures isotropic micellar phases (L_1) are formed.

Schematic drawings of the cubic I_1 phase, the hexagonal H_1 phase, the bicontinuous cubic V_1 phase and the lamellar L_α phase are depicted in Figure 2.7. The cubic I_1 phase which occurs between the micellar phase and the hexagonal H_1 phase consists of spherical micelles which arrange in a cubic lattice at a certain surfactant concentration. It is characterized by a high viscosity and optical isotropy. The three-dimensional positional order of the spherical micelles, i.e. the cubic arrangement, is caused by the high number of micelles which finally leads to repulsive forces between the micelles. Due to the symmetry of the spherical micelles, the cubic I_1 phase has no orientational order and is thus referred to as plastic crystal. At higher surfactant concentrations, spherical micelles are transformed into cylindrical micelles with an indefinite length. The latter arrange in a hexagonal lattice and form the lyotropic liquid crystalline hexagonal H_1 phase with a two-dimensional positional order. The hexagonal H_1 is also highly viscous but is characterized by optical anisotropy in contrast to the cubic I_1 phase.

Between the hexagonal H_1 phase and the lamellar L_α phase, a bicontinuous cubic V_1 phase might be formed. It possesses a three-dimensional positional order and is characterized by a high viscosity and optical isotropy in line with the cubic I_1 phase. However, its building blocks are not symmetric. As the term bicontinuous implies, it consists of two continuous channels of water on the one hand and the surfactant on the other of which the latter aggregates into extended surfactant bilayers. The lamellar L_α phase, which is formed at high surfactant mass fractions, consist of bilayers of surfactants that are separated by water. It is less viscous than the cubic and the hexagonal phases and is characterized by a one-dimensional positional order and optical anisotropy. Note that lyotropic nematic liquid crystals are also formed in binary systems water – surfactant, such as the nematic phases of the systems H_2O – caesium pentadecane fluoro octanoate (CsPFO) and H_2O – cetyltrimethylammonium bromide (CTAB). However due to their rarity in binary systems of water and a surfactant, they are not discussed in the thesis at hand.

Although the packing parameter *P* was introduced in order to predict the shape of micelles based on the molecular structure of the surfactant, it also explains the order of possible occurring lyotropic liquid crystals in one system with increasing surfactant concentration. It is recalled that the packing parameter *P* is the ratio of the area of the hydrophobic alkyl chain and the effective size of the hydrophilic head group. If a surfactant is added to water, its hydrophilic head group becomes hydrated, i.e. the effective head group area is the sum of the actual size of the head group and its hydration shell. Increasing the surfactant concentration leads to a smaller hydration shell which, in turn, increases the ratio of the hydrocarbon chain to the effective head group area. As consequence, micelles of different shapes are formed with increasing surfactant concentration such as cylindrical micelles or bilayers which are the building blocks of the lyotropic liquid crystalline phases.

Lyotropic Liquid Crystals can be recognized by different methods such as deuterium NMR (^{2}H-NMR), small angle X-ray scattering (SAXS), polarizing optical microscopy (POM) and transmission electron microscopy (TEM). These techniques were also used in the thesis at hand and will be described in Section 3. But first, the second parent system will be introduced, i.e. molecular gels formed by self-assembled fibrillar networks of low molecular weight gelators (LMWG).

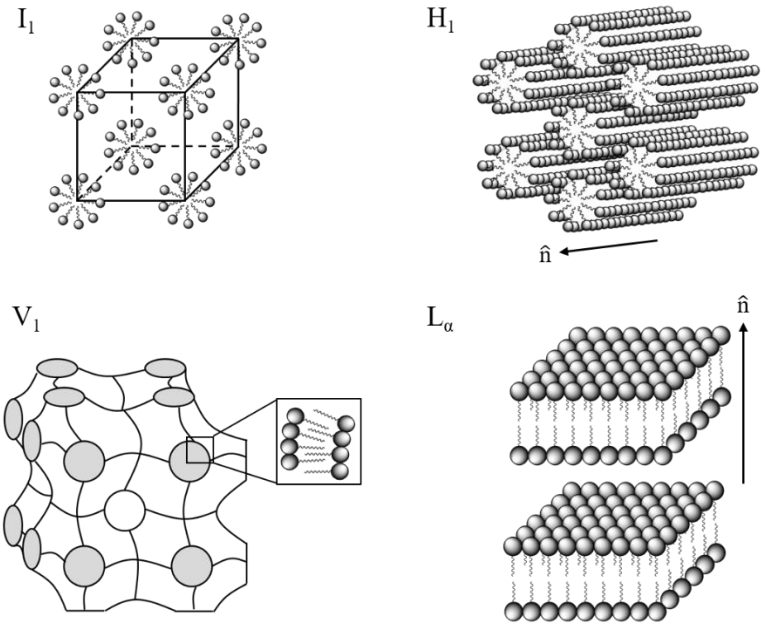

Figure 2.7: Schematic drawings of the cubic I_1 phase, hexagonal H_1 phase, the bicontinuous cubic V_1 phase and the lamellar L_α phase. The I_1 phase is referred to plastic crystal, the V_1, H_1 and L_α phase are lyotropic liquid crystals. For the H_1 and the L_α phase, the director n̂ is shown.

2.3 Molecular Gels

In the wide field of gels, the interest in molecular gels grew rapidly over the years. Molecular gels are formed by low molecular weight gelators (LMWG) that aggregate into so-called self-assembled fibrillar networks (SAFiNs) due to non-covalent, i.e. physical interactions. The latter include hydrophobic interactions such as London dispersion forces and π-π-stacking as well as hydrophilic interactions like hydrogen bonding. Unlike chemical gels which involves covalent bonds between polymers, molecular gels are often thermoreversible. The gel can be transformed into a sol and vice versa by simply heating and cooling the solution, whereby the composition is not changed. Molecular gels are thus mostly prepared by the dissolution of a LMWG at low concentrations, i.e. < 2 wt.%, in a solvent at high temperatures followed by cooling down to the so-called sol-gel transition temperature ($T_{\text{sol-gel}}$) below which the gel is formed. The $T_{\text{sol-gel}}$ depends on the properties of the solvent, in some case on the heating/cooling mechanism, and on the concentration of the LMWG. With increasing gelator concentration, the $T_{\text{sol-gel}}$ increases until it reaches a plateau. Mésini *et al*. indicated that this plateau is due to a miscibility gap of solvent and gelator above a critical gelator concentration [Més16]. In Figure 2.8, a simplified phase diagram of a molecular gel is shown. Below $T_{\text{sol-gel}}$, the LMWG molecules self-assemble into one-dimensional gel fibers which, in turn, form a

three-dimensional gel network via non-covalent interactions. The solvent is encapsulated in the meshes of the three-dimensional gel network and hence exhibits no flow. Since gelation can be seen as a microscopic phase separation, i.e. for some LMWG even comparable to crystallization, the gelation process is a balance of opposing influences such as solubility of the gelator and phase separation. In fact, temperature, age, the type of solvent and the LMWG concentration are important factors which determine the gelation process and the properties of molecular gels. In addition, the type of LMWG is a major factor. As mentioned before, LMWGs can be categorized dependent on the nature of the solvent, i.e. an organogelator gels organic solvents, whereas a hydrogelator gels a hydrophilic solvent. Furthermore, they can be classified dependent on structural units such as alkane-based gelators, sugar-based gelators or fatty acid derivatives etc.

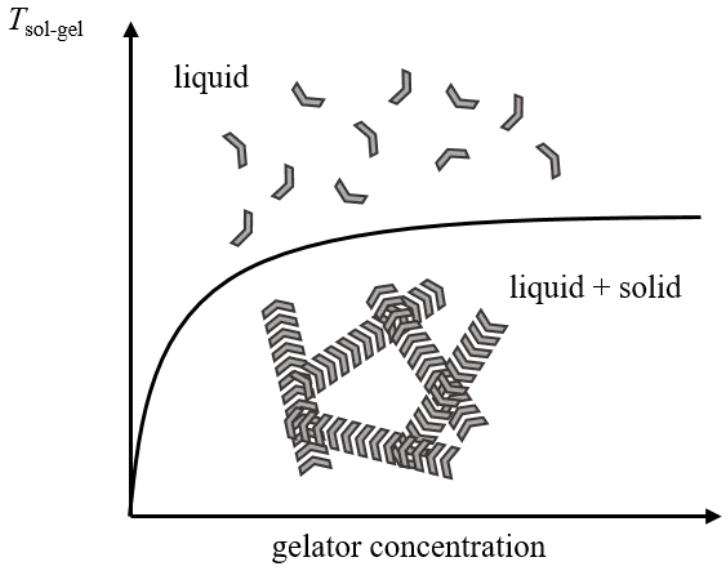

Figure 2.8: Schematic drawing of the sol-gel transition temperature $T_{sol\text{-}gel}$ of a molecular gel as function of the low molecular weight gelator (LMWG) concentration.

From the wide variety of LMWGs, four different LMWGs were chosen in order to investigate their capability of gelling lyotropic liquid crystals, i.e. the organogelators 12-hydroxyoctadecanoic acid (12-HOA) and 1,3:2,4-dibenzylidene-D-sorbitol (DBS) as well as the hydrogelators *N*,*N*'-dibenzoyl-L-cystine (DBC) and HG1 (a tris-amido cyclohexane derivative). Since they are all LMWGs, they are simply referred to as organogelators and hydrogelators in the following. In Figure 2.9, the molecular structures of the gelators are shown. The organogelator 12-HOA is a chiral fatty acid derivative with a carbon chain length of C_{18}

and a hydroxyl group at the C_{12} position. In industry, for instance, 12-HOA is used as thickening agent for greases [Ter91]. It is known to gel various organic solvents such as benzene, carbon tetrachloride, nitrobenzene, dodecane, toluene and decane [Tac91, Tec94, Ter00, Lau15]. In addition, 12-HOA turned out to be a potent gelator for gelling bicontinuous microemulsions in an orthogonal self-assembled way, i.e. both the bicontinuous microemulsion and the gelator fibers still form in the presence of the other and coexist [Lau13a, Lau14]. The structure of the self-assembled fibrillar networks has been reported as well. The dominating physical interactions are hydrogen bonds between the carboxyl groups on the one hand and the hydroxyl group at the C_{12} position, on the other [Ter94]. The former leads to the formation of dimers of 12-HOA molecules which, in turn, are stacked on top of one another to form helical gel fibers. Interestingly, although 12-HOA is indeed a classic organogelator, hydrogels formed by surfactant-mediated gelation of 12-HOA have been recently reported [Ara19].

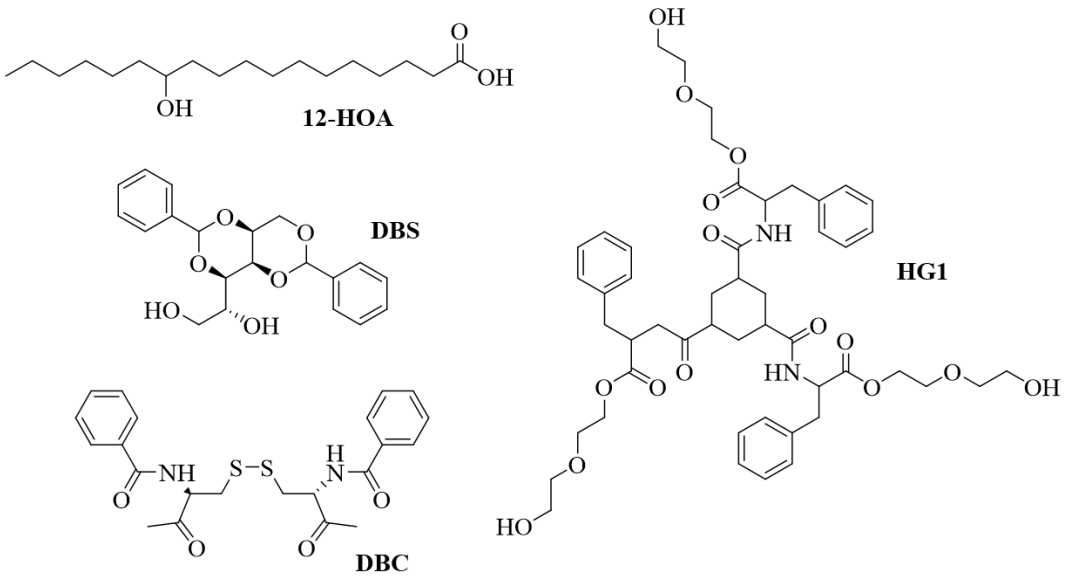

Figure 2.9: Molecular structures of the organogelators 12-hydroxyoctadecanoic acid (12-HOA) and 1,3:2,4-dibenzylidene-D-sorbitol (DBS) as well as of the hydrogelators *N*,*N*'-dibenzoyl-L-cystine (DBC) and HG1. Note that stereocenters are not marked.

The organogelator DBS [Oke15] is a chiral, butterfly-shaped sorbitol derivative with a sugar-based backbone and two phenyl groups which represent the wings. It is a versatile gelator of which gels with typical organic compounds such as 1,4-dioxane, *p*-Xylene, dimethyl sulfoxide (DMSO) [Yam95a], ethanol, chlorobenzene [San11] and ethylene glycol (EG) [Yam94a, Yam94b, Yam96], with polymers such as poly(ethylene glycol) PEG [Wil03a], poly(propylene glycol) (PPG) [Lai09] and amphiphilic block copolymers [Wil03b] as well as

gels with a thermotropic liquid crystal [Jan00] have been reported. DBS and its derivatives are widely used in industry, such as in cosmetics and health care [Roe79, Roe82], in adhesive technology [And74], as matrix for gel electrolytes [Moh04] etc. The interactions which lead to the self-assembly of DBS has been investigated dependent on the polarity of the solvent [Yam95a, Yam95b, Wat98, Wat99]. In general, the sugar-backbone and the phenyl rings are the two potential motifs for physical interactions, i.e. hydrogen bonding and π-π-stacking. In non-polar solvents, however, hydrogen bonding between DBS molecules was found to be the driving force for the self-assembly of DBS into helical gel fibers [Yam95a, Yam95b]. In contrast, in polar, protic solvents, π-π-stacking between the phenyl rings of the DBS molecules become the predominant interactions for gel fiber formation [Wat98, Wat99] since hydrogen bonding between DBS molecules was found to be less favoured than hydrogen bonding between the solvent and DBS [Yam95a, Yam95b]. One important feature of DBS is the possibility of modifying its molecular structure such that it turns form an organogelator into a hydrogelator, for instance, by introducing carboxylic groups at the aromatic wings [Vie17, Vie18].

A classic hydrogelator is DBC whose hydrogels were found to be potential candidates for controlled drug release systems [Fri04]. In contrast to 12-HOA and DBS organogels, hydrogels formed by DBC are pH-sensitive in addition to its thermoreversible property, which results from the two carboxylic groups in the molecule. DBC and its derivatives were studied in mixtures of ethanol(5%)/ H_2O and DMSO(10%)/H_2O in order to obtain information on the intermolecular interactions between DBC molecules which lead to the self-assembled gelator fibers [Men78, Men95, Men00]. In the case of the DBC-derivative di(*p*-tolouyl)-L-cystine (DTC) it was found that DTC molecules linearly stack on top of one another which is enhanced by hydrogen bonds between the carboxylic CO and the amide NH groups. Possibly, π-π-stacking also occurs and stabilizes the fibers since the tolouyl groups were found to be situated and stacked on one side. In addition, hydrogen bonding between amide oxygens and carboxylic oxygens was found to be the predominating interaction between two DBC gel fibers. [Men78]

The hydrogelator HG1 is a 1,3,5-tris-amido cyclohexane derivative and is known to be a potent gelator for gelling aqueous surfactant solutions such that micelles of different shape are immobilized within the meshes of the self-assembled gel network of HG1 [Bri09b]. The shape and type of the micelles ranges thereby from spherical micelles [Hee03], worm-like micelles [Bri08], liposomes [Bri09a] and phospholipids [Boe16]. In all cases, the gel network and the micellar solutions are formed independently, i.e. they are orthogonal self-assembled systems. The self-assembly process of HG1 is mainly driven by hydrogen bonding between the

1,3,5-trisamide cyclohexane motives which stack one top of one another to form one-dimensional arrays of HG1 molecules.

3 Methods

The gelled lyotropic liquid crystals were studied by a broad variety of different methods, namely **visual phase studies**, **deuterium (^{2}H) NMR** [Jel86, Bla92, Dav83, See77, Sto76, Ste99] **rheology** [Mez16, Goo08, Bru06, Rao07, www01], **small-angle X-ray scattering (SAXS)** [Sed98, Ste99, Gla82], **dynamic light scattering (DLS)** [www02], **polarizing optical microscopy (POM)** [Col97, Ste99], and **transmission electron microscopy (TEM)** [Ste99, www03]. Unless otherwise stated, the relevant theory was taken from the given references and references therein. This section will give a short overview of each method and their use in **Paper I** [Ste18], **II** [Ste19a], **III** [Ste19b], and **IV** [Ste19c]. However, since the experimental conditions for ^{2}H-NMR, rheology, SAXS, DLS, POM, and FFEM are described in detail in the publications, they will not be discussed in this section. In line with the publications, it begins with the used chemicals, the sample preparation and the visual phase studies.

3.1 Chemicals, Sample Preparation and Visual Phase Studies

Chemicals. In Table 3.1, all chemicals used in this study are listed. The chemicals were used without further purification.

Table 3.1: Chemicals used in this study. The hydrogelator HG1 was synthesized by the group of van Esch as described before [Bom04].

Name	Abbreviation	Supplier	Purity
water	H_2O		bidistilled
deuterium oxide	D_2O	Eurisotop	99.9%
heptaethylene glycol monododecyl ether	$C_{12}E_7$	Sigma Aldrich	≥ 98.0%
		Santa Cruz	≥ 95.0%
		Nikkol	n/a
		TCI	n/a
Genapol LA070		Clariant	technical grade
12-hydroxyoctadecanoic acid	12-HOA	Alfa Aesar	95.0%
1,3:2,4-dibenzylidene-D-sorbitol	DBS	NJC Europe	n/a
N,*N*'-dibenzoyl-L-cystine	DBC	Santa Cruz	> 98%
HG1			n/a

Sample preparation. In **Paper I-IV** the samples were prepared with the surfactant mass fraction

$$\gamma_a = \frac{m_{\text{surfactant}}}{m_{\text{surfacatant}} + m_{H_2O}} \tag{3.1}$$

using bidistilled water and with the gelator mass fractions

$$\eta = \frac{m_{\text{gelator}}}{m_{\text{surfactant}} + m_{\text{water}} + m_{\text{gelator}}} \tag{3.2}$$

or in general

$$\eta = \frac{m_{\text{gelator}}}{m_{\text{total}}} \tag{3.3}$$

with *m* being the mass of the respective compound.

All components were weighed in glass tubes, sealed with plugs and heated in water baths to the temperature at which the gelator was dissolved. The samples were stirred for at least 15 min at the respective temperature to ensure homogeneity. In **Paper I**, the organogelator 12-HOA was added to the binary system H_2O – $C_{12}E_7$ at three 12-HOA mass fractions, i.e. η = 0.015, 0.025 and 0.05. No specific cooling protocol was followed, though. In **Paper II**, the system H_2O/NaCl – Genapol LA070 was studied in the presence of the organogelators 12-HOA and DBS, as well as in the presence of the hydrogelators DBC and HG1 at two gelator mass fractions, i.e. η = 0.0075 and η = 0.015. As in Paper I, no specific cooling protocol was applied. In **Paper III** and **IV**, the binary system H_2O – $C_{12}E_7$ was studied in the presence of the organogelator DBS at DBS mass fractions of η = 0.0075 and η = 0.015. Since the focus was on the chronology of gel and lyotropic liquid crystal formation, the samples were cooled as follows: (1) At η = 0.015 the samples were cooled to a temperature low enough to allow gel formation in a reasonable time, but still to be in the isotropic phase. After gel formation, the sample was put to room temperature at which the isotropic phase transformed into a lyotropic liquid crystal. (2) At η = 0.0075 the samples were cooled to room temperature at which first the lyotropic liquid crystal was formed first, followed by gel formation after a couple of hours.

Visual Phase Studies. The investigation of the phase behavior of the lyotropic liquid crystalline phases in the presence of the different gelators was always a first hint on whether a gelator is a potential candidate for gelling LLCs in an orthogonal self-assembled way. Visual

phase studies were thus the starting point in **Paper I**, **II** and **III**. The LLC phase boundaries in the absence and presence of the different gelators were determined by visual observations in water basins (Figure 3.1). The samples were fixed in the water basins equipped with a *Thermo Scientific* DC30 Thermostat which allowed to adjust the water temperature in steps of 0.1 K. For temperature control, a digital thermometer with an accuracy of +/- 0.01 K was used. As stirring was required, the vessels were equipped with magnetic stir bars and the water basin was placed on a magnetic stirrer. In order to detect the phase boundaries by anisotropy, a microscopy lamp was placed behind the water basins and two crossed polarizers, one behind and one in front of the sample, were used. Phase boundaries were determined by heating the samples starting from T = 21 °C up to T = 95 °C. Phase transitions were determined by temperatures steps of +/- 0.1 K.

Figure 3.1: Experimental set-up for the visual phase studies of gelled lyotropic liquid crystals in the absence and presence of different gelators: **A** thermostat, **B** water basin, **C** microscopy lamp, **D** polarisation filter, **E** digital thermometer with temperature sensor, **F** magnetic stirrer, **G** sample holder with samples.

3.2 Deuterium (^{2}H) NMR

Visual phase studies are often impeded by phase transitions which occur in very narrow temperature ranges, by multiphase regions or by turbidity of the samples such as it might be the case in the presence of gelators. In the study at hand, the presence of the organogelator 12-HOA in the system H_2O – $C_{12}E_7$ lead to turbid samples, which complicated the determination of the phase boundaries especially at low surfactant concentrations, i.e. at high water content. As a quick reminder, gelation is a balance between solubility and precipitation and 12-HOA is a classic organogelator and not soluble in water. At low surfactant concentrations, the gelation/precipitation of 12-HOA is more likely than at high surfactant concentrations, i.e. the gelation leads to very turbid samples at low surfactant concentrations. A useful method to overcome these difficulties is ^{2}H-NMR. It allows the unequivocal determination of phase boundaries under these limitations and thus complemented the visual phase studies in **Paper I**. Note that H_2O had to be replaced by D_2O for the ^{2}H-NMR measurements, which, in turn, influenced the phase boundaries of the lyotropic liquid crystalline phases. The lyotropic liquid crystalline phases of the system D_2O – $C_{12}E_7$ were marginally shifted to smaller surfactant mass fractions compared to the system with H_2O. In addition, the phase boundaries were shifted to slightly lower temperatures for the H_1 phase and slightly higher temperatures for the L_α phase. This effect was also observed for the lyotropic liquid crystals of the system D_2O – $C_{12}E_7$ in the presence of the organogelator 12-HOA. Replacing H_2O by D_2O thus leads to a more hydrophobic surfactant [Stu04]. In the following, the basics of ^{2}H-NMR will be shortly described.

The deuterium (^{2}H) nucleus has a spin quantum number of $I = 1$, i.e. three equidistant energy levels with the magnetic spin quantum number $m_I = +1, 0, -1$ occur in the presence of an external magnetic field. This is known as the Zeeman splitting. Moreover, the ^{2}H nucleus is quadrupolar and possesses a non-spherical charge distribution at the nucleus due to which an interaction of the quadrupole moment and the electric field tensor emerges at the nucleus. This, in turn, leads to a perturbation of the Zeeman splitting, which is so strong that the quadrupole coupling dominates the ^{2}H-NMR spectra over other nuclear spin interactions. The resulting splitting, in turn, depends on the local orientation of the D_2O molecules and, for anisotropic media such as lyotropic liquid crystals, on the orientation of the director with respect to the external magnetic field. In an aqueous surfactant solution, the D_2O molecules are slightly aligned due to interactions with the aligned surfactant molecules which, in turn, leads to a non-zero residual quadrupole splitting. In an isotropic phase, however, since the molecules have no

preferred orientation, this splitting vanishes and a single peak is detected. In contrast, in an anisotropic phase, in which the surfactant molecules are aligned leading to aligned D_2O molecules, a quadrupole splitting is observed. Due to their high viscosity, lyotropic liquid crystals are often not macroscopically aligned and LLC domains with all possible director orientations with respect to the magnetic field are present. As a result, the spectral contributions from all domains are superimposed and lead to a characteristic line shape, known as the Pake powder pattern (Figure 3.2) [Pak48]. For uniformly aligned samples with the director axis at an angle θ with respect to the magnetic field two peaks are yielded. The splitting $\Delta\nu$ is proportional to $(3\cos^2\theta - 1)$. The maximum splitting is observed for a uniform director alignment parallel to the magnetic field axis, i.e. at $\theta = 0\,°$. When the director is aligned perpendicular to the magnetic field ($\theta = 90\,°$), half of the maximum splitting is observed.

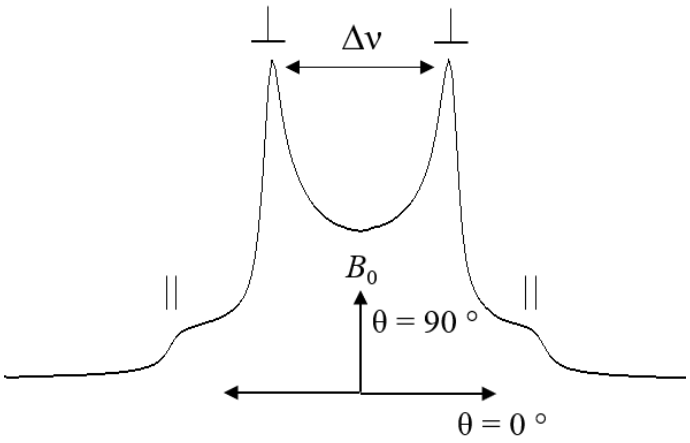

Figure 3.2: A schematic ^{2}H-NMR line shape (Pake powder pattern) of an anisotropic phase with splitting $\Delta\nu$**.** At a parallel director alignment ($\theta = 0\,°$) with respect to the direction of the magnetic field B_0, the maximum splitting is observed; for a perpendicular aligned director ($\theta = 90\,°$) half of the splitting is detected.

The magnetic susceptibility χ is the proportional constant between the magnetic field intensity and the magnetic moment which results from the magnetic polarization. In all cases, molecules have an opposing impact on the magnetic susceptibility, i.e. they are diamagnetic. Lyotropic liquid crystals possess an anisotropic diamagnetic susceptibility $\Delta\chi = \chi(\text{parallel}) - \chi(\text{perpendicular})$, which results in a preferred director orientation with respect to the magnetic field. Thus, dependent on the algebraic sign of $\Delta\chi$, either the parallel or the perpendicular orientation of the director is favoured. This, in turn, allows to distinguish between different lyotropic liquid crystals in one system, such as L_α and H_1 phases. If the latter are formed by

cooling from the isotropic phase, the director of the L_α phase is uniformly aligned, whereas that of the H_1 phase only shows partial alignment as a result of the higher viscosity [Stu02]. Another possibility to distinguish lyotropic liquid crystal phases is a change of the magnetic field direction with respect to the director. The director of a nematic phase almost instantaneously orients in the direction of the magnetic field, whereas the viscosity of the L_α and the H_1 phases is too high for a fast reorientation of their directors.

^{2}H-NMR measurements are usually performed by using a quadrupole echo pulse sequence (Figure 3.3). The latter is applied since the free induction decay (FID) signal vanishes rapidly due to the broad ^{2}H-NMR line shapes. In fact, the FID is so fast that the signal disappears during the so-called dead time, i.e. the time between the pulse and data acquisition. At the beginning of the experiment, all spins are oriented in the direction of the magnetic field (z-direction). After the excitation pulse ($90°_x$), the spins rapidly dephase which limits the time for the detection of the FID. A second pulse ($90°_y$) at a time t_1 after the excitation pulse leads to refocusing of the spins and, in turn, to the generation of a quadrupole echo at a time t_2. The echo maximum at t_2 indicates that all spins are rephased and is usually the start of data acquisition.

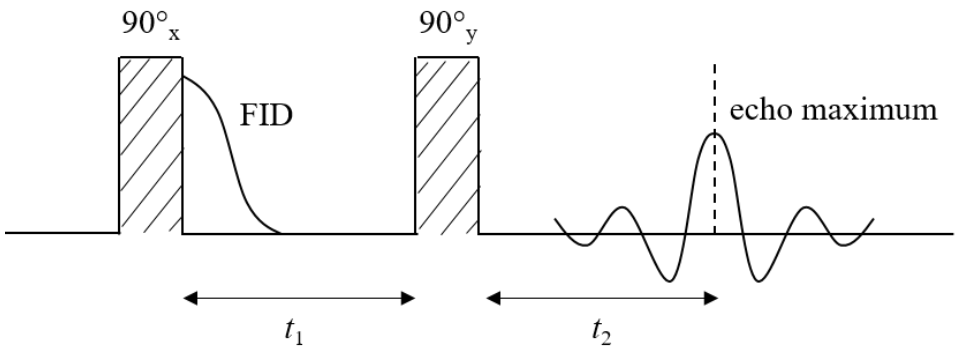

Figure 3.3: The quadrupole echo pulse sequence with t_1 the time between the two pulses ($90°_x$ and $90°_y$) and t_2 the time between the second pulse ($90°_y$) and the occurrence of the quadrupole echo maximum at which data acquisition starts. At the beginning all spins are oriented in the direction of the magnetic field (z). The indices x, y for the pulses indicate the direction in which the spins are flipped.

3.3 Rheology

As mentioned in Section 2.1, definitions of gels are very ambiguous. One approach to define a gel, however, is by determining its rheological, i.e. mechanical, properties. Gels are characterized by a viscoelastic mechanical behaviour, i.e. they show liquid-like as well as solid-

like mechanical properties dependent on the time scale of observation. So far, the basic rheological definition of a gel is that the storage modulus *G*' is larger than the loss modulus *G*'' in a frequency range of $\omega = 10^{-3}$-10^{2} rad/s which is accessible by most ordinary rheometers [Nis09, Alm93]. Whereas *G*' indicates the ability to store deformation energy, and thus represents the elastic component, *G*'' represents the viscous component and is a measure of the energy which is lost as heat during the deformation. In **Paper I**, **II** and **III**, rheological measurements complemented the visual phase studies since the latter only allowed to qualitatively determine whether a gelled lyotropic liquid crystal was formed. Note that gelation was visually determined by either loss of flow ability or turbidity. Rheology, in contrast, enabled to quantify the mechanical properties and thus confirmed whether or not gelled lyotropic liquid crystals were formed. Note that it was therefore necessary to carry out rheological measurements on three systems, i.e. the lyotropic liquid crystals in the presence of different gelators and on the respective binary systems, i.e. the pure lyotropic liquid crystals and the binary gels composed of an organic solvent and the respective LMWG. In the following, a short introduction to rheology is given with a special focus on viscoelasticity.

The term rheology is derived from the Greek word *"rheo"*, which means "flow, move". It describes the flow behaviour of liquids as well as the deformation of solids and is based on the fact that materials start to flow when exposed to a shear stress τ. Note that the technique of the investigation of rheological properties is referred to as rheometry which includes the measuring geometry (cone-plate, plate-plate, couette), the device and the methods. Basic rheological definitions are best described by the two-plates model (Figure 3.4) for which two conditions are required, i.e. (1) the sample adheres on the walls of the plates and (2) only laminar flow occurs.

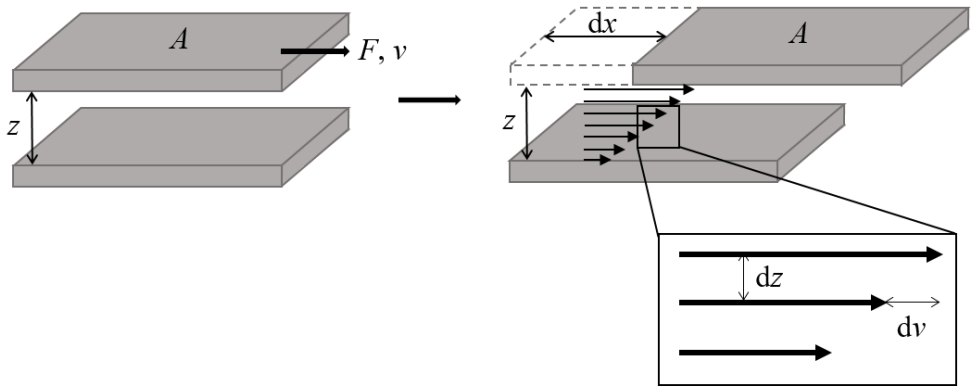

Figure 3.4: Two-plates model with shear area *A*, gap width *z*, shear force *F* and shear velocity *v*. Samples are sheared exhibiting laminar flow with the distance d*z* between the planar layers of the fluid which move with different velocities (d*v*) by moving the upper plate by a distance d*x*. The lower plate is stationary.

The sample is located between two plates, one of which is stationary, usually the lower plate and the upper one is moved. The shear stress τ is the ratio of the force *F*, which is directed parallel to the plates and the area *A* of the plates

$$\tau = \frac{F}{A}. \tag{3.4}$$

The unit of the shear stress is Pascal (Pa). The resulting shear deformation or shear strain is defined as

$$\gamma = \frac{\mathrm{d}x}{z} \tag{3.5}$$

with the distance *z* between the two plates and the deflection d*x* of the upper plate with regard to the lower plate. The shear rate $\dot{\gamma}$ is the shear strain per time unit d*t* and is given as

$$\dot{\gamma} = \frac{\gamma}{\mathrm{d}t} = \frac{1}{z} \cdot \frac{\mathrm{d}x}{\mathrm{d}t} = \frac{v}{z} \tag{3.6}$$

with the velocity *v*. The shear rate is usually given in s^{-1}. In general, materials can be categorized into viscous liquids and elastic solids. Ideal viscous fluids, also called Newtonian Fluids, are characterized by a linear relation of the shear stress τ and the shear rate $\dot{\gamma}$ with the viscosity η as the constant of proportionality

$$\tau = \eta \cdot \dot{\gamma} \,. \tag{3.7}$$

This is also known as the law of viscosity or Newton's Law. The deformation of an ideal viscous liquid is irreversible since the opposing force to the shear stress τ is a frictional force between the particles and is not restored. Ideal viscous behaviour is thus best described by the model of a dashpot. In contrast, ideal elastic behaviour is best depicted by a spring. An elastic solid shows a reversible deformation as a result of an internal restoring force due to which a material completely returns to its initial shape once the deformation stops. Ideal elastic solids are thus characterized by a linear relation of the shear stress τ and the shear strain γ, which is known as law of elasticity or Hooke's Law

$$\tau = G \cdot \gamma \tag{3.8}$$

with the shear modulus *G* as the proportionality constant. However, many materials possess viscoelastic properties, i.e. their mechanical behaviour is determined by both elastic and viscous contributions. Viscoelastic materials are often described by the Kelvin-Voigt model and the Maxwell model, which both represent viscoelastic behaviour by connecting a dashpot and a spring. However, wherever the Kelvin-Voigt model describes a solid-like response to deformation, the Maxwell model represents liquid-like behaviour.

The viscosity and the flow behaviour of a fluid is often measured by rotational tests. The mechanical properties of viscoelastic materials, however, are usually determined by oscillation shear tests. The latter can also be described with the two-plates model (Figure 3.5, left). In the case of oscillation shear rheology, the shear strain is a measure for the deflection of the upper plate, whereas the shear stress τ is an indication for the force that acts upon the lower plate to remain stationary. Oscillation shear tests can be controlled either by the shear strain γ or the shear stress τ, i.e. either the strain or the stress is the preset curve; the other the so-called response curve. However, independent on which parameter is controlled, the shear strain γ and the shear stress τ as a function of time result in sinusoidal curves with amplitudes γ_{max} and τ_{max} and frequency ω (Figure 3.5, right).

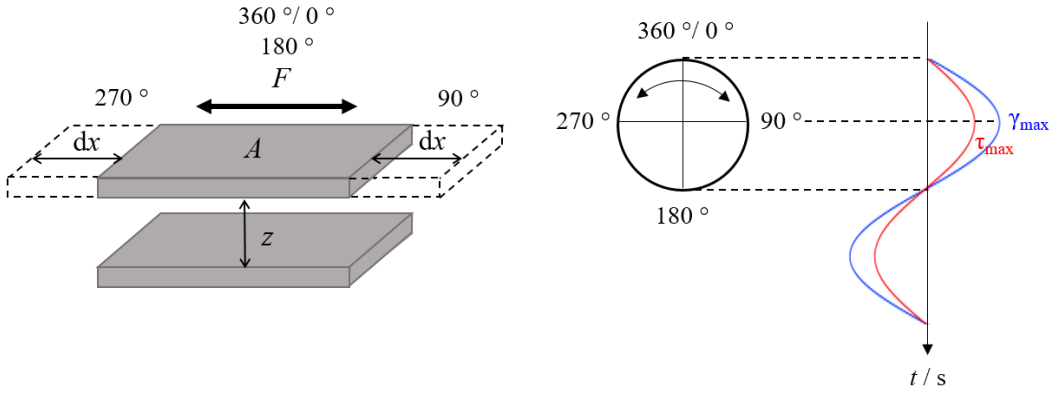

Figure 3.5: (left) Two-plates model for oscillation shear experiments with shear area *A*, gap width *z* and shear force *F*. The sample is sheared by moving the upper plate by a distance *dx* at angle positions of 0 °/360 °, 90 °, 180 °, 270 °. The lower plate is stationary. (right) The sinusoidal curves of shear strain γ and shear stress τ versus time with amplitudes γ_{max} and τ_{max} and frequency ω after a full oscillation cycle.

In Figure 3.6, the sine curves of the shear strain γ and the shear stress τ of a strain controlled oscillation experiment are shown for ideal elastic, ideal viscous and viscoelastic behaviour. While no phase shift is observed for ideal elastic behaviour, i.e. the amplitudes γ_{max} and τ_{max} of the sine curves are reached at the same time, the sine curves of ideal viscous materials are shifted by $\delta = 90$ °. Viscoelastic materials thus show phase shifts between these two extremes.

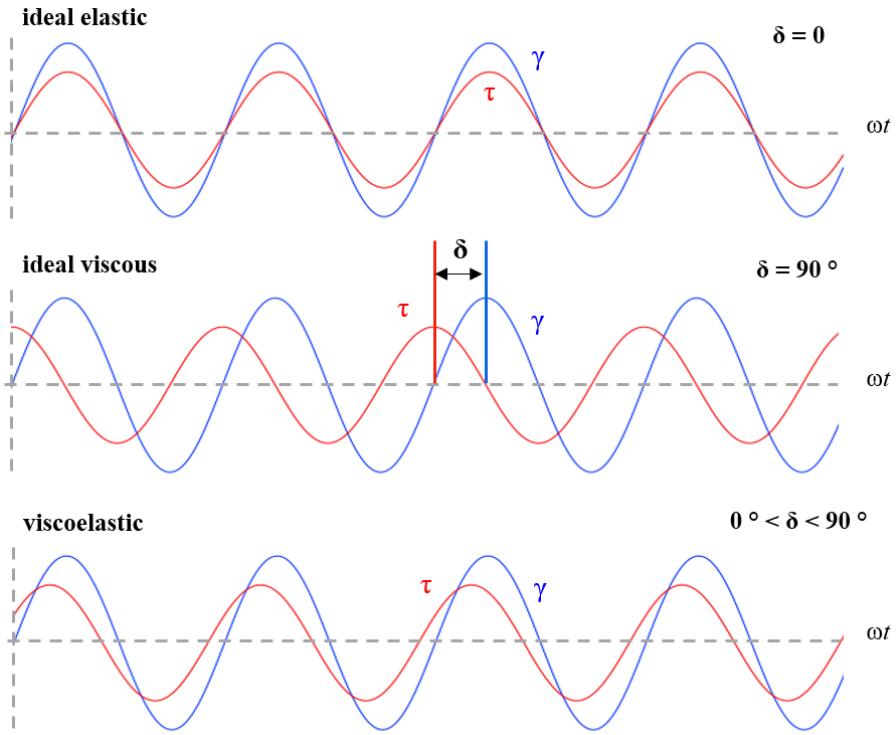

Figure 3.6: Sine curve versus time of the shear strain γ and of the resulting shear stress τ for ideal elastic, ideal viscous and viscoelastic behaviour. The sine curves are characterized by their amplitude and frequency ω after a full oscillation cycle. The phase shift δ is zero for ideal elastic behaviour and 90 ° for ideal viscous behaviour. For viscoelastic behaviour a phase shift δ in between these two ideal cases occurs.

The entire viscoelastic behaviour is described by the complex shear modulus G^* which is defined as the ratio of the amplitudes of the sine curves γ_{max} and τ_{max}

$$G^*(\omega) = \frac{\tau_{max}(\omega)}{\gamma_{max}(\omega)}, \tag{3.9}$$

also known as the law of elasticity. The complex shear modulus G^* is given in Pascal (Pa). The complex shear modulus G^* can be expressed by

$$G^*(\omega) = G'(\omega) + iG''(\omega). \tag{3.10}$$

with the storage modulus G' and the loss modulus G'', the former being the real, the latter the imaginary component, respectively. In Figure 3.7, the relationship between the complex shear modulus G^*, the storage modulus G', the loss modulus G'' and the phase shift δ, which is recorded for each measuring point, is depicted graphically. The angle by which the sine curves

are shifted is placed below the vector of the complex shear modulus *G**, which can be projected onto the x- and the y-axis. The latter represent the real and the imaginary parts, i.e. they represent the elastic and the viscous contribution and thus the storage (*G*') and the loss (*G*'') modulus. The unit of both moduli is Pascal.

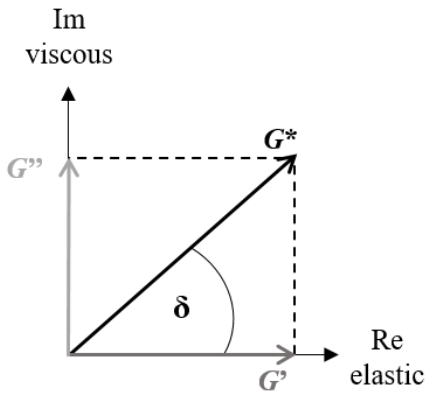

Figure 3.7: Relationship between complex shear modulus *G**, storage modulus *G*', loss modulus *G*'' and the phase shift δ of the sine curves of shear strain γ and shear stress τ in the complex plane with real axis (Re) and imaginary axis (Im). The real axis presents the elastic component; the imaginary axis the viscous component.

The storage modulus *G*' is thus a measure for the energy which is stored during deformation and describes the solid-like behaviour of materials. In contrast, the loss modulus *G*'' is a measure for the absorbed energy which is lost due to frictional forces and is also referred to as energy dissipation during deformation. The damping factor tan δ is the ratio of the viscous and the elastic component

$$\tan \delta = \frac{G''}{G'}. \tag{3.11}$$

It is dimensionless and is an indication of whether the elastic or the viscous contribution dominates the viscoelastic behaviour. The smaller tan δ, the more predominant is the elastic behaviour.

The viscoelastic behaviour of materials can be determined by different oscillation shear experiments, such as amplitude sweeps, frequency sweeps or temperature sweeps. In these experiments, the storage modulus *G*' and the loss modulus *G*'' are determined as function of the shear strain γ, the oscillation frequency ω and the temperature, respectively. Amplitude sweeps are performed to determine the linear viscoelastic (LVE) region of materials. During

the measurement the amplitude of either the shear strain γ or the shear stress τ is increased while the oscillation frequency and the temperature are kept constant. The LVE region is the range of the shear strain or shear stress in which measurements can be conducted without irreversibly changing the sample's structure. Amplitude sweeps are thus usually the starting point in the rheological investigation of viscoelastic materials. In frequency and temperature sweeps, the amplitude is thus set such that the sample is in its LVE region. Frequency sweeps are performed in order to simulate the time-dependent behaviour of viscoelastic materials, i.e. slow and fast motion on large and short time scales is mimicked at low and high frequencies, respectively. In this study, frequency sweeps were carried out in order to confirm that indeed gelled lyotropic liquid crystals were formed (**Paper I-III**). As the name indicates, only the frequency is varied in frequency sweeps, whereas the amplitude and the temperature is kept constant. In temperature sweeps, only the temperature is varied. In the case of gels, temperature sweeps are usually used to determine the sol-gel transition temperature $T_{\text{sol-gel}}$. Following the basic rheological definition, the storage modulus G' is higher than the loss modulus G'' in the gel state. The sol-gel transition temperature $T_{\text{sol-gel}}$ is indicated by a sudden drop of both moduli and a change of the viscoelastic behaviour from solid-like ($G' > G''$) to liquid-like ($G' < G''$) after crossing the $T_{\text{sol-gel}}$. In **Paper II** and **III**, the $T_{\text{sol-gel}}$ of gelled lyotropic liquid crystals were determined via oscillation shear temperature sweeps. Note that amplitude sweeps needed to be performed for each sample in advance.

3.4 Small-Angle X-ray Scattering

Scattering methods, such as light scattering, neutron scattering, and X-ray scattering are versatile methods to obtain information of the microstructure of materials. In the case of liquid crystals, small angle X-ray scattering is a common method to identify the type of liquid crystal and to obtain information on the microstructure. In **Paper IV,** small angle X-ray scattering (SAXS) measurements were carried out in order to determine whether the gel network influences the microstructure of the lyotropic liquid crystalline phases. As it was the case for the rheological investigations, SAXS measurements were performed for three systems, i.e. the gelled lyotropic liquid crystals, the pure lyotropic liquid crystals and the binary gels.

In general, X-ray scattering is based on the fact that an incident X-ray beam with wavelength λ is scattered in all directions by the electron clouds of atoms. If applied on samples with periodic structures of distance *d*, the scattered X-ray waves with same wavelength λ as the

incident beam interfere constructively when the path difference $2d \sin \theta$ of the X-ray waves is an integer n of the wavelength λ (Bragg's Law)

$$2d \sin \theta = n\lambda. \tag{3.12}$$

In other words, the two waves remain in phases if the Bragg condition is met. An illustration of Bragg's Law is given in Figure 3.8. The scattered intensity at different scattering angles is measured by a detector, which yields a characteristic pattern. As the name implies in the case of small-angle X-ray scattering, the scattered intensity of the X-ray beams is measured at small Bragg angles θ, i.e. periodical structures in the nm range are detected.

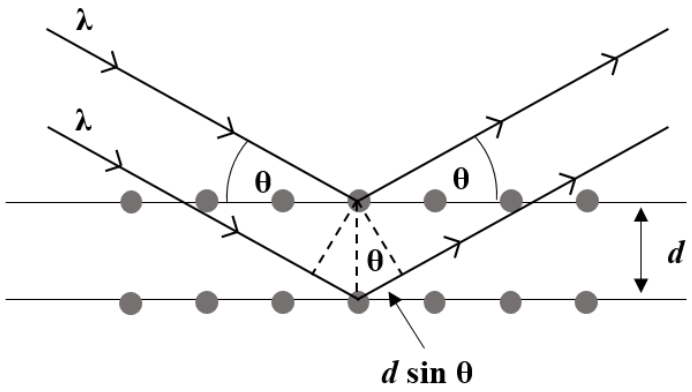

Figure 3.8: Illustration of Bragg's Law with wavelength λ, the distance between crystal planes d and θ the angle between a crystal plane and the incident and scattered beam, also referred to as the glancing angle.

Lyotropic liquid crystals, such as the hexagonal H_1 phase and the lamellar L_α phases consist of cylindrical micelles and surfactant bilayers, respectively, with a periodicity d in the nm range. Thus, their investigation with SAXS yields a characteristic pattern, i.e. SAXS allows the unequivocal determination of the existence of a certain lyotropic liquid crystalline phase. SAXS is thus often used to complement polarizing optical microscopy (POM, section 3.6). From the position of the first order Bragg peak, the distance d_0 can be estimated via the amount q of the scattering vector, which is defined as

$$q = \frac{4d \sin \theta}{\lambda} = \frac{2\pi}{d_0}. \tag{3.13}$$

The repeat distance d of the lyotropic liquid crystalline phases is in turn estimated from d_0 (Figure 3.9). Note that the characteristic pattern of hexagonal H_1 and lamellar L_α phases show Bragg peaks with a ratio of $q_1 / q_2 / q_3 = 1 / \sqrt{3} / \sqrt{4}$ etc. and $q_1 / q_2 / q_3 = 1 / 2 / 3$ etc., respectively.

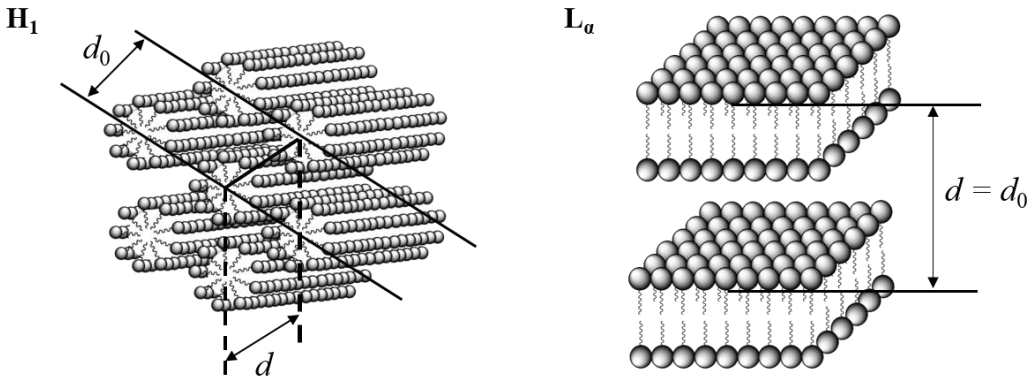

Figure 3.9: Schematic drawings of the lyotropic hexagonal H_1 phase and the lyotropic lamellar L_α phase with the repeat distances d and the distance d_0 derived from the first order Bragg peak obtained via small angle X-ray scattering. In the case of the hexagonal H_1 phase, the repeat distance is $d = 2/\sqrt{3}\, d_0$.

3.5 Dynamic Light Scattering

In order to gain information on the mesh size of the gel networks, dynamic light scattering (DLS) was performed in **Paper IV**. Before describing how this information can be extracted from the dynamic light scattering data, a short overview of the basics of DLS is given in the following.

In general, DLS is a common method to determine particle size distributions of molecules which are dispersed in a liquid medium. It is based on the Brownian motion of particles in a liquid medium, i.e. the particles movement is random in all directions. If a laser is focused on a sample in which particles are dispersed, the laser light is scattered in all directions. The intensity of the scattered laser light is detected at a scattering angle θ. Due to the movement of the particles, the scattered intensity fluctuates over time (Figure 3.10 a). With the help of the initial detected intensity, a correlation function C is generated (Figure 3.10 b and c). The latter is the average of the initial detected intensity $I(t)$ multiplied with an intensity $I(t + \tau)$ of the same intensity trace after different delay times τ divided by the square of the average of the initial detected intensity $I(t)$

$$C(\tau) = \frac{< I(t) \cdot I(t+\tau) >}{< I(t) >^2}. \tag{3.14}$$

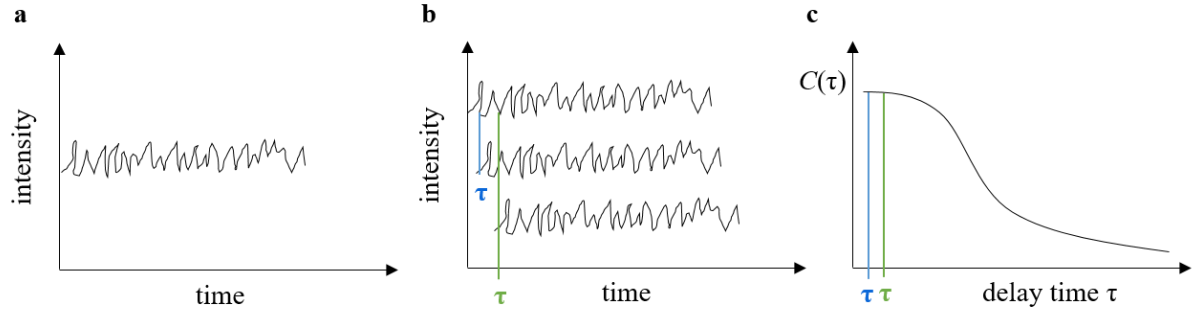

Figure 3.10: (a) Intensity fluctuations over time of a particle dispersion in a dynamic light scattering measurement. (b) Illustration of the derivation of the correlation function $C(\tau)$. (c) Correlation function $C(\tau)$, i.e. intensity as function of the delay time τ.

At the beginning, the correlation function is at the highest value and almost constant, i.e. the particle hasn't moved yet. At increasing delay times τ, the correlation function decays exponentially which indicates the movement of the particle. The decay gives information on the size of the particle, i.e. small particles show a faster decay than large particles due to their faster movement. After the decay, the initial spot and the spot at delay time τ do not show any similarity which result in a linear correlation function, also referred to as baseline, at large values of τ. For the determination of particle size distributions, the correlation functions are fitted by CUMULANT algorithms which yields the decay rate Γ

$$\Gamma = q^2 D \tag{3.15}$$

with the squared amount of the scattering vector q (Equation 3.13) and the diffusion coefficient D. The latter can, in turn, be calculated by the Stokes-Einstein equation

$$D = \frac{k_B T}{6\pi\eta R_H} \tag{3.16}$$

with Boltzmann's constant k_B, temperature T, viscosity η and hydrodynamic radius of the particles R_H.

The correlation function of gels, however, is often characterized by fast and slow relaxation modes [Mar88, Shi00] of which the former shows a decay which is either steeper or

more compressed than a single exponential decay. The correlation function is then best fitted with a compressed exponential

$$C(\tau) = \mathrm{A} + \exp\left(-\left(\frac{1}{x} \cdot \tau\right)^{\beta}\right) \tag{3.17}$$

with initial amplitude A, the relaxation time of the fast relaxation mode x and the compressed exponent β. The latter are, in turn, related to the average relaxation time of the fast mode $\langle x \rangle$

$$\langle x \rangle = \frac{x}{\beta}\,\Gamma\left(\frac{1}{\beta}\right) \tag{3.18}$$

with the gamma function $\Gamma(\frac{1}{\beta})$. From the average relaxation time of the fast mode $\langle x \rangle$, the apparent diffusion coefficient D_{app} is obtained

$$D_{\mathrm{app}} = \frac{1}{q^2 \langle x \rangle} \tag{3.19}$$

with the square of the amount of the scattering vector q (Equation 3.13). Finally, a correlation length ξ, which represents the average mesh size of a gel network [Mei07], is calculated via the Stokes-Einstein equation

$$\xi = \frac{k_{\mathrm{B}} T}{6\pi\eta D_{\mathrm{app}}}. \tag{3.20}$$

Since gels are non-ergodic media [Pus89], in which local scatterers only show limited Brownian motion, i.e. their scattering intensity is strongly position-dependent, it is important to scan different scattering volumes for the determination of the average mesh size. This can either be done by measuring the intensity of the scattered light at different scattering angles or by simply rotating the cuvette. In this study, however, no fast relaxation mode could be detected for the gelled lyotropic liquid crystals and the binary gel. The correlation functions remain independent on the delay time τ with a final relaxation at high values of τ in some cases, which indicates that gel networks with frozen mobility were formed. It was thus not possible to determine an average mesh size of the gel networks.

3.6 Polarizing Optical Microscopy and Transmission Electron Microscopy

Polarizing Optical Microscopy (POM) and Transmission Electron Microscopy (TEM) were used to determine whether the gel network influences the microstructure of the lyotropic liquid crystalline phases (POM, **Paper III**) on the one hand, and to visualize the gelled lyotropic liquid crystals on the other (TEM, **Paper IV**). In the following, the two methods will be shortly described.

Polarizing Optical Microscopy (POM). The refractive index of lyotropic liquid crystals is dependent on the direction, in which light propagates and, on the polarization, i.e. lyotropic liquid crystals are birefringent. Under a polarizing microscope, they show characteristic textures which are often used to determine the type of lyotropic liquid crystals. In Figure 3.11 (left), a basic set-up of a polarizing optical microscope is shown. It differs from a conventional microscope by two polarisation filters, one of which is in front of the sample (polarizer) and one behind (analyzer) arranged perpendicular (90 °) with respect to the polarizer. The latter linearly polarizes the light, i.e. it oscillates parallel with respect to the polarizer. For an isotropic sample, the polarisation of the light is not changed and thus the light is fully blocked by the analyzer. For birefringent materials, such as lyotropic liquid crystals, however, the polarization of the light is changed. Some parts of the light are thus passed through the analyzer, which leads to characteristic textures. In Figure 3.11, a POM image of a lyotropic lamellar L_α phase is depicted, which shows characteristic mosaic textures on the left part of the image and characteristic oily streaks on the right part. Nematic and hexagonal H_1 phases are usually characterized by so-called Schlieren textures and fan-like textures, respectively.

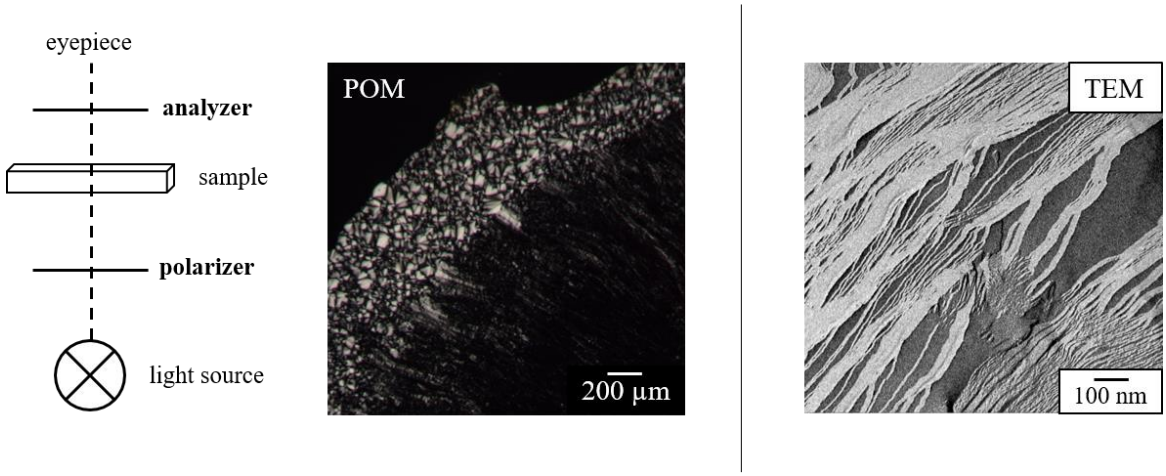

Figure 3.11: (left) Schematic set-up of a polarizing optical microscope with two polarization filter, i.e. the polarizer and the analyzer, arranged 90° to each other. Polarizing optical microscopy (POM) picture of a lamellar L_α phase which shows typical mosaic structures and oily streaks. (right) Transmission electron microscopy (TEM) picture of a lamellar L_α phase (taken by Dr. Natalie Preisig) which shows the typical layered microstructure.

Transmission Electron Microscopy (TEM). In general, the principles of a transmission electron microscope are the same as for conventional light microscopes. However, instead of lights, TEM uses electrons which yields a higher resolution due to the much smaller wavelength of electrons than that of light. TEM is thus a powerful method for the visualization of the microstructure of lyotropic liquid crystals (Figure 3.11, right). The set-up usually consists of an electron source, condenser lenses which focus the beam onto the sample and objective lenses which are placed behind the sample and focus the transmitted light on a charge coupled device (CCD) camera. The transmission of the electrons depends on the transparency of the sample on the one hand and on the sample thickness on the other. In addition, the fact that electrons are transmitted through the samples, allows to extract diffraction data as well. In this study, however, only TEM images were taken. The samples in this study were prepared via freeze fracture, i.e. they were rapidly frozen and fractured afterwards. Thus, the method is referred to as Freeze Fracture Electron Microscopy (FFEM) in **Paper IV**.

4 Summary of Research

Generally, this study can be divided into three stages: (a) Testing the capability of different low molecular weight gelators to gel LLCs without influencing their phase boundaries; (b) measuring the phase behaviour and the sol-gel transitions of the gelled LLCs of the system of choice; (c) studying the microstructure of the gelled LLCs of the system of choice. The results have been published in four publications [Ste18 (**Paper I**), Ste19a (**Paper II**), Ste19b (**Paper III**), Ste19c (**Paper IV**)]. In the following sections, the most important findings of the publications will be shortly summarized and connected with one another.

4.1 The Twofold Role of 12-Hydroxyoctadecanoic Acid (12-HOA) in a Ternary Water – Surfactant – 12-HOA System: Gelator and Co-surfactant (Paper I)

The organogelator 12-hydroxyoctadecanoic acid (12-HOA) was known to gel bicontinuous microemulsions in an orthogonal self-assembled way [Lau13a, Lau13b, Lau14] and also showed potential for gelling LLCs via orthogonal self-assembly [Koi17]. However, it was also found that 12-HOA not only gels LLCs but also is partly incorporated in the amphiphilic film due to its surface activity [Lau14, Xu15]. Therefore, 12-HOA was first added to the LLCs of the system H_2O – $C_{12}E_7$ in order to find out its function and to probe whether it gels the LLCs of the binary system H_2O – $C_{12}E_7$.

The starting point was to determine the phase boundaries of the LLCs of the system H_2O – $C_{12}E_7$, i.e. of the lamellar L_α phase, the hexagonal H_1 phase, and the bicontinuous cubic V_1 phase, in the presence of the organogelator 12-HOA at various 12-HOA mass fractions η. We first remeasured the phase boundaries of the binary system H_2O – $C_{12}E_7$ by means of visual observation of birefringence (Figure 4.1, black circles). One sees that the phase boundaries are in good agreement with literature data [Ino01]. The highly viscous and transparent H_1 and V_1 phases occur at surfactant mass fractions of $\gamma_a \approx 0.40$-0.68 and $\gamma_a \approx 0.68$-0.72, respectively. The less viscous and slightly turbid L_α phase occurs at higher surfactant mass fractions of $\gamma_a \approx 0.72$-0.85. For all three LLCs, the phase transitions of the LLCs to the isotropic phase (L phase) occur at moderate temperatures, i.e. $T_{LLC\text{-}iso} \approx 50$ °C for the H_1 and the L_α phase and $T_{LLC\text{-}iso} \approx 46$ °C for the V_1 phase. Note that in contrast to the anisotropic H_1 and L_α phases, the bicontinuous cubic V_1 phase is characterized by isotropy, i.e. the V_1-to-isotropic phase transition was determined by a decreasing viscosity. Due to the difficulty in identifying the V_1 phase, especially in the presence of a gel network, it will not be discussed further, though.

Typical for oligo (ethylene oxide) alkyl ethers, the upper miscibility gap (2ϕ) was detected at higher temperatures and at surfactant mass fractions up to $\gamma_a = 0.50$.

The influence of 12-HOA on the phase boundaries of the system H_2O – $C_{12}E_7$ is represented by the open symbols in Figure 4.1. Three 12-HOA mass fractions were investigated, namely $\eta = 0.015$, $\eta = 0.025$ and $\eta = 0.05$. In Figure 4.1, however, only the influence of 12-HOA at $\eta = 0.015$ and $\eta = 0.05$ on the phase boundaries of the LLCs are shown, since they best describe the behaviour of 12-HOA in the system H_2O – $C_{12}E_7$. At a 12-HOA mass fraction of $\eta = 0.015$ (Figure 4.1, left), the phase boundaries of the H_1 phase are shifted to lower temperatures by $\Delta T \approx 8$ °C, whereas those of the L_α phase are shifted to higher temperatures by the same value. Thus, adding 12-HOA to the system H_2O – $C_{12}E_7$ leads to a destabilized H_1 phase and a stabilized L_α phase. In addition, the upper miscibility gap (2ϕ) is also shifted to lower temperatures. This effect is more pronounced with increasing 12-HOA mass fraction, i.e. at $\eta = 0.025$ the H_1 phase is even more destabilized and the L_α phase in turn more stabilized than at $\eta = 0.015$ (data not shown). The phase boundaries of the H_1 phase at $\eta = 0.025$ could still be detected though, in contrast to those of the H_1 phase at $\eta = 0.05$ (Figure 4.1, right). For the L_α phase at a 12-HOA mass fraction of $\eta = 0.05$ (Figure 4.1, right), however, one sees that it extends up to the upper miscibility gap at lower surfactant mass fractions and at higher temperatures. As discussed in the pioneering work of Laupheimer *et al.* [Lau14], 12-HOA is partly incorporated in the surfactant layer of the system H_2O – $C_{12}E_7$ due to its surface activity. This leads to an increase of the packing parameter, i.e. the ratio of the hydrophobic area and the effective hydrophilic head group area, and thus to a lower curvature of the surfactant layer. In other words, 12-HOA also acts as co-surfactant, which, in turn, hinders its gelation capacity at the same time.

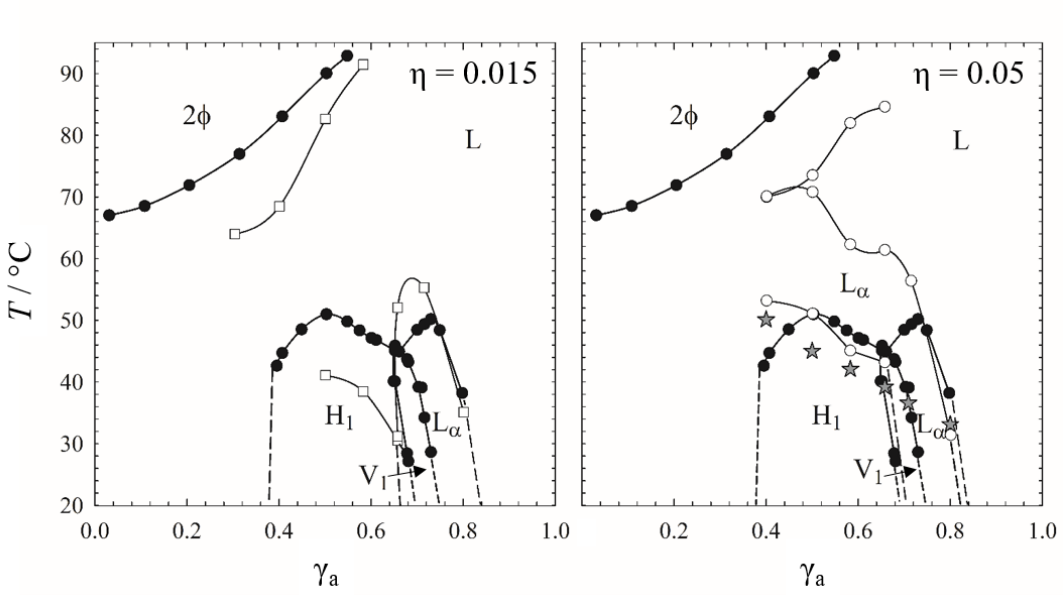

Figure 4.1: Temperature (*T*) – surfactant mass fraction (γ_a) phase diagram of the binary system H_2O – $C_{12}E_7$ in the absence (black circles) and in the presence of the organogelator 12-HOA at 12-HOA mass fractions of η = 0.015 (left, open squares) and η = 0.05 (right, open circles) determined by visual observation of birefringence. For the system at η = 0.05 approximate sol-gel transition temperatures (grey stars) are also shown. Gelation could not be observed for the system at η = 0.015. Adapted from [Ste18] with permission of MDPI, open access journal.

At the lowest 12-HOA mass fraction of η = 0.015, no change in the appearance of the L_α phase is observed. It keeps its flow ability, i.e. no gelled L_α phase is formed. In contrast, the initially transparent H_1 phase becomes slightly turbid in the presence of 12-HOA at η = 0.015 which indicates that a gelled H_1 phase is formed. However, since the turbidity vanishes at temperatures slightly larger than room temperature, it is not possible to reproducibly detect a sol-gel transition temperature. As opposed to the L_α phase, the viscosity is not indicative of gelation in the case of the H_1 phase since it is high prior to gelation. Note that additional deuterium (^2H) NMR were performed in order to complement the visual observations for the H_1 phase at a 12-HOA mass fraction of η = 0.015 since the latter were complicated by the turbidity of the H_1 phase caused by gelation. ^2H-NMR confirmed the phase behaviour of the system H_2O – $C_{12}E_7$ – 12-HOA at η = 0.015 and the role of 12-HOA as co-surfactant, but will not be discussed in detail in this section. At a 12-HOA mass fraction of η = 0.05, gelled L_α phases are formed at high surfactant mass fractions of $\gamma_a \approx 0.70$-0.80 which is indicated by the loss of the flow ability and the increase of turbidity. At lower surfactant mass fractions of $\gamma_a \approx$ 0.40-0.65, gelled isotropic phases are formed since the H_1 phase does not occur anymore. In addition, the sol-gel transition temperatures $T_{sol\text{-}gel}$ (Figure 4.1, right, grey stars) are below the lower phase boundary of the extended L_α phase, although they increase with decreasing

surfactant mass fraction γ_a. For the gelled L_α phases at $\gamma_a \approx 0.70\text{-}0.80$, the sol-gel transition temperatures $T_{sol\text{-}gel}$ are in the range of the L_α phase, i.e. below the L_α-to-isotropic phase transition. Note that the $T_{sol\text{-}gel}$ are approximate values which were visually determined by a decrease in viscosity.

To summarize, the organogelator 12-HOA has two functions in the ternary system H_2O – $C_{12}E_7$ – 12-HOA, namely co-surfactant and gelator with the former being more pronounced. Its role as co-surfactant is caused by its surface activity due to which 12-HOA is incorporated in the surfactant layer. This, in turn, leads to a destabilized H_1 phase and a stabilized L_α phase. At the same time, the gelation capacity is lowered, i.e. a 12-HOA mass fraction of $\eta \approx 0.05$ is necessary for reproducibly gel the L_α phase. Since the function as co-surfactant is enhanced with increasing 12-HOA mass fraction, shown by the disappearance of the H_1 phase at a 12-HOA mass fraction of $\eta = 0.05$, the gelled L_α phases at this high 12-HOA mass fraction are no example of an orthogonal self-assembled system. Furthermore, using 12-HOA it is not possible to adjust two sol-gel transition temperatures such that (a) $T_{sol\text{-}gel} > T_{LLC\text{-}iso}$ and vice versa, i.e. (b) $T_{sol\text{-}gel} < T_{LLC\text{-}iso}$. The next step hence was to find a potent low molecular weight gelator, which gels the LLCs without influencing the phase boundaries and with which the $T_{sol\text{-}gel}$ can be adjusted as required.

4.2 Tuning gelled lyotropic liquid crystals (LLCs) – probing the influence of different low molecular weight gelators on the phase diagram of the system H_2O/NaCl – Genapol LA070 (Paper II)

In order to find a potent gelator which gels lyotropic liquid crystals without influencing their phase boundaries, we studied the system H_2O/NaCl (0.1 wt.%) – Genapol LA070 (Figure 4.2, left) in the presence of four different low molecular weight gelators (Figure 4.2, right). Since Genapol LA070 is the technical analogue to $C_{12}E_7$, we used the system H_2O/NaCl (0.1 wt.%) – Genapol LA070 as scouting system for economic reasons. Looking at the T – γ_a phase diagram of the system H_2O/NaCl (0.1 wt.%) – Genapol LA070 (Figure 4.2, left), one sees that it forms two lyotropic liquid crystals, namely the hexagonal H_1 phase and the lamellar L_α phase at surfactant mass fractions of $\gamma_a = 0.30\text{-}0.60$ and $\gamma_a = 0.60\text{-}0.84$, respectively. Whereas the H_1 phase melts at moderate temperatures ($T \approx 40$ °C), the L_α phase extends to the upper miscibility gap (2ϕ) at high temperatures and lower surfactant mass fractions. The occurrence of an extended L_α phase in the system H_2O/NaCl (0.1 wt.%) – Genapol LA070 (not formed in the system H_2O – $C_{12}E_7$) is due to the

technical grade surfactant Genapol LA070 whose alkyl chain length varies from C_{12}-C_{14}. As a result, the packing parameter, i.e. the ratio of the hydrophobic area to the effective hydrophilic head group area, is increased which leads to a lower curvature of the amphiphilic film and, in turn, to the extension of the L_α phase [Sel02, Isr76, Stu02, Var06, Kra93, Kra95].

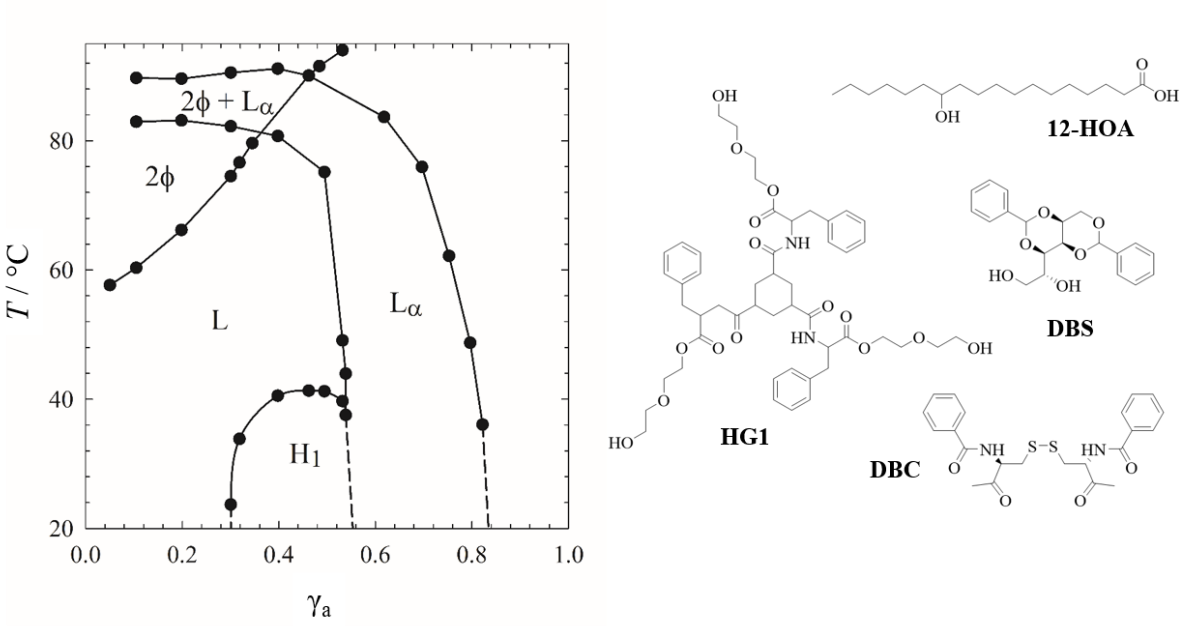

Figure 4.2: (left) T – γ_a phase diagram of the system H_2O/NaCl (0.1 wt.%) – Genapol LA070. (right) Molecular structures of the low molecular weight organogelators 12-HOA and DBS as well as of the hydrogelators HG1 and DBC. Adapted from [Ste19a] with permission from The Royal Society of Chemistry.

Having determined the phase boundaries of the system H_2O/NaCl (0.1 wt.%) – Genapol LA070 by means of visual observation of birefringence, we studied the phase boundaries in the presence of four different low molecular weight gelators (Figure 4.2, right), namely (a) the organogelators 12-HOA and 1:3,2:4-dibenzylidene-D-sorbitol (DBS) [Oke15] and (b) the hydrogelators *N*,*N*'-dibenzoyl-L-cystine (DBC) [Fri04] and HG1, a tris-amido cyclohexane derivative [Hee03, Bri08, Bri09a, Bri09b]. What they all have in common is that the sol-gel transition temperature $T_{sol\text{-}gel}$ is dependent on the gelator mass fraction. We thus investigated the influence of two gelator mass fractions, i.e. $\eta = 0.0075$ and $\eta = 0.015$, on the phase boundaries of the LLCs of the system H_2O/NaCl (0.1 wt.%) – Genapol LA070 and qualitatively determined whether gelled LLCs were formed.

The organogelator DBS and the hydrogelator HG1 turned out to be suitable gelators for gelling LLCs in an orthogonal self-assembled way. The phase boundaries of the LLCs of the system H_2O/NaCl (0.1 wt.%) – Genapol LA070 are only marginally shifted to lower

temperatures in the presence of DBS and HG1 at mass fractions of η = 0.0075 and η = 0.015 and both gelled L_α and gelled H_1 phases are formed. The latter is proved by rheometry, i.e. oscillation shear frequency sweeps. Note that 12-HOA and DBC turned out to be no suitable gelators for gelling LLCs of the scouting system. Whereas the twofold role of 12-HOA as co-surfactant and gelator was confirmed, no gelled LLCs were formed in the presence of DBC.

The visual phase studies enabled us to determine the sol-gel transition temperatures of the gelled LLCs formed by DBS and HG1 at mass fractions of η = 0.0075 and η = 0.015 by a decrease in viscosity. For both the gelled LLCs in the presence of DBS and those in the presence of HG1, the sol-gel transition temperatures $T_{\text{sol-gel}}$ depend on the gelator mass fraction. Since the visual determination of the $T_{\text{sol-gel}}$ is only qualitatively, we performed oscillation shear temperature (T) – sweeps. In this summary, the emphasis is on the organogelator DBS, though the results are very similar for the hydrogelator HG1.

In Figure 4.3 the T – sweeps of the pure L_α phase (left) and of the gelled L_α phases of the system H_2O/NaCl (0.1 wt.%) – Genapol LA070 at DBS mass fractions of η = 0.0075 (middle) and η = 0.015 (right) are shown. For the pure L_α phase, the storage modulus G' is higher than the loss modulus G'' at the initial temperature, i.e. the L_α phase shows solid-like, elastic behaviour at room temperature [Ném98]. With increasing temperature, G' and G'' slightly decrease until a sharp drop of G' at $T \approx 70$ °C indicates the L_α-to-isotropic phase transition [Mez05]. Looking at the T-sweeps of the gelled L_α phases, one thus must consider that both the sol-gel transition and the L_α-to-isotropic phase transition contributes to the temperature-dependent G' and G'' values. In the case of the gelled L_α phase at a DBS mass fraction of η = 0.0075 (Figure 4.3, middle), G' is also larger than G'' at the initial temperature but at much higher G' and G'' values than for the pure L_α phase. This proves that the L_α phase is indeed gelled in the presence of DBS at η = 0.0075, which leads to a higher mechanical strength. G' and G'' decrease with further increasing temperature until G' drops below G'' which is caused by the loss of interconnectivity of the gelator fibers, hence indicating the sol-gel transition temperature $T_{\text{sol-gel}}$ [Ter00]. Since the $T_{\text{sol-gel}}$ is equal to the L_α-to-isotropic phase transition temperature $T_{\text{LLC-iso}}$, i.e. $T_{\text{sol-gel}} \approx T_{\text{LLC-iso}} \approx 70$ °C, they cannot be separated from each other, i.e. the L_α-to-isotropic phase transition is "hidden" in the sol-gel transition. For the gelled L_α phase at the higher DBS mass fraction (Figure 4.3, right), $G' > G''$ at the initial temperature with slightly larger values than for the gelled L_α phase at η = 0.0075. With increasing temperature, G' and G'' slightly decrease until a small drop occurs in both moduli at $T \approx 68$ °C which is assigned to the L_α-to-isotropic phase transition in accordance with the visual phase studies. After this phase transition, G' and G'' decrease further until the sol-gel phase transition

is reached at $T \approx 82$ °C. The fact that the $T_{sol\text{-}gel}$ is increased by $\Delta T \approx 10$ °C by doubling the DBS mass fraction enables to separate the L_α-to-isotropic phase and the sol-gel transition from each other.

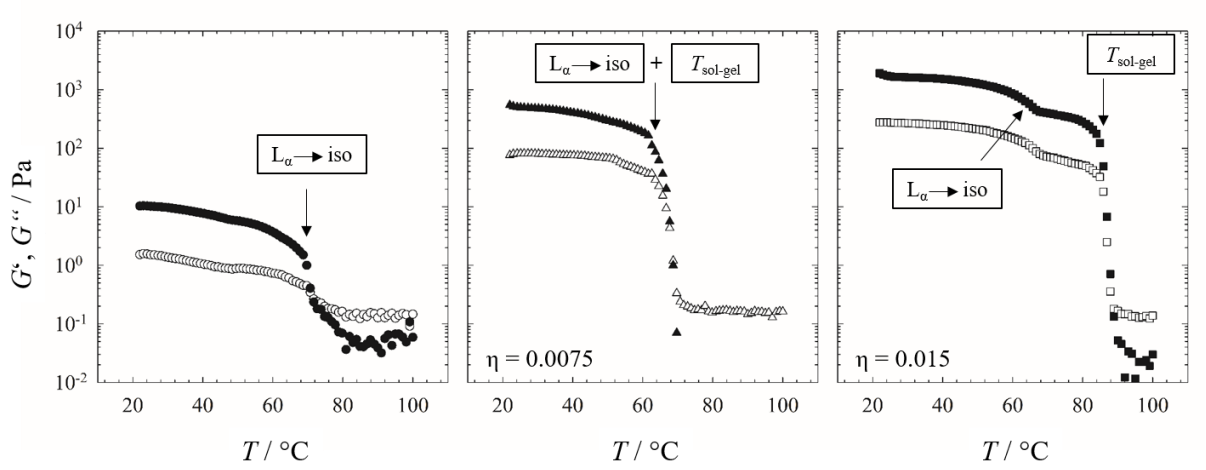

Figure 4.3: Storage modulus G' (filled symbols) and loss modulus G'' (open symbols) of the pure L_α phase of the system H_2O/NaCl (0.1 wt.%) – Genapol LA070 at a surfactant mass fraction of $\gamma_a = 0.70$ (left) and of the gelled L_α phases ($\gamma_a = 0.70$) at DBS mass fractions of $\eta = 0.0075$ (middle) and $\eta = 0.015$ (right) as function of the temperature T. Data were determined by oscillation shear T – sweeps at constant strain amplitude $\gamma_{max} = 1\%$ and constant frequency $\omega = 10\ s^{-1}$. Adapted from [Ste19a] with permission from The Royal Society of Chemistry.

The T-sweeps of the pure H_1 phase and of the gelled H_1 phases of the system H_2O/NaCl (0.1 wt.%) – Genapol LA070 in the presence of DBS at $\eta = 0.0075$ and $\eta = 0.015$ are interpreted in the same way. For the pure H_1 phase (Figure 4.4, left), one observes $G' > G''$ with decreasing values until a sharp drop at $T \approx 40$ °C is assigned to the H_1-to-isotropic phase transition. Note that the G' and G'' values are much higher for the H_1 phase than for the L_α phase. This reflects the higher viscosity of the H_1 phase due to its two-dimensional translational order, whereas the L_α phase possesses a one-dimensional order only [Dun98]. For the gelled H_1 phases at DBS mass fractions of $\eta = 0.0075$ (Figure 4.4, middle) and $\eta = 0.015$ (right), one observes an equal viscoelastic behaviour. At the initial temperature it again holds $G' > G''$ until a drop at $T \approx 40$ °C indicates the H_1-to-isotropic phase transition in both cases. After this phase transition, G' and G'' remain constant but with $G' > G''$, which shows that the system is still gelled at both DBS mass fractions and medium temperatures ($T \approx 40$-70 °C). On increasing the temperature, G' and G'' increase until sharp drops occur at $T \approx 74$ °C for the gelled H_1 phase

at η = 0.0075 and at $T \approx 94$ °C for the gelled H_1 phase at η = 0.015 which are assigned to the sol-gel phase transitions.

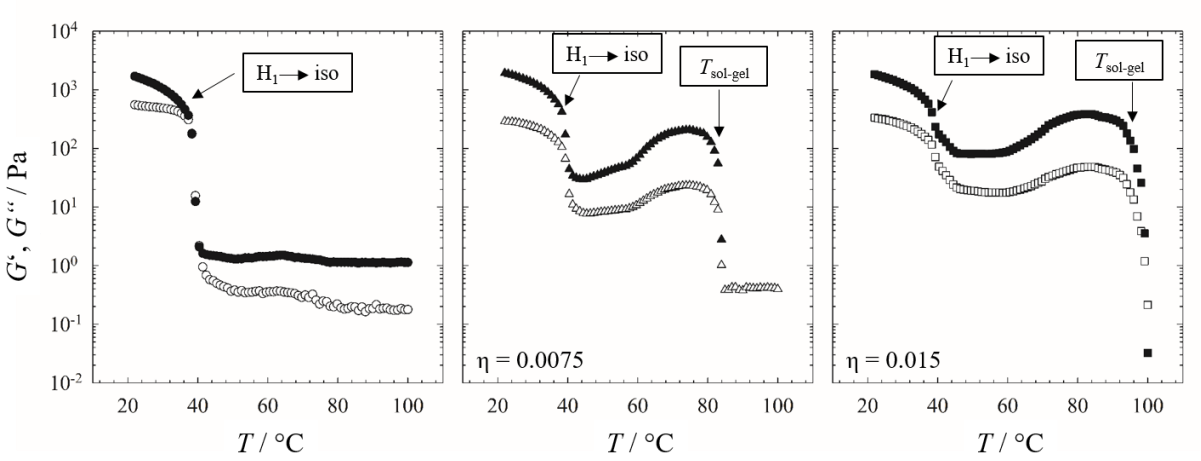

Figure 4.4: Storage modulus *G*' (filled symbols) and loss modulus *G*'' (open symbols) of the pure H_1 phase of the system H_2O/NaCl (0.1 wt.%) – Genapol LA070 at a surfactant mass fraction of $\gamma_a = 0.40$ (left) and of the gelled H_1 phases ($\gamma_a = 0.40$) at DBS mass fractions of η = 0.0075 (middle) and η = 0.015 (right) as function of the temperature *T*. Data were determined by oscillation shear *T* – sweeps at constant strain amplitude $\gamma_{max} = 1\%$ and constant frequency $\omega = 10\ s^{-1}$. Adapted from [Ste19a] with permission from The Royal Society of Chemistry.

In Figure 4.5, the sol-gel transition temperatures $T_{sol\text{-}gel}$ of the gelled LLCs at DBS mass fractions of η = 0.0075 (grey stars) and η = 0.015 (open stars) are added to the $T - \gamma_a$ phase diagram of the system H_2O/NaCl (0.1 wt.%) – Genapol LA070. Generally, the $T_{sol\text{-}gel}$ decrease with increasing surfactant mass fraction γ_a due to the good solubility of both gelators in the pure surfactant, i.e. the binary system is a better solvent at high γ_a. In the case of the gelled H_1 phases, the $T_{sol\text{-}gel}$ are above the H_1-to-isotropic phase transition at both DBS mass fraction. For the gelled L_α phases, however, the $T_{sol\text{-}gel}$ are below the L_α-to-isotropic phase transition at η = 0.0075 and above at η = 0.015.

To conclude, studying the system H_2O/NaCl (0.1 wt.%) – Genapol LA070 in the presence of four different LMWG, we identified two gelators as promising candidates for gelling LLCs in an orthogonal self-assembled way, namely the organogelator DBS and the hydrogelator HG1. Both gelators gel the L_α phase and the H_1 phase by only marginally influencing their phase boundaries. Moreover, it is possible to adjust the $T_{sol\text{-}gel}$ of the gelled L_α phases, such that (a) the $T_{sol\text{-}gel}$ is higher than the L_α-to-isotropic phase transition temperature ($T_{LLC\text{-}iso}$) at a DBS mass fraction of η = 0.015 and (b) $T_{sol\text{-}gel} < T_{LLC\text{-}iso}$ at η = 0.0075. This enables us to study the influence of the gel network on the L_α phase and vice versa, the influence of the

L_α phase on the gel network. For the simple reason that it is commercially available, DBS is chosen for gelling the LLCs of the system H_2O – $C_{12}E_7$.

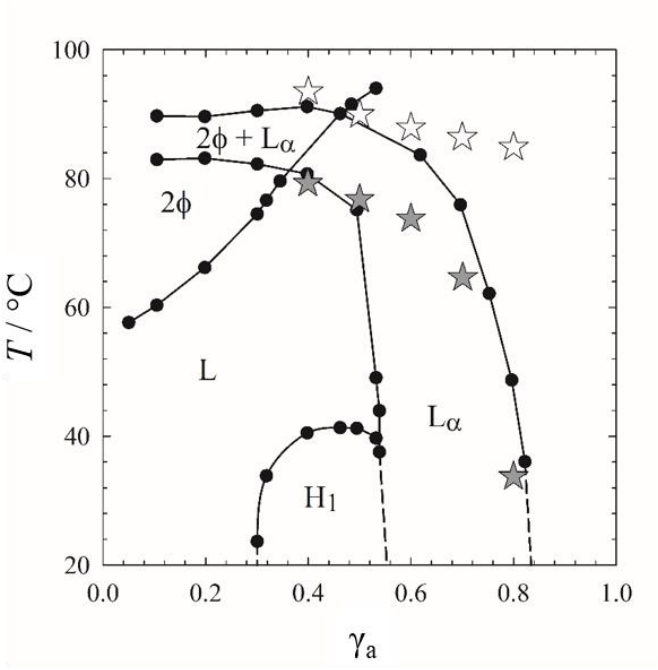

Figure 4.5: $T - \gamma_a$ phase diagram of the system H_2O/NaCl (0.1 wt.%) – Genapol LA070 (black circles) with the sol-gel transition temperatures $T_{sol\text{-}gel}$ of the gelled lyotropic liquid crystals (L_α and H_1 phase) at DBS mass fractions of η = 0.0075 (grey stars) and η = 0.015 (open stars). Adapted from [Ste19a] with permission from The Royal Society of Chemistry.

4.3 Gelling Lyotropic Liquid Crystals with the Organogelator 1,3:2,4-Dibenzylidene-D-sorbitol Part I: Phase Studies and Sol-Gel Transitions (Paper III)

Since DBS turned out to be a potent gelator for gelling the LLCs of the scouting system H_2O/NaCl (0.1 wt.%) – Genapol LA070, we investigated its capability of gelling the LLCs of the binary system H_2O – $C_{12}E_7$. Comparing the $T - \gamma_a$ phase diagrams of the system H_2O – $C_{12}E_7$ (Figure 4.6) in the absence (black circles) and in the presence of DBS at DBS mass fractions of η = 0.0075 (left, open triangles) and η = 0.015 (right, open squares), one sees that DBS has only marginal influence on the LLC phase boundaries irrespective of its mass fraction. The melting points of the L_α phase are only slightly shifted to lower temperatures ($T \approx$ 2-4 °C) by the presence of DBS, whereas those of the H_1 and V_1 phases are not altered. The visual phase studies also qualitatively showed that DBS gelled all LLCs of the system H_2O – $C_{12}E_7$ at both DBS mass fractions η = 0.0075 and η = 0.015. Moreover, one observes two sol-gel transition

temperatures $T_{sol\text{-}gel}$ of the gelled LLCs dependent on the DBS mass fractions, i.e. (a) $T_{sol\text{-}gel} > T_{LLC\text{-}iso}$ at $\eta = 0.015$ and (b) $T_{sol\text{-}gel} < T_{LLC\text{-}iso}$ at $\eta = 0.0075$.

Thus, varying the DBS mass fraction in the system $H_2O - C_{12}E_7$, it is possible to adjust the $T_{sol\text{-}gel}$ values of three gelled LLCs, namely gelled H_1, gelled V_1 and gelled L_α phases. Moreover, it is possible to study whether the chronology of gel and LLC formation does influence the microstructure and properties of the gelled LLCs. Note that the $T_{sol\text{-}gel}$ were determined in oscillation shear *T*-sweeps which are not further discussed in this Section since they can be interpreted in the same way as those described in Section 4.2. However, we performed oscillation shear frequency (ω) – sweeps in order to prove that gelled LLCs are formed and to additionally examine in which way the replacement of an organic solvent by an LLC influences the frequency dependent viscoelastic behaviour of the gel. Note that the focus is on the gelled L_α and the gelled H_1 phases since the V_1 phase occurs in a narrow concentration range and is difficult to access.

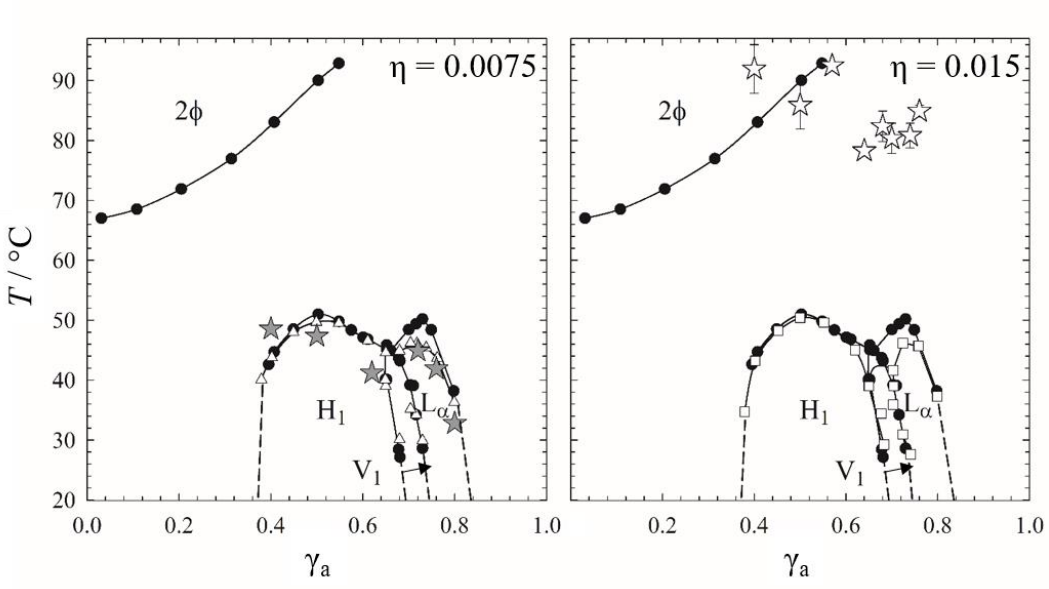

Figure 4.6: $T - \gamma_a$ phase diagram of the binary system $H_2O - C_{12}E_7$ in the absence (black circles) and in the presence of DBS at mass fractions of $\eta = 0.0075$ (left, open triangles) and $\eta = 0.015$ (right, open squares) with added sol-gel transition temperatures $T_{sol\text{-}gel}$ of the gelled LLCs (grey and open stars). Adapted with permission from [Ste19b]. Copyright (2019) American Chemical Society.

In Figure 4.7, the ω-sweeps of the gelled L_α phases (middle) and those of the binary counterparts, i.e. the pure L_α phase (left), and the binary gels ethylene glycol (EG) – DBS (right) at DBS mass fractions of $\eta = 0.0075$ (triangles) and $\eta = 0.015$ (squares) are shown. Note that

we chose the binary gel EG-DBS as parent system since ethylene glycol better mimics the "hydrophobicity" of the H_2O – $C_{12}E_7$ mixture than an alkane. For the pure L_α phase, the storage modulus *G*' is higher than the loss modulus *G*'' in the frequency range of ω = 0.01-100 s^{-1}, i.e. the L_α phase shows solid-like viscoelastic behaviour [Ném98]. However, the low absolute values of *G*' and *G*'' indicate a low viscosity, which is due to a one-dimensional translational order [Dun98, Col97]. In the case of the binary gels at DBS mass fraction of η = 0.0075 and η = 0.015, one observes *G*' > *G*'' at both mass fractions with higher values at the higher DBS mass fraction, i.e. the mechanical strength of the gel network increases with increasing DBS mass fraction [Nis09, Dou18]. In addition, *G*' is almost frequency independent at both DBS mass fractions which indicates that DBS forms rigid gel networks in ethylene glycol. For both the gelled L_α phase at η = 0.0075 and that at η = 0.015, *G*' > *G*'' at values in the same range as for the binary gels, i.e. at much higher values than for the pure L_α phase. This proves that indeed gelled L_α phases are formed at both DBS mass fractions with an equal mechanical strength as the binary gels, i.e. the mechanical strength increases with increasing DBS mass fraction. Thus, replacing ethylene glycol by the L_α phase in the DBS gel network, the gel-like viscoelastic behaviour is mostly retained. *G*' is slightly more frequency dependent in the case of the gelled L_α phases, though, which indicates that the gelled L_α phases at DBS mass fractions of η = 0.0075 and η = 0.015 are slightly softer gels than the binary gels.

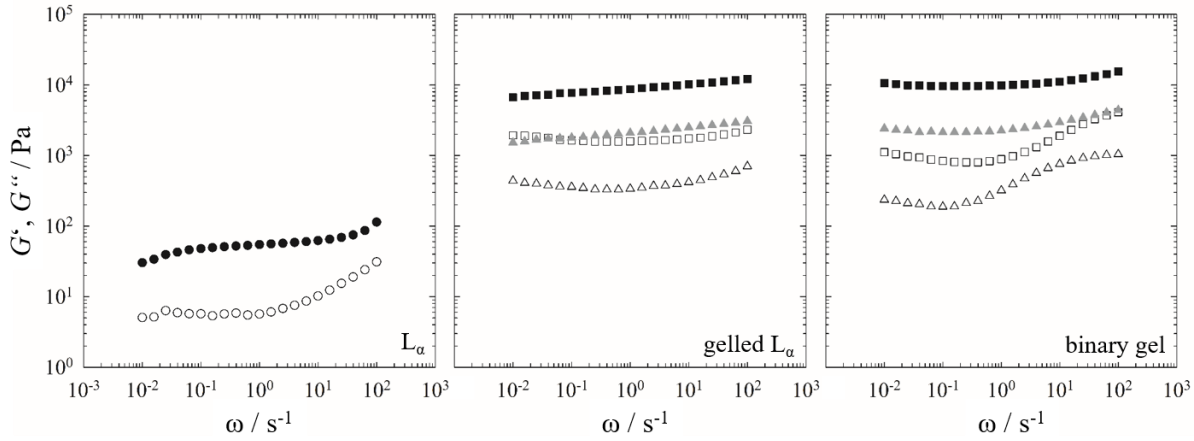

Figure 4.7: Storage modulus *G*' (filled symbols) and loss modulus *G*'' (open symbols) of the pure L_α phase of the system H_2O – $C_{12}E_7$ at a surfactant mass fraction of γ_a = 0.76 (left), the gelled L_α phases (middle, γ_a = 0.76) at DBS mass fractions of η = 0.0075 (triangles) and η = 0.015 (squares), and the binary gels (ethylene glycol – DBS) at η = 0.0075 and η = 0.015 (right) as function of the frequency ω. Data were determined by oscillation shear ω – sweeps at constant strain amplitude γ_{max} = 1% and constant temperature *T* = 22 °C. Adapted with permission from [Ste19b]. Copyright (2019) American Chemical Society.

For the pure H_1 phase (Figure 4.8, left), one observes a crossover of *G*' and *G*'' at $\omega = 0.015\ s^{-1}$, i.e. the viscoelastic behaviour of the H_1 phase changes form solid-like, elastic behaviour (*G*' > *G*'') at high frequencies to liquid-like viscous behaviour (*G*' < *G*'') at low frequencies [Ném98]. The larger absolute *G*' and *G*'' values for the H_1 phase compared to the pure L_α phase indicate a higher viscosity due to a two-dimensional translational order. In the case of the gelled H_1 phases at DBS mass fractions of $\eta = 0.0075$ and $\eta = 0.015$, the crossover of *G*' and *G*'' does not occur anymore. We found *G*' > *G*'' in the measured frequency range which shows that gelled H_1 phases were formed at both DBS mass fractions. The absolute values of *G*' and *G*'' are in the same range for both gelled H_1 phases and are only slightly higher than those of the pure H_1 phase. Hence, gelled H_1 phases with almost equal mechanical strength are formed at DBS mass fractions of $\eta = 0.0075$ and $\eta = 0.015$. In addition, in line with the gelled L_α phases, the gelled H_1 phases are softer gels than the binary gels at both DBS mass fractions, i.e. the storage modulus *G*' of the gelled H_1 phases shows a stronger frequency dependence than that of the binary gels. This is also reflected in a lower sol-gel transition temperature for the gelled LLCs, i.e. $T_{sol\text{-}gel} \approx 40\text{-}50$ °C at a DBS mass fraction of $\eta = 0.0075$ and $T_{sol\text{-}gel} \approx 80\text{-}90$ °C at $\eta = 0.015$, compared to those of the binary gels ($T_{sol\text{-}gel} \approx 90\text{-}100$ °C) at both DBS mass fractions (Figure 4.9). Interestingly, the higher the DBS mass fraction, i.e. the stronger the gel network, the less $T_{sol\text{-}gel}$ is affected by the exchange of ethylene glycol by one of the LLCs.

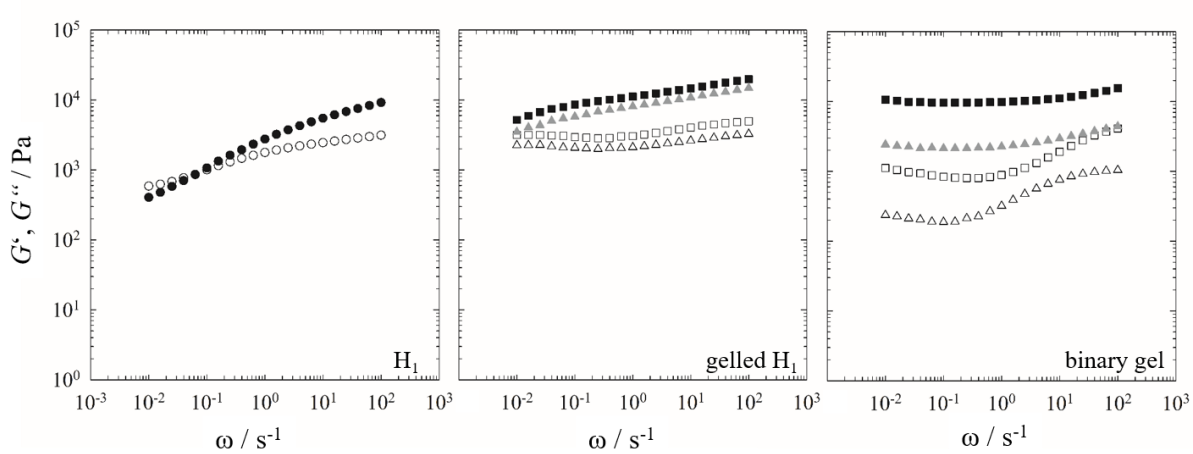

Figure 4.8: Storage modulus *G*' (filled symbols) and loss modulus *G*'' (open symbols) of the pure H_1 phase of the system H_2O – $C_{12}E_7$ at a surfactant mass fraction of $\gamma_a = 0.50$ (left), the gelled H_1 phases (middle, $\gamma_a = 0.50$) at DBS mass fractions of $\eta = 0.0075$ (triangles) and $\eta = 0.015$ (squares), and the binary gels (ethylene glycol – DBS) at $\eta = 0.0075$ and $\eta = 0.015$ (right) as function of the frequency ω. Data were determined by oscillation shear ω – sweeps at constant strain amplitude γ_{max} = 1% and constant temperature T = 22 °C. Adapted with permission from [Ste19b]. Copyright (2019) American Chemical Society.

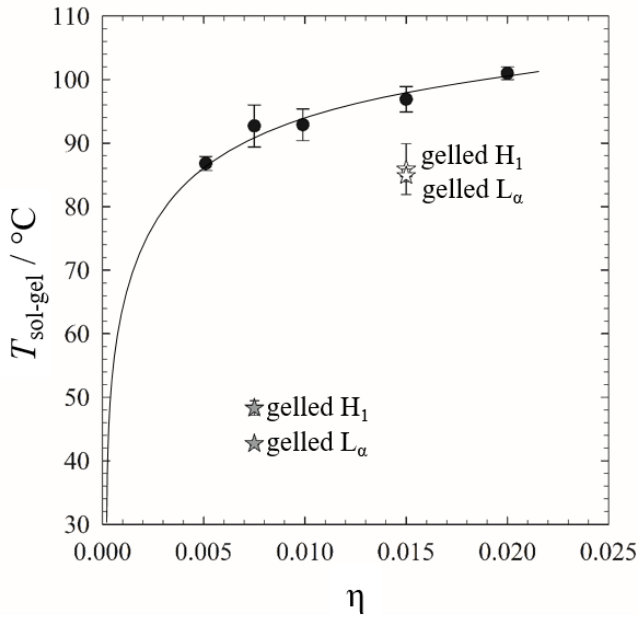

Figure 4.9: Sol-gel transition temperatures $T_{sol\text{-}gel}$ of the binary gel ethylene glycol – DBS as a function of the DBS mass fraction (black circles). The added line is a guide for the eye. For comparison, the $T_{sol\text{-}gel}$ of the gelled H_1 and the gelled L_α phases of the system H_2O – $C_{12}E_7$ in the presence of DBS at DBS mass fractions of $\eta = 0.0075$ (light grey stars) and $\eta = 0.015$ (open stars) are shown. Data was determined by oscillation shear *T* – sweeps. Adapted with permission from [Ste19b]. Copyright (2019) American Chemical Society.

In conclusion, the organogelator DBS gels the LLCs of the system $H_2O - C_{12}E_7$, i.e. the H_1, the L_α and the V_1 phases, at DBS mass fractions of $\eta = 0.0075$ and $\eta = 0.015$ with only marginal influence on the LLC phase boundaries. Oscillation shear ω – sweeps prove that gelled L_α and gelled H_1 phases are indeed formed. In addition, the sweeps show that the solid-like viscoelastic behaviour and the mechanical strength of the DBS gel network is retained in the presence of an LLC instead of ethylene glycol. Varying the DBS mass fraction η, it is possible to adjust two sol-gel transition temperatures $T_{\text{sol-gel}}$ such that (a) $T_{\text{sol-gel}}$ is above the melting points of the LLCs $T_{\text{LLC-iso}}$ at $\eta = 0.015$ and (b) $T_{\text{sol-gel}} < T_{\text{LLC-iso}}$ at $\eta = 0.0075$. This enables to form gelled L_α and gelled H_1 phases via two ways, which, in turn, allows to study the influence of the gel network on the LLC and vice versa: (1) At $\eta = 0.015$, the gel is formed in the isotropic phase on cooling down. The isotropic phase then becomes an LLC on further cooling. (2) At $\eta = 0.0075$, the gel is formed in the already existing LLC on cooling down. A first hint on how the two structures influence one another was given by polarizing optical microscopy. The pictures showed that both parent systems, i.e. the pure LLCs and the binary gel EG-DBS, are birefringent and, if combined, that the structure which is formed first dominates the optical properties. However, whether this is an effect of the chronology of gel and LLC formation or an effect of the increasing DBS mass fraction, i.e. larger structures, requires more sophisticated techniques. In the following Section, the focus is on the microstructure of the gelled LLCs which was studied via small-angle X-ray scattering (SAXS), dynamic light scattering (DLS) and freeze fracture electron microscopy (FFEM).

4.4 Gelling Lyotropic Liquid Crystals with the Organogelator 1,3:2,4-Dibenzylidene-D-sorbitol (DBS) Part II: Microstructure (Paper IV)

To finally answer the question whether the chronology of gel and LLC formation influences the microstructure of gelled LLCs, we used small-angle X-ray scattering (SAXS), dynamic light scattering (DLS) and freeze fracture electron microscopy (FFEM). In this summary, though, the focus is on SAXS and TEM since it was not possible to extract quantitative data from the DLS measurements. As a reminder, varying the DBS mass fraction in the system $H_2O - C_{12}E_7$ one can adjust the sol-gel transition temperatures $T_{\text{sol-gel}}$ of the gelled H_1 phase and the gelled L_α phase. This allows to form the gelled LLCs via two ways: (a) At a DBS mass fraction $\eta = 0.015$, the gel is formed in the isotropic phase on cooling down, which transforms into an LLC on further cooling down ($T_{\text{sol-gel}} > T_{\text{LLC-iso}}$). (b) At $\eta = 0.0075$, the LLC is formed first on cooling down, which is then followed by gel formation ($T_{\text{sol-gel}} < T_{\text{LLC-iso}}$).

In Figure 4.10, the SAXS curves of the gelled L_α phases and the gelled H_1 phases of the system H_2O – $C_{12}E_7$ in the presence of DBS at η = 0.0075 and η = 0.015 are shown. For comparison, the SAXS curves of the pure LLCs and the binary gels ethylene glycol – DBS are added. In the case of the pure L_α phase, one sees two Bragg peaks with a scattering vector ratio of $q_1 / q_2 = 1 / 2$, which is characteristic for L_α phases [Sed98, Hil94]. For the gelled L_α phases, one also observes the characteristic L_α phase pattern, which proves that the L_α phase still forms in the presence of the gel network at both DBS mass fractions. The Bragg peaks are slightly broader and less intense in the presence of the gel network at η = 0.0075 and η = 0.015 which is a result of a shorter correlation length and thus a reduced translational order [Sed98]. Comparing the repeat distances, which can be calculated from the first order Bragg peak, one sees that the repeat distance is slightly increased in the presence of the gel network. For the pure L_α phase, the repeat distance is $d_{LLC} \approx 4.1$ nm, which does not change much for the gelled L_α phases ($d_{LLC} \approx 4.2$ nm) independent on the DBS mass fraction, i.e. independent on which structure is formed first.

Looking at the SAXS curve of the pure H_1 phase and the gelled H_1 phases, one observes three Bragg peaks with a ratio of $q_1 / q_2 / q_3 = 1 / \sqrt{3} / \sqrt{4}$, which is characteristic for H_1 phases [Sed98, Hil94]. In line with the gelled L_α phases, the peaks of the gelled H_1 phases are broader and less intense compared to those of the pure H_1 phase. In addition, the repeat distance of the H_1 phase is hardly increased for the gelled phases at both DBS mass fraction, i.e. the repeat distance is $d_{LLC} \approx 5.5$ nm for both the pure H_1 phase and the gelled H_1 phases. This is again independent on the DBS mass fraction and hence independent on whether the gel is formed in the isotropic phase or the H_1 phase. Note that the SAXS curves of the binary gels ethylene glycol – DBS are also shown for comparison in Figure 4.10. No Bragg peaks are detected, though.

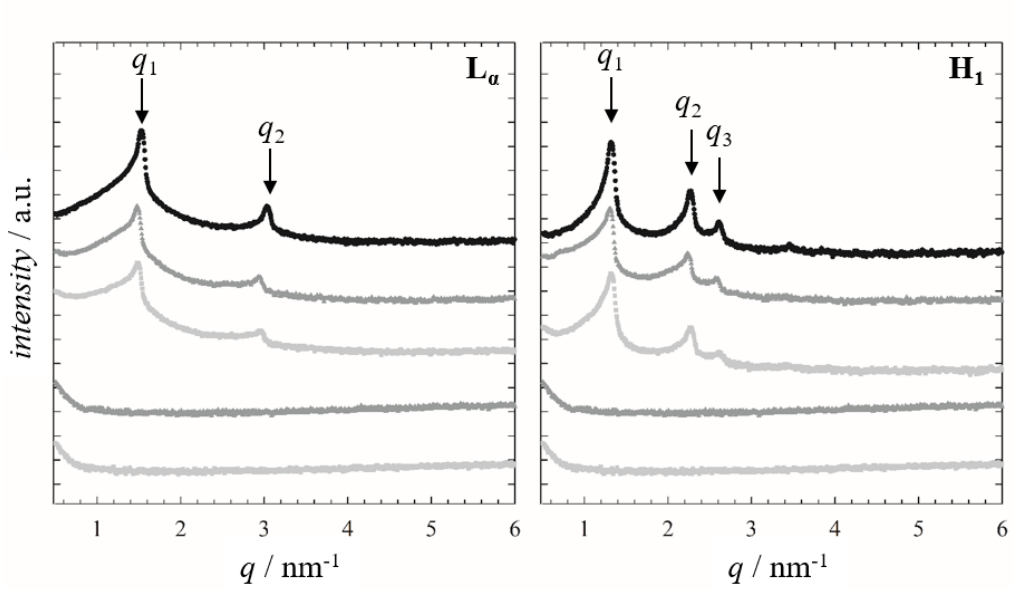

Figure 4.10: (left, top) SAXS curves of the L_α phase (black circles) of the system H_2O – $C_{12}E_7$ at a surfactant mass fraction of $\gamma_a = 0.76$ and of the gelled L_α phases ($\gamma_a = 0.76$) at DBS mass fractions of $\eta = 0.0075$ (dark grey symbols) and $\eta = 0.015$ (light grey symbols). (right, top) SAXS curves of the H_1 phase (black circles, $\gamma_a = 0.50$) of the system H_2O – $C_{12}E_7$ and of the gelled H_1 phases ($\gamma_a = 0.50$) at $\eta = 0.0075$ (dark grey symbols) and $\eta = 0.015$ (light grey symbols). (bottom) SAXS curves of the binary gels ethylene glycol – DBS at $\eta = 0.0075$ (dark grey symbols) and $\eta = 0.015$ (light grey symbols). Adapted with permission from [Ste19c]. Copyright (2019) American Chemical Society.

Freeze fracture electron microscopy (FFEM) was used in order to visualize the microstructure of the gelled LLCs. In Figure 4.11, the FFEM pictures of the pure LLCs and of the binary gels at DBS mass fractions of $\eta = 0.0075$ and $\eta = 0.015$ are shown. In the case of the pure LLCs, one observes the characteristic layered structure for the pure L_α phase and the also layered, but rather step-like and uneven structure for the pure H_1 phase [Mül99]. In line with SAXS, repeat distances of $d_{LLC} \approx 4$ nm (L_α phase) and $d_{LLC} \approx 5$ nm (H_1 phase) are estimated. The pictures of the binary gels show twisted and randomly distributed gel fibers with diameters of $d_{fibril} \approx$ 5-8 nm at both DBS mass fractions.

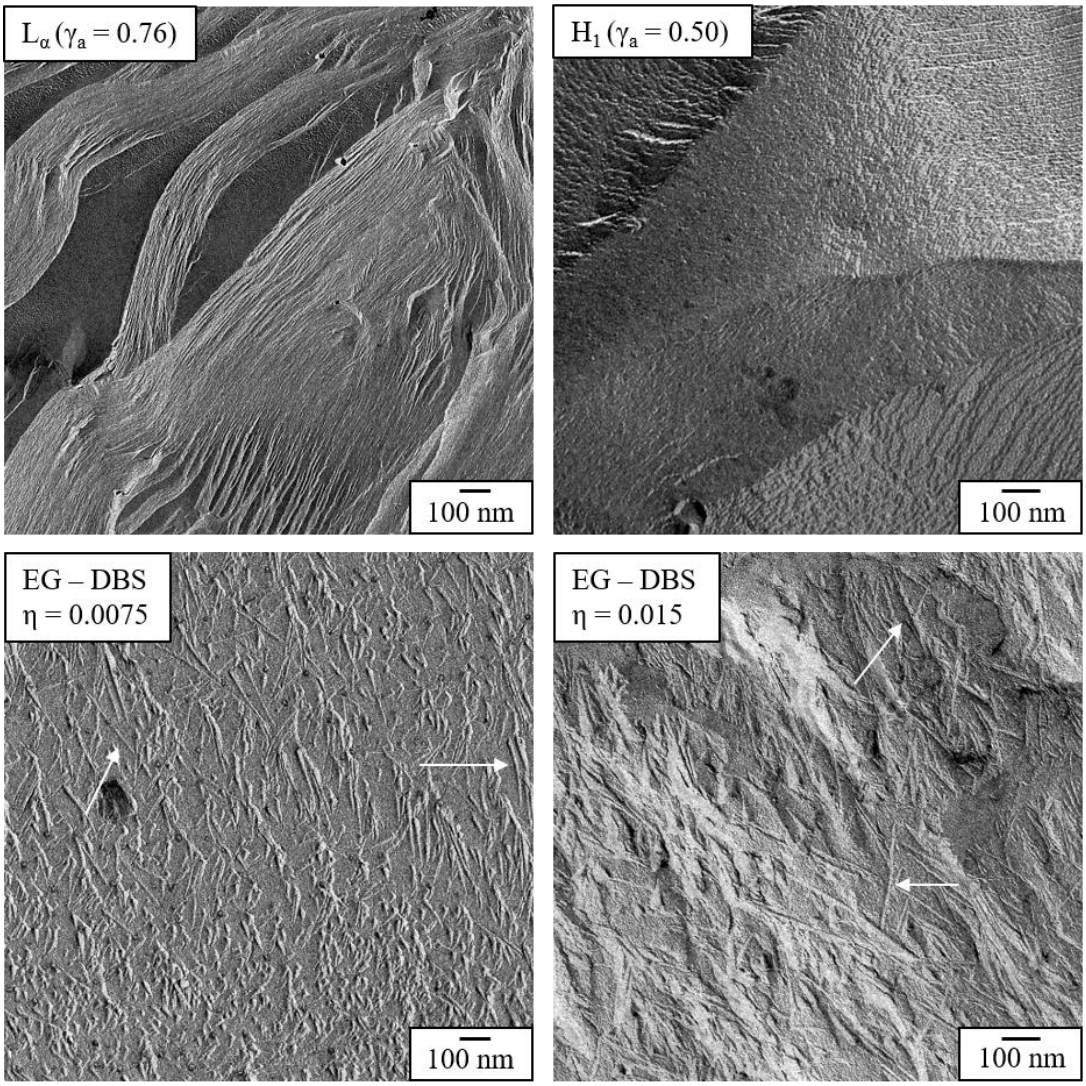

Figure 4.11: (top) Freeze fracture electron microscopy (FFEM) pictures of the pure L_α phase (left) and the pure H_1 phase (right) of the system H_2O – $C_{12}E_7$ at surfactant mass fractions γ_a. (bottom) FFEM pictures of the binary gels ethylene glycol – DBS at DBS mass fractions of η = 0.0075 (left) and η = 0.015 (right). The white arrows point to gel fibers. Note that the scale bars are slightly different. Reproduced with permission from [Ste19c]. Copyright (2019) American Chemical Society.

Looking at the FFEM pictures of the gelled L_α phases (Figure 4.12), one sees that the L_α phase and the gel network still form in the presence of each other at both DBS mass fractions. For both gelled L_α phases, twisted gel fibers which preferably occur in bundles parallel to the L_α bilayers, are detected. The twisted structure of the gel fibers is thus retained if one replaces ethylene glycol by the L_α phase. However, the occurrence in bundles is in contrast to the binary gels, for which mainly single fibers are detected. Occasionally also bundles of a small number of fibers can be observed, though. In line with SAXS, repeat distances of $d_{LLC} \approx 4$ nm and gel

fiber thicknesses of $d_{\text{fibril}} \approx$ 6-18 nm are estimated for both gelled L_α phases. The structure of the gelled L_α phases is thus independent on the DBS mass fraction, i.e. independent on whether the gel is formed in the isotropic phase or the L_α phase.

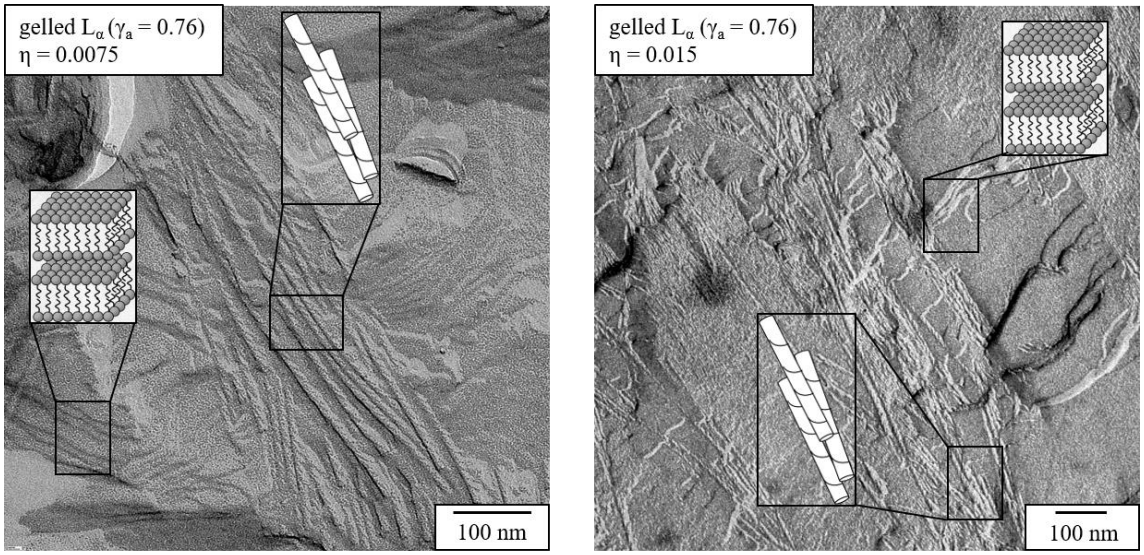

Figure 4.12: FFEM pictures of the gelled L_α phases of the system H_2O – $C_{12}E_7$ at surfactant mass fraction γ_a = 0.76 in the presence of DBS at DBS mass fraction of η = 0.0075 (left) and η = 0.015 (right). The insets highlight gelator fibers and the L_α phase. The scale bars are slightly different. Reproduced with permission from [Ste19c]. Copyright (2019) American Chemical Society.

In Figure 4.13, the FFEM images of the gelled H_1 phases at DBS mass fractions of η = 0.0075 and η = 0.015 are shown. For both gelled H_1 phases, one observes that the H_1 phase and the gel network coexist. As compared to the L_α phases, the gel fibers are twisted and preferably occur in bundles parallel to the cylindrical micelles independent on the DBS mass fraction. Thus, in line with the L_α phases, the twisted structure of the gel fibers is retained if one replaces ethylene glycol by the H_1 phase, though the arrangement of the gel fibers is different to the binary gels. At both DBS mass fraction, a repeat distance of $d_{\text{LLC}} \approx$ 5 nm is estimated. The gel fibers, though, are thicker at the higher DBS mass fraction. However, since the range of the gel fiber thickness overlap, i.e. $d_{\text{fibril}} \approx$ 8-15 nm at η = 0.0075 and $d_{\text{fibril}} \approx$ 8-25 nm at η = 0.015, this is rather an effect of the higher DBS mass fraction than of the chronology of gel and H_1 phase formation. The structures of the two gelled H_1 phases are hence equal, i.e. independent on which structure is formed first.

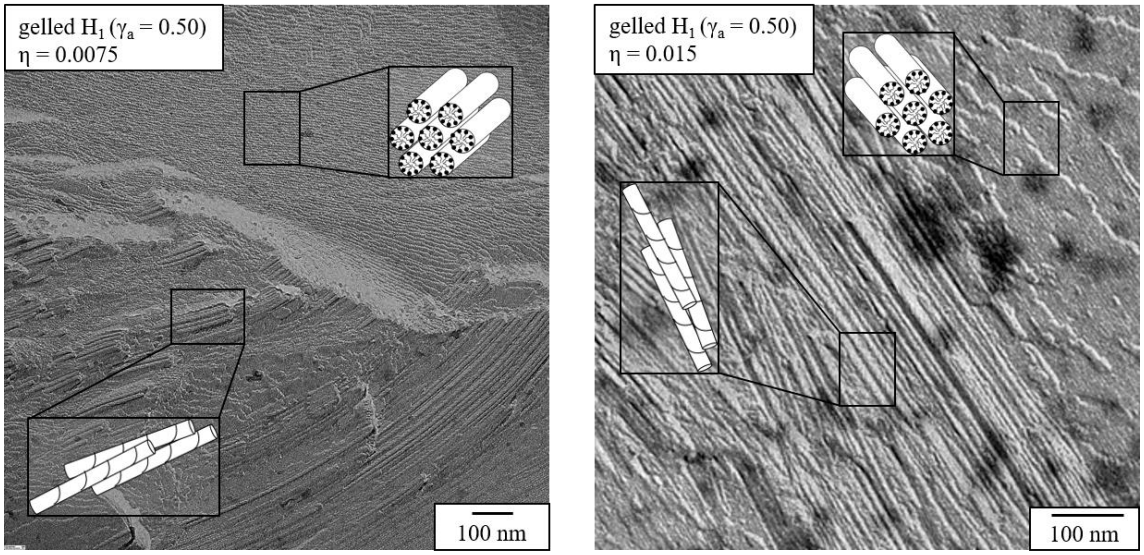

Figure 4.13: FFEM pictures of the gelled H_1 phases of the system H_2O – $C_{12}E_7$ at surfactant mass fraction γ_a = 0.50 in the presence of DBS at DBS mass fraction of η = 0.0075 (left) and η = 0.015 (right). The insets highlight gelator fibers and the H_1 phase. The scale bars are slightly different. Reproduced with permission from [Ste19c]. Copyright (2019) American Chemical Society.

To summarize, SAXS and FFEM showed that the chronology of gel and LLC formation has no influence on the microstructure of both the gelled L_α phases and the gelled H_1 phases. In fact, the gelator and the surfactant self-assemble in the presence of each other to form a gel network and an LLC, respectively. The most distinctive difference of the gelled LLCs to the binary systems, i.e. the pure LLCs and the binary gel, is the arrangement of the gel fibers. The latter are bundled in the gelled LLCs. However, since this is independent on whether the gel is formed in the isotropic or in the LLC phase, we assign this difference to different interactions of the organogelator DBS with the system H_2O – $C_{12}E_7$ and with ethylene glycol, respectively. Apart from the different arrangement of the gel fibers, only marginal differences compared to the binary systems were detected. In a nutshell, in gelled L_α and gelled H_1 phase two self-assembled, supramolecular structures coexist with their final microstructure uninfluenced by the chronology of gel and LLC formation. In other words, gelled L_α and gelled H_1 phases are orthogonal self-assembled systems!

5 Conclusion & Outlook

The thesis at hand aimed to give further insight on two fundamental questions in the field of gelled lyotropic liquid crystals: (1) Does the chronology of LLC and gel formation influence the size and orientation of the LLC domains and the alignment of the gel fibers? (2) Do the gel network and the LLC form simultaneously but independently, i.e. are gelled LLCs orthogonal self-assembled systems?

First and foremost, however, this study showed that the gelator must be carefully chosen for gelling LLCs via orthogonal self-assembly. In **Paper I**, the organogelator 12-HOA, which was known to gel bicontinuous microemulsions via orthogonal self-assembly, was investigated at different mass fractions. However, visual observations of birefringence revealed that 12-HOA acted as gelator and co-surfactant such that the H_1 phase of the system H_2O – $C_{12}E_7$ is destabilized, whereas the L_α phase is stabilized. Due to the loss of gelator as co-surfactant, high gelator concentrations were needed to gel the LLCs in the first place. This is in clear contradiction to an orthogonal self-assembled system, though. In **Paper II**, the scouting system H_2O/NaCl – Genapol LA070 was studied in the presence of a selection of LMWG in order to find promising candidates for gelling LLCs in an orthogonal self-assembled way. Both organogelators (12-HOA and 1,3:2,4-dibenzylidene-D-sorbitol (DBS)) and hydrogelators (*N*,*N*'-dibenzoyl-L-cystine (DBC) and a tris-amido cyclohexane derivative (HG1)) were investigated. The starting point was again the visual determination of the temperature (T) – surfactant mass fraction (γ_a) phase diagrams of the system H_2O/NaCl – Genapol LA070 in the presence of the gelators. The role of 12-HOA as co-surfactant and gelator was confirmed since the phase boundaries of the H_1 phase and the L_α phase were strongly influenced. The hydrogelator DBC turned out not to be a potent gelator for gelling LLCs. Although the phase boundaries were not as strongly affected as in the presence of 12-HOA, no gelled LLCs were formed with DBC. The organogelator DBS and the hydrogelator HG1 were found to be the most promising gelators for gelling LLCs via orthogonal self-assembly. Both DBS and HG1 gelled the LLCs of the system H_2O/NaCl – Genapol LA070 without noticeably influencing their phase boundaries. The gelation was confirmed by oscillation shear frequency sweeps. In addition, using DBS and HG1 at two mass fractions, it was possible to adjust the sol-gel transition temperature $T_{sol\text{-}gel}$ of the gelled L_α phase. (a) At a gelator mass fraction of $\eta = 0.015$, the $T_{sol\text{-}gel}$ were above the melting points of the L_α phase ($T_{LLC\text{-}iso}$). (b) At $\eta = 0.0075$, $T_{sol\text{-}gel} < T_{LLC\text{-}iso}$. Interestingly, both the hydrogelator HG1 and the organogelator DBS are potent gelators for gelling LLCs via orthogonal self-assembly.

The organogelator DBS was chosen for further investigations of the system H_2O – $C_{12}E_7$ for the simple reason that it is commercially available. In **Paper III**, the T – γ_a phase diagram of the system H_2O – $C_{12}E_7$ – DBS was determined by visual observations of birefringence. DBS was added at the two mass fractions, i.e. $\eta = 0.0075$ and $\eta = 0.015$, with which it was possible to adjust the $T_{sol\text{-}gel}$. At both DBS mass fractions gelled LLCs were formed without the phase boundaries being affected by the presence of the gel network. In order to confirm gelation, oscillation shear frequency sweeps of the gelled LLCs and their binary counterparts, i.e. the binary system H_2O – $C_{12}E_7$ and the binary gel ethylene glycol – DBS were again conducted. In the case of the LLCs, gelation lead to an increase of the storage (G') and the loss (G'') modulus with larger values at the higher DBS mass fraction. Compared to the binary gel ethylene glycol – DBS, the gelled L_α and the gelled H_1 phases are slightly softer gels which was indicated by a more frequency dependent storage modulus G'. Performing oscillation shear temperature sweeps enabled to detect the sol-gel transition temperatures $T_{sol\text{-}gel}$ of the gelled LLCs next to the LLC to isotropic phase transition temperatures $T_{LLC\text{-}iso}$. For all gelled LLCs of the system H_2O – $C_{12}E_7$ it held: (a) $T_{sol\text{-}gel} > T_{LLC\text{-}iso}$ at $\eta = 0.015$ and (b) $T_{sol\text{-}gel} < T_{LLC\text{-}iso}$ at $\eta = 0.0075$.

This allowed to form the gelled LLCs via two ways: (a) At $\eta = 0.015$, the gel network is formed in the isotropic phase which transforms into an LLC on cooling down. (b) At $\eta = 0.0075$, the gel network is formed in the LLC on cooling down. This enabled us to investigate (a) the influence of the gel network on the microstructure of the LLC phase and (b) the influence of the LLC on the alignment of the gel fibers. In **Paper IV**, the microstructure of the gelled LLCs and the binary counterparts was studied by means of small angle X-ray scattering (SAXS), dynamic light scattering (DLS) and freeze fracture electron microscopy (FFEM). The focus was thereby on the gelled L_α and the gelled H_1 phases. For both the gelled L_α phases and the gelled H_1 phases it was found that the chronology of gel and LLC formation has no influence on the final microstructure. The following findings are valid for the gelled L_α and the gelled H_1 phases at both DBS mass fractions and hence are independent on whether the gel network is formed in the isotropic phase or in one of the LLCs. (1) The interlayer spacing of the LLCs is slightly increased in the presence of the gel network compared to the pure LLCs. (2) The gel networks of all gelled LLCs and the binary gels have frozen mobility indicated by intensity correlation functions that are independent on the delay time and only show a final relaxation at long delay times. (3) The gel fibers of the gelled LLCs preferably occur in bundles parallel to the surfactant bilayers of the L_α phase and parallel to the cylindrical micelles of the H_1 phase. For the binary gel, in contrast, the fibers preferably occur as randomly distributed single fibers,

though bundles of a small number of fibers are detected as well. In addition, the fibers of the gelled LLCs have slightly larger diameters compared to the binary gel. These observations showed that the organogelator DBS interacts differently with the system H_2O – $C_{12}E_7$ than with ethylene glycol. Nevertheless, the gel fibers retain their general structure, i.e. they are twisted in the gelled LLCs as is the case for the binary gels.

Altogether, the gelled LLCs only show marginal differences to their binary counterparts. This proves that gelled L_α phases and gelled H_1 phases of the system H_2O – $C_{12}E_7$ in the presence of DBS at DBS mass fractions of $\eta = 0.0075$ and $\eta = 0.015$ are indeed formed by the self-assembly of a gelator and the self-assembly of a surfactant. In a nutshell, they are orthogonal self-assembled systems.

This study helps to better understand the interactions of a gel network and an LLC. Furthermore, it showed that the gelator is a crucial component in gelled LLCs and requires thorough optimization to avoid interactions of the gel network and the LLC, i.e. the surfactant layer. Future work will have to address a fundamental question about the interactions of the LLC and the gel network. The thickness of the gel fibers in gelled LLCs was found to be different for the organogelators DBS and 12-HOA. The gel fibers in the gelled LLCs of the present study are 8-25 nm thick, whereas fibers in L_α phases gelled by the organogelator 12-HOA are much thicker (35-70 nm) [Xu15]. Thus, the question arises whether there is a critical fiber thickness up to which gelled LLCs are formed via the orthogonal self-assembly of a gelator and a surfactant. In order to answer this question, LLCs gelled by a selection of LMWGs which form gel fibers of different thicknesses have to be studied. Moreover, future studies should address the formulation of stimuli-responsive gelled LLCs for a wide range of applications. For a potential use as drug delivery systems, $C_{12}E_7$ needs to be replaced by a biologically and dermatologically compatible surfactant and the thermo-sensitive LMWGs by a potent photo-sensitive gelator whose sol-gel transitions can be induced by UV irradiation. Hydrogels formed by the latter have been reported as systems with a controlled drug release [Tom11]. The advantage of gelled LLCs compared to hydrogels is the capability to dissolve both hydrophobic and hydrophilic drugs. The goal is to load gelled LLCs with both hydrophobic and hydrophilic drugs and to carry out penetration and skin permeability tests. Stimuli-responsive gels are further used in art conservation. Weiss *et al*. reported on gels whose sol-gel transition can be induced by introducing CO_2 gas in solutions of an amine-based gelator and can be reversed by addition of small amounts of a weak acid [Wei05]. Transferring this concept

to gelled LLCs via this route, gelled LLCs might be used in art conservation with the advantage that both hydrophobic and hydrophilic grime can be removed. Moreover, embedding electrically stimulating compounds such as metal-based nanocomposite materials [Raf19] in gelled LLCs formed with LMWGs opens the possibility to design a new class of stimuli-responsive anisotropic gels with potential use as actuators. In addition, incorporating different types of nanocomposites will allow to tune the properties of gelled LLCs for different applications [Raf19].

6 Abbreviations

Numerical & Latin.

12-HOA	12-hydroxyoctadecanoic acid
$2C_{12}$DAB	didodecyldimethylammonium bromide
^{2}H-NMR	deuterium nuclear magnetic resonance
2ϕ	two-phase region
a_0	effective head group area
a_{chain}	area of hydrophobic part
A	area
B_0	magnetic field
$C_{10}E_4$	tetraethylene glycol monodecyl ether
$C_{12}E_7$	heptaethylene glycol monododecyl ether
C	correlation function
CAPB	cocamidopropyl betaine
cmc	critical micelle concentration
CsPFO	caesium pentadecane fluoro octanoate
CTAB	cetyltrimethylammonium bromide
D_2O	deuterated water
d_{fibril}	diameter of gel fibers
d_{LLC}	repeat distance of lyotropic liquid crystals
dv	velocity gradient
dx	deflection
dz	distance
D	diffusion coefficient
D_{app}	apparent diffusion coefficient
DBC	*N*,*N*'-dibenzoyl-L-cystine
DBS	1,3:2,4-dibenzylidene-D-sorbitol
DLS	dynamic light scattering
DMPC	dimyristoyl phosphatidyl choline
EG	ethylene glycol
F	shear force

FFEM	freeze fracture electron microscopy
FID	free induction decay
G^*	complex shear modulus
G'	storage modulus
G''	loss modulus
H_2O	water
H_1	hexagonal phase
HG1	short name of a tris-amido cyclohexane derivative
H-bonds	hydrogen bonds
I	(a) spin quantum number; (b) intensity
Im	imaginary part
k_B	Boltzmann's constant
l_c	length of hydrocarbon chain
L_1	normal micellar phase
L_α	lamellar phase
LC	liquid crystal
LMWG	low molecular weight gelator
LLC	lyotropic liquid crystal
LVE	linear viscoelastic region
m_I	magnetic spin quantum number
m_X	mass of component X
n	(a) integer; (b) refractive index
$\hat{n}$	director of orientational order
P	Packing parameter
PAAm	polyacrylamide
PDGI	poly(dodecyl glyceryl itaconate)
PEG-lipid	poly(ethylene glycol)-derived polymer lipids
POM	polarized optical microscopy
q	scattering vector
Re	real part
R_H	hydrodynamic radius
S	orientational order parameter
SAFiNs	self-assembled fibrillar networks

SAXS	small angle X-ray scattering
SDS	sodium dodecyl sulfate
t	time
tan δ	damping factor
T	temperature
$T_{\text{LLC-iso}}$	lyotropic liquid crystal-to-isotropic phase transition temperature
$T_{\text{sol-gel}}$	sol-gel transition temperature
V_1	bicontinuous cubic phase
v	velocity
V_c	volume of hydrocarbon chain
x	fast relaxation mode
z	distance

Greek.

β	stretching exponent
γ	shear strain
γ_a	surfactant mass fraction
γ_{max}	amplitude of shear strain
$\dot{\gamma}$	shear rate
δ	phase shift of sine curves of shear stress and shear deformation
Δν	splitting of deuterium NMR lineshape
η	(a) viscosity; (b) gelator mass fraction
η_{app}	apparent viscosity
θ	(a) angle between two axes; (b) scattering angle
λ	wavelength
ξ	correlation length
τ	(a) shear stress; (b) delay time
τ_{max}	amplitude of shear stress
Γ	(a) decay rate; (b) gamma function
χ	magnetic susceptibility
ω	oscillation shear/angular frequency

7 References

[Alm93] K. Almdal, J. Dyre, S. Hvidt, O. Kramer, *Poly. Gels Netw.* **1993**, *1*, 5-17.

[And74] T. Ando, Y. Yamazaki, *US Pat.*, 3846363, 1974.

[Ara19] K. Aramaki, S. Koitani, E. Takimoto, M. Kondo, C. Stubenrauch, *Soft Matter* **2019**, *15*, 8896-8904.

[Bla92] J. C. Blackburn, P. K. Kilpatrick, *Langmuir* **1992**, *8*, 1679-1687.

[Bom04] K. J. van Bommel, C. van der Pol, I. Muizebelt, A. Friggeri, A. Heeres, A. Meetsma, B. L. Feringa, J. van Esch, *Angew. Chem. Int. Ed.* **2004**, *43*, 1663-1667.

[Bri08] A. Brizard, M. Stuart, K. Van Bommel, A. Friggeri, M. De Jong, J. van Esch, *Angew. Chem. Int. Ed.* **2008**, *47*, 2063-2066.

[Bri09a] A. M. Brizard, J. H. van Esch, *Soft Matter* **2009**, *5*, 1320-1327.

[Bri09b] A. M. Brizard, M. C. A. Stuart, J. H. van Esch, *Faraday Discuss.* **2009**, *143*, 345-357.

[Bru06] R. Brummer, *Rheology Essentials of Cosmetic and Food Emulsions*, Springer, Berlin-Heidelberg, 2006.

[Boe16] J. Boekhoven, A. M. Brizard, M. C. A. Stuart, L. Florusse, G. Raffy, A. Del Guerzo, J. H. van Esch, *Chem. Sci.* **2016**, *7*, 6021-6031.

[Col97] P. J. Collings, M. Hird, *Introduction to Liquid Crystals: Chemistry and Physics* (Eds.: G. W. Gray, J. W. Goodby, A. Fukuda), Taylor & Francis Ltd.: London, UK, 1997.

[Dav83] J. H. Davis, *Biochim. Biophys. Acta* **1983**, *737*, 117-171.

[Dou18] J. Douglas, *Gels* **2018**, *4*, 19.

[Dun98] D. Dunmur, K. Toriyama, Elastic Properties. In *Handbook of Liquid Crystals Vol. 1 Fundamentals*, Wiley-VHC, Weinheim, 1998, 253-280.

[Eva99] D. F. Evans, H. Wennerström, *The Colloidal Domain where Physics, chemistry, biology and technology meet,* Second Edition, Wiley-VHC, New York, 1999.

[Flo74] P. J. Flory, *Faraday Discuss. Chem. Soc.* **1974**, *57*, 7-18.

[Fri04] A. Friggeri, B. L. Feringa, J. van Esch, *Journal of Controlled Release* **2004**, *97*, 241-248.

[Gla82] O. Glatter, O. Kratky, *Small Angle X-ray Scattering.* Academic Press Inc., London, 1982.

[Goo08] J. W. Goodwin, R. W. Hughes, *Rheology for Chemists: An Introduction – 2nd Edition*, RCS Publishing, Cambridge, 2008.

[Hee03] A. Heeres, C. van der Pol, M. Stuart, A. Friggeri, B. L. Feringa, J. van Esch, *J. Am. Chem. Soc.* **2003**, *125*, 14252-14253.

[Hil94] K. Hiltrop, Lyotropic Liquid Crystals. In *Liquid Crystals* (Ed.: H. Stegemeyer), First Edition, Steinkopff, Darmstadt, 1994, 143-171.

[Hu14] X. Hu, T. Xiao, C. Lin, F. Huang, L. Wang, *Acc. Chem. Res.* **2014**, *47*, 2041-2051.

[Ily17] M. Ilyas, Md. Anamul Haque, Y. Yue, T. Kurokawa, T. Nakajima, T. Nonoyama, J. P. Gong, *Macromolecules* **2017**, *50* (20), 8169-8177.

[Ino01] T. Inoue, M. Matsuda, Y. Nibu, Y. Misono, M. Suzuki, *Langmuir* **2001**, *17*, 1883-1840.

[Isr76] J. N. Israelachvili, D. J. Mitchell, B. W. Ninham, *J. Chem. Soc., Faraday Trans. 2* **1976**, *72*, 1525-1568.

[Jan00] R. H. C. Janssen, V. Stümpflen, M. C. W. van Boxtel, C. W. M. Bastiaansen, D. J. Broer, T. A. Tervoort, P. Smith, *Macromol. Symp.* **2000**, *154*, 117-126.

[Jel86] L. W. Jelinski, Deuterium NMR of Solid Polymers. In *High resolution NMR Spectroscopy of Synthetic Polymers in Bulk*. (Ed.: R.A. Komorowski), VHC Publishers, 1986, 335-364.

[Kat02] T. Kato, T. Kutsuna, K. Yabuuchi, N. Mizoshita, *Langmuir* **2002**, *18*, 7086-7088.

[Kat07] T. Kato, Y. Hirai, S. Nakaso, M. Moriyama *Chem. Soc. Rev.* **2007**, *36*, 1857-1867.

[Kel09] C.V.-D. Kelly, Perturbations of cellular membranes with synthetic polymers and ultrafast lasers, PhD Thesis, University of Michigan (2009) and ref. 12 therein.

[Koi17] S. Koitani, S. Dieterich, N. Preisig, K. Aramaki, C. Stubenrauch, *Langmuir* **2017**, *33*, 12171-12179.

[Kra93] K. Kratzat, H. Finkelmann, *Liquid Crystals* **1993**, *13* (5), 691-699.

[Kra95] K. Kratzat, C. Stubenrauch, H. Finkelmann, *Colloid Polym. Sci.* **1995**, *273*, 257-262.

[Kum14] D. K. Kumar, J. W. Steed, *Chem. Soc. Rev.* **2014**, *43*, 2080-2088.

[Lai10] W.-C. Lai, C.-H. Wu, *J. Appl. Polym. Sci.* **2010**, *115*, 1113-1119.

[Lai79] P. E. Laibinis, J. J. Hickman, M. S. Wrighton, G. M. Whitesides, *Science* **1989**, *245*, 845-847.

[Lau94] R. G. Laughlin, *The Aqueous Phase Behaviour of Surfactants* (Eds.: R. H. Ottewill, R. L. Rowell), Academic Press Limited, London, UK, 1996.

[Lau13a] M. Laupheimer, Gelled Bicontinuous Microemulsions – A New Type of Orthognal Self-Assembled Systems. Springer, **2013**.

[Lau13b] M. Laupheimer, K. Jovic, F. E. Antunes, M. da Graça Martins Miguel, C. Stubenrauch, *Soft Matter* **2013**, *9*, 3661-3670.

[Lau14] M. Laupheimer, T. Sottmann, R. Schweins, C. Stubenrauch, *Soft Matter* **2014**, *10*, 8744-8757.

[Lau15] M. Laupheimer, N. Preisig, C. Stubenrauch, *COLSUA* **2015**, *469*, 315-325.

[Li12] S. Li, T. Xiao, C. Lin, L. wang, *Chem. Soc. Rev.* **2012**, *42*, 6860-6909.

[Mar88] J. E. Martin, J. P. Wilcoxon, *Phys. Rev. Lett.* **1988**, *61*, 373-376.

[Mei07] A. Meister, M. Bastrop, M. Koschorek, V. M. Garamus, T. Sinemus, G. Hempel, S. Drescher, B. Dobner, W. Richtering, K. Huber, A. Blume, *Langmuir* **2007**, *23*, 7715-7723.

[Men75] F. M. Menger, K. S. Venkatasubban, *J. Org. Chem.* **1978**, *43*, 3413-3414.

[Men95] F. M. Menger, Y. Yamasaki, K. K. Catlin, T. Nishimi, *Angew. Chem. Int. Ed. Engl.* **1995**, *34*, 585-586.

[Men00] F. M. Menger, K. L. Caran, *J. Am. Chem. Soc.* **2000**, *122*, 11679-11691.

[Més16] E. Christ, C. Blanc, A. Al Ouahabi, D. Maurin, R. Le Parc, J.-L. Bantignies, J.-M. Guenet, D. Collin, P. J. Mésini, *Langmuir* **2016**, *32*, 4975-4982.

[Mez05] R. Mezzenga, C. Meyer, C. Servais, A. I. Romoscanu, L. Sagalowicz, R. C. Hayward, *Langmuir* **2005**, *21*, 3322-3333.

[Mez16] T. G. Mezger, *Das Rheologie-Handbuch. (Fifth Edition)* Vincentz, Hannover, 2016.

[Mit17] K. Mito, Md. A. Haque, T. Nakajima, M. Uchiumi, T. Kurokawa, T. Nonoyama, J. P. Gong, *Polymer* **2017**, *128*, 373-378.

[Miz99] N. Mizoshita, T. Kutsuna, K. Hanabusa, T. Kato, *Chem. Commun.* **1999**, 781-782.

[Miz03] K. Mizoshita, K. Hanabusa, T. Kato, *Adv. Funct. Mater.* **2003**, *13*, 313-317.

[Moh04] N. Mohmeyer, P. Wang, H.-W. Schmidt, S. M. Zakeeruddin, M. Grätzel *J. Mater. Chem.*, **2004**, *14*, 1905-1909.

[Mül99] C. C. Müller-Goymann, Anwendung lyotroper Flüssigkristalle in Pharmazie und Medizin. In *Lyotrope Flüssigkristalle*, Steinkopff, Darmstadt, 1999, 141-167.

[Ném98] Zs. Németh, L. Halász, J. Pálinkás, A. Bóta, T. Horányi, *Colloids Surf. A* **1998**, *145*, 107-119.

[Nij97] K. Nijenhuis, *Adv. Poly. Sci.* **1997**, *130*.

[Nis09] K. Nishinari, *Progr. Colloid Polym. Sci.* **2009**, *136*, 87-94.

[Oke15] B. O. Okesola, V. M. P. Vieira, D. J. Cornwell, N. K. Whitelaw, D. K. Smith, *Soft Matter* **2015**, *11*, 4768-4787.

[Pak48] G. E. Pake, *J. Chem. Phys.* **1948**, *16*, 327-336.

[Pus87] P. N. Pusey, W. Van Megen, *Physica A.* **1989**, *157*, 705-741.

[Raf19] S. Rafieian, H. Mirzadeh, H. Mahdavi, M. E. Masoumi, *Sci. Eng. Compos. Mater.* **2019**, 154-174.

[Rao07] M. A. Rao, *Rheology of Fluid and Semisolid Foods: Principles and Applications – Second Edition*, (Ed.: Gustavo V. Brabosa-Cánovas), Springer, New York, 2007.

[Roe79] E. L. Roehl, H. B. Tan, *US Pat.*, 4154816, 1979.

[Roe82] E. L. Roehl, *US Pat.*, 4346079, 1982.

[Sah13] M. L. Saha, S. De, S. Pramanik, M. Schmittel, *Chem. Soc. Rev.* **2013**, *42*, 6860-6909.

[San11] P. S. Santos, M. G. Abiad, M. A. Carignano, O. H. Campanella, *Rheol. Acta* **2012**, *51*, 3-11.

[Sed98] J. M. Seddon, Structural Studies of Liquid Crystals by X-ray Diffraction. In *Handbook of Liquid Crystals Vol. 1 Fundamentals*, Wiley-VHC, Weinheim, 1998, 635-679.

[See77] J. Seelig, *Q. Rev. Biophys.* **1977**, *10*, 353-418.

[Sel02] K. Selber, S. Müller, H. Gieren, J. Thömmes, T. Sottmann, R. Strey, M.-R. Kula, *Bioseparation* **2002**, *10*, 243-253.

[Shi00] M. Shibayama, M. Tsujimoto, F. Ikkai, *Macromolecules* **2000**, *33*, 7868-7876.

[Ste99] (a) K. Hiltrop, Grundlagen und Historie. In *Lyotrope Flüssigkristalle* (Ed.: H. Stegemeyer), First Edition, Steinkopff, Darmstadt, 1999, 1-24. (b) K. Hiltrop, Lyotrope Flüssigkristallphasen mizellarer Tensidlösungen. In *Lyotrope Flüssigkristalle* (Ed.: H. Stegemeyer), First Edition, Steinkopff, Darmstadt, 1999, 25-57.

[Ste18] K. Steck, C. Schmidt, C. Stubenrauch, *Gels* **2018**, *4*, 78.

[Ste19a] K. Steck, J. H. van Esch, D. K. Smith, C. Stubenrauch, *Soft Matter* **2019**, *15*, 3111-3121.

[Ste19b] K. Steck, C. Stubenrauch, *Langmuir* **2019**, *35*, 17132-17141.

[Ste19c] K. Steck, N. Preisig, C. Stubenrauch, *Langmuir* **2019**, *35*, 17141-17149.

[Sto76] G. W. Stockton, C. F. Polnaszek, A. P. Tulloch, F. Hasan, I. C. P. Smith, *Biochemistry* **1976**, *15* (5), 954-966.

[Stu02] C. Stubenrauch, C. Frank, R. Strey, D. Burgmeister, C. Schmidt, *Langmuir* **2002**, *18*, 5027-5030.

[Stu04] C. Stubenrauch, S. Burauer, R. Strey, *Liquid Crystals* **2004**, *31*, 39-53.

[Stu16] C. Stubenrauch, F. Gießelmann, *Angew. Chem. Int. Ed.* **2016**, *55*, 3268-3275.

[Tac91] T. Tachibana, T. Mori, K. Hori, *Bull. Chem. Soc. Jpn.* **1981**, *54*, 73-80.

[Ter91] P. Terech, *Colloid. Polym. Sci.* **1991**, *269*, 490-500.

[Ter94] P. Terech, V. Rodriguez, J. D. Barnes, G. B. McKenna, *Langmuir* **1994**, *10*, 3406-3418.

[Ter97] P. Terech, R. G. Weiss, *Chem. Rev.* **1997**, *97*, 3113-3159.

[Ter00] P. Terech, C. Rossat, F. Volino, *J. Colloid Interface Sci.* **2000**, *227*, 363-370.

[Tid80] G. J. T Tiddy, *Phys. Rep.* **1980**, *57*, 1-46.

[Tom11] I. Tomatsu, K. Peng, A. Kros, *Adv. Drug Deliv. Rev.* **2011**, *63*, 1257-1266.

[Var06] D. Varade, H. Kunieda, R. Strey, C. Stubenrauch, *J. Colloid Interface Sci.* **2006**, *300*, 338-347.

[Vie17] V. M. P. Viera, L. L. Hay, D. K. Smith, *Chem. Sci.* **2017**, *8*, 6981-6990.

[Vie18] V. M. P. Vieira, A. C. Lima, M. de Jong and D. K. Smith, *Chem. – Eur. J.* **2018**, *24*, 15112-15119.

[War96] H. E. Warriner, S. H. J. Idziak, N. L. Slack, P. Davidson, C. R. Safinya, *Science* **1996**, *271* (5251), 969-973.

[Wat98] M. Watase, H. Itagaki, *Bull. Chem. Soc. Jpn.* **1998**, *71*, 1457-1466.

[Wat99] M. Watase, Y. Nakatani, H. Itagaki, *J. Phys. Chem. B* **1999**, *103*, 2366-2373.

[Wei05] E. Carretti, L. Dei, R. G. Weiss, *Soft Matter* **2005**, *1*, 17-22.

[Wei06] (a) R. G. Weiss, P. Terech. In *Molecular Gels, Materials with Self-Assembled Fibrillar Networks* (Eds.: R. G. Weiss, P. Terech), Springer, Dordrecht, 2006, 1-13. (b) M. George, R. G. Weiss. In *Molecular Gels, Materials with Self-*

Assembled Fibrillar Networks (Eds.: R. G. Weiss, P. Terech), Springer, Dordrecht, 2006, 449-551.

[Wil03a] E. A. Wilder, C. K. Hall, S. A. Khan, R. J. Spontak, *Langmuir* **2003**, *19*, 6004-6013.

[www01] https://wiki.anton-paar.com/de-de/grundlagen-der-rheologie/ (18.12.2019)

[www02] (a) https://wiki.anton-paar.com/de-de/das-prinzip-der-dynamischen-lichtstreuung/ (18.12.2019) (b) https://lsinstruments.ch/en/technology/dynamic-light-scattering-dls/dynamic-light-scattering-theory (18.12.2019)

[www03] https://warwick.ac.uk/fac/sci/physics/current/postgraduate/regs/mpagswarwick/ex5/techniques/structural/tem (18.12.2019)

[Xu15] Y. Xu, M. Laupheimer, N. Preisig, T. Sottmann, C. Schmidt, C. Stubenrauch, *Langmuir* **2015**, *31*, 8589-8598.

[Yam94a] S. Yamasaki, H. Tsutsumi, *Bull. Chem. Soc. Jpn.* **1994**, *67*, 906-911.

[Yam94b] S. Yamasaki, H. Tsutsumi, *Bull. Chem. Soc. Jpn.* **1994**, *67*, 2053-2056.

[Yam95a] S. Yamasaki, H. Tsutsumi, *Bull. Chem. Soc. Jpn.* **1995**, *68*, 123-127.

[Yam95b] S. Yamasaki, H. Tsutsumi, *Bull. Chem. Soc. Jpn.* **1995**, *68*, 146-151.

[Yam96] S. Yamasaki, H. Tsutsumi *Bull. Chem. Soc. Jpn.* **1996**, *69*, 561-564.

Paper I

gels

MDPI

Article

The Twofold Role of 12-Hydroxyoctadecanoic Acid (12-HOA) in a Ternary Water—Surfactant—12-HOA System: Gelator and Co-Surfactant

Katja Steck [1], Claudia Schmidt [2] and Cosima Stubenrauch [1,*]

[1] Institute of Physical Chemistry, University of Stuttgart, Pfaffenwaldring 55, 70569 Stuttgart, Germany; katja.steck@ipc.uni-stuttgart.de

[2] Department of Chemistry, University of Paderborn, Warburger Straße 100, 33098 Paderborn, Germany; claudia.schmidt@uni-paderborn.de

* Correspondence: cosima.stubenrauch@ipc.uni-stuttgart.de; Tel.: +49-711-685-64470

Received: 19 July 2018; Accepted: 10 September 2018; Published: 12 September 2018

Abstract: Gelled lyotropic liquid crystals can be formed by adding a gelator to a mixture of surfactant and solvent. If the gel network and the liquid-crystalline phase coexist without influencing each other, the self-assembly is called orthogonal. In this study, the influence of the organogelator 12-hydroxyoctadecanoic acid (12-HOA) on the lamellar and hexagonal liquid crystalline phases of the binary system H_2O–$C_{12}E_7$ (heptaethylene glycol monododecyl ether) is investigated. More precisely, we added 12-HOA at mass fractions from 0.015 to 0.05 and studied the resulting phase diagram of the system H_2O–$C_{12}E_7$ by visual observation of birefringence and by ^2H NMR spectroscopy. In addition, the dynamic shear moduli of the samples were measured in order to examine their gel character. The results show that 12-HOA is partly acting as co-surfactant, manifested by the destabilization of the hexagonal phase and the stabilization of the lamellar phase. The higher the total surfactant concentration, the more 12-HOA is incorporated in the surfactant layer. Accordingly, its gelation capacity is substantially reduced in the surfactant solution compared to the system 12-HOA–*n*-decane, and large amounts of gelator are required for gels to form, especially in the lamellar phase.

Keywords: gelled complex fluids; gelator; lyotropic liquid crystals; phase diagram

1. Introduction

Gelled complex fluids [1], in which the mechanical stability of a gel is combined with the microstructure of a complex fluid, are interesting candidates for (trans-)dermal drug delivery systems and tissue healing applications [1,2]. Additional applications of this class of materials can be found in a recent review by Stubenrauch and Gießelmann [1]. Gelled complex fluids can be obtained by either adding a gelator to a complex fluid or by replacing the solvent of a gel by a complex fluid. A special class of gelled complex fluids are gelled lyotropic liquid crystals (gelled LCs), such as gelled lamellar phases L_α (gelled L_α). Examples of gelled L_α phases, known in literature are the cell [3], lamellar biogels [4], and gelled lamellar phases of synthetic surfactants. Only two systems of the latter type have been studied to date: The gelled lamellar phase of the system H_2O–*n*-decane/12-hydroxyoctadecanoic acid (12-HOA)—tetraethylene glycol monodecyl ether ($C_{10}E_4$) [5] and the gelled lamellar phase L_α of the system H_2O–$2C_{12}$DAB–12-HOA [6]. The cell surely is the most prominent example. Proteins form filaments, which provide mechanical stability of the cell and coexist independently with the lipid bilayer of phospholipids, i.e., the building block of the cell membrane [3]. Warriner et al. introduced lamellar biological hydrogels that consist of the lipid dimyristoyl phosphatidyl choline (DMPC), the co-surfactant pentanol and tiny amounts of poly (ethylene glycol)-derived polymer lipids

(PEG-lipids) [4]. The domains of the lamellar membranes built by DMPC and pentanol are randomly orientated and provide the gel properties, while the PEG-lipids are attached to these membranes, but can diffuse freely within the lamellar bilayers, which are separated by water. These PEG-lipids stabilize defects occurring in high curvature regions and lead to highly flexible membranes with large distances from each other caused by long-range repulsive forces of the PEG-lipids. Xu et al. studied the gelled lamellar phase L_α of the system H_2O–*n*-decane/12-HOA–$C_{10}E_4$ with a focus on the question whether the formation of the gel network and of the lamellar phase formation is simultaneous, but independent [5]. Koitani et al. tried to answer the same question by studying the lamellar phase L_α of the system H_2O–$2C_{12}$DAB–12-HOA [6].

Introduced by Laibinis et al. for alkanethiols and alkane carboxylic acids on gold and alumina, respectively, the simultaneous (but independent) formation of two coexisting structures is called orthogonal self-assembly [7]. However, the term orthogonal self-assembly is not restricted to surface chemistry. Orthogonal self-assembled structures have been studied in bulk systems as well [8–12]. The cell, once again, is the most prominent example of an orthogonal self-assembled system, since proteins self-assemble to fibers forming the cytoskeleton, while phospholipids self-assemble to membranes [3]. The expression orthogonal self-assembly was first used for gelled complex fluids by the group of van Esch [13]. They reported on surfactant micelles, worm-like micelles, liposomes and phospholipids entrapped in self-assembled fibrillary networks of low molecular weight gelators (LMWG) [13–17]. Laupheimer studied the system H_2O–*n*-decane/12-HOA–$C_{10}E_4$ and proved that the gelled bicontinuous microemulsion is an orthogonal self-assembled system in which the formation of the nanostructured microemulsion is nearly independent on the formation of the gel network [18–20]. In the special case of the gelled L_α phase of the very same system, the question whether it is a truly orthogonal self-assembled system could not be answered satisfactorily. On the one hand, phase behaviour and rheological studies supported the idea of an orthogonal self-assembled gelled lamellar L_α phase. On the other hand, freeze fracture electron microscopy revealed that the gel network and the lamellar L_α phase influence each other: The presence of the gel network leads to a higher order of the L_α phase while the presence of the L_α phase results in gel fibers which are not twisted anymore [5]. Moreover, Laupheimer et al. showed in a previous SANS study of the system H_2O–*n*-decane/12-HOA–$C_{10}E_4$ that 12-HOA is only partly involved in the gel formation, since it also acts as co-surfactant, which results in a shift of the phase boundaries to lower temperatures [20]. Koitani et al. studied the gelled lamellar phase L_α of the system H_2O–didodecyldimethylammonium bromide ($2C_{12}$DAB)–12-HOA at surfactant mass fractions $\gamma_a = 0.10$ and $\gamma_a = 0.20$ in order to answer the question of orthogonal self-assembly [6]. However, they also found that 12-HOA seems to have two roles in surfactant-containing systems, namely as gelator and as co-surfactant. The slightly surface active 12-HOA molecules are partly incorporated in the surfactant bilayers of the system H_2O–$2C_{12}$DAB–12-HOA and are thus not available for the gel formation which leads to a weaker gel compared to the binary gel *n*-decane–12-HOA. Additionally, the incorporation of 12-HOA in the bilayers caused a slightly larger interlayer spacing compared to the non-gelled L_α phase. In order to elucidate the role of 12-HOA in surfactant-containing systems and its ability of gelling lyotropic liquid crystals of different phase structures, we chose the binary system H_2O–heptaethylene glycol monododecyl ether ($C_{12}E_7$) instead of the ternary system H_2O–*n*-decane–$C_{10}E_4$ or the system H_2O–$2C_{12}$DAB, for the following reasons. Firstly, studying the system H_2O–$C_{12}E_7$ ensures easy handling and a broader access to gelled lyotropic liquid crystals as it forms three lyotropic liquid crystalline phases, namely the hexagonal phase H_1, the bicontinuous cubic phase V_1 and the lamellar phase L_α in specific surfactant concentration ranges and with melting points at moderate temperatures ($T \approx 50$ °C) [21]. Secondly, it allows us to prove the concept of gelling lyotropic liquid crystals of binary water–surfactant systems with the organogelator 12-HOA at much higher surfactant concentrations as compared to the binary system H_2O–$2C_{12}$DAB. We first investigated the influence of the 12-HOA concentration on the phase boundaries of the system H_2O–$C_{12}E_7$ by means of visual observation in water basins and determined qualitatively whether a gelled lyotropic liquid crystalline phase was

formed. ^{2}H NMR spectroscopy complemented the visual phase studies, since it is a well-known and powerful tool to detect phase transitions of lyotropic liquid crystalline phases to an isotropic phase and the coexistence of two phases, respectively [22–30]. In addition, we investigated the rheological properties of the lyotropic liquid crystalline phases in the presence of 12-HOA in order to identify gelled lyotropic liquid crystalline phases.

2. Results and Discussion

2.1. Visual Phase Studies

The visual phase studies allowed us to determine the occurrence of lyotropic liquid crystals via optical birefringence. In addition, they helped identifying transition temperatures, namely the melting points of the lyotropic liquid crystals and the sol-gel transition of the gel network. Therefore, we were able to measure the influence of 12-HOA on the phase boundaries of the lyotropic liquid crystalline phases of the system H_2O–$C_{12}E_7$. As already mentioned, the system H_2O–$C_{12}E_7$ forms three liquid crystalline phases as a function of the surfactant concentration, namely the hexagonal phase H_1, the bicontinuous cubic phase V_1 and the lamellar phase L_α. The visually determined T-γ_a phase diagram of the binary system H_2O–$C_{12}E_7$, as well as those of the systems in the presence of 12-HOA, i.e., H_2O–$C_{12}E_7$–12-HOA with 12-HOA mass fractions η = 0.015, 0.025, 0.05, are shown in Figure 1.

The black circles refer to the binary system H_2O–$C_{12}E_7$ and we note that the phase boundaries are in good agreement with literature data [21]. The highly viscous and transparent hexagonal H_1 phase occurs at a surfactant concentration range of $\gamma_a \approx 0.40$–0.68 and melts at temperatures $T \approx 50$ °C. At higher surfactant concentrations, in a range of $\gamma_a \approx 0.72$–0.85, the lamellar L_α phase is formed. The L_α phase melts at about the same temperatures as the hexagonal H_1 phase, but is less viscous and appears slightly turbid. The highly viscous, transparent bicontinuous cubic phase V_1 occurs between the hexagonal phase H_1 and the lamellar phase L_α in a surfactant concentration range $\gamma_\alpha \approx 0.68$–$0.72$ and melts at temperatures $T \approx 46$ °C. In contrast to the anisotropic H_1 and L_α phases, the bicontinuous cubic phase V_1 is characterized by optical isotropy. The V_1 phase will not be discussed further as it is difficult to identify, especially in the presence of 12-HOA. The upper miscibility gap (2φ), which is typical for oligo (ethylene oxide) alkyl ethers, was detected at higher temperatures for surfactant concentrations up to $\gamma_a = 0.50$.

The open circles in Figure 1 represent the phase boundaries of the system H_2O–$C_{12}E_7$ at three different 12-HOA concentrations. Comparing the binary system with the systems in the presence of 12-HOA, it is obvious that 12-HOA has an enormous influence on the phase boundaries of the liquid crystalline phases. For a 12-HOA mass fraction of η = 0.015, the melting point of the lamellar phase L_α is increased by $\Delta T \approx 5$ K, whereas at the same time the melting point of the hexagonal phase H_1 is decreased by the same value. The upper miscibility gap is also shifted towards lower temperatures in the presence of 12-HOA. The influence of 12-HOA on the upper miscibility gap at surfactant concentrations $\gamma_a < 0.3$ could not be determined via visual observations, because 12-HOA precipitated at these surfactant concentrations. After addition of 12-HOA (η = 0.015) the appearance and viscosity of the lamellar phase L_α did not change. It maintained its slight turbidity and also its flow ability, i.e., no gelled lamellar L_α phase was formed. On the contrary, the initially transparent hexagonal phase H_1 became turbid after addition of 12-HOA (η = 0.015), but whether a gel was formed, could not be detected by visual observation, because the viscosity of the hexagonal phase H_1 is high a priori. Moreover, the turbidity of the hexagonal phase complicated the visual observation, especially at low temperatures. For a 12-HOA concentration of η = 0.025 we observed the same trend, i.e., a stabilized lamellar L_α phase and a destabilized hexagonal H_1 phase, but a bit more pronounced as for η = 0.015. Again, even after increasing the 12-HOA concentration to η = 0.025, the appearance of the lamellar phase L_α did not change, i.e., still no gelled lamellar phase L_α was formed. In the case of the hexagonal phase H_1, the effect of 12-HOA is also slightly more pronounced for η = 0.025 than for

η = 0.015. The hexagonal H_1 phase is marginally less temperature stable for η = 0.025, but again its appearance changes from transparent to turbid. For the highest 12-HOA concentration, i.e., η = 0.05, the lamellar phase L_α is extended to higher temperatures and lower surfactant concentrations γ_a, i.e., it additionally occurs in the range of γ_a = 0.40–0.60 at temperatures T = 50–70 °C. Unlike for η = 0.015 and 0.025, gelled L_α phases were obtained for η = 0.05 in a surfactant concentration range of γ_a = 0.72–0.85. In addition, gelled isotropic solutions were formed at lower concentrations of γ_a = 0.40–0.60, since the hexagonal H_1 phase did not form anymore in the presence of 12-HOA at η = 0.05. In Figure 1, bottom, the approximate sol-gel transition temperature line is added to the phase diagram of the system H_2O–$C_{12}E_7$–12-HOA (η = 0.05) and it can be seen that the sol-gel transition temperatures decrease with increasing surfactant concentration γ_a.

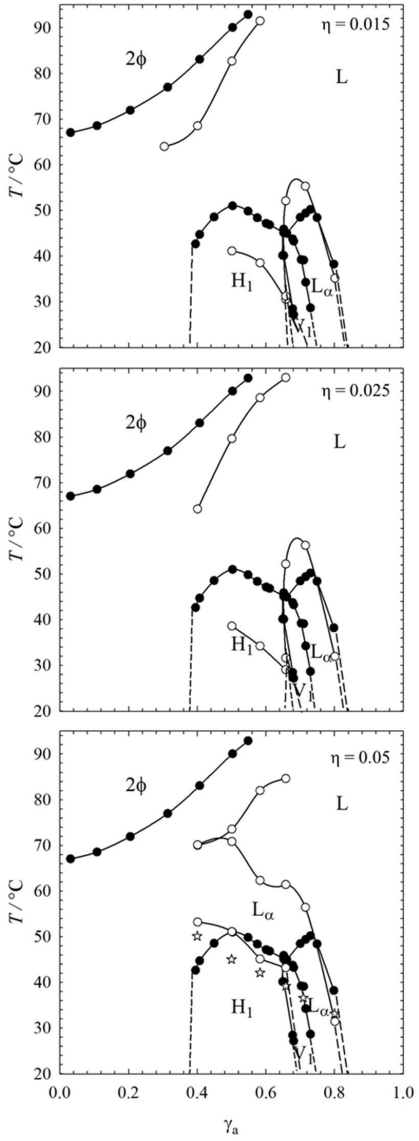

Figure 1. T–γ_a phase diagrams of the binary system H_2O–$C_{12}E_7$ (black circles) and of the systems H_2O–$C_{12}E_7$–12-HOA (open circles) with 12-hydroxyoctadecanoic acid (12-HOA) mass fractions η = 0.015, 0.025, and 0.05 (from top to bottom). The phase transition temperatures were determined by visual observations in water basins. The stars in the phase diagram of the system H_2O–$C_{12}E_7$–12-HOA with η = 0.05 indicate the approximate sol-gel transition temperatures. Gelation could not be observed for H_2O–$C_{12}E_7$–12-HOA with 12-HOA mass fractions of η = 0.015 and η = 0.025. The error is within the size of the symbols.

Based on these results it is clear that 12-HOA has two roles in the system H_2O–$C_{12}E_7$–12-HOA. On the one hand, it acts as co-surfactant, which results in the stabilization of the lamellar phase L_α and at the same time in the destabilization of the hexagonal phase H_1. This effect can be explained by Israelachvili's packing parameter, which is the ratio of hydrophobic area to the effective hydrophilic head group area [31]. By adding 12-HOA to the system H_2O–$C_{12}E_7$, a C_{18} chain is introduced which increases the volume of the hydrophobic chains. As a consequence, the packing parameter is increased, and the surfactant layer has a lower curvature. This stabilizes the lamellar phase L_α, and simultaneously destabilizes the hexagonal phase H_1 [31–33]. On the other hand, it seems that at sufficient high gelator concentrations, i.e., for $\eta > 0.025$–0.05, the bilayers of the lamellar phase are saturated by 12-HOA and 12-HOA starts to act as gelator. The sol-gel transition temperature of the system H_2O–$C_{12}E_7$–12-HOA ($\eta = 0.05$) decreases with increasing surfactant concentration γ_a which can be explained by an increasing surfactant layer at higher surfactant concentrations γ_a. The higher the surfactant concentrations γ_a, the more likely 12-HOA is incorporated in the surfactant layer instead of forming the gelator network, which leads to weaker gels with lower sol-gel transition temperatures $T_{\text{sol-gel}}$. The system H_2O–$C_{12}E_7$ thus is a better solvent for 12-HOA at high surfactant concentrations γ_a than at low ones. This concentration dependence is already evident at the lowest 12-HOA concentration $\eta = 0.015$. While the appearance of the lamellar L_α phase at high surfactant mass fractions does not change in the presence of 12-HOA at $\eta = 0.015$, the otherwise clear hexagonal H_1 phase becomes turbid, which may indicate the start of a gel formation. Therefore, we focused our study on the system H_2O–$C_{12}E_7$–12-HOA at $\eta = 0.015$, in order to answer the question whether 12-HOA acts as both gelator and co-surfactant already at the lowest 12-HOA mass fraction.

2.2. ^2H NMR

We performed ^{2}H NMR measurements in order to complement the visual phase studies of the system H_2O–$C_{12}E_7$–12-HOA at $\eta = 0.015$ as the determination of the phase boundary of the hexagonal phase H_1 at surfactant concentrations $\gamma_a \approx 0.40$ is difficult by means of visual observation, in particular, in the presence of 12-HOA which makes the sample turbid. For this purpose, H_2O needed to be replaced by D_2O, which, in turn, requires a phase study of D_2O–$C_{12}E_7$. The phase diagram of D_2O–$C_{12}E_7$ is available in the Appendix A (Figure A1). It was found that the lyotropic liquid crystalline phases were shifted to slightly smaller surfactant mass fractions γ_a. Moreover, the phase boundary of the hexagonal phase H_1 was shifted by $\Delta T = 1$–2 °C to lower values, whereas the phase boundary of the lamellar phase L_α was shifted to higher temperatures by $\Delta T = 2$–3 °C. The miscibility gap at low surfactant concentrations and at high temperatures was shifted to lower temperatures by $\Delta T = 2$–3 °C, i.e., it seems that the surfactant is more hydrophobic in the presence of D_2O [29]. The temperature shifts caused by replacing H_2O by D_2O are the same for the systems without and with 12-HOA. We performed temperature dependent ^{2}H NMR measurements at $\gamma_a = 0.37$ and 0.38 for the system D_2O–$C_{12}E_7$ and at $\gamma_a = 0.36$ and 0.38 for the system D_2O–$C_{12}E_7$–12-HOA ($\eta = 0.015$). In the following, we will discuss the ^{2}H NMR spectra of the systems D_2O–$C_{12}E_7$ and D_2O–$C_{12}E_7$–12-HOA ($\eta = 0.015$) at $\gamma_a = 0.38$. The spectra of the systems D_2O–$C_{12}E_7$ at $\gamma_a = 0.37$ and D_2O–$C_{12}E_7$–12-HOA ($\eta = 0.015$) at $\gamma_a = 0.36$ are shown in the Appendix A (Figure A2).

In the anisotropic hexagonal phase H_1, the quadrupolar ^{2}H nucleus with a spin quantum number $I = 1$ shows a splitting which depends on the local orientation order of the D_2O molecules, as well as on the orientation of the director of the hexagonal phase with respect to the magnetic field. The D_2O molecules are on average slightly aligned, since they interact with the aligned surfactant molecules resulting in a non-zero residual quadrupole coupling. Hexagonal phases H_1 are not macroscopically aligned by the magnetic field, because of their high viscosity, i.e., domains with all possible orientations of the hexagonal axis are present in the sample. The superposition of the spectral contributions from all domains leads to a characteristic line shape, called the Pake powder pattern [34]. On the contrary, isotropic phases are indicated by a single peak, since the temporal average over the random orientations

of the molecules, which have no preferred orientation with respect to the magnetic field eliminates the quadrupole coupling.

In Figure 2a, the ^{2}H NMR spectra of the system D_2O–$C_{12}E_7$ at γ_a = 0.38 as a function of temperature are shown. The bottom two spectra show the Pake powder pattern with two inner peaks and two outer shoulders, corresponding to domains with the hexagonal axis perpendicular and parallel to the magnetic field, respectively. The shape of the Pake pattern represents the isotropic distribution of domains in a macroscopically unaligned sample. As we studied the system D_2O–$C_{12}E_7$ by means of visual observation, and since the general phase behavior is known in literature, the splitting can be assigned to the hexagonal phase H_1. The spectrum at T = 33 °C shows an additional peak that can be assigned to an isotropic phase that coexists with the hexagonal phase. The two phase region can be detected up to T = 40 °C, though the peaks that indicate the hexagonal phase are at minimum intensity. At T = 41 °C the single peak corresponds to an isotropic phase, therefore this temperature is set as phase transition temperature from the hexagonal phase H_1 to the isotropic phase. The ^{2}H NMR spectra of the system D_2O–$C_{12}E_7$ at γ_a = 0.37 shown in the Appendix A indicate that the system consists of an isotropic and a hexagonal phase H_1 from room temperature up to T = 42 °C.

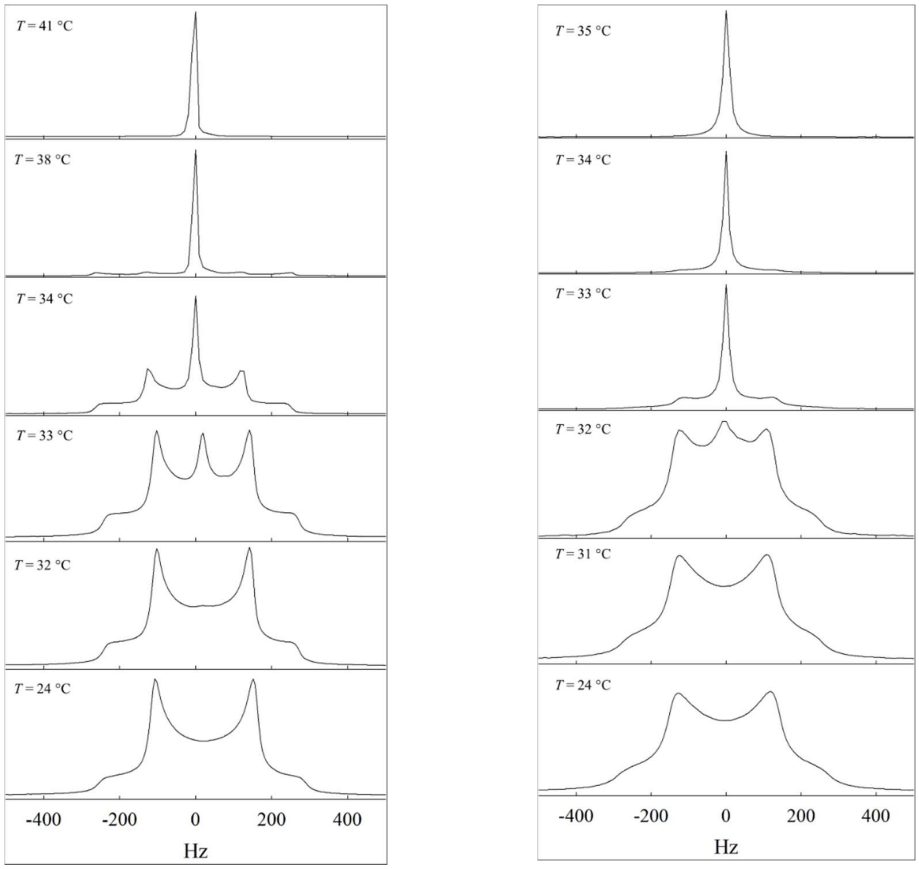

(**a**) (**b**)

Figure 2. (**a**) Temperature dependent ^{2}H NMR spectra of the system D_2O–$C_{12}E_7$, recorded at γ_a = 0.38. (**b**) Temperature dependent ^{2}H NMR spectra of the system D_2O–$C_{12}E_7$–12-HOA, recorded at γ_a = 0.38 and η = 0.015.

The respective temperature dependent ^{2}H NMR spectra of the system D_2O–$C_{12}E_7$–12-HOA (η = 0.015) at γ_a = 0.38 are shown in Figure 2b. As opposed to the spectra of the system D_2O–$C_{12}E_7$, the line shape is less sharp in the presence of 12-HOA, though the general phase behavior is maintained in presence of 12-HOA, but shifted to lower temperatures by ΔT = 8 °C, which is in accordance with the visual phase studies. At T = 25 °C up to T = 31 °C again the Pake pattern can be observed and

can also be assigned to the hexagonal phase H_1. At $T > 32$ °C an additional peak occurs, which can be assigned to the isotropic phase. At $T = 34$ °C, the Pake spectrum is still visible, indicating that the system is still in the two phase region. The phase transition temperature from the hexagonal phase H_1 to the isotropic phase was set to $T = 35$ °C—since a single peak, indicative of a pure isotropic phase, was recorded. In the Appendix A the spectra of the 12-HOA containing sample at $\gamma_a = 0.36$ are shown.

In Figure 3, the phase transitions determined by ^{2}H NMR are added to the phase diagram of the system H_2O–$C_{12}E_7$–12-HOA ($\eta = 0.015$) determined by visual observation in water basins (see Figure 1, top). We added $\Delta T = +1$ to the phase transitions determined by ^{2}H NMR before we added them to the phase diagram, since D_2O influences the phase boundaries in that way (see Figure A1). The results of visual observations and ^{2}H NMR are in good agreement and complement each other. We were able to detect the phase boundaries of the hexagonal phase H_1 at $\gamma_a < 0.40$ in the presence of 12-HOA, which was difficult by means of visual observations, due to turbidity caused by 12-HOA. Moreover, the ^{2}H NMR measurements enabled the detection of the two-phase region of isotropic and hexagonal phase at $\gamma_a = 0.38$–0.40. To summarize, ^{2}H NMR measurements confirm the phase behavior and the role of 12-HOA as co-surfactant determined by visual observations.

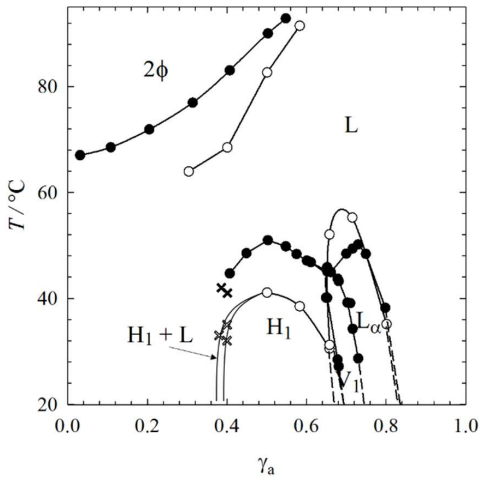

Figure 3. T–γ_a phase diagram of the binary system H_2O–$C_{12}E_7$ (black symbols) and of the system H_2O–$C_{12}E_7$–12-HOA (open symbols) at $\eta = 0.015$. The phase transition temperatures were determined by visual observation in water basins (circles) and by ^{2}H NMR (crosses). For the sake of clarity, the two-phase region is not drawn for the system H_2O–$C_{12}E_7$.

2.3. Rheometry

Looking at the phase diagrams and the NMR spectra one can conclude that 12-HOA acts as co-surfactant up to $\eta = 0.015$. Somewhere between a 12-HOA concentration of $\eta = 0.025$ and $\eta = 0.05$ its second role of a gelator becomes obvious. However, at the lowest 12-HOA concentration of $\eta = 0.015$, the hexagonal H_1 phase went turbid as discussed in Section 2.1, which could indicate the beginning of a gel formation. In other words, it can well be that 12-HOA acts already as both co-surfactant and gelator at $\eta = 0.015$. In order to determine whether or not the hexagonal phase H_1 was gelled at a 12-HOA concentration of $\eta = 0.015$, we performed frequency sweeps by oscillation shear rheometry and compared the results with the pure hexagonal phase H_1 at $\gamma_a = 0.50$ and with the binary gel *n*-decane–12-HOA at $\eta = 0.015$. For comparison, we also studied the lamellar L_α phase at $\gamma_a = 0.76$ under the same conditions. The results of the frequency sweeps are shown in Figure 4 for the lamellar phase L_α and in Figure 5 for the hexagonal phase H_1, respectively.

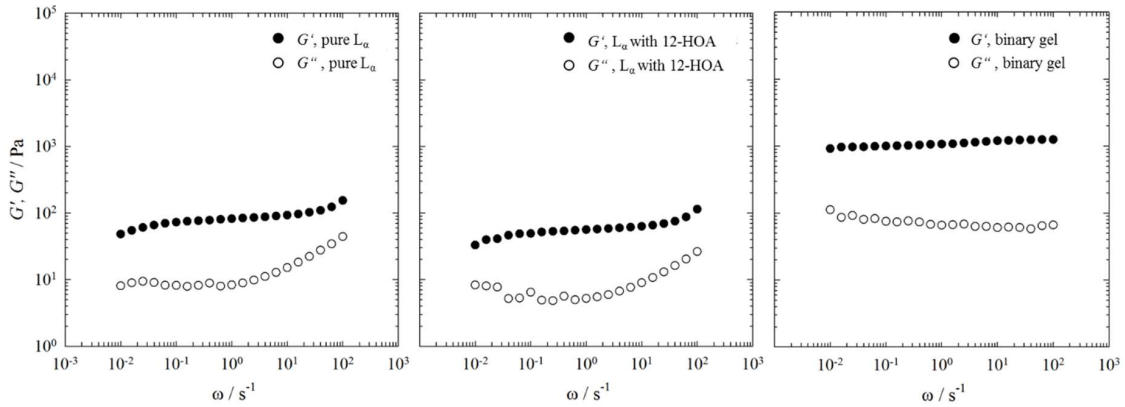

Figure 4. Storage modulus G' and loss modulus G'' (filled and open circles) of the pure lamellar phase L_α at $\gamma_a = 0.76$ (**left**), of the lamellar phase L_α at $\gamma_a = 0.76$ in presence of 12-HOA at $\eta = 0.015$ (**middle**), and of the binary gel n-decane–12-HOA at $\eta = 0.015$ (**right**) determined by frequency sweeps at T = 22 °C and a strain amplitude of $\gamma = 1\%$.

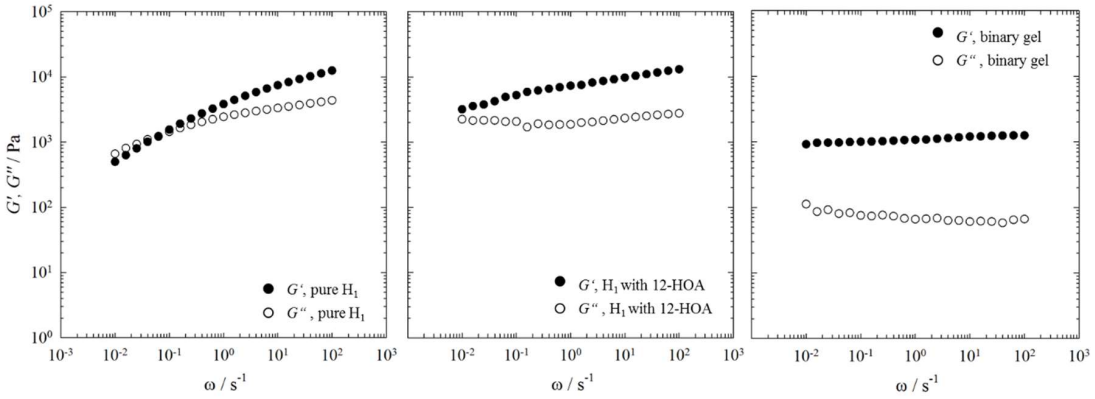

Figure 5. Storage modulus G' and loss modulus G'' (filled and open circles) of the pure hexagonal phase H_1 at $\gamma_a = 0.50$ (**left**), of the hexagonal phase H_1 at $\gamma_a = 0.50$ in presence of 12-HOA at $\eta = 0.015$ (**middle**), and of the binary gel n-decane–12-HOA at $\eta = 0.015$ (**right**) determined by frequency sweeps at $T = 22$ °C and a strain amplitude of $\gamma = 1\%$.

For all systems, except for the pure hexagonal phase H_1 (Figure 5, left) the storage modulus G' is higher than the loss modulus G'' over the whole frequency range investigated, i.e., the binary gel *n*-decane–12-HOA, the pure lamellar phase L_α, as well as both the lamellar phase L_α and the hexagonal phase H_1 in presence of 12-HOA at $\eta = 0.015$ show solid like behavior. In case of the pure hexagonal phase H_1 a crossover point between G' and G'' is observed at frequencies of $\omega \approx 0.1\ s^{-1}$, which indicates a change from solid like, elastic behavior ($G' > G''$) to liquid like, viscous behavior ($G' < G''$) [35]. Moreover, G' of the pure hexagonal phase H_1 changes with the frequency. Characteristic for gels and soft solids is the frequency independence of G' as can be seen in the frequency sweep of the binary gel *n*-decane–12-HOA [36–39]. The frequency sweeps of the pure lamellar phase L_α, as well as of the lamellar phase L_α and the hexagonal phase H_1 in presence of 12-HOA show a slight frequency dependence of G'. Comparing the absolute values of G' and G'', one sees that the pure hexagonal phase H_1 is much more viscous than the pure lamellar phase L_α. This results from the densely packed cylinders compared to the parallel orientated lamellar bilayers, which can easily slip against each other [40]. Moreover, the absolute G' and G'' values of the pure lamellar phase L_α are lower than those of the binary gel and do not change in the presence of 12-HOA. This shows that no gel was formed in case of the lamellar phase L_α. In the frequency sweep of the hexagonal phase H_1 in presence of 12-HOA no crossover between G' and G'' can be seen anymore, since the slope of G' is lower, i.e., the solid like behavior predominates in the whole frequency range and indicates that a gel

was indeed formed. However, as the storage modulus G' is still frequency dependent, a gel weaker (but stiffer) than the binary gel was formed. Note that the absolute values of G' and G'' cannot be used as measure for gel formation as they are a priori high for the pure hexagonal phase H_1. In conclusion, one can say that for the lowest 12-HOA mass fraction of $\eta = 0.015$, 12-HOA is only co-surfactant in case of the lamellar L_α phase, but acts as both co-surfactant and gelator in case of the hexagonal phase. Again, it becomes obvious that 12-HOA is more likely incorporated in the surfactant layer of the system H_2O–$C_{12}E_7$ at higher surfactant mass fractions than at low ones—since at higher surfactant mass fractions most of the 12-HOA molecules are dissolved in the surfactant layer, no gel can be formed.

3. Conclusions

Both visual observation and ^{2}H NMR clearly show that 12-HOA stabilizes the lamellar phase and destabilizes the hexagonal phase of the binary system H_2O–$C_{12}E_7$ (heptaethylene glycol monododecyl ether). The strong influence of 12-HOA on the phase behavior is clear evidence that the organogelator acts as a co-surfactant. With increasing mass fraction η of 12-HOA the effect is more pronounced (at the highest gelator mass fraction investigated, namely $\eta = 0.05$, the hexagonal phase is completely absent), but the gelation capacity is increased, too. At $\eta = 0.05$, a sol-gel transition can be observed by visual inspection. The sol-gel transition temperature decreases with increasing surfactant concentration, which proves a decreasing gelation capacity, due to an increasing incorporation of 12-HOA in the surfactant layer. Note that the total gelator mass fraction is kept constant, while the amount of surfactant thus the surfactant layer increases.

The ^{2}H NMR measurements show broadened features of the Pake powder pattern of the hexagonal phase, which indicates an increased viscosity, even at the lowest gelator mass fraction of $\eta = 0.015$. Dynamic rheometry proves that a weak gel is formed at this low gelator concentration in the case of the hexagonal phase (i.e., at low surfactant concentrations), whereas no gel is formed in the case of the lamellar phase (i.e., at high surfactant concentrations). This is in excellent agreement with the decreasing gelation capacity deduced from decrease of the sol-gel transition temperature as a function of surfactant concentration.

Our investigations clearly show that 12-HOA is not a suitable gelator for binary systems consisting of H_2O and an alkyl polyglycol ether (C_iE_j), since its gelation capacity is hampered by its competing role as co-surfactant. The search for a suitable gelator for H_2O–C_iE_j systems that solely acts as gelator is continued; tests of other organogelators, as well as hydrogelators, are in progress. Once a suitable gelator is found, we will investigate (a) if the lyotropic liquid crystalline phases serve as template for the gelator network leading to well aligned gelator fibers and (b) if the gel network influences the structure of the lyotropic liquid crystalline phases. For this purpose, the sol-gel transition line has to be adjusted via the gelator concentration, such that (a) the sol-gel transition temperature $T_{\text{sol-gel}}$ of the gelator is lower than the melting point of the lyotropic liquid crystalline phases, and (b) the sol-gel transition temperature $T_{\text{sol-gel}}$ of the gelator is higher than the melting point of the lyotropic liquid crystalline phases. First experimental evidence that the chronology—that is, whether gelation or liquid crystal phase formation occurs first—may indeed play a role is the work published by Kato et al. They studied gelled thermotropic liquid crystals (thermotropic LC), focusing on the influence of the chronology on the resulting structure [41].

4. Materials and Methods

4.1. Materials and Sample Preparation

We purchased heptaethylene glycol monododecyl ether ($C_{12}E_7$) from Sigma Aldrich ($\geq$98%) (St. Louis, MO, USA), Nikkol (Tokyo, Japan) and TCI (Tokyo, Japan), 12-hydroxyoctadecanoic acid (12-HOA) from Alfa Aesar (95%) (Karlsruhe, Germany), and D_2O from euriso-top (99.9 atom % D). Note that Alfa Aesar does not specify whether 12-HOA is a racemate or a pure enantiomer. We thus measured the optical rotation angle of 12-HOA in methanol and found out that the substance is the

(*R*)-enantiomer. In a previous study we proved that 12-HOA provided by Sigma Aldrich is also (*R*)-12-HOA. [42] All chemicals were used without further purification.

The composition of the systems is defined by the surfactant mass fraction,

$$\gamma_a = \frac{m_{C_{12}E_7}}{m_{C_{12}E_7} + m_{H_2O}}, \quad (1)$$

and the 12-HOA mass fraction,

$$\eta = \frac{m_{12\text{-HOA}}}{m_{C_{12}E_7} + m_{H_2O} + m_{12\text{-HOA}}}. \quad (2)$$

We used η = 0.015, 0.025, 0.05 as 12-HOA mass fractions. The samples were weighed in glass tubes, equipped with a stirring bar and sealed with plugs. The samples had to be heated in a water bath up to T = 85 °C as 12-HOA has to be molten and they were then stirred at this temperature for at least 5 min in order to ensure homogenous mixing. Subsequently, the samples were put into an ice bath for gelation for 5 min. Gelation was indicated by a change of turbidity in the case of the otherwise clear hexagonal phase and a change in viscosity in the case of the lamellar phase L_α. It is important to note that changes in turbidity and viscosity are no proofs of gelation per se. However, in the present case they can be used to identify gelation, since there are no other (phase) transitions, which could explain these changes. The samples measured by ^{2}H NMR were prepared with D_2O instead of H_2O, but the surfactant mass fraction, as well as the 12-HOA mass fraction were calculated in the same way.

4.2. Visual Phase Studies

The phase boundaries of the binary system H_2O–$C_{12}E_7$ and of the systems H_2O–$C_{12}E_7$–12-HOA with η = 0.015, 0.025, 0.05 were determined by visual observation in water basins equipped with a thermostat (Thermo Scientific DC30, Waltham, MA, USA). The phase boundaries of the anisotropic lyotropic LC phases to the transparent, isotropic phase were detected with the help of a lamp behind the water basin and two crossed polarizers, one behind and one in front of the sample. The lyotropic LC phases were distinguished due to anisotropy, viscosity and turbidity. The hexagonal phase H_1 is transparent and highly viscous, whereas the lamellar phase L_α is slightly turbid and less viscous. Accordingly, the turbid upper miscibility gap at higher temperature was identified. The approximate sol-gel transition temperature was determined by fading turbidity in the case of the hexagonal phase H_1 and by a change in viscosity in the case of the lamellar phase L_α.

4.3. 2H NMR

^{2}H NMR measurements were carried out with a Tecmag Apollo 300 MHz spectrometer (Erfurt, Germany) at a ^{2}H resonance frequency of 46.02 MHz with a pulse width of 6.4 µs and a relaxation delay time of 2 s. The samples were filled in 4 cm glass tubes with a diameter of 5 mm. The tubes, equipped with a Teflon spacer and sealed with a Teflon plug and parafilm, were put in a goniometer probe such that its axis was perpendicular to the magnetic field. By applying a quadrupole echo pulse sequence, temperature-dependent ^{2}H-NMR spectra of each sample were recorded. The sample temperature in the goniometer probe was set according to the temperature calibration of a reference probe, which was calibrated by a known phase transition of the system that was determined by visual observation before. The target temperatures were reached after a 30 min heating ramp followed by an additional 30 min equilibration time. 64 scans were averaged before Fourier transformation was applied.

4.4. Rheometry

The measurements were carried out with a Physica MCR 501 rheometer from Anton Paar (Ostfildern, Germany). A cone-plate geometry was used with an upper moving cone of 2.5 cm diameter and a cone angle of 1°. The samples were transferred to the plate with a spatula. After the

upper cone was lowered to the measuring position (gap width z = 1 mm), the samples were kept at T = 22 °C for 30 min to reach equilibrium. Then, frequency (ω) sweeps were performed with a constant strain amplitude γ = 1% and constant temperature T = 22 °C of the lower plate. The frequency $\omega = 0.01\ s^{-1}$ is the lower limit of our rheometer. The temperature was set with a precision of ±0.1 K by a Peltier element. The strain amplitude γ was set such that it was in the linear viscoelastic (LVE) region determined through prior oscillating stress sweeps. The storage modulus G' and the loss modulus G'' were determined in the frequency sweeps. The pure hexagonal H_1 phase at a surfactant mass fraction $\gamma_a = 0.50$ and the pure lamellar L_α phase at $\gamma_a = 0.76$ as well as both lyotropic liquid crystalline phases in the presence of 12-HOA with a gelator mass fraction $\eta = 0.015$ were measured. For comparison, the rheological behaviour of the binary gel *n*-decane–12-HOA at $\eta = 0.015$ was investigated.

Author Contributions: K.S. performed the experiments and wrote the first version of the article, C.Sch. and C.S. contributed to the discussion of the results and revised the first version of the article.

Funding: This research was funded by the Deutsche Forschungsgemeinschaft grant number STU287/6-1.

Acknowledgments: We thank Marco Grunwald for his help with the phase studies, Dmitry Kushnikovskiy for his help with the NMR measurements and Waldemar Keil for his help with the fine-tuning of the NMR spectra.

Conflicts of Interest: The authors declare no conflict of interest.

Appendix A

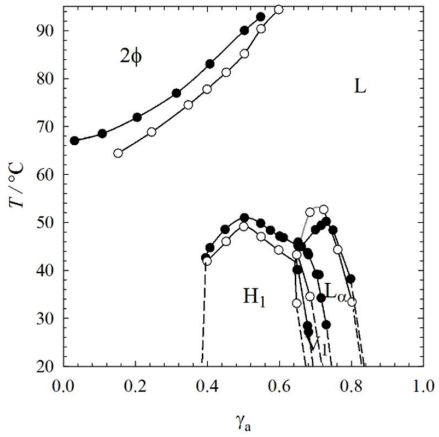

Figure A1. T–γ_a phase diagrams of the binary systems H_2O–$C_{12}E_7$ (black circles) and D_2O–$C_{12}E_7$ (open circles). The phase transition temperatures were determined by visual observation in water basins.

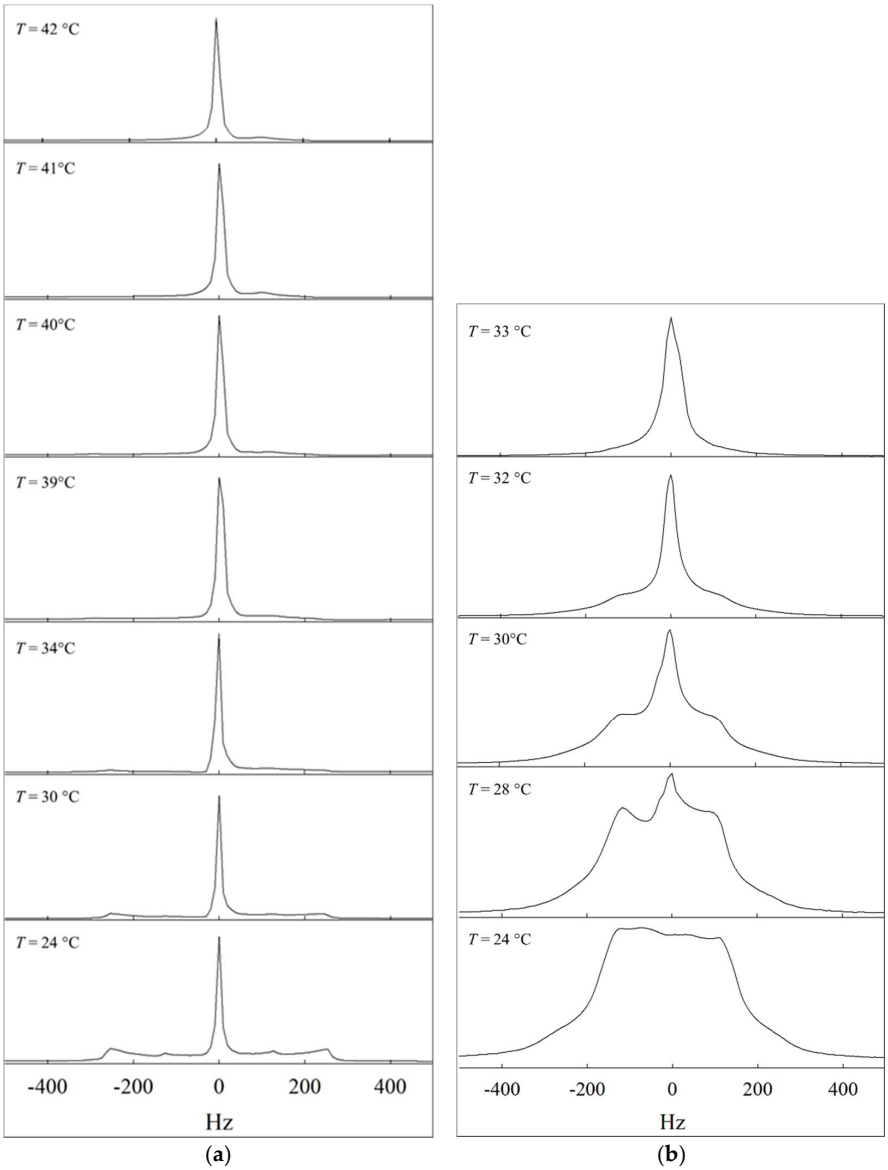

Figure A2. (**a**) Temperature dependent ^{2}H NMR spectra of the system D_2O–$C_{12}E_7$ recorded at $\gamma_a = 0.37$. (**b**) Temperature dependent ^{2}H NMR spectra of the system D_2O–$C_{12}E_7$–12-HOA recorded at $\gamma_a = 0.36$ and at $\eta = 0.015$. The asymmetry seen in the spectra may have several reasons. One is the local anisotropy, which causes an anisotropy of the magnetic susceptibility and therefore an orientation dependent shift in addition to the orientation dependent quadrupolar splitting. Therefore, the isotropic peak is not exactly in the center of the two maxima (which correspond to domains aligned with the phase axis perpendicular to the magnetic field), and the maxima are not exactly in the middle of the two outer shoulders (which correspond to domains aligned with the phase axis parallel to the magnetic field). Additional asymmetries arise from shim and phase errors.

References

1. Stubenrauch, C.; Gießelmann, F. Gelled Complex Fluids: Combining Unique Structures with Mechanical Stability. *Angew. Chem. Int. Ed.* **2016**, *55*, 3268–3275. [CrossRef] [PubMed]
2. Kim, D.-H.; Jahn, A.; Cho, S.-J.; Kim, J.S.; Ki, M.-H.; Kim, D.-D. Lyotropic liquid crystal systems in drug delivery: A review. *J. Pharm. Investig.* **2015**, *45*, 1–45. [CrossRef]
3. Kelly, C.V.-D. Perturbations of Cellular Membranes with Synthetic Polymers and Ultrafast Lasers. Ph.D. Thesis, University of Michigan, Ann Arbor, MI, USA, 2009.

4. Warriner, H.E.; Idziak, S.H.J.; Slack, N.L.; Davidson, P.; Safinya, C.R. Lamellar Biogels: Fluid-Membrane-Based Hydrogels Containing Polymer Lipids. *Science* **1996**, *271*, 969–973. [CrossRef] [PubMed]
5. Xu, Y.; Laupheimer, M.; Preisig, N.; Sottmann, T.; Schmidt, C.; Stubenrauch, C. Gelled Lyotropic Liquid Crystals. *Langmuir* **2015**, *31*, 8589–8598. [CrossRef] [PubMed]
6. Koitani, S.; Dieterich, S.; Preisig, N.; Aramaki, K.; Stubenrauch, C. Gelling Lamellar Phases of the Binary System Water–Didodecyldimethylammonium Bromide with an Organogelator. *Langmuir* **2017**, *33*, 12171–12179. [CrossRef] [PubMed]
7. Laibinis, P.E.; Hickman, J.J.; Wrighton, M.S.; Whitesides, G.M. Orthogonal Self-Assembled Monolayers: Alkanethiols on Gold and Alkane Carboxylic Acids on Alumina. *Science* **1989**, *245*, 845–847. [CrossRef] [PubMed]
8. Hu, X.; Xiao, T.; Lin, C.; Huang, F.; Wang, L. Dynamic Supramolecular Complexes Constructed by Orthogonal Self-Assembly. *Acc. Chem. Res.* **2014**, *47*, 2041–2051. [CrossRef] [PubMed]
9. Kumar, D.K.; Steed, J.W. Supramolecular gel phase crystallization: Orthogonal self-assembly under non-equilibrium conditions. *Chem. Soc. Rev.* **2014**, *43*, 2080–2088. [CrossRef] [PubMed]
10. Li, S.; Xiao, T.; Lin, C.; Wang, L. Advanced supramolecular polymers constructed by orthogonal self-assembly. *Chem. Soc. Rev.* **2012**, *41*, 5950–5968. [CrossRef] [PubMed]
11. Saha, M.L.; De, S.; Pramanik, S.; Schmittel, M. Orthogonality in discrete self-assembly—Survey of current concepts. *Chem. Soc. Rev.* **2013**, *42*, 6860–6909. [CrossRef] [PubMed]
12. Wei, P.; Yan, X.; Huang, F. Supramolecular polymers constructed by orthogonal self-assembly based on host–guest and metal–ligand interactions. *Chem. Soc. Rev.* **2015**, *44*, 815–832. [CrossRef] [PubMed]
13. Heeres, A.; van der Pol, C.; Stuart, M.; Friggeri, A.; Feringa, B.L.; van Esch, J. Orthogonal self-assembly of Low Molecular Weight Hydrogelators and Surfactants. *J. Am. Chem. Soc.* **2003**, *125*, 14252–14253. [CrossRef] [PubMed]
14. Brizard, A.; Stuart, M.; van Bommel, K.; Friggeri, A.; de Jong, M.; van Esch, J. Preparation of Nanostructures by Orthogonal Self-Assembly of Hydrogelators and Surfactants. *Angew. Chem. Int. Ed.* **2008**, *47*, 2063–2066. [CrossRef] [PubMed]
15. Brizard, A.M.; van Esch, J.H. Self-assembly approaches for the construction of cell architecture mimics. *Soft Matter* **2009**, *5*, 1320–1327. [CrossRef]
16. Brizard, A.M.; Stuart, M.C.A.; van Esch, J.H. Self-assembled interpenetrating networks by orthogonal self-assembly of surfactants and hydrogelators. *Faraday Discuss.* **2009**, *143*, 345–357. [CrossRef] [PubMed]
17. Boekhoven, J.; Brizard, A.M.; Stuart, M.C.A.; Florusse, L.; Raffy, G.; Del Guerzo, A.; van Esch, J.H. Bio-inspired supramolecular materials by orthogonal self-assembly of hydrogelators and phospholipids. *Chem. Sci.* **2016**, *00*, 1–11. [CrossRef] [PubMed]
18. Laupheimer, M. Gelled Bicontinuous Micoremulsions: A New Type of Orthogonal Self-Assembled Systems. Ph.D. Thesis, University of Stuttgart, Stuttgart, Germany, 2013.
19. Laupheimer, M.; Jovic, K.; Antunes, F.E.; da Graça Martins Miguel, M.; Stubenrauch, C. Studying orthogonal self-assembled systems: Phase behaviour and rheology of gelled microemulsions. *Soft Matter* **2013**, *9*, 3661–3670. [CrossRef]
20. Laupheimer, M.; Sottman, T.; Schweins, R.; Stubenrauch, C. Studying orthogonal self-assembled systems: Microstructure of gelled bicontinuous microemulsions. *Soft Matter* **2014**, *10*, 8744–8757. [CrossRef] [PubMed]
21. Inoue, T.; Matsuda, M.; Nibu, Y.; Misono, Y.; Suzuki, M. Phase Behavior of Heptaethylene Glycol Dodecyl Ether and Its Aqueous Mixture Revealed by DSC and FT-IR Spectroscopy. *Langmuir* **2001**, *17*, 1833–1840. [CrossRef]
22. Blackburn, J.C.; Kilpatrick, P.K. Using Deuterium NMR Line Shapes to Analyze Lyotropic Liquid Crystalline Phase Transitions. *Langmuir* **1992**, *8*, 1679–1687. [CrossRef]
23. Davis, J.H. The description of membrane lipid conformation, order and dynamics by ^{2}H-NMR. *Biochim. Biophys. Acta* **1983**, *737*, 117–171. [CrossRef]
24. Dufourc, E.J.; Parish, E.J.; Chitrakorn, S.I.C.P. Smith Structural and Dynamical Details of Cholesterol-Lipid Interaction as Revealed by Deuterium NMR. *Biochemistry* **1984**, *23*, 6062–6071. [CrossRef]
25. Jelinski, L.W. Deuterium NMR of Solid Polymers. In *High resolution NMR Spectroscopy of Synthetic Polymers in Bulk*; Komorowski, R.A., Ed.; VHC Publishers: New York, NY, USA, 1986; pp. 335–364.
26. Lukaschek, M.; Grabowski, D.A.; Schmidt, C. Shear-Induced Alignment of a Hexagonal Lyotropic Liquid Crystal as Studied by Rheo-NMR. *Langmuir* **1995**, *11*, 3590–3594. [CrossRef]

27. Seelig, J. Deuterium magnetic resonance: Theory and application to lipid membranes. *Q. Rev. Biophys.* **1977**, *10*, 353–418. [CrossRef] [PubMed]
28. Stubenrauch, C.; Frank, C.; Strey, R.; Burgmeister, D.; Schmidt, C. Lyotropic Mesophases Next to Highly Efficient Microemulsions: A ^{2}H NMR Study. *Langmuir* **2002**, *18*, 5027–5030. [CrossRef]
29. Stubenrauch, C.; Burauer, S.; Strey, R. A new approach to lamellar phases (Lα) in water–non-ionic surfactant systems. *Liq. Cryst.* **2004**, *31*, 39–53. [CrossRef]
30. Stockton, G.W.; Polnaszek, C.F.; Tulloch, A.P.; Hasan, F.; Smith, I.C.P. Molecular Motion and Order in Single-Bilayer Vesicles and Multilamellar Dispersions of Egg Lecithin and Lecithin-Cholesterol Mixtures. A Deuterium Nuclear Magnetic Resonance Study of Specifically Labeled Lipids. *Biochemistry* **1976**, *15*, 954–966. [CrossRef] [PubMed]
31. Israelachvili, J.N.; Mitchell, D.J.; Ninham, B.W. Theory of Self-Assembly of Hydrocarbon Amphiphiles into Micelles and Bilayers. *J. Chem. Soc. Faraday Trans. 2* **1976**, *72*, 1525–1568. [CrossRef]
32. Mitchell, D.J.; Tiddy, G.J.T.; Waring, L.; Bostock, T.; McDonald, M.P. Phase behaviour of Polyoxyethylene Surfactants with Water. *J. Chem. Soc. Faraday Trans. 1* **1983**, *79*, 975–1000. [CrossRef]
33. Hoffmann, H.; Ulbricht, W. Faszinierende Phänomene in Tensidlösungen. *Chemie Unserer Zeit* **1995**, *29*, 76–86. [CrossRef]
34. Pake, G.E. Nuclear Resonance Absorption in Hydrated Crystals: Fine Structure of the Proton Line. *J. Chem. Phys.* **1948**, *16*, 327–336. [CrossRef]
35. Nishinari, K. Some Thoughts on the Defnition of a Gel. *Prog. Colloid Polym. Sci.* **2009**, *136*, 87–94. [CrossRef]
36. Terech, P.; Rodriguez, V.; Barnes, J.D.; McKenna, G.B. Organogels and Aerogels of Racemic and Chiral 12-Hydroxyoctadecanoic Acid. *Langmuir* **1994**, *10*, 3406–3418. [CrossRef]
37. Terech, P.; Weiss, R.G. Low Molecular Mass Gelators of Organic Liquids and the Properties of Their Gels. *Chem. Rev.* **1997**, *97*, 3113–3160. [CrossRef]
38. Terech, P.; Pasquier, D.; Bordas, V.; Rossat, C. Rheological Properties and Structural Correlations in Molecular Organogels. *Langmuir* **2000**, *16*, 4485–4494. [CrossRef]
39. Weiss, R.G.; Terech, P. *Molecular Gels: Materials with Self-Assembled Fibrillar Networks*; Springer: Dordrecht, The Netherlands, 2005; ISBN 978-1-4020-3689-7.
40. Collings, P.J.; Hird, M. *Introduction to Liquid Crystals: Chemistry and Physics*; Taylor & Francis Ltd.: London, UK, 1997; ISBN 9780748404834.
41. Kato, T.; Hirai, Y.; Nakaso, S.; Moriyama, M. Liquid Crystalline physical gels. *Chem. Soc. Rev.* **2007**, *36*, 1857–1867. [CrossRef] [PubMed]
42. Laupheimer, M.; Preisig, N.; Stubenrauch, C. The Molecular Organogel *n*-Decane/12-Hydroxyoctadecanoic Acid: Sol-Gel Tranisition, Rheology and Microstructure. *COLSUA* **2015**, *469*, 315–325. [CrossRef]

Paper II

Volume 15 | Number 15 | 21 April 2019 | Pages 3067–3274

Soft Matter

rsc.li/soft-matter-journal

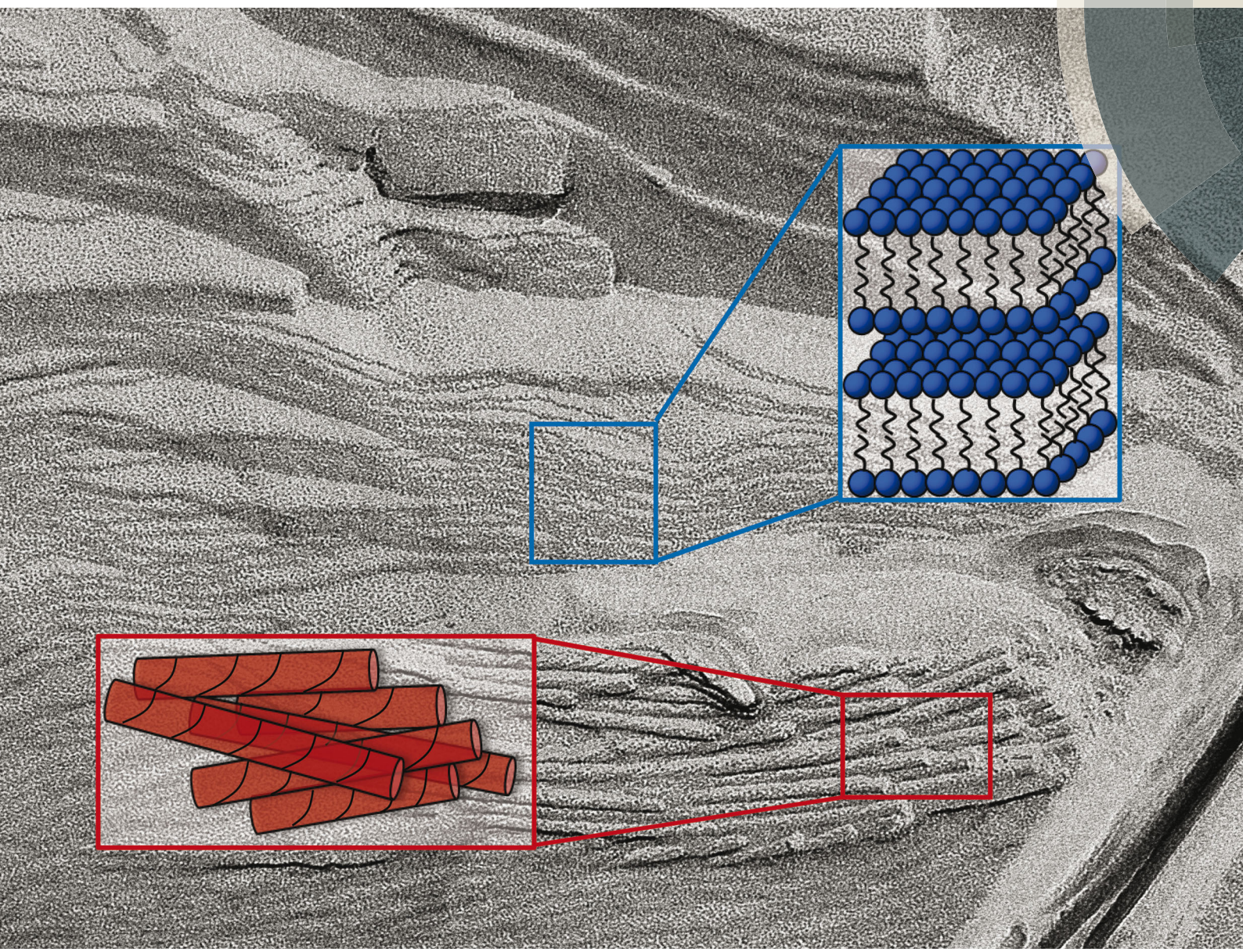

ISSN 1744-6848

ROYAL SOCIETY OF CHEMISTRY | Celebrating IYPT 2019

PAPER
Cosima Stubenrauch *et al.*
Tuning gelled lyotropic liquid crystals (LLCs) – probing the influence of different low molecular weight gelators on the phase diagram of the system H_2O/NaCl–Genapol LA070

Soft Matter

PAPER

View Article Online
View Journal | View Issue

Cite this: *Soft Matter*, 2019, **15**, 3111

Tuning gelled lyotropic liquid crystals (LLCs) – probing the influence of different low molecular weight gelators on the phase diagram of the system H_2O/NaCl–Genapol LA070

Katja Steck,[a] Jan H. van Esch,[b] David K. Smith[c] and Cosima Stubenrauch*[a]

Gelled lyotropic liquid crystals (LLCs) are highly tunable multi-component materials. By studying a selection of low molecular weight gelators (LMWGs), we find gelators that form self-assembled gels in LLCs without influencing their phase boundaries. We studied the system H_2O/NaCl–Genapol LA070 in the presence of (a) the organogelators 12-hydroxyoctadecanoic acid (12-HOA) and 1,3:2,4-dibenzylidene-D-sorbitol (DBS) and (b) the hydrogelators *N*,*N*′-dibenzoyl-L-cystine (DBC) and a tris-amido-cyclohexane derivative (HG1). Visual phase studies and oscillation shear frequency sweeps confirmed that 12-HOA acts as co-surfactant (stabilizing the lamellar L_α phase and destabilizing the hexagonal H_1 phase), thus preventing gelation. Conversely, DBS was a potent gelator for LLCs, with the phase boundaries un-influenced by the presence of DBS; gelled lamellar L_α, and softly-gelled hexagonal H_1 phases are formed. For the hydrogelator DBC, the LLC phase boundaries were only slightly altered, but no gelled LLCs were formed. For the hydrogelator HG1, however, the phase boundaries were unaffected while gelled lamellar L_α and softly-gelled hexagonal H_1 phases were formed. Temperature-dependent rheology measurements demonstrated that by changing the DBS or the HG1 concentration, the sol–gel transition temperature of the gelled lamellar L_α phase can be adjusted such that (a) $T_{sol-gel}$ is below the L_α-isotropic phase transition (DBS, HG1 mass fraction η = 0.0075) and (b) $T_{sol-gel}$ is above the gelled L_α-isotropic phase transition (DBS, HG1 η = 0.015). This opens the possibility of temporal materials control by addressing phase transitions in different orders. As this system contains oil and water, both the organogelator DBS and the hydrogelator HG1 can gel these LLCs, but this clearly does not apply to all organogelators/hydrogelators. The study indicates that careful optimization of LMWGs is required to avoid interaction with the surfactant layer and to optimize the $T_{sol-gel}$ value, which is important for the application of LMWGs in gelled LLCs.

Received 14th November 2018,
Accepted 6th February 2019

DOI: 10.1039/c8sm02330a

rsc.li/soft-matter-journal

Introduction

Gelled lyotropic liquid crystals (gelled LLCs) are one example of gelled complex fluids.[1] They combine the mechanical stability of a gel with the microstructure of a lyotropic liquid crystalline phase, which makes them interesting new materials in tissue healing applications and (*trans*-)dermal drug delivery systems.[1,2] If the two structures, *i.e.* the lyotropic liquid crystal and the gel network, form simultaneously but independently, gelled LLCs can be called orthogonal self-assembled systems.[1] Introduced by Laibinis *et al.* for alkanethiols on gold and alkane carboxylic acids on alumina,[3] the term orthogonal self-assembly was first used for gelled complex fluids by the group of van Esch, who gelled micellar solutions by adding a low molecular weight gelator (LMWG) to aqueous surfactant solutions.[4–8] Kato *et al.* reported on thermotropic liquid-crystalline physical gels and showed that the anisotropic environment leads to controlled self-aggregation of the gelator molecules.[9–12] For the special case of gelled LLCs, the cell is the most prominent example of an orthogonal self-assembled system.[13] The liquid crystalline phospholipid membrane coexists independently with the protein filaments that give the cell mechanical stability. Smith and co-workers explored cationic micelles in several hydrogels, showing that depending on the chemical functionality of the hydrogelator, the self-assembled systems can either be orthogonal or non-orthogonal, depending on the absence or presence of non-covalent interactions between

[a] *Institute of Physical Chemistry, University of Stuttgart, Pfaffenwaldring 55, 70569 Stuttgart, Germany. E-mail: cosima.stubenrauch@ipc.uni-stuttgart.de; Tel: +49-711-685-64470*
[b] *Department of Chemical Engineering, Faculty of Applied Sciences, Delft University of Technology, Julianalaan 136, 2628BL Delft, The Netherlands. E-mail: j.h.vanesch@tudelft.nl*
[c] *Department of Chemistry, University of York, Heslington, York, YO10 5DD, UK. E-mail: david.smith@york.ac.uk*

the two components.[14,15] Lamellar biogels, described by Warriner *et al.*, are an example of a non-orthogonal self-assembled gelled LLC.[16] The gel character of the latter is provided by the random orientation of lamellar bilayers, resulting from defects in high curvature regions which are stabilized by short poly(ethylene glycol)-based amphiphilic block copolymers attached to the lamellar bilayers. Gelled LLCs, more specifically gelled lamellar phases, formed by adding a LMWG to a lamellar phase were studied focussing on the concept of orthogonal self-assembly.[17,18] Koitani *et al.* found that the gelled lamellar phase of the system H_2O–$2C_{12}DAB$ (didodecyldimethylammonium bromide)–12-HOA (12-hydroxyoctadecanoic acid) is an orthogonal self-assembled system,[17] whereas Xu *et al.* found for the very same gelator that the gelled lamellar phase of the system H_2O–*n*-decane/12-HOA–$C_{10}E_4$ (tetraethylene glycol monodecyl ether) is not compatible with the concept of orthogonal self-assembly since the gel network and the lamellar phase influence each other.[18] Thus, the question under which conditions gelled lamellar phases, or more generally gelled LLC, are truly orthogonal self-assembled systems still has to be fully understood.

In order to answer this question, the system H_2O–$C_{12}E_7$ (heptaethylene glycol monododecyl ether) is our system of choice since it forms three lyotropic liquid crystalline phases, namely the hexagonal H_1 phase, the bicontinuous cubic V_1 phase and the lamellar L_α phase, with moderate melting points ($T \approx 50$ °C) which ensures easy handling.[19] In our previous study,[20] we investigated the influence of the organogelator 12-HOA on the phase boundaries of the LLC phases of the system H_2O–$C_{12}E_7$ since 12-HOA has turned out to be a potent gelator for complex fluids.[21–23] However, we made an unexpected observation. We found that 12-HOA has two roles, namely as co-surfactant and as gelator with the former being more pronounced. In its role as co-surfactant, 12-HOA influences the LLC phases such that the hexagonal phase is destabilized and the lamellar phase is stabilized. The "loss" of gelator, *i.e.* the incorporation of 12-HOA in the surfactant layer, is directly reflected in a reduced gelation capacity,[20] *i.e.* that the system H_2O–$C_{12}E_7$–12-HOA is not appropriate to answer the question.

Since 12-HOA turned out not to be a suitable gelator for gelling the LLCs of the system H_2O–$C_{12}E_7$ in an orthogonal self-assembled way, a gelator has to be found, which gels the lyotropic liquid crystals of the system H_2O–$C_{12}E_7$ without influencing the phase boundaries. For economic reasons, we chose the system H_2O/NaCl–Genapol LA070 as "scouting" system for further investigations. Genapol LA070 is the technical analogue to $C_{12}E_7$ with an alkyl chain length varying between C_{12}–C_{14}. We first determined the phase diagram of the system H_2O/NaCl–Genapol LA070 and subsequently the influence of the organogelators 12-HOA (as reference) and DBS (Dibenzylidene-D-sorbitol)[24] as well as of the hydrogelators DBC (*N*,*N*′-dibenzoyl-L-cystine)[25] and HG1[4–7] on its phase boundaries by means of visual observations of birefringence. At the same time, we qualitatively determined the capability of the gelators to gel the LLCs. The molecular structures of the gelators are shown in Fig. 1. Note that all gelators are low molecular weight gelators (LMWG), with sol–gel transition temperatures that can be adjusted *via* the concentration of the gelator in a suitable solvent.[26] In addition to the visual phase studies, we performed oscillation shear frequency sweeps in order to clarify whether gelled lyotropic liquid crystalline phases are formed. In case a gelled LLC was formed we carried out oscillation shear temperature sweeps in order to detect the sol–gel transition temperatures.

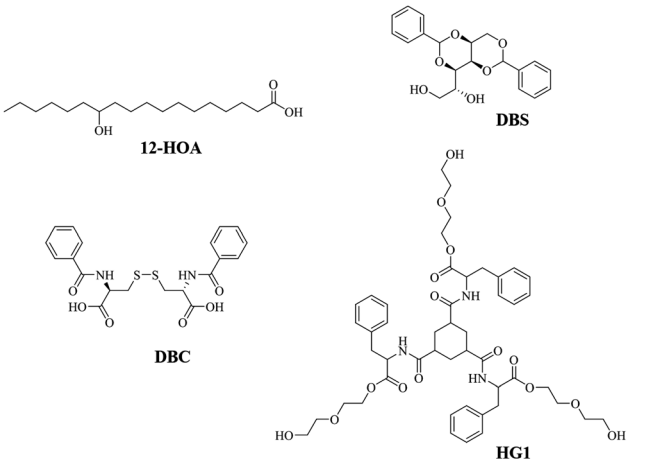

Fig. 1 Molecular structures of the organogelators 12-hydroxyoctadecanoic acid (12-HOA), 1,3:2,4-dibenzylidene-D-sorbitol (DBS) and of the hydrogelators *N*,*N*′-dibenzoyl-L-cystine (DBC) and HG1.

Experimental

Materials and sample preparation

We purchased Genapol LA070 from Clariant, 12-hydroxyoctadecanoic acid (12-HOA, *R*-enantiomer) from Alfa Aesar (95%), *N*,*N*′-dibenzoyl-L-cystine (DBC) from Santa Cruz and DBS as 'Geniset D' from NJC Europe. HG1 was synthesized as described before.[27] The chemicals were used without further purification.

The samples were prepared by using bi-distilled water with the salt mass fraction

$$\varepsilon = \frac{m_{\mathrm{NaCl}}}{m_{\mathrm{NaCl}} + m_{\mathrm{H_2O}}} \tag{1}$$

and the surfactant mass fraction

$$\gamma_{\mathrm{a}} = \frac{m_{\text{Genapol LA070}}}{m_{\text{Genapol LA070}} + m_{\mathrm{H_2O/NaCl}}}. \tag{2}$$

Gelator mass fractions were calculated by

$$\eta = \frac{m_{\mathrm{gelator}}}{m_{\text{Genapol LA070}} + m_{\mathrm{H_2O/NaCl}} + m_{\mathrm{gelator}}}. \tag{3}$$

We used $\varepsilon = 0.001$ for all samples and $\eta = 0.0075$ and $\eta = 0.015$ for gelator-containing samples. All components were weighed in glass tubes and sealed with plugs. The samples were heated up to $T = 95$ °C in a water bath as the gelators had to be dissolved. To ensure homogeneity, the samples were stirred at $T = 95$ °C for at least 10 min. Subsequently, the samples were cooled to room temperature for gelation. In the case of the lamellar phase, changes in viscosity indicated the process of

gelation since no other phase transition occurred in this temperature range. The change of turbidity was used as indication for gelation in the case of the otherwise clear hexagonal phase.

Visual phase studies

The T–γ_a – phase diagram of the system H_2O/NaCl–Genapol LA070 as well as the influence of various low molecular weight gelators on the phase boundaries of the lyotropic liquid crystalline phases were determined by visual observation of birefringence in water basins. The water basins are equipped with a thermostat (Thermo Scientific DC30), a thermometer, a sample holder, a lamp behind the samples and two crossed polarizers, one in front of and one behind the samples. First, we determined eventual LLC to isotropic phase transitions in intervals of ΔT = 5 K, followed by a second temperature scan changing the temperature increment to ΔT = 0.1 K at about 2 K below the roughly determined phase transitions. A waiting time of 3 min was kept for each increment. The phase boundaries of the lyotropic liquid crystalline phases were determined by anisotropy, viscosity and turbidity. The transparent hexagonal H_1 phase is highly viscous as compared to the slightly turbid and less viscous lamellar L_α phase. Accordingly, the upper miscibility gap at high temperatures was identified by turbidity.

Rheometry

The rheological properties of the samples were determined by oscillation shear rheometry using a Physica MCR 501 rheometer from Anton Paar. We used a cone-plate geometry with an upper moving cone of 2.5 cm diameter and a cone angle of 1°. After the samples were transferred with a spatula to the lower plate, the upper cone was lowered to the measuring position (gap width z = 1 mm). In order to reach equilibrium, the samples were kept at T = 22 °C for 30 min, before starting the measurements. In preliminary oscillation strain sweeps at constant frequency ω = 10 s^{-1} and constant temperature T = 22 °C the linear viscoelastic (LVE) region of each sample was determined. The constant strain amplitude was set such that all tests were within the strain limit of the LVE region for each sample. The storage modulus G' and the loss modulus G'' were then determined by frequency (ω) sweeps at a constant strain amplitude γ = 1% and a constant temperature T = 22 °C. We calculated the average G' and G'' values and their standard deviations of three ω-sweeps (Table 1).

Additional T-sweeps enabled us to monitor the sol–gel transition temperatures as well as the lyotropic liquid crystal to isotropic phase transitions of the gelator containing samples. Therefore, the samples were heated from T = 22 °C up to T = 100 °C in temperature steps of 2 K min^{-1} at a constant strain amplitude γ = 1% and at a constant frequency ω = 10 s^{-1}. The average sol–gel transition temperatures of two T-sweeps were calculated.

Results & discussion

Visual phase studies

Visual observations of birefringence as function of the temperature T and the surfactant mass fraction γ_a enabled us to determine the T–γ_a phase diagram of the system H_2O/NaCl–Genapol LA070 (Fig. 2, black symbols). The system forms two lyotropic liquid crystalline phases, namely the hexagonal H_1 phase and the lamellar L_α phase, in specific ranges of temperature and surfactant mass fraction.

Table 1 Standard deviations of the storage modulus G' and the loss modulus G'' averaged over three frequency sweep measurements for the pure lamellar L_α and the pure hexagonal H_1 phase as well as for both phases in the presence of the gelators 12-HOA, DBS, DBC and HG1 at gelator mass fractions η

		Standard deviation of L_α phase		Standard deviation of H_1 phase	
Gelator	η	G'/%	G''/%	G'/%	G''/%
	0	61	52	66	67
12-HOA	0.0075	34	20	42	37
	0.015	59	51	56	53
DBS	0.0075	33	35	59	53
	0.015	35	32	15	12
DBC	0.0075	85	74	47	40
	0.015	51	48	25	22
HG1	0.0075	49	48	60	70
	0.015	76	73	36	30

The highly viscous and transparent hexagonal H_1 phase occurs at surfactant mass fractions $\gamma_a \approx$ 0.30–0.60 and melts at temperatures between $T \approx$ 25–41 °C. The less viscous and slightly turbid lamellar L_α phase is formed at higher surfactant mass fractions ($\gamma_a \approx$ 0.60–0.84) but extends to the upper miscibility gap (2ϕ) at low surfactant mass fractions γ_a and high temperatures T. Note that an extended lamellar L_α phase does not occur in the system H_2O–$C_{12}E_7$. Its formation in the system H_2O/NaCl–Genapol LA070 is caused by the technical grade surfactant Genapol LA070 whose alkyl chain length varies from C_{12}–C_{14}. Due to the presence of longer alkyl chains in Genapol LA070, the packing parameter, *i.e.* the ratio of hydrophobic area to effective hydrophilic head group area, is reduced which leads to a lower curvature of the surfactant layer, and hence to an extended lamellar phase.[28–33]

Having measured the phase diagram of the binary base system, we investigated the influence of the organogelators 12-HOA and DBS as well as of the hydrogelators DBC and HG1 at gelator mass fractions of η = 0.0075 and η = 0.015 on the phase boundary of the hexagonal H_1 phase at surfactant mass fractions γ_a = 0.40 and 0.50 as well as on the phase boundary of the lamellar L_α phase at γ_a = 0.60, 0.70 and 0.80. (Fig. 2, open symbols). Looking at the T–γ_a phase diagram of H_2O/NaCl–Genapol LA070 in the presence of the organogelator 12-HOA at η = 0.0075 and η = 0.015 (Fig. 2, top left), the role of 12-HOA as co-surfactant becomes obvious. Whereas it has no influence on the phase boundary of the lamellar L_α phase at surfactant mass fractions γ_a = 0.60–0.80, the influence on the phase boundary of the hexagonal H_1 phase at γ_a = 0.40–0.50 is enormous, *i.e.* its melting point is shifted towards lower temperatures by ΔT = 5–6 °C at both 12-HOA mass fractions. In addition, the lower phase boundary of the three-phase region (upper miscibility gap 2ϕ and lamellar L_α phase) is shifted towards lower temperatures in the presence of 12-HOA, but since the main interest at γ_a = 0.40 is on

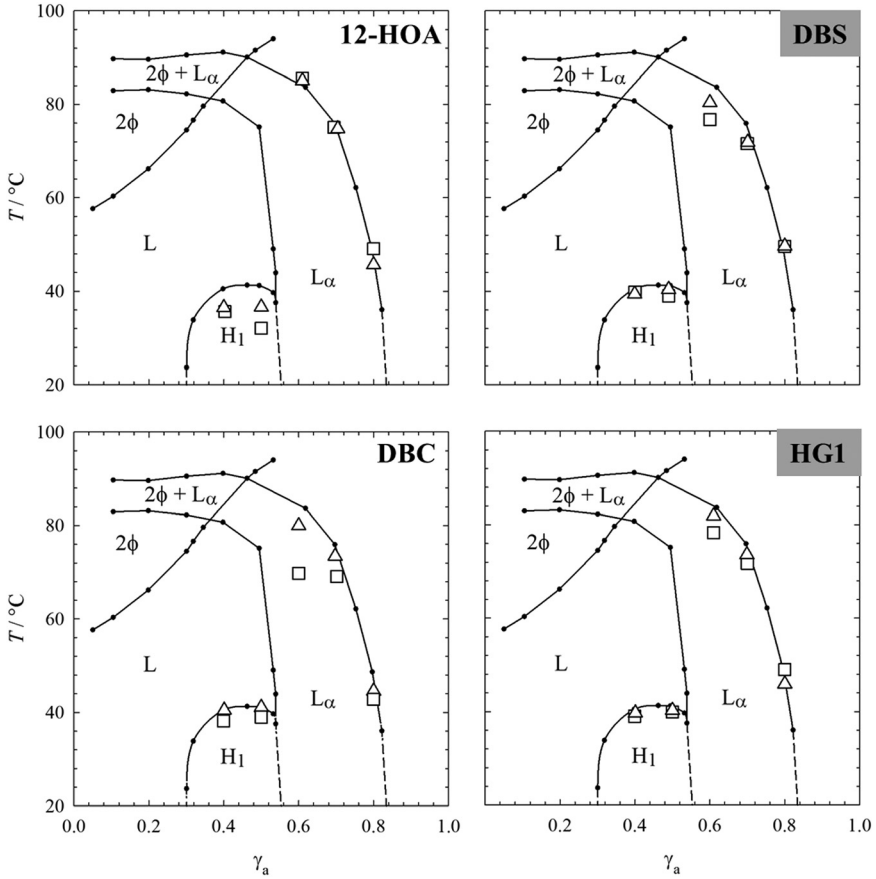

Fig. 2 T–γ_a phase diagram of the system H_2O/NaCl–Genapol LA070 (black symbols) and the influence of the organogelators 12-HOA, DBS (top) and of the hydrogelators DBC and HG1 (bottom) on the phase boundaries of the lyotropic liquid crystalline phases at the surfactant mass fractions of γ_a = 0.40, 0.50, 0.60, 0.70 and 0.80 determined by visual observations of birefringence in water basins. The open triangles indicate the influence of the gelators at a gelator mass fraction η = 0.0075 and the open squares the influence at η = 0.015. The gelators capable of gelling lyotropic liquid crystals are highlighted in grey. The error of the phase boundaries is within the size of the symbols.

the phase boundary of the H_1 phase, we didn't add the influence on the lower phase boundary of the three-phase region in Fig. 1. Adding 12-HOA at a mass fraction of η = 0.075, one sees that the initially transparent hexagonal H_1 phase does not change its appearance and that the slightly turbid lamellar L_α phase maintained its flow ability, *i.e.* no gelled LLCs are formed. At a 12-HOA mass fraction of η = 0.015, still no gelled lamellar L_α phase was formed. However, the hexagonal H_1 phase at γ_a = 0.40 became turbid which is taken as hint for the beginning of a gel formation. A detailed discussion of the latter observation can be found in our previous work.[20]

Contrary to 12-HOA, the organogelator DBS does not influence the phase boundaries of the hexagonal H_1 phase at the surfactant mass fractions γ_a = 0.40 and 0.50 as well as of the lamellar L_α phase at γ_a = 0.60, 0.70 and 0.80 (Fig. 2, top right). However, the lamellar L_α phase lost its flow ability and the transparent hexagonal H_1 phase became turbid at both DBS mass fractions. We ascribed this to gel formation as will be discussed further below (Section Rheometry). In the presence of the hydrogelator DBC (Fig. 2, bottom left) the phase boundaries were also not influenced at a DBC mass fraction of η = 0.0075, but were decreased (ΔT = 2–4 °C) at η = 0.015. No gelled lyotropic liquid crystalline phases were formed though. The lamellar L_α phase maintained its slight turbidity and its flow ability, while the hexagonal H_1 phase maintained its optical transparence. Thus, DBC is only solubilized but does not act as gelator for the system H_2O/NaCl–Genapol LA070. Finally, we found that the hydrogelator HG1 also does not influence the LLC phase boundaries of the system H_2O/NaCl–Genapol LA070 but forms gelled lyotropic liquid crystalline phases at both gelator mass fractions similar to the organogelator DBS.

Based on the results obtained so far, one can conclude that the organogelator DBS and the hydrogelator HG1 are suitable gelators for gelling the lyotropic liquid crystals of the system H_2O/NaCl–Genapol LA070. Both gelled hexagonal H_1 phases and gelled lamellar L_α phases were formed in their presence. In the following section our focus is the gelling capacity of DBS and HG1. Since the visual phase studies allowed us to only qualitatively determine whether a gelled LLC was formed, we performed oscillation shear rheometry experiments, more precisely frequency (ω) sweeps at constant strain amplitude and constant temperature to investigate whether indeed gelled lamellar L_α phases and gelled hexagonal H_1 phases are formed in the presence of DBS and HG1. For comparison, we also

performed ω-sweeps of the pure lamellar L_α phase, the pure hexagonal H_1 phase and in the presence of the gelators 12-HOA and DBC.

Rheometry

Frequency sweeps. The ω-sweeps of the pure lamellar L_α phase at a surfactant mass fraction of $\gamma_a = 0.70$ and those of the lamellar L_α phase in the presence of the organogelators 12-HOA and DBS as well as in the presence of the hydrogelators DBC and HG1 at gelator mass fractions of $\eta = 0.0075$ and $\eta = 0.015$ are shown in Fig. 3. For all systems, the storage modulus G' is higher than the loss modulus G'', *i.e.* all systems show solid-like, elastic behaviour in the frequency range $\omega = 0.01$–$100\ s^{-1}$.[34] The absolute G' and G'' values of the pure L_α phase (Fig. 3, left) are low, due to the parallel lamellar bilayers which can easily slide over each other.[35,36] G' and G'' are not significantly altered in the presence of the organogelator 12-HOA (Fig. 3, top middle) or of the hydrogelator DBC (Fig. 3, bottom middle) at the mass fractions $\eta = 0.0075$ and $\eta = 0.015$, which confirms that no gelled L_α phases were formed, irrespective of the 12-HOA and of the DBC mass fraction. However, adding the organogelator DBS or the hydrogelator HG1 at mass fractions of $\eta = 0.0075$ and $\eta = 0.015$, one clearly sees that that G' and G'' are significantly higher compared to the values of the pure L_α phase. However, the storage modulus G' is still frequency dependent in the presence of DBS and HG1, which is characteristic for soft solids and soft gels.[34] These observations prove, in accordance to the visual phase studies, that gelled L_α phases are formed in the presence of DBS and HG1 at both gelator mass fractions. Note that the sol–gel transition temperature of LMWGs depends on the gelator concentration, *i.e.* that it increases with increasing gelator concentration up until a plateau is reached. Although we studied only two gelator concentrations we can conclude from the data shown in Fig. 3 that this plateau is reached in case of HG1 (no concentration dependence of G', G''), while this is not the case for DBS (higher G' and G'' values at $\eta = 0.015$ as compared to $\eta = 0.0075$). These observations are in line with previous studies. For DBS it was found that G' and G'' of liquid paraffin gelled with DBS increases significantly between $\eta = 0.002$ and $\eta = 0.01$.[24] On the other hand, the sol–gel transition temperature of H_2O gelled with HG1 stays constant at concentrations as low as $\sim$6 mM, which corresponds to $\eta = 0.006$.[7]

Looking at the ω-sweeps of the pure hexagonal H_1 phase (Fig. 4, left), one can see higher values of G' and G'' than for the less viscous lamellar L_α phase, due to densely packed cylinders.[35] In addition, there is a crossover point of the storage modulus G' and the loss modulus G'' at low frequencies. At this

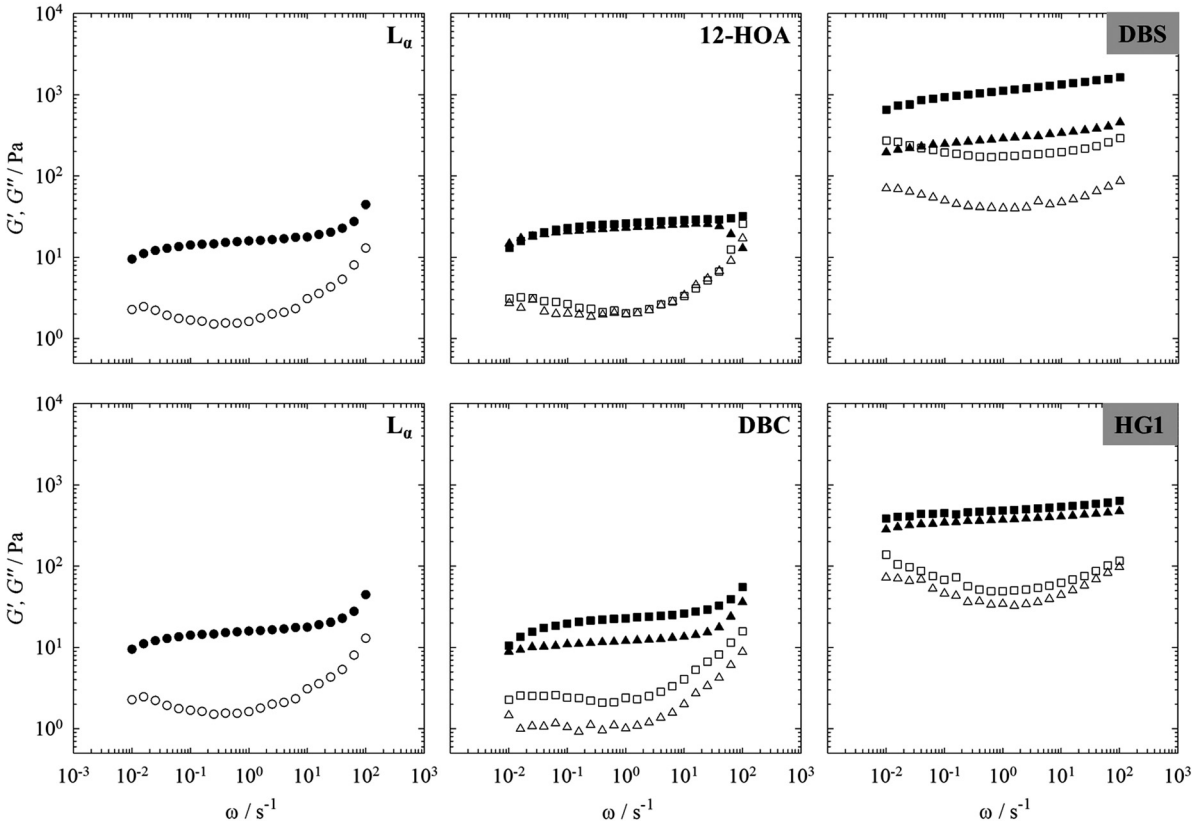

Fig. 3 Storage modulus G' (filled symbols) and loss modulus G'' (open symbols) of the pure lamellar phase at a surfactant mass fraction of $\gamma_a = 0.70$ (left) and in the presence of the organogelators 12-HOA, DBS (top) and of the hydrogelators DBC, HG1 (bottom) at two gelator mass fractions $\eta = 0.0075$ (triangles) and $\eta = 0.015$ (squares) determined by frequency (ω) – sweeps at constant temperature $T = 22\ ^\circ C$ and constant strain amplitude $\gamma = 1\%$. The grey highlighted gelators are capable of gelling the L_α phase.

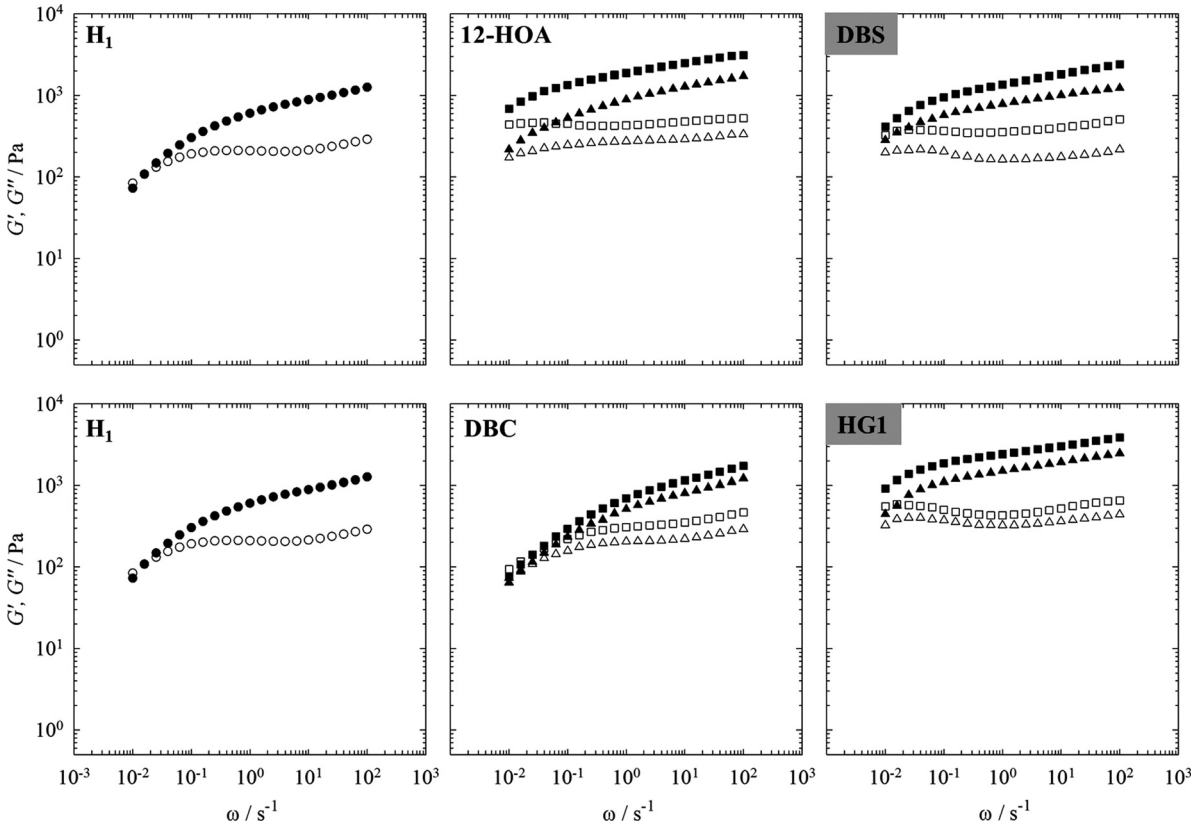

Fig. 4 Storage modulus G' (filled symbols) and loss modulus G'' (open symbols) of the pure hexagonal phase at a surfactant mass fraction of γ_a = 0.40 (left) and in the presence of the organogelators 12-HOA, DBS (top) and of the hydrogelators DBC, HG1 (bottom) at two gelator mass fractions η = 0.0075 (triangles) and η = 0.015 (squares) determined by frequency (ω) – sweeps at constant temperature T = 22 °C and constant strain amplitude γ = 1%. The grey highlighted gelators are capable of gelling both the hexagonal H_1 phase and the lamellar L_α phase.

crossover point, the rheological behaviour of the hexagonal H_1 phase changes from liquid-like, viscous behaviour ($G'' > G'$) at lower frequencies to solid-like, elastic behaviour ($G' > G''$) at higher frequencies.[36]

For a gelled hexagonal H_1 phase one would expect that $G' > G''$ in the measured frequency range. In the presence of the organogelator 12-HOA at both 12-HOA mass fractions η = 0.0075 and η = 0.015, the crossover of G' and G'' does not occur anymore in the measured frequency range, but seems to be shifted to lower frequencies, since G' and G'' approach each other at low frequencies (Fig. 4, top middle). Furthermore, the G' value is slightly enhanced by the presence of the organogelator. Taken together, these observations would suggest that the hexagonal H_1 phase forms a soft gel in the presence of 12-HOA. Contrary to the hexagonal H_1 phase in the presence of 12-HOA, the crossover of G' and G'' still occurs at low frequencies in the presence of DBC at both gelator mass fractions, and furthermore, the absolute value of G' is near identical in the presence or absence of the gelator. These observations confirm that no gelled hexagonal H_1 phase was formed in the presence of DBC. The hexagonal H_1 phase in the presence of the organogelator DBS (Fig. 4, top right) and the hydrogelator HG1 (Fig. 4, bottom right) show the same viscoelastic behaviour as the H_1 phase in the presence of 12-HOA. The storage moduli G' are higher than the loss moduli G'' in the measured frequency range, but G' still is strongly frequency dependent and approaches G'' at low frequencies in the presence of DBS and HG1. The presence of the gelator slightly enhances the absolute values of G'. The results of the ω-sweeps of the hexagonal H_1 phase in the presence of the organogelators 12-HOA, DBS and of the hydrogelator HG1 therefore suggest that gelled hexagonal H_1 phases are formed. However, the strong frequency dependence of G' indicates that the gel is very soft and that the viscoelastic behaviour dominates.

To summarize, the oscillation shear ω-sweeps confirm the visual observations and show that the organogelator 12-HOA is not suitable for gelling liquid crystals, since no gelled lamellar L_α phase and only a softly gelled hexagonal H_1 phase are formed. In the presence of the hydrogelator DBC no gelled lyotropic liquid crystals are formed either. In contrast to 12-HOA and DBC, gelled lamellar L_α phases and softly gelled hexagonal H_1 phases are formed in the presence of the organogelator DBS and of the hydrogelator HG1 at both mass fractions. Interestingly, since the system H_2O/NaCl–Genapol LA070 is partly oil and partly water, both the organogelator and the hydrogelator are capable of gelling the lyotropic liquid crystals.

Note that due to the large standard deviations (see Table 1 in the Experimental section), we do not discuss the actual G' and G'' values but only the qualitative trends which were always the same: (a) increasing G' and G'' values in the case of the gelled

lamellar L_α phases and (b) $G' > G''$ in the whole frequency range for the gelled hexagonal phases.

Temperature sweeps. We decided to additionally perform *T*-sweeps of the gelled lamellar L_α phase and the gelled hexagonal H_1 phase in the presence of the organogelator DBS and of the hydrogelator HG1 in order to determine the sol–gel transition temperatures. The *T*-sweeps of the pure lamellar L_α phase and of the L_α phase in the presence of DBS and HG1 at mass fractions of $\eta = 0.0075$ and $\eta = 0.015$ are shown in Fig. 5. In the case of the pure lamellar L_α phase (Fig. 5, left), the storage modulus G' is higher than the loss modulus G'' at the initial temperature $T = 22$ °C in accordance with the frequency sweeps. On increasing the temperature, G' and G'' slightly decrease until G' drops below G'' at $T \approx 70$ °C, which can be assigned to the lamellar to isotropic phase transition.[36] Looking at the *T*-sweeps of the gelled lamellar L_α phase in the presence of DBS at $\eta = 0.0075$ (Fig. 5, top middle), one can see that, in accordance to the frequency sweeps, G' and G'' have considerably higher values than G' and G'' of the pure L_α phase. G' and G'' decrease with increasing temperature until the sol–gel boundary is approached. Due to the loss of interconnectivity of the gelator fibers, a sharp drop of G' and G'' as well as $G' < G''$ indicate the sol–gel transition temperature.[37] Due to the fact that the lamellar to isotropic and sol–gel transitions occur at about the same temperature (*ca.* 70 °C), the lamellar to isotropic phase transition cannot be isolated and is "hidden" in the sol–gel transition. In the case of the gelled lamellar L_α phase in the presence of DBS at $\eta = 0.015$ (Fig. 5, top right) the same temperature-dependent viscoelastic behaviour is observed with slightly larger absolute values of G' and G''. Both moduli again decrease with increasing temperature, however, in this case, there is a small drop at $T \approx 68$ °C. According to the optical phase studies, we assigned this drop to the lamellar to isotropic phase transition. After crossing this phase boundary, the values of G' and G'' remain high with $G' > G''$ until the sol–gel boundary is reached at $T \approx 82$ °C, indicated by the sharp drop of the moduli. As such, doubling the concentration of gelator increases the $T_{sol-gel}$ value by *ca.* 10 °C, and consequently allows the lamellar-to-isotropic and gel-to-sol transitions to be thermally separated from one another.

For the gelled lamellar L_α phase in the presence of the hydrogelator HG1 at $\eta = 0.0075$ (Fig. 5, bottom middle), the collapse of G' and G'' is not as sharp as for the gelled lamellar phases L_α in the presence of DBS. Instead, G' and G'' decrease continuously with increasing temperature. However, one can see two small drops of the storage modulus G' and the loss modulus G'' at $T \approx 68$ °C and $T \approx 77$ °C, which indicate phase transitions. According to the visual observations, the first drop at $T \approx 68$ °C can be identified as the lamellar to isotropic phase transition, whereas the second drop indicates the sol–gel transition

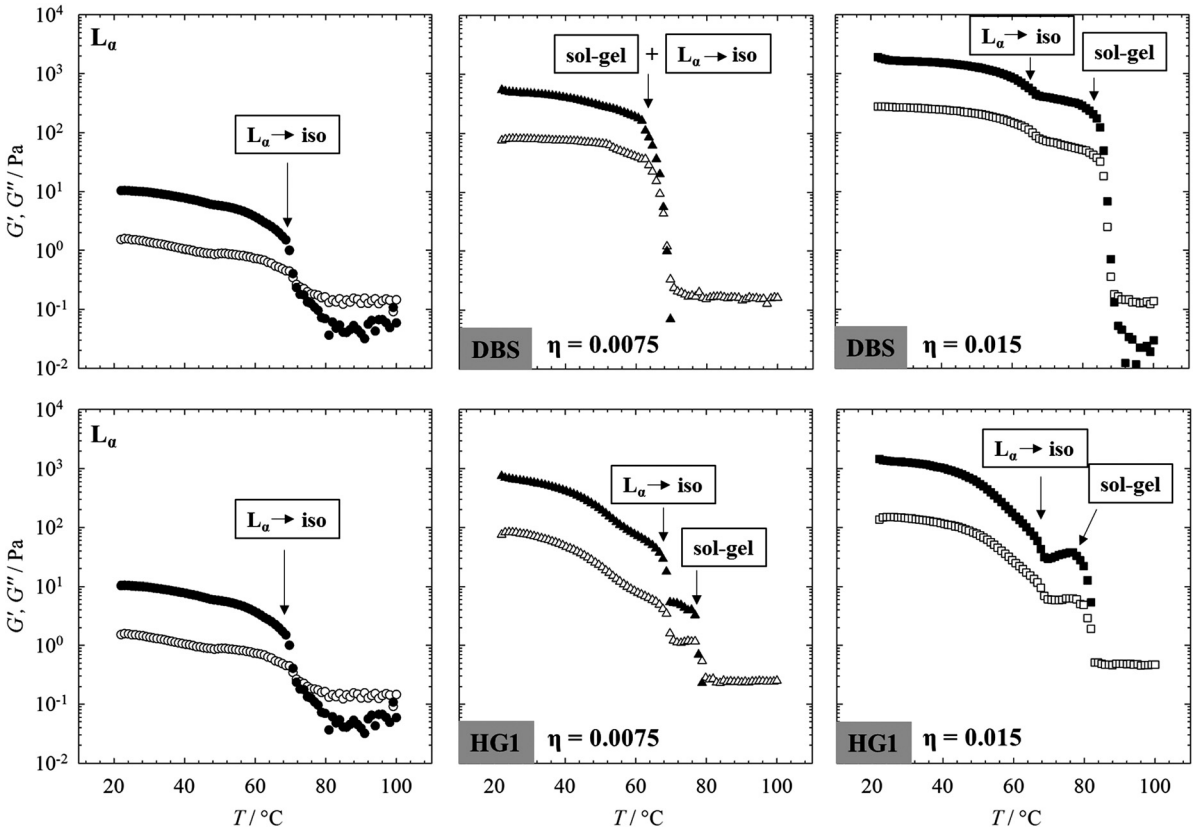

Fig. 5 Storage modulus G' (filled symbols) and loss modulus G'' (open symbols) of the pure lamellar phase at a surfactant mass fraction of $\gamma_a = 0.70$ (left) and in the presence of the organogelator DBS (top) and of the hydrogelator HG1 (bottom) at gelator mass fractions of $\eta = 0.0075$ (triangles) and $\eta = 0.015$ (squares) determined by temperature sweeps (heating rate 2 K min^{-1}) at constant frequency $\omega = 10$ s^{-1} and constant strain amplitude $\gamma = 1\%$.

temperature. In the presence of HG1 at η = 0.015 (Fig. 5, bottom right), the same temperature-dependent viscoelastic behaviour can be observed. The drop at $T \approx 66$ °C is due the lamellar to isotropic phase transition and the one at $T \approx 85$ °C is due to sol–gel transition temperature.

The T-sweeps of the pure hexagonal H_1 phase and those of the softly gelled H_1 phases in the presence of the organogelator DBS and of the hydrogelator HG1 can be interpreted in the same way (Fig. 6). For the pure hexagonal H_1 phase, the sharp collapse of G' and G'' at $T \approx 40$ °C can be assigned to the hexagonal to isotropic phase transition.

The hexagonal to isotropic phase transition is also visible in the temperature-dependent viscoelastic behaviour of the softly gelled hexagonal H_1 phases. In case of the gelled H_1 phase in the presence of DBS at η = 0.0075 (Fig. 6, top middle), the first drop of G' and G'' indicates the hexagonal to isotropic phase transition after which the values of G' and G'' again increase until a second drop occurs at $T \approx 79$ °C, which can be assigned to the sol–gel transition temperature. However, in the presence of DBS at η = 0.015 (Fig. 6, top right) the hexagonal to isotropic phase transition can be detected at $T \approx 40$ °C, after which G' and G'' first remain constant before they increase with increasing temperature. The increase of G' and G'', *i.e.* the observed thermo-thickening, may be due to the fact that the gel network is able to reorganize and thus strengthen itself in the isotropic phase once the hexagonal phase is molten. We would like to emphasize that this observation is not in contradiction to orthogonal self-assembly: orthogonal self-assembly refers to a self-assembly on a molecular level, while the observed thermo-thickening happens on a supramolecular level. In the latter case we are talking about the rearrangement of already formed fibers (formed *via* self-assembly) in a solvent in which the self-assembly of surfactants leads to an anisotropic and an isotropic surrounding, respectively. The sharp drop of G' and G'' at high temperatures ($T \approx 92$ °C) can be assigned to the sol–gel transition temperature in accordance with the visual observations.

The temperature dependent viscoelastic behaviour of the gelled hexagonal H_1 phase in the presence of the hydrogelator HG1 at η = 0.0075 is dominated by the viscoelastic behaviour of the hexagonal H_1 phase (Fig. 6, bottom middle). Comparing the visual observations with the T-sweep, the first drop in G' and G'' can be assigned to the hexagonal to isotropic phase transition. Similar to the gelled H_1 phase in the presence of DBS at η = 0.0075, the drop of G' and G'' at $T \approx 74$ °C can be assigned to the sol–gel transition temperature. For the softly gelled H_1 phase in the presence of HG1 at η = 0.015 the same temperature-dependent viscoelastic behaviour can be observed. The hexagonal to isotropic phase transition is assigned to the first drop of G' and G''. With increasing temperature, G' and G''

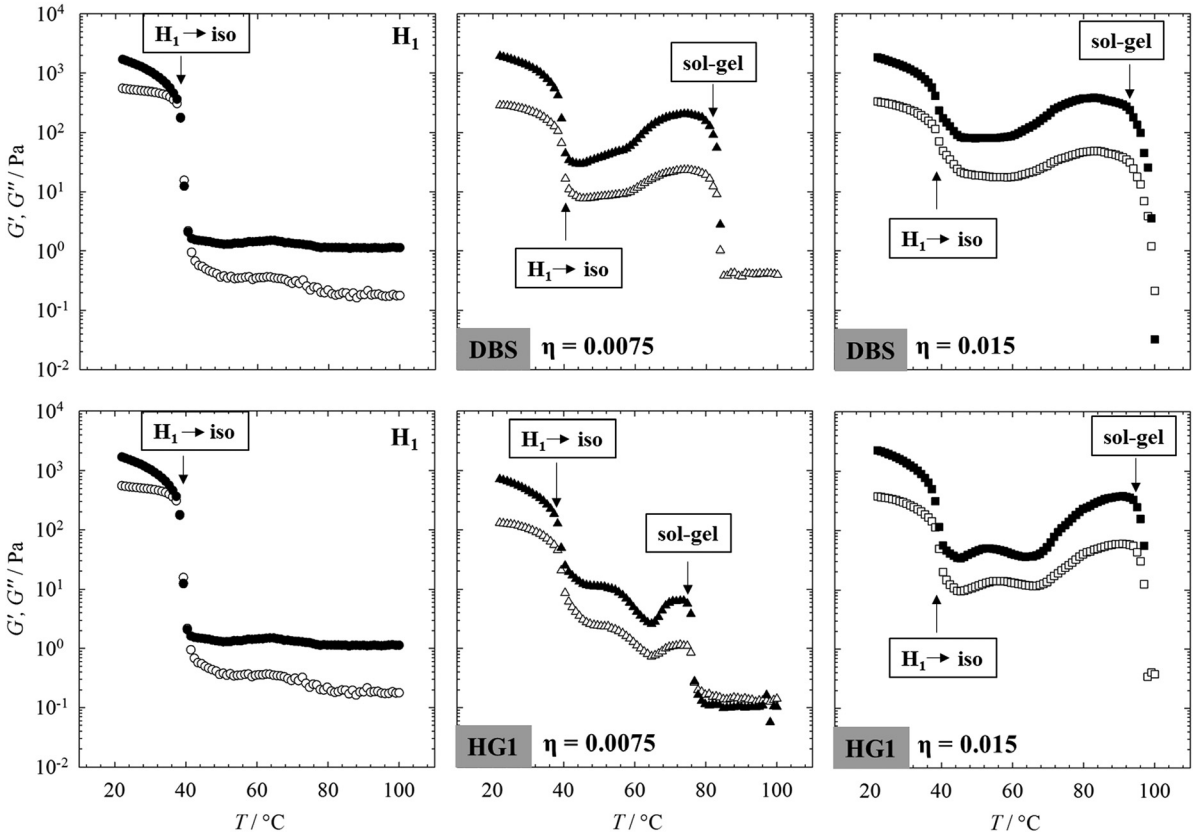

Fig. 6 Storage modulus G' (filled symbols) and loss modulus G'' (open symbols) of the pure hexagonal H_1 phase at a surfactant mass fraction γ_a = 0.40 (left) and in the presence of the organogelator DBS (top) and of the hydrogelator HG1 (bottom) at gelator mass fractions of η = 0.0075 (triangles) and η = 0.015 (squares) determined by temperature sweeps (heating rate 2 K min^{-1}) at constant frequency ω = 10 s^{-1} and constant strain amplitude γ = 1%.

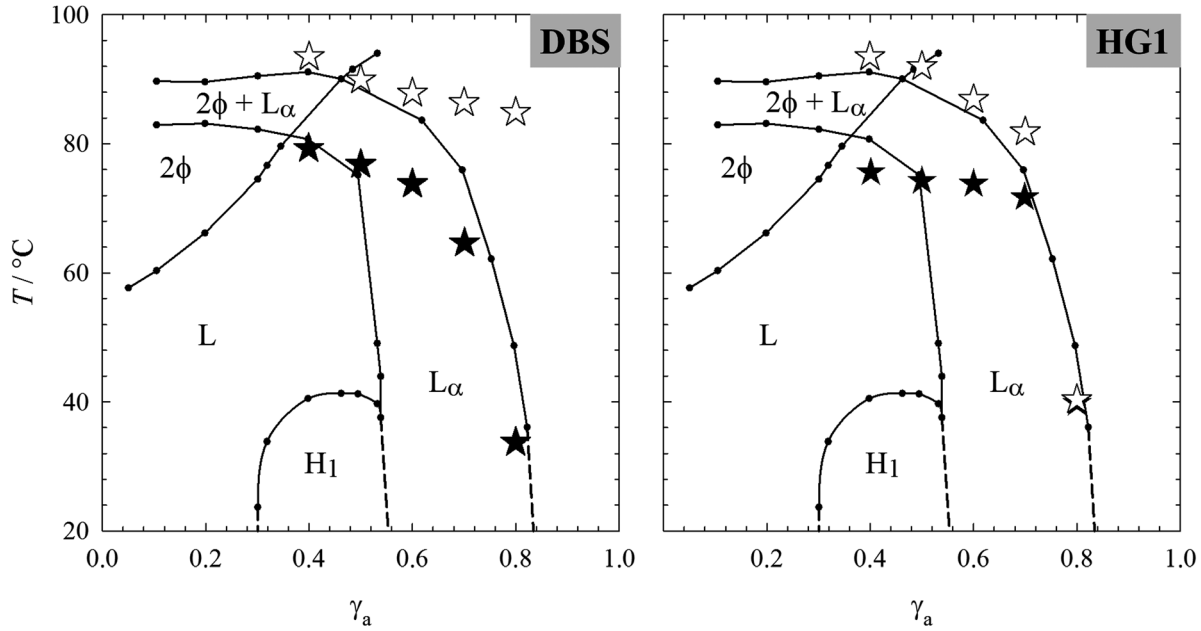

Fig. 7 T–γ_a phase diagram of the system H_2O/NaCl–Genapol LA070 (black circles) with added sol–gel transition temperatures $T_{sol-gel}$ of the gelled H_1 phase at γ_a = 0.40 and the gelled L_α phase γ_a = 0.70 in the presence of the organogelator DBS (left) and of the hydrogelator HG1 (right) at gelator mass fractions of η = 0.0075 (black stars) and η = 0.015 (open stars) determined by oscillation shear temperature sweeps. The error of the sol–gel transition temperature is $\Delta T_{sol-gel} = \pm$ 1–5 °C. Since the phase boundaries of the LLCs did not change in the presence of DBS and HG1 (see Fig. 2), they are not added to the phase diagrams.

increase again until the sharp drop at $T \approx 94$ °C, which is assigned to the sol–gel transition temperature.

To conclude, the T-sweeps enabled us to detect the lyotropic liquid crystal to isotropic phase transitions as well as the sol–gel phase transitions of the gelled lamellar L_α phase and the gelled hexagonal H_1 phase in the presence of the organogelator DBS and the hydrogelator HG1. In Fig. 7, we added the sol–gel transition temperatures to the T–γ_a phase diagram of the system H_2O/NaCl–Genapol LA070. For the gelled LLC phases in the presence of DBS (Fig. 7, left), we were able to detect the sol–gel transition temperatures of the gelled L_α phases and the gelled hexagonal H_1 phases at both gelator mass fractions η = 0.0075 and η = 0.015. In the case of the lamellar L_α phase, the sol–gel transition temperature is below the melting point of the lamellar L_α phase ($T_{sol-gel} < T_{LLC-iso}$) at the DBS mass fraction η = 0.0075, whereas it is above the melting point of the L_α phase ($T_{sol-gel} > T_{LLC-iso}$) at η = 0.015. In analogy to Kato *et al.*,[10] we name the former situation Type II LLC gel and the latter Type I LLC gel. In the case of the gelled H_1 phase the sol–gel transition temperatures are above the melting point of the hexagonal H_1 phase at both DBS mass fraction. For the gelled LLCs in the presence of HG1 (Fig. 7, right), the same situation can be observed. We could also detect the sol–gel transition temperatures of the gelled H_1 phases and of the gelled L_α phases at both mass fractions, *i.e.* η = 0.0075 and η = 0.015. The sol–gel transition temperature of the gelled lamellar L_α phases at η = 0.0075 is below the lamellar to isotropic phase transition (Type II LLC gel) and it is above the melting point of the lamellar L_α phase for η = 0.015 (Type I LLC gel). The sol–gel transition temperatures of the gelled hexagonal H_1 phase in the presence of HG1 are above the melting point of the hexagonal H_1 phase at both HG1 mass fractions with a higher sol–gel transition temperature at η = 0.015. The decrease of the sol–gel transition temperatures with increasing surfactant concentration for DBS and HG1 is due to the fact that both gelators are soluble in the pure surfactant. In other words, the binary water-surfactant mixture becomes a better solvent for the gelators with increasing surfactant mass fraction.

Conclusions

In order to find a gelator which forms self-assembled gels in LLCs without influencing their phase boundaries, we studied the LLCs of the system H_2O/NaCl–Genapol LA070 in the presence of organogelators 12-HOA and DBS as well as in the presence of hydrogelators DBC and HG1 at gelator mass fractions η = 0.0075 and η = 0.015. 12-HOA is partly incorporated in the surfactant layer and acts as co-surfactant such that the lamellar L_α phase is stabilized and the hexagonal H_1 phase is destabilized, which results in a reduced gelation capacity, *i.e.* no gelled LLCs are formed. The organogelator DBS is a potent gelator for LLCs. The LLC phase boundaries are not influenced by the presence of DBS and softly gelled hexagonal H_1 phases as well as gelled lamellar L_α phases are formed at both DBS mass fractions. In the case of hydrogelator DBC, the LLC phase boundaries are only slightly altered by its presence but since no gelled LLCs are formed, DBC was not studied further. For hydrogelator HG1, similar to DBS, the LLC phase

boundaries are not influenced by its presence and softly gelled hexagonal H_1 phases as well as lamellar L_α phases are formed at both HG1 mass fractions. Since we studied the phase behaviour at surfactant mass fractions γ_a = 0.40–0.80, the system contains both oil and water, and thus organogelator DBS and hydrogelator HG1 are capable of gelling the LLCs.

For both gelators, DBS and HG1, the sol–gel transition temperatures of the gelled lamellar L_α phases could be adjusted such that (a) $T_{sol-gel}$ is below the melting point of the gelled lamellar L_α phase at the gelator mass fractions η = 0.0075 and (b) $T_{sol-gel}$ is above the melting point of the gelled L_α phase at η = 0.015. In the case of the gelled hexagonal H_1 phase however, the sol–gel transition temperatures are above the melting point of the H_1 phase at both DBS and HG1 mass fractions. Since DBS and HG1 are soluble in the pure Genapol LA070, the $T_{sol-gel}$ value decreases with increasing surfactant mass fraction for both gelators.

Orthogonal self-assembly requires simultaneous but independent formation of two self-assembled structures. The observation that DBS and HG1 gel LLCs without altering the phase boundaries and that the gelators indeed self-assemble into gel fibers prove that the gelled LLCs of this study are indeed orthogonal self-assembled systems from a molecular point of view. In a follow-up study we will characterize the two coexisting structures. Another focus will be on the chronology of lyotropic liquid crystal and gel formation, *i.e.* we want to study if (a) the LLC can serve as template for the gel network leading to aligned gelator fibers and (b) if the gel network has influence on the LLC structure.[38] If both answers were yes, we would have an orthogonal self-assembled system in which the two coexisting self-assembled supramolecular structures interact with each other. The study published here has allowed us to identify two gelators, DBS and HG1, with which it is possible two adjust the sol–gel transition temperatures of the gelled lamellar L_α phases *via* the gelator mass fraction as required, in order to answer the question whether the chronology of gel and LLC formation does play a role regarding orthogonal self-assembly. For the simple reason of commercial availability, we choose DBS for further investigations.

Conflicts of interest

The authors declare no conflict of interest.

Acknowledgements

We thank David Moser for carrying out parts of the visual and rheological phase studies. Financial Support by the Deutsche Forschungsgemeinschaft (grant number: STU287/6-1) is gratefully acknowledged.

Notes and references

1 C. Stubenrauch and F. Gießelmann, *Angew. Chem., Int. Ed.*, 2016, **55**, 3268.
2 D.-H. Kim, A. Jahn, S.-J. Cho, J. S. Kim, M.-H. Ki and D.-D. Kim, *J. Pharm. Invest.*, 2015, **45**, 1.
3 P. E. Laibinis, J. J. Hickman, M. S. Wrighton and G. M. Whitesides, *Science*, 1989, **245**, 845.
4 A. Heeres, C. van der Pol, M. Stuart, A. Friggeri, B. L. Feringa and J. van Esch, *J. Am. Chem. Soc.*, 2003, **125**, 14252.
5 A. Brizard, M. Stuart, K. Van Bommel, A. Friggeri, M. De Jong and J. van Esch, *Angew. Chem., Int. Ed.*, 2008, **47**, 2063.
6 A. M. Brizard and J. H. van Esch, *Soft Matter*, 2009, **5**, 1320.
7 A. M. Brizard, M. C. A. Stuart and J. H. van Esch, *Faraday Discuss.*, 2009, **143**, 345.
8 J. Boekhoven, A. M. Brizard, M. C. A. Stuart, L. Florusse, G. Raffy, A. Del Guerzo and J. H. van Esch, *Chem. Sci.*, 2016, **00**, 1.
9 N. Mizoshita, T. Kutsuna, K. Hanabusa and T. Kato, *Chem. Commun.*, 1999, 781.
10 T. Kato, T. Kutsuna, K. Yabuuchi and N. Mizoshita, *Langmuir*, 2002, **18**, 7086.
11 K. Mizoshita, K. Hanabusa and T. Kato, *Adv. Funct. Mater.*, 2003, **13**, 313.
12 T. Kato, N. Mizoshita and K. Kishimoto, *Angew. Chem., Int. Ed.*, 2006, **45**, 38.
13 C. V.-D. Kelly, *Perturbations of cellular membranes with synthetic polymers and ultrafast lasers*, *PhD thesis*, University of Michigan, Michigan, 2009.
14 V. M. P. Vieira, L. L. Hay and D. K. Smith, *Chem. Sci.*, 2017, **8**, 6981.
15 V. M. P. Vieira, A. C. Lima, M. de Jong and D. K. Smith, *Chem. – Eur. J.*, 2018, **24**, 15112.
16 H. E. Warriner, S. H. J. Idziak, N. L. Slack, P. Davidson and C. R. Safinya, *Science*, 1996, **271**, 969.
17 S. Koitani, S. Dieterich, N. Preisig, K. Aramaki and C. Stubenrauch, *Langmuir*, 2017, **33**, 12171.
18 Y. Xu, M. Laupheimer, N. Preisig, T. Sottmann, C. Schmidt and C. Stubenrauch, *Langmuir*, 2015, **31**, 8589.
19 T. Inoue, M. Matsuda, Y. Nibu, Y. Misono and M. Suzuki, *Langmuir*, 2001, **17**, 1883.
20 K. Steck, C. Schmidt and C. Stubenrauch, *Gels*, 2018, **4**, 78.
21 M. Laupheimer, *Gelled Bicontinuous Micoremulsions: A New Type of Orthogonal Self-Assembled Systems*, PhD thesis, University of Stuttgart, Stuttgart, 2013.
22 M. Laupheimer, K. Jovic, F. E. Antunes, M. da Graça Martins Miguel and C. Stubenrauch, *Soft Matter*, 2013, **9**, 3661.
23 M. Laupheimer, T. Sottman, R. Schweins and C. Stubenrauch, *Soft Matter*, 2014, **10**, 8744.
24 B. O. Okesola, V. M. P. Vieira, D. J. Cornwell, N. K. Whitelaw and D. K. Smith, *Soft Matter*, 2015, **11**, 4768.
25 A. Friggeri, B. L. Feringa and J. van Esch, *J. Controlled Release*, 2004, **97**, 241.
26 R. G. Weiss and P. Terech, *Molecular Gels: Materials with Self-Assembled Fibrillar Networks*, Springer, The Netherlands, 2005.
27 K. J. van Bommel, C. van der Pol, I. Muizebelt, A. Friggeri, A. Heeres, A. Meetsma, B. L. Feringa and J. van Esch, *Angew. Chem., Int. Ed.*, 2004, **43**, 1663.

28 K. Selber, S. Müller, H. Gieren, J. Thömmes, T. Sottmann, R. Strey and M.-R. Kula, *Bioseparation*, 2002, **10**, 243.
29 J. N. Israelachvili, D. J. Mitchell and B. W. Ninham, *J. Chem. Soc., Faraday Trans. 2*, 1976, **72**, 1525.
30 C. Stubenrauch, C. Frank, R. Strey, D. Burgmeister and C. Schmidt, *Langmuir*, 2002, **18**, 5027.
31 D. Varade, H. Kunieda, R. Strey and C. Stubenrauch, *J. Colloid Interface Sci.*, 2006, **300**, 338.
32 K. Kratzat and H. Finkelmann, *Liq. Cryst.*, 1993, **13**, 691.
33 K. Kratzat, C. Stubenrauch and H. Finkelmann, *Colloid Polym. Sci.*, 1995, **273**, 257.
34 K. Nishinari, *Prog. Colloid Polym. Sci.*, 2009, **136**, 87.
35 P. J. Collings and M. Hird, *Introduction to Liquid Crystals: Chemistry and Physics*, Taylor & Francis Ltd, United Kingdom, 1997.
36 R. Mezzenga, C. Meyer, C. Servais, A. I. Romoscanu, L. Sagalowicz and R. C. Hayward, *Langmuir*, 2005, **21**, 3322.
37 P. Terech, C. Rossat and F. Volino, *J. Colloid Interface Sci.*, 2000, **227**, 363.
38 T. Kato, Y. Hirai, S. Nakaso and M. Moriyama, *Chem. Soc. Rev.*, 2007, **36**, 1857.

Paper III

LANGMUIR Article
Cite This: Langmuir 2019, 35, 17132−17141
pubs.acs.org/Langmuir

Gelling Lyotropic Liquid Crystals with the Organogelator 1,3:2,4-Dibenzylidene-D-sorbitol Part I: Phase Studies and Sol−Gel Transitions

Katja Steck and Cosima Stubenrauch*

Institute of Physical Chemistry, University of Stuttgart, Pfaffenwaldring 55, 70569 Stuttgart, Germany

ABSTRACT: Gelled lyotropic liquid crystals (gelled LLCs) are the combination of an LLC and a gel network. One method for obtaining gelled LLCs is the addition of a low molecular weight gelator, which forms gels via self-assembled fibrillar networks, to an aqueous surfactant solution. A potent gelator for LLCs is the LMW organogelator 1,3:2,4-dibenzylidene-D-sorbitol (DBS). This gelator gels the lamellar L_α phase, the bicontinuous cubic V_1 phase, and the hexagonal H_1 phase of the system $H_2O-C_{12}E_7$ (heptaethylene glycol monododecyl ether) without influencing the phase boundaries as visual phase studies and rheometry show. Varying the DBS mass fraction η, one can adjust the sol−gel transition temperature $T_{sol-gel}$ of the gelled LLCs. At η = 0.0075, all $T_{sol-gel}$ values are below the LLC-to-isotropic phase transition temperatures $T_{LLC-iso}$, that is, the LLCs are formed first while cooling down, followed by gel formation. At η = 0.015, however, $T_{sol-gel} > T_{LLC-iso}$, that is, the gel is formed in an isotropic solvent, which becomes an LLC while cooling down. The system $H_2O-C_{12}E_7$ is the first where an adjustment of the gelator concentration allowed us to decouple gel and LLC formation for all three LLCs, that is, gel and LLC formation happen one after the other and not simultaneously. This allows us to study whether the structure and thus the properties of gelled LLCs can be manipulated by the order of gel and LLC formation. We discuss our findings in light of the following question: are our gelled LLCs truly orthogonal self-assembled systems, that is, do the LLCs and the gel network form and coexist independently?

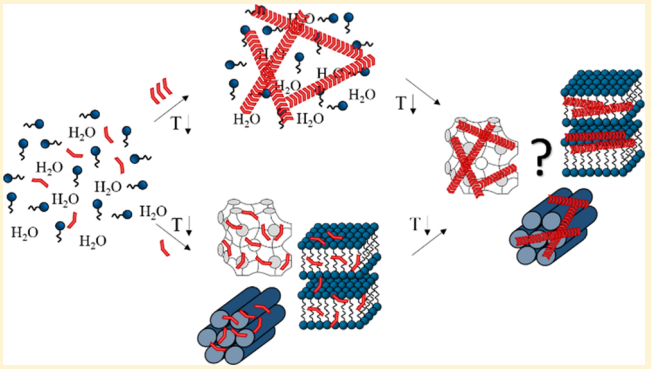

1. INTRODUCTION

Gelled complex fluids combine the microstructure of a complex fluid and the mechanical stability of a gel.[1] If the two structures, that is, the complex fluid and the gel network, form simultaneously but independently via self-assembly, gelled complex fluids can be called orthogonal self-assembled systems.[1,2] For example, this is the case for gelled micellar solutions and gelled bicontinuous microemulsions formed by adding low molecular weight hydro-/organogelators to aqueous surfactant solutions[3−7] or bicontinuous microemulsions,[8,9] respectively. Gelled thermotropic liquid crystals are a borderline case between orthogonal self-assembly and soft templating. Kato et al. found that the chronology of thermotropic liquid crystal and physical gel formation has crucial influence on the resulting microstructure of the gelled thermotropic LC phases and their properties. Varying the gelator, they studied gelled nematic and gelled smectic liquid crystals with different sol−gel transition temperatures ($T_{sol-gel}$) and anisotropic-to-isotropic phase transition temperatures (T_{LC-iso}). In case gel formation occurred at temperatures higher than the liquid crystal formation, that is, $T_{sol-gel} > T_{LC-iso}$, randomly distributed gelator fibers coexisting with LC polydomains were detected while cooling down. In contrast, the growth of the gelator fibers in an already existing liquid crystalline phase, that is, $T_{sol-gel} < T_{LC-iso}$, led to well-aligned gelator fibers while cooling from the isotropic phase. The former situation ($T_{sol-gel} > T_{LC-iso}$) is referred to as "Type I" gel by Kato et al. and the latter ($T_{sol-gel} < T_{LC-iso}$) as "Type II" gel.[10−17] In the special case of gelled lyotropic liquid crystals (gelled LLC) formed by adding the organogelator 12-hydroxyoctadecanoic acid (12-HOA), gelled lamellar L_α phases have been studied with a particular focus on orthogonal self-assembly.[18−20] With 12-HOA, however, truly orthogonal self-assembled systems were not obtained because the surface-active gelator 12-HOA was partly incorporated in the surfactant layers, which led to both a slightly higher order and slightly larger interlaying spacing of the L_α phase on the one hand, and to a reduced gelation capacity as well as gel weakening on the other. These observations raised two questions. (1) Is there a gelator which does not interfere with the surfactant, that is, which is not surface-active? (2) Can the structure of gelled LLC phases be manipulated in the same way as that of thermotropic LC physical gels?

Received: June 4, 2019
Revised: July 4, 2019
Published: July 29, 2019

DOI: 10.1021/acs.langmuir.9b01688
Langmuir 2019, 35, 17132−17141

Following Kato's concept, we studied (a) the influence of the gel network on the liquid crystalline phase formation (Type I gel) and (b) the influence of the lyotropic liquid crystal on the gel network formation (Type II gel). For that purpose, we chose the binary system $H_2O-C_{12}E_7$ (heptaethylene glycol monododecyl ether) (Figure 1) as it forms

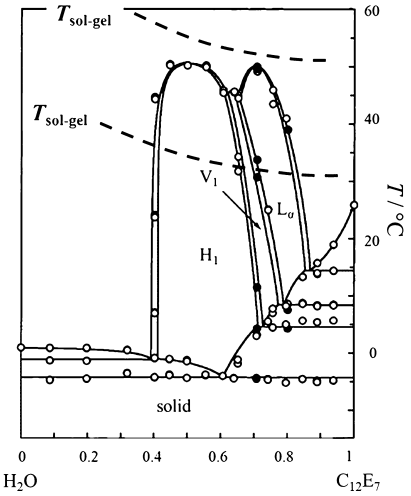

Figure 1. Phase diagram of the binary system $H_2O-C_{12}E_7$ with two schematic sol–gel transition lines (modified from[21]).

three lyotropic liquid crystalline phases, namely, the lamellar L_α phase, the bicontinuous cubic V_1 phase, and the hexagonal H_1 phase depending on the surfactant mass fraction γ_a and the temperature T.[21] Moreover, the moderate melting points of the LLCs ($T \approx 50$ °C) ensure easy handling. For our study, two sol–gel transition temperature lines had to be adjusted such that the $T_{sol-gel}$ is either higher or lower than the melting points of the lyotropic liquid crystalline phases (Figure 1). This can be achieved with a low molecular weight gelator which is not surface-active and whose sol–gel transition temperature $T_{sol-gel}$ can be adjusted via its concentration. In our previous study, we found that the organogelator 1,3:2,4-dibenzylidene-D-sorbitol (DBS) and the hydrogelator HG1 are potent gelators for the L_α phase of the binary system H_2O/NaCl–Genapol LA070. For economic reasons, we chose Genapol LA070 as the "scouting" system to identify suitable gelators for the model system $H_2O-C_{12}E_7$: Genapol LA070 is the technical analogue to $C_{12}E_7$ with an alkyl chain length varying between C12–C14.[22] Not for the hexagonal H_1 phase but indeed for the lamellar L_α phase, it was possible to adjust two sol–gel transition temperatures via the gelator's mass fractions such that $T_{sol-gel} > T_{LLC-iso}$ and $T_{sol-gel} < T_{LLC-iso}$, respectively. Having identified two suitable gelators, we chose DBS for the present study for the simple reason that it is commercially available.

The starting point of our study was the visual determination of the temperature (T)–surfactant mass fraction (γ_a) phase diagram of the system $H_2O-C_{12}E_7$ in the presence of DBS at two different DBS mass fractions. At the same time, the sol–gel transition temperatures were determined for the two gelator mass fractions as a function of the surfactant mass fraction γ_a. To confirm whether or not gelled LLCs were formed, we performed oscillation shear frequency sweeps of the pure LLCs, the gelled LLCs and the binary gel. In addition, we carried out oscillation shear temperature sweeps to detect the sol–gel transition temperatures as well as the transitions from the LLCs to the isotropic phase. Finally, we used polarizing optical microscopy to study if the formation of the gel network and the LLC influence each other. In a follow-up study, we will quantify the length scales of both the LLCs and the gel fibers by using small angle X-ray scattering (SAXS) and dynamic and time-resolved static light scattering (DLS/SLS) as well as transmission electron microscopy (TEM). The data obtained from these techniques will allow us to answer the question raised above, namely, can the structure of gelled LLC phases be manipulated in the same way as that of thermotropic LC physical gels? Or more generally, are the gelled LLCs of the system under study further examples of orthogonal self-assembled systems?

2. EXPERIMENTAL SECTION

2.1. Materials and Sample Preparation. We purchased heptaethylene glycol monododecyl ether ($C_{12}E_7$) from Santa Cruz, TCI and Nikkol and DBS as "Geniset D" from NJC Europe. The chemicals were used as received. The samples were prepared with the surfactant mass fraction

$$\gamma_a = \frac{m_{C_{12}E_7}}{m_{C_{12}E_7} + m_{H_2O}} \quad (1)$$

using bi-distilled water. Gelator mass fractions were calculated by

$$\eta = \frac{m_{DBS}}{m_{C_{12}E_7} + m_{H_2O} + m_{DBS}} \quad (2)$$

for the system $H_2O-C_{12}E_7$–DBS and by

$$\eta = \frac{m_{DBS}}{m_{ethylene\ glycol} + m_{DBS}} \quad (3)$$

for the binary gel ethylene glycol (EG)–DBS. For the system $H_2O-C_{12}E_7$–DBS, we chose DBS mass fractions of $\eta = 0.0075$ and $\eta = 0.015$ because we could gel LLCs with these DBS mass fractions in our previous study. At DBS mass fractions $\eta < 0.0075$, it was difficult to reproducibly gel the LLCs. The components were weighed in glass tubes, sealed with plugs, and heated to $T = 95$ °C in water baths as the gelator had to be dissolved. For the system $H_2O-C_{12}E_7$–DBS at a DBS mass fraction of $\eta = 0.015$ and at surfactant mass fractions of $\gamma_a \leq 0.50$ as well as for the binary gel EG–DBS at $\eta \geq 0.015$, the samples were shortly heated with a heat gun to dissolve DBS. The samples were then stirred for at least 15 min at $T = 95$ °C to ensure homogeneity. Subsequently, the samples of the system $H_2O-C_{12}E_7$–DBS at $\eta = 0.0075$ were cooled to room temperature and the samples at $\eta = 0.015$ to $T = 47$ °C for gelation. In the case of the binary gel EG–DBS, all samples were transferred into a small Petri dish, in which the gel was formed at room temperature. Gelation was indicated by turbidity in the case of the transparent and highly viscous hexagonal H_1 phase and by increasing viscosity, that is, the loss of flow ability, in the case of the slightly turbid and less viscous lamellar L_α phase and the binary gel.

2.2. Visual Phase Studies. The influence of the organogelator DBS at mass fractions of $\eta = 0.0075$ and $\eta = 0.015$ on the LLC phase boundaries of the system $H_2O-C_{12}E_7$ was determined by visual observation of birefringence in water basins equipped with a thermostat (Thermo Scientific DC30), a thermometer, a sample holder, a lamp behind the samples, and two crossed polarizers, one behind and one in front of the samples. The LLC to isotropic phase transitions in the presence of DBS was roughly determined in a quick temperature scan with an increment of $\Delta T = 5$ K, followed by a second temperature scan with a change of the temperature increment of $\Delta T = 0.1$ K at 3 K below the roughly determined phase transitions temperatures. After each temperature increment, we waited 3 min before the next temperature was set. The lyotropic liquid crystalline to isotropic phase transitions in the presence of DBS were determined by anisotropy, viscosity, and turbidity.

DOI: 10.1021/acs.langmuir.9b01688
Langmuir 2019, 35, 17132–17141

2.3. Rheometry. The viscoelastic behavior of the samples was determined with a Physica MCR 501 rheometer from Anton Paar using a cone-plate geometry with an upper moving cone with a cone angle of 1° and a cone diameter of 2.5 cm. The samples were transferred with a spatula to the lower plate, and subsequently, the upper cone was lowered to the measuring gap (z = 1 mm). In order to reach equilibrium, the samples were kept at T = 22 °C for 30 min before starting the measurements. For each sample, we determined the linear viscoelastic (LVE) region in preliminary oscillation strain (γ) sweeps at constant temperature T = 22 °C and constant frequency ω = 10 s^{-1}. The constant strain amplitude was set to γ = 1% for each sample such that all measurements are within the strain limit of the LVE region. In oscillation shear frequency (ω) sweeps at constant T = 22 °C and constant γ = 1%, the storage modulus G' and the loss modulus G'' were determined. The measurements were carried out for the binary system $H_2O-C_{12}E_7$ at surfactant mass fractions of γ_α = 0.76 (L_α phase) and γ_α = 0.50 (H_1 phase), the systems $H_2O-C_{12}E_7$–DBS (γ_a = 0.76, 0.50) at DBS mass fractions of η = 0.0075 and η = 0.015 and for the binary gel EG–DBS at the same DBS mass fractions. The average G' and G'' values of three ω—sweeps and their standard deviations were calculated (Table 1). In general, the standard deviations of the LLC-based systems are higher than those of the binary gel, which is most likely caused by shear-induced reorientation of the LLCs.

Table 1. Standard edviations of the storage modulus G' and the loss modulus G'' averaged over three frequency sweeps of each system, that is, the pure LLCs (η = 0), the gelled LLCs in the presence of DBS at η = 0.0075 and η = 0.015 as well as the binary gel EG–DBS at η = 0.0075 and η = 0.015

	standard deviation of/%					
	L_α		H_1		binary gel	
	G'	G''	G'	G''	G'	G''
η = 0	40	39	28	26		
η = 0.0075	24	23	10	11	12	8
η = 0.015	33	36	21	54	4	6

In additional oscillation temperature (T) sweeps at constant frequency ω = 10 s^{-1} and constant strain amplitude γ = 1%, the sol–gel transition temperatures $T_{sol-gel}$ were determined. We used a heating rate of 1 K·min^{-1} for the binary system $H_2O-C_{12}E_7$, the system $H_2O-C_{12}E_7$–DBS at η = 0.0075, and for the binary gel EG–DBS. In the case of the system $H_2O-C_{12}E_7$–DBS at η = 0.015, a heating rate of 2 K·min^{-1} had to be used because otherwise no phase transition could be detected. The average $T_{sol-gel}$ of two T-sweeps and their absolute deviations were calculated.

2.4. Polarizing Optical Microscopy. Polarizing optical microscopy was used to study the textures of the pure lyotropic liquid crystals, the gelled LLCs, and the binary gel EG–DBS. The samples were filled in single rubbed polyimide cells, sealed and subsequently observed at room temperature using a Leica DMLP polarization microscope. The images of the textures were taken with a Nikon D5300 reflex camera.

3. RESULTS AND DISCUSSION

3.1. Visual Phase Studies. The visual phase studies enabled us to determine the phase boundaries of the system $H_2O-C_{12}E_7$ in the presence of the organogelator DBS at gelator mass fractions of η = 0.0075 (Figure 2 left, open triangles) and η = 0.015 (Figure 2 right, open squares) as a function of the surfactant mass fraction (γ_a) and the temperature (T). The rationale for choosing these two DBS mass fraction is given in the Experimental Section. The $T-\gamma_a$ phase diagram of the binary system $H_2O-C_{12}E_7$ determined by visual observations in our previous study is also shown in Figure 2 (black circles) for comparison. As mentioned before, the binary system forms three liquid crystalline phases, namely, the hexagonal H_1 phase, the bicontinuous cubic V_1 phase, and the lamellar L_α phase. Looking at the phase boundaries of the LLCs in the presence of DBS at η = 0.0075 (Figure 2 left, open triangles), one sees that the phase boundaries of the hexagonal H_1 and the bicontinuous cubic V_1 phase are not altered, whereas the melting point of the lamellar L_α phase is slightly shifted to lower temperatures by $\Delta T \approx 2-4$ °C. In addition, the phase boundaries of the upper miscibility gap (2ϕ) at high temperatures are not influenced by DBS. Adding DBS at η = 0.0075, one can observe that the appearances of the liquid crystalline phases change. The initially transparent H_1 phase and V_1 phases became turbid after addition of DBS, which was taken as a hint of gelation. Note that we can exclude that turbidity is caused by a phase separation since the H_1 and the V_1 phases again became transparent after the gel was molten. In the case of the initially slightly turbid L_α phase, gel formation was indicated by its loss of flow ability. Note that the viscosity of the H_1 and the V_1 phase is high prior to gelation, that is a change in viscosity is not indicative of gelation in these cases. In addition, we visually determined approximate sol–gel transition temperatures $T_{sol-gel}$ by a decrease in turbidity for the gelled H_1 and the gelled V_1 phase and by a decrease in viscosity for the gelled L_α phase. For all gelled LLCs at a DBS mass fraction of η = 0.0075, the $T_{sol-gel}$ were just below the

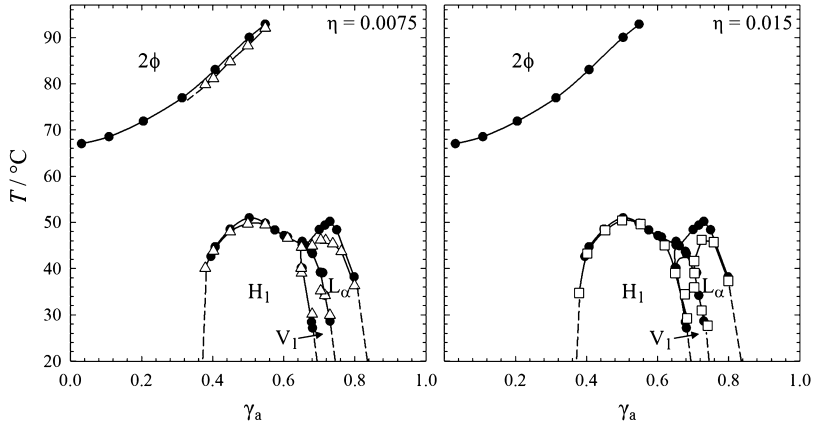

Figure 2. $T-\gamma_a$ phase diagram of the binary system $H_2O-C_{12}E_7$ in the absence (black circles) and in the presence of DBS at mass fractions of η = 0.0075 (open triangles, left) and η = 0.015 (open squares, right).

DOI: 10.1021/acs.langmuir.9b01688
Langmuir 2019, 35, 17132–17141

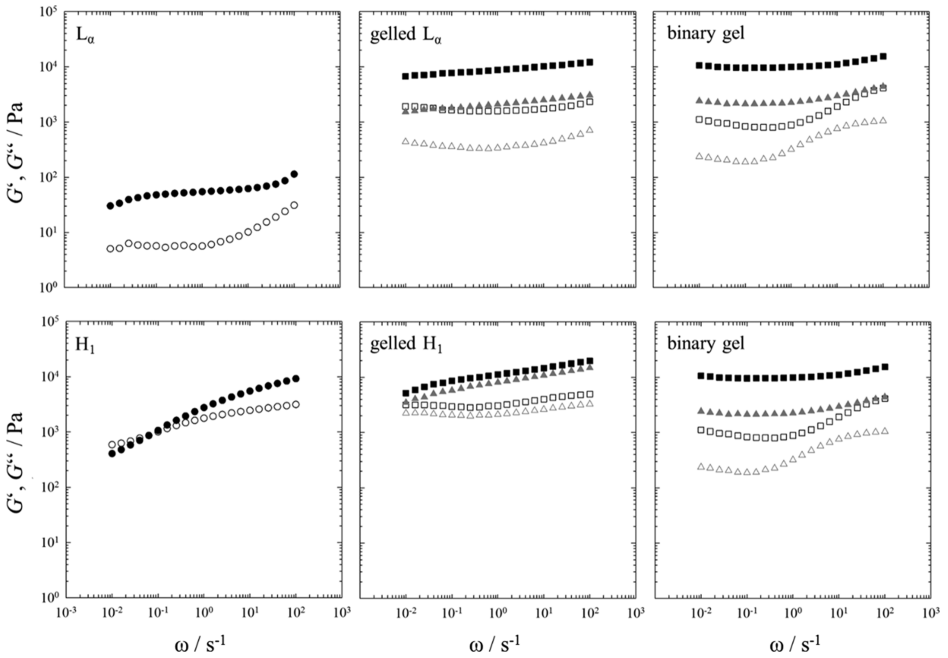

Figure 3. Storage modulus G' (filled symbols) and loss modulus G'' (open symbols) of the pure L_α phase at a surfactant mass fraction of $\gamma_a = 0.76$ (top left), of the pure H_1 phase at $\gamma_a = 0.50$ (bottom left), of the gelled L_α and H_1 phases in the presence of the organogelator DBS (middle) at gelator mass fractions of $\eta = 0.0075$ (triangles) and $\eta = 0.015$ (squares) and of the binary gel EG−DBS (right) at the same DBS mass fractions. Data were determined by frequency (ω)—sweeps at constant temperature $T = 22$ °C and constant strain amplitude $\gamma = 1\%$.

melting points of the LLC phases. We will come back to this point further below.

The $T-\gamma_a$ phase diagram of the system $H_2O-C_{12}E_7$ in the presence of DBS at $\eta = 0.015$ is shown in Figure 2 right (open squares). As was the case for a DBS mass fraction of $\eta = 0.0075$, the phase boundaries of the hexagonal H_1 phase and the bicontinuous cubic V_1 phase are not influenced and those of the lamellar L_α phase are slightly shifted to lower temperatures by $\Delta T \approx 2-4$ °C. Note that the influence on the upper miscibility gap is not shown for the DBS mass fraction $\eta = 0.015$ because it is difficult to measure it for the following reason: at surfactant mass fractions $\gamma_a < 0.40$, the gelator cannot be dissolved (it precipitates) which renders the samples turbid. At higher surfactant mass fractions, however, DBS can be dissolved but because we are at the limit of the gelator's solubility, DBS also precipitates after the gel is molten. Adding DBS at $\eta = 0.015$, one sees that the initially transparent H_1 and V_1 phases become even more turbid than at $\eta = 0.0075$. For the L_α phase, the loss of its flow ability was again taken as a hint of gel formation. However, the L_α phase also became noticeably turbid in the presence of DBS at $\eta = 0.015$. As opposed to the $T_{sol-gel}$ at $\eta = 0.0075$, the $T_{sol-gel}$ at a DBS mass fraction of $\eta = 0.015$ were found to be above the melting points of the LLCs. After crossing the LLC-to-isotropic phase boundaries on heating up, the gel network was still present in the isotropic phase, which enabled us to determine the $T_{sol-gel}$ by a decreasing viscosity in all cases as shown further below. Interestingly, the gel network itself is birefringent, which was also observed for the binary gel EG−DBS at DBS mass fractions of $\eta = 0.0075$ and $\eta = 0.015$ and will be further discussed in the Section 3.3.

In the following, we will focus on the rheological properties of the gelled H_1 phases ($\gamma_a = 0.50$) and the gelled L_α phases ($\gamma_a = 0.76$) at both DBS mass fractions of $\eta = 0.0075$ and $\eta = 0.015$. The V_1 phase will not be discussed further because it appears in a very narrow surfactant mass fraction range and thus is difficult to access. With oscillation shear frequency (ω) sweeps, we determined whether the LLCs are indeed gelled at both DBS mass fractions because the visual phase studies only allowed us to qualitatively study this question. For comparison, we also investigated the rheological properties of the pure H_1 phase at $\gamma_a = 0.50$, the pure L_α phase at $\gamma_a = 0.76$ and of the binary gel EG−DBS at $\eta = 0.0075$ and $\eta = 0.015$. Note that EG was chosen as solvent for DBS because it better mimics the polarity of the $H_2O-C_{12}E_7$ mixtures than pure water or pure oil. In other words, exchanging EG by the $H_2O-C_{12}E_7$ mixture, one can focus on the structural differences of the two "solvents" rather than on the different polarities.

3.2. Rheology. *3.2.1. Frequency Sweeps.* Looking at the ω-sweeps of the pure L_α phase at a surfactant mass fraction of $\gamma_a = 0.76$ (Figure 3, top left), one sees that the storage modulus G' is higher than the loss modulus G'' in the whole frequency range, that is, the L_α phase shows solid-like elastic behavior, although the low absolute G' and G'' values indicate a low viscosity due to a one-dimensional translational order.[23−25] In the case of the binary gel (top right) at $\eta = 0.0075$ (triangles) and $\eta = 0.015$ (squares), $G' > G''$ but at much larger values than for the pure L_α phase as expected. In addition, the storage modulus G' is frequency-independent at low frequencies and only shows slight frequency dependence at high frequencies, which is characteristic for "strong" gels following classical rheological definitions for physical gels.[26−28] In the paper at hand, however, we relate the terms "strong" and "weak" gel to the magnitude of G' and G'' and the terms "rigid" and "soft" gel to the frequency dependence. Thus, looking at the ω-sweep of the binary gel, one sees that the binary gels are equally rigid but that the absolute G' and G'' values are higher at a DBS mass fraction of $\eta = 0.015$ than at $\eta = 0.0075$. Thus, a gel with a higher mechanical strength is formed at $\eta = 0.015$, that is, the gel network becomes "stronger" with increasing DBS mass

DOI: 10.1021/acs.langmuir.9b01688
Langmuir 2019, 35, 17132−17141

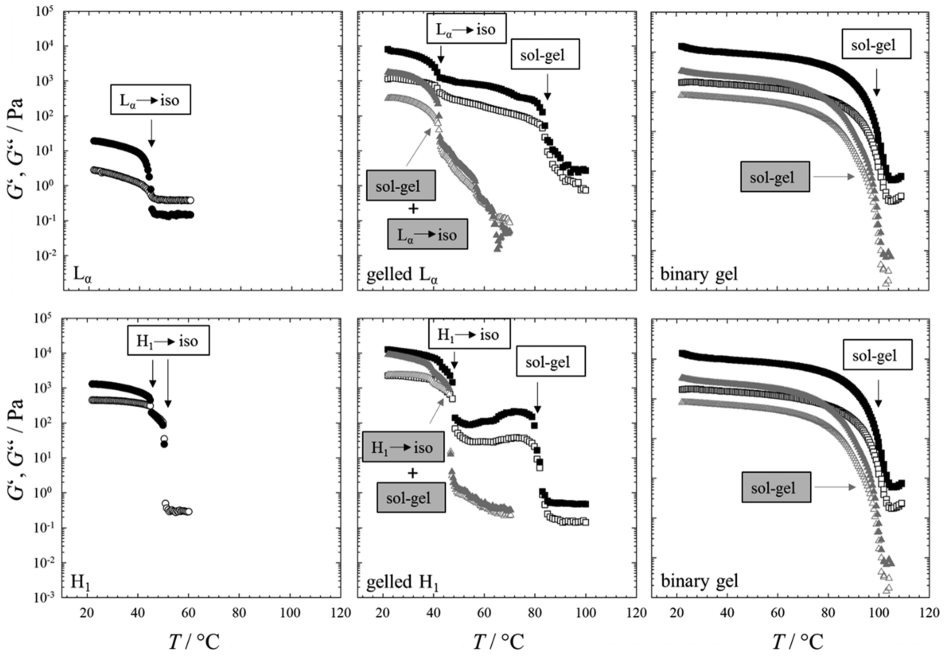

Figure 4. Storage modulus G' (filled symbols) and loss modulus G'' (open symbols) of the pure lamellar phase at a surfactant mass fraction of γ_a = 0.76 (top left), of the pure H_1 phase at γ_a = 0.50 (bottom left), of the gelled lamellar and H_1 phases in the presence of the organogelator DBS (middle) at gelator mass fractions of η = 0.0075 (triangles) and η = 0.015 (squares) and of the binary gel EG−DBS (right) at the same DBS mass fractions. Data were determined by temperature (T) − sweeps at constant frequency ω = 10 s^{-1} and constant strain amplitude γ = 1%.

fraction. For the gelled L_α phases (top middle) at γ_a = 0.76 and DBS mass fractions of η = 0.0075 (triangles) and η = 0.015 (squares), one observes $G' > G''$ with significantly larger absolute values than for the pure L_α phase. The G' and G'' values are at the same order of magnitude as those for the binary gel which proves that indeed gelled L_α phases are formed. As was the case for the binary gel, one can observe higher absolute G' and G'' values for the gelled L_α phase at η = 0.015 compared to the values obtained at η = 0.0075. Generally, the storage moduli are of the same order of magnitude for the gelled L_α phase and the binary gel at both gelator mass fractions, that is, exchanging EG by the L_α phase forms gels with same mechanical strength. However, the storage modulus G' of the gelled L_α phase is slightly frequency-dependent at both DBS mass fractions, which indicates that the gelled L_α phases are a bit softer gels than the binary gels.[27]

For the H_1 phase (Figure 3, bottom left), the absolute G' and G'' values are higher than for the L_α phase, which is related to a higher viscosity because the H_1 phase possesses a two-dimensional translational order as opposed to the L_α phase with a one-dimensional translational order.[23] Unlike the L_α phase, the H_1 phase shows a frequency-dependent viscoelastic behavior with a crossover of G' and G'' at $\omega \approx 0.015$ s^{-1}.[29] It shows liquid-like viscous behavior ($G' < G''$) at low frequencies, whereas at high frequencies, the solid-like elastic behavior ($G' > G''$) predominates. In the case of the gelled H_1 phases (Figure 3, bottom middle) at DBS mass fractions of η = 0.0075 and η = 0.015, one observes $G' > G''$ in the measured frequency range with slightly larger values than for the pure H_1 phase which proves that indeed gelled H_1 phases are formed at both DBS mass fractions. However, the viscoelastic properties of the H_1 phase seem to predominate the viscoelastic behavior of the gelled H_1 phases because G' is frequency-dependent and approaches G'' at low frequencies, that is, the crossover is most likely shifted to even lower frequencies. In accordance with the gelled L_α phases, the gelled H_1 phases thus are slightly softer gels than the binary counterparts. Interestingly, the absolute G' and G'' values are at the same order of magnitude at both DBS mass fractions for the gelled H_1 phases, whereas they differ for the gelled L_α phase and for the binary gel. Thus, the gelled H_1 phases show similar mechanical strength independent of the DBS mass fraction which might be due to the high impact of the H_1 phase on the viscoelastic behavior. Note that because of the high standard deviations for the LLCs and the gelled LLCs (see Section 2.3), we only discuss trends, that is, an increase of G' and G'' for the gelled L_α phases and an increasing DBS mass fraction as well as the disappearance of the crossover of G' and G'' in the measured frequency range for the gelled H_1 phases.

To conclude so far, the oscillation shear frequency sweeps confirm the visual phase studies and prove that indeed gelled L_α phases and gelled H_1 phases are formed at DBS mass fractions of η = 0.0075 and η = 0.015. Moreover, they show that the exchange of the organic solvent EG by either the L_α phase or the H_1 phase leads to softer gels. This may be caused by a different gel network formed in the LLCs or simply by the fact that the $H_2O-C_{12}E_7$ mixture interacts differently with the gel fibers than EG.

3.2.2. Temperature Sweeps. Additional temperature (T) sweeps enabled us to determine the sol−gel transition temperatures of the gelled LLCs as well as the LLC-to-isotropic phase transitions. For all samples, the viscoelastic behavior was in accordance with the frequency sweeps at the initial temperature of T = 22 °C. Starting with the pure L_α phase (Figure 4, top left), one sees that G' and G'' decrease continuously with increasing temperature until G' drops below G'' at $T \approx 44$ °C, which can be assigned to the L_α-to-isotropic phase transition. In the case of the binary gel EG−DBS (Figure 4, right), G' and G'' also decrease with increasing temperature until the sharp drops at $T \approx 96$ °C for η = 0.0075 (gray triangles) and $T \approx 103$ °C for η = 0.015 (black squares)

DOI: 10.1021/acs.langmuir.9b01688
Langmuir 2019, 35, 17132−17141

indicate the sol−gel transition temperatures.[30,31] The $T_{sol-gel}$ were assigned to the temperatures at which $G' = G''$. In the case of the binary gel at $\eta = 0.0075$, G' remained higher than G'', although the drop indicated that the gel is melting. We thus assigned the sol−gel transition temperature for the binary gel at $\eta = 0.0075$ to the temperature where the G' and G'' values were closest to each other. For the T-sweeps of the gelled L_α phases, hence, one must consider that both the sol−gel transition temperatures and L_α-to-isotropic phase transitions contribute to the temperature-dependent viscoelastic behavior.

Looking at the T-sweep of the gelled L_α phase at $\eta = 0.0075$ (Figure 4, top middle, gray triangles), one sees that G' and G'' drop to lower values at $T \approx 42$ °C. On the one hand, we assign this drop to the sol−gel transition temperature because we expect the gel network to have high impact on the temperature-dependent viscoelastic behavior of the gelled L_α phase in accordance to the frequency-dependent viscoelastic behavior. On the other hand, because the drop occurs at about the same temperature as the L_α-to-isotropic phase transition of the pure L_α phase, we assign it to the L_α-to-isotropic phase transition as well. This observation is in accordance to the visual phase studies, which showed that the sol−gel phase transitions of the gelled LLCs at a DBS mass fraction of $\eta = 0.0075$ are just below the LLC-to-isotropic phase transitions, that is, the L_α-to-isotropic phase transition cannot be thermally isolated from the sol−gel phase transition.

For the gelled L_α phase at $\eta = 0.015$ (Figure 4, top middle, black squares), two drops of G' and G'' can be clearly distinguished. The first drop at $T \approx 42$ °C is assigned to the L_α-to-isotropic phase transition after which G' and G'' remain at high values with $G' > G''$, that is, the gel network still exists but now in an isotropic environment. Further temperature increase leads to a continuous decrease of G' and G'' until the drop at $T \approx 84$ °C indicates the sol−gel phase transition. Due to the increase of the sol−gel transition temperatures (ca. 40 °C) by doubling the DBS mass fraction, the L_α-to-isotropic and the sol−gel boundary can be thermally separated from one another.

As was the case for the gelled L_α phases, the contribution of the H_1-to-isotropic phase transition to the temperature-dependent viscoelastic behavior of the gelled H_1 phases (Figure 4, bottom middle) must be considered. Looking at the T-sweep of the pure H_1 phase (Figure 4, bottom left), one can see that G' drops below G'' at $T \approx 45$ °C, after which both moduli decrease continuously with increasing temperature until a second drop of G' and G'' at $T \approx 50$ °C is assigned to the final H_1-to-isotropic phase transition. The first drop indicates that the temperature-dependent viscoelastic behavior of the pure H_1 phase changes from solid-like ($G' < G''$) to liquid-like ($G' < G''$) close to the H_1-to-isotropic phase transition temperature.

In the case of the gelled H_1 phase at $\eta = 0.0075$ (Figure 4, bottom middle, gray triangles), a small drop of G' and G'' occurs at $T \approx 39$ °C but G' remains higher than G'' as opposed to the pure H_1 phase, that is, the H_1 phase is still gelled at this temperature. With increasing temperature, G' and G'' decrease continuously until both moduli drop to low absolute values at $T \approx 46$ °C which we assign to both the H_1-to-isotropic phase transition and the sol−gel boundary in accordance to the visual phase studies.

For the gelled H_1 phase at a DBS mass fraction of $\eta = 0.015$, G' and G'' decrease with increasing temperature until a first drop at $T \approx 49$ °C indicates the H_1-to-isotropic phase transition after which G' remains higher than G'', that is, the gel network still exists. The gel obviously strengthens itself in the isotropic phase because thermo-thickening can be observed after crossing the H_1-to-isotropic phase transition temperature, that is, G' increases with increasing temperature until the sol−gel boundary indicated by the second drop of G' and G'' at $T \approx 86$ °C is reached.

In addition to the samples shown in Figure 4, we carried out temperature sweeps (data not shown) at other surfactant mass fractions (see Table 2 for sample compositions). In Figure 5,

Table 2. DBS mass fractions η and surfactant mass fractions γ_a of the samples used for the determination of the $T_{sol-Gel}$ via oscillation shear temperature Sweeps

	η	γ_a
binary gel	0.0050, 0.0075, 0.010, 0.015, 0.020	0
$H_2O-C_{12}E_7$	0	0.50, 0.76
$H_2O-C_{12}E_7$−DBS	0.0075	0.40, 0.50, 0.62, 0.72, 0.76, 0.80
	0.015	0.40, 0.50, 0.57, 0.68, 0.70, 0.74, 0.76

we added all measured sol−gel transition temperatures $T_{sol-gel}$ to the $T-\gamma_a$ phase diagrams of the systems $H_2O-C_{12}E_7$−DBS at $\eta = 0.0075$ (Figure 5, left) and at $\eta = 0.015$ (Figure 5, right). One can see that the $T_{sol-gel}$ are just below the melting points of the LLC phases at $\eta = 0.0075$ and clearly above the LLC melting points at $\eta = 0.015$ which enabled us to study the chronology of gel and LLC formation. In the presence of DBS at $\eta = 0.0075$, the LLC is formed first on cooling down, that is, the gel network forms in the LLC phase because $T_{sol-gel} < T_{LLC-iso}$. Using DBS at $\eta = 0.0075$ hence allows us to study the influence of the LLC phase on the structure and/or formation of the gel network. For the gelled LLCs at $\eta = 0.015$, however, $T_{sol-gel} > T_{LLC-iso}$, that is, the gel network is formed in the isotropic phase which becomes a lyotropic liquid crystal at lower temperatures. Thus, using a DBS mass fraction of $\eta = 0.015$ allows us to investigate the influence of the gel network on the structure and/or formation of the LLC phase. In accordance to Kato et al., the former case is referred to as Type II LLC gel ($T_{sol-gel} < T_{LLC-iso}$) and the latter as Type I LLC gel ($T_{sol-gel} > T_{LLC-iso}$).[13]

The oscillation shear temperature sweeps also enabled us to detect the sol−gel transition temperature of the binary gel EG−DBS as a function of the DBS mass fraction (see Table 2 for sample compositions, data of the T-sweeps are not shown). As expected, the data seen in Figure 6 show that the sol−gel transition temperatures increase with increasing DBS mass fraction. So far, we discussed the influence of DBS on the phase boundaries of the LLC system. In Figure 6, we added the $T_{sol-gel}$ of the gelled LLC phases to see how the replacement of an organic solvent by a LLC, that is, an aqueous surfactant solution, affects the sol−gel transition temperature. One can see that the sol−gel transition temperatures of the gelled LLCs also increase with increasing DBS mass fraction, but they are below those of the binary gel EG−DBS. In the presence of DBS at $\eta = 0.0075$, the $T_{sol-gel}$ are $\Delta T \approx 40-60$ °C below those of the binary gel, with a slightly lower value for the gelled L_α phases at the surfactant mass fraction $\gamma_a = 0.76$ compared to the gelled H_1 phases at $\gamma_a = 0.50$. For a DBS mass fraction of $\eta = 0.015$; however, the exchange of EG by the LLCs led to a

DOI: 10.1021/acs.langmuir.9b01688
Langmuir 2019, 35, 17132−17141

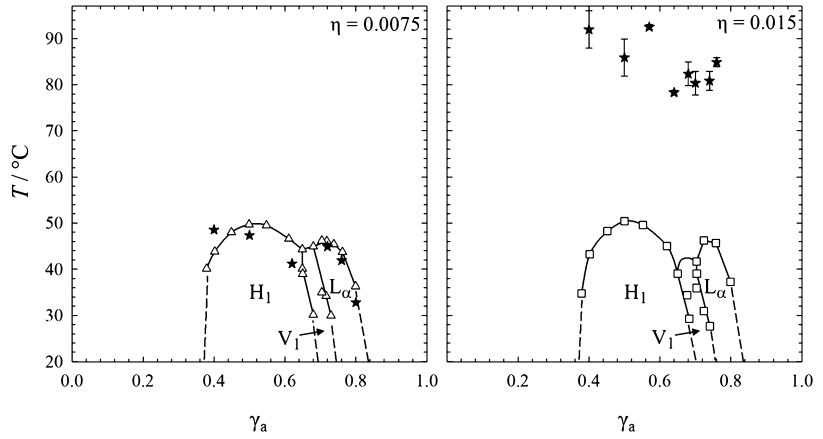

Figure 5. $T-\gamma_a$ phase diagram of the system $H_2O-C_{12}E_7$ in the presence of DBS at the mass fractions η = 0.0075 (open triangles, left) and η = 0.015 (open squares, right) with the sol−gel transition temperatures $T_{sol-gel}$ at both DBS mass fractions (black crosses) determined by oscillation shear temperature sweeps at constant frequency ω = 10 s^{-1} and constant strain amplitude γ = 1%. Note that the $T_{sol-gel}$ values are the average value of two T-sweeps. Unless an error bar is shown, the error is within the size of the symbols.

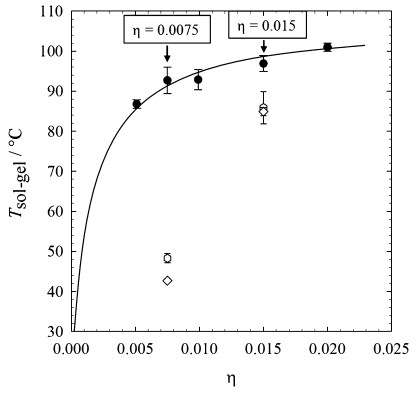

Figure 6. Sol−gel transition temperatures $T_{sol-gel}$ of the binary gel EG−DBS (black circles) as a function of the DBS mass fraction η determined by rheometry. For comparison, the $T_{sol-gel}$ of the gelled H_1 phases (γ_a = 0.50, white hexagons) and of the gelled L_α phases (γ_a = 0.76, white diamonds) at the two DBS mass fractions studied here are also shown. The solid line is drawn as a guide for the eyes.

rather moderate decrease of the sol−gel transition temperatures by roughly 10 °C. Generally speaking, the replacement of EG by the $H_2O-C_{12}E_7$ mixture leads to a decrease of the $T_{sol-gel}$. The stronger the gel network though, the less its $T_{sol-gel}$ is affected. The decrease of the sol−gel transition temperatures might be caused by different interactions between the gelator and the solvent (the LLC phase) compared to the binary gel EG−DBS. Another possibility would be that a fraction of DBS is trapped in the LLC phase because of molecular interactions of the surfactant and gelator which leads to a less dense gel network. However, this only seems to be reasonable for the L_α phase because DBS solely affects the phase boundaries of the L_α phase according to the visual phase studies.

Having determined the phase behavior and the viscoelastic behavior of the gelled LLCs, the question of how the microstructure of the LLCs is affected by the gel network and how the gel network is influenced by the LLCs has to be addressed. This question can be answered qualitatively with polarizing optical microscopy, which will be described in the following.

3.3. Polarizing Optical Microscopy. The polarizing optical microscope pictures (a) of the pure lamellar L_α phase (γ_a = 0.76), (b) of the gelled L_α phases (γ_a = 0.76) at DBS mass fractions of η = 0.0075 and η = 0.015, and (c) of the binary gels EG−DBS at the same DBS mass fractions are shown in Figure 7. Visual phase studies have shown that both the LLCs and the gel network are birefringent between crossed polarizers. For the pure L_α phase, one observes characteristic oily streaks that merge into focal conics.[32−34] In the case of the binary gel EG−DBS, the optical micrographs (Figure 7, right) show spherulitic structures that coexist with isotropic phases at

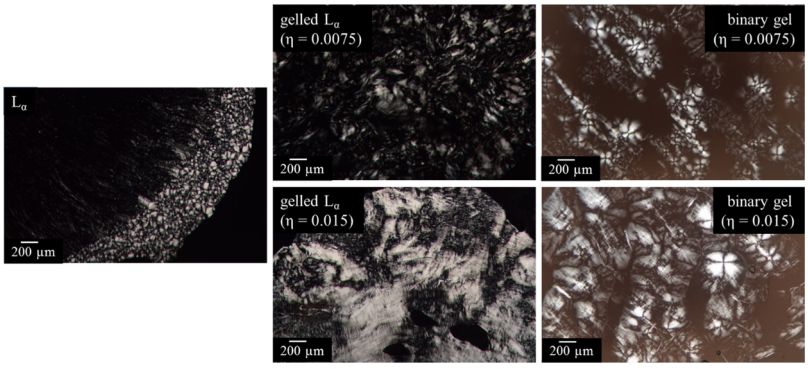

Figure 7. Polarizing optical microscope pictures of the pure lamellar L_α phase (γ_a = 0.76, left), the gelled lamellar L_α phases (γ_a = 0.76) at η = 0.0075 (top middle) and at η = 0.015 (bottom middle) as well as of the binary gels at η = 0.0075 (top right) and η = 0.015 (bottom right).

DOI: 10.1021/acs.langmuir.9b01688
Langmuir 2019, 35, 17132−17141

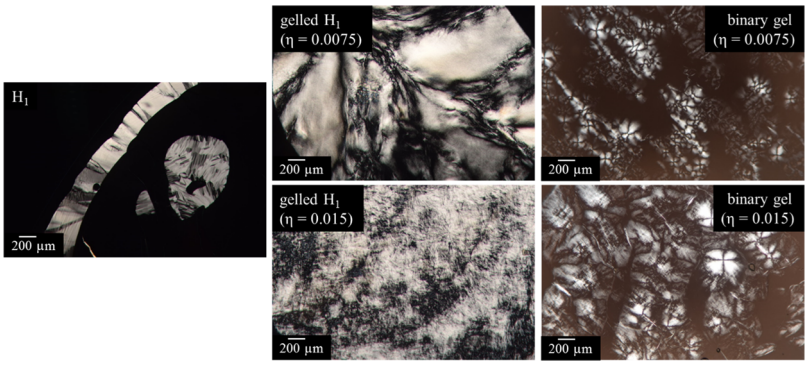

Figure 8. Polarizing optical microscope pictures of the pure hexagonal H_1 phase (γ_a = 0.50, left), the gelled hexagonal H_1 phases (γ_a = 0.50) at η = 0.0075 (top middle) and at η = 0.015 (bottom middle) as well as of the binary gels at η = 0.0075 (top right) and η = 0.015 (bottom right).

both DBS mass fractions.[35] At the higher DBS mass fraction, the structures are larger though. Hence, looking at the optical micrographs of the gelled LLCs, one must consider that both the LLCs and the gel network show birefringence between crossed polarizers.

For the gelled L_α phases (Figure 7, middle), one observes different textures for the two DBS mass fractions. At η = 0.0075, one sees white spots and a dark background, that is, the gel network seems to induce partial disorder in an otherwise homeotropic aligned L_α phase.[17] We recall that at a DBS mass fraction of η = 0.0075, the LLC was formed first while cooling down, followed by gel formation. By contrast, the picture of the gelled L_α phase at η = 0.015 shows a non-geometric texture with light and dark parts which is similar to that of the binary gel at η = 0.015. Here, the gel was formed first while cooling down, followed by LLC formation. As speculative it may be, one can argue that the presence of the gel fibers induced the formation of domains of the L_α phase in the gel network, which are aligned in different orientations. Generally speaking, one can conclude that the structure which is formed first predominates the optical properties, that is, at η = 0.0075 the L_α phase and at η = 0.015 the gel network. This can be observed for the gelled H_1 phases as well (Figure 8, middle). The picture of the pure H_1 phase (γ_a = 0.50) shows two light parts, that is, a typical fan-like texture on the left-hand side of the picture and a rectangular texture on the right-hand side.[32−34] At a DBS mass fraction of η = 0.0075 (Figure 8, top middle), one sees a texture that resembles the fan-like texture of the pure H_1 phase on the left-hand side. As was the case for the gelled L_α phase, the texture of the gelled H_1 at η = 0.0075 resembles the texture of the structure that is formed first while cooling down, that is, the H_1 phase in this case. For the gelled H_1 at a DBS mass fraction of η = 0.015 (Figure 8, bottom middle), a non-geometric texture similar to that of the gelled L_α phase at η = 0.015 was detected. One sees that the gel network which is formed first, determines the optical properties of the gelled H_1 phase at η = 0.015 in accordance to the gelled L_α phase at the same DBS mass fraction.

To summarize, the gelled LLCs combine two birefringent systems and show textures that resemble the texture of the structure, which is formed first while cooling down, that is, at η = 0.0075 the L_α phase and H_1 phase, respectively, and at η = 0.015 the gel network. However, the question of whether the chronology of LLC and gel formation indeed affects the microstructure of the gelled LLCs cannot be answered by POM. A quantitative characterization of the structure requires more sophisticated techniques such as SAXS, DLS/SLS, and TEM.

4. CONCLUSIONS AND OUTLOOK

Visual phase studies and rheometry showed that the organogelator DBS gels the L_α phase and the H_1 phase of the system H_2O−$C_{12}E_7$ at DBS mass fractions of η = 0.0075 and η = 0.015. The two DBS mass fractions were used to adjust the sol−gel transition temperature lines. (a) At η = 0.015, the $T_{sol-gel}$ values are above the LLC-to-isotropic phase transition temperatures $T_{LLC-iso}$, that is, the gel network is formed in the isotropic phase, which becomes an LLC while further cooling down. (b) At η = 0.0075, $T_{sol-gel} < T_{LLC-iso}$, that is, the LLC is formed first while cooling down, followed by gel formation. Independent of the DBS mass fraction, the gel network does not affect the phase boundaries of the LLC. Whether this is also true for the microstructure of the LLCs still needs to be examined. The first idea about structural details was obtained by means of polarizing optical microscopy, which showed that the gel network influences the alignment of the LLC domains differently, depending on the timing of gel formation. A quantitative analysis of the microstructure of the gelled LLCs, however, is not possible by POM, so further investigations are required.

The higher sol−gel transition temperatures of the gelled LLCs at η = 0.015 are also reflected in "stronger" gel networks, as is the case for the binary gel EG−DBS. Comparing the $T_{sol-gel}$ values of the gelled LLCs with those of the binary gel, one sees that the LLCs reduce the $T_{sol-gel}$ values quite significantly at a DBS mass fraction of η = 0.0075, whereas the $T_{sol-gel}$ values are moderately reduced at η = 0.015. In other words, the stronger the gel network, the less the temperature-dependent sol−gel boundary is affected by replacing EG with an LLC. In addition, the exchange of EG by the LLCs leads to a more frequency-dependent viscoelastic behavior, that is, the gelled LLCs are softer than the binary gels. The question of whether this is caused by a structural change of the gel fibers due to the LLC environment or simply by different interactions between the gel network and the H_2O−$C_{12}E_7$ mixture still needs to be studied.

In a follow-up study, we will focus on structural changes of the LLCs caused by the presence of the gel network and vice versa. We recall that (a) a DBS mass fraction of η = 0.015, that is, $T_{sol-gel} > T_{LLC-iso}$, allows us to study in what way the presence of the gel network affects the formation and structure of the LLCs. (b) Using a DBS mass fraction of η = 0.0075, that is, $T_{sol-gel} < T_{LLC-iso}$, allows us to investigate the influence of

DOI: 10.1021/acs.langmuir.9b01688
Langmuir 2019, 35, 17132−17141

the LLC on the structure and arrangement of the gel fibers. We used SAXS, DLS/SLS, and TEM for studying the pure LLCs, the gelled LLCs, and the binary gel. SAXS provides information on the layer spacing and the lattice parameters of the LLCs in the absence and presence of the gel network, while DLS/SLS gives us further insight into the gel network, that is, the mesh size and the growth of the gelator fibers in isotropic and anisotropic environments, respectively. Additionally, TEM allows us to visualize and quantify structural details. With these measurements, which we will present in a follow-up study (Part II), we are able to answer the questions (a) as to whether the chronology of gel and LLC formation has any influence on the microstructure of the gelled LLCs and (b) as to whether gelled LLCs are truly orthogonal self-assembled systems in the sense that the two supramolecular structures, that is, the LLC and the gel network, coexist and form independently.

AUTHOR INFORMATION

Corresponding Author

*E-mail: cosima.stubenrauch@ipc.uni-stuttgart.de. Phone: +49-711-685 64470.

ORCID

Cosima Stubenrauch: 0000-0002-1247-4006

Notes

The authors declare no competing financial interest.

ACKNOWLEDGMENTS

We thank Birgit Feucht for her help with the phase diagram measurements and David K. Smith for the provision of DBS. Financial Support by the Deutsche Forschungsgemeinschaft (grant number: STU287/6-1) is gratefully acknowledged.

REFERENCES

(1) Stubenrauch, C.; Gießelmann, F. Gelled Complex Fluids: Combining Unique Structures with Mechanical Stability. *Angew. Chem., Int. Ed.* **2016**, *55*, 3268−3275.

(2) Laibinis, P. E.; Hickman, J. J.; Wrighton, M. S.; Whitesides, G. M. Orthogonal Self-Assembled Monolayers: Alkanethiols on Gold and Alkane Carboxylic Acids on Alumina. *Science* **1989**, *245*, 845−847.

(3) Heeres, A.; van der Pol, C.; Stuart, M.; Friggeri, A.; Feringa, B. L.; van Esch, J. Orthogonal Self-Assembly of Low Molecular Weight Hydrogelators and Surfactants. *J. Am. Chem. Soc.* **2003**, *125*, 14252−14253.

(4) Brizard, A.; Stuart, M.; van Bommel, K.; Friggeri, A.; de Jong, M.; van Esch, J. Preparation of Nanostructures by Orthogonal Self-Assembly of Hydrogelators and Surfactants. *Angew. Chem., Int. Ed.* **2008**, *47*, 2063−2066.

(5) Brizard, A. M.; van Esch, J. H. Self-assembly approaches for the construction of cell architecture mimics. *Soft Matter* **2009**, *5*, 1320−1327.

(6) Brizard, A. M.; Stuart, M. C. A.; van Esch, J. H. Self-assembled interpenetrating networks by orthogonal self assembly of surfactants and hydrogelators. *Faraday Discuss.* **2009**, *143*, 345−357.

(7) Boekhoven, J.; Brizard, A. M.; Stuart, M. C. A.; Florusse, L.; Raffy, G.; Del Guerzo, A.; van Esch, J. H. Bio-inspired supramolecular materials by orthogonal self-assembly of hydrogelators and phospholipids. *Chem. Sci.* **2016**, *7*, 6021−6031.

(8) Laupheimer, M.; Jovic, K.; Antunes, F. E.; da Graça Martins Miguel, M.; Stubenrauch, C. Studying orthogonal self-assembled systems: phase behaviour and rheology of gelled microemulsions. *Soft Matter* **2013**, *9*, 3661−3670.

(9) Laupheimer, M.; Sottmann, T.; Schweins, R.; Stubenrauch, C. Studying orthogonal self-assembled systems: microstructure of gelled bicontinuous microemulsions. *Soft Matter* **2014**, *10*, 8744−8757.

(10) Kato, T.; Kutsuna, T.; Hanabusa, K.; Ukon, M. Gelation of Room-Temperature Liquid Crystals by the Association of atrans-1,2-Bis(amino)cyclohexane Derivative. *Adv. Mater.* **1998**, *10*, 606−608.

(11) Kato, T.; Kondo, G.; Hanabusa, K. Thermoreversible Self-Organized Gels of a Liquid Crystal Formed by Aggregation of *trans*-1,2-Bis(acylamino)cyclohexane Containing a Mesogenic Moiety. *Chem. Lett.* **1998**, *27*, 193−194.

(12) Mizoshita, N.; Kutsuna, T.; Kato, T.; Hanabusa, K. Smectic liquid-crystalline physical gels. Anisotropic self-aggregation of hydrogen-bonded molecules in layered structures. *Chem. Commun.* **1999**, 781−782.

(13) Kato, T.; Kutsuna, T.; Yabuuchi, K.; Mizoshita, N. Anisotropic Self-Aggregation of an Anthracene Derivative: Formation of Liquid-Crystalline Physical Gels in Oriented States. *Langmuir* **2002**, *18*, 7086−7088.

(14) Mizoshita, N.; Hanabusa, K.; Kato, T. Fast and High-Contrast Electro-optical Switching of Liquid-Crystalline Physical Gels: Formation of Oriented Microphase-Separated Structures. *Adv. Funct. Mater.* **2003**, *13*, 313−317.

(15) Moriyama, M.; Mizoshita, N.; Yokota, T.; Kishimoto, K.; Kato, T. Photoresponsive Anisotropic Soft Solids: Liquid-Crystalline Physical Gels Based on a Chiral Photochromic Gelator. *Adv. Mater.* **2003**, *15*, 1335−1338.

(16) Kato, T.; Mizoshita, N.; Kishimoto, K. Functional Liquid-Crystalline Assemblies: Self-Organized Soft Materials. *Angew. Chem., Int. Ed.* **2006**, *45*, 38−68.

(17) Kato, T.; Hirai, Y.; Nakaso, S.; Moriyama, M. Liquid-crystalline physical gels. *Chem. Soc. Rev.* **2007**, *36*, 1857−1867.

(18) Xu, Y.; Laupheimer, M.; Preisig, N.; Sottmann, T.; Schmidt, C.; Stubenrauch, C. Gelled Lyotropic Liquid Crystals. *Langmuir* **2015**, *31*, 8589−8598.

(19) Koitani, S.; Dieterich, S.; Preisig, N.; Aramaki, K.; Stubenrauch, C. Gelling Lamellar Phases of the Binary System Water-Didodecyldimethylammonium Bromide with an Organogelator. *Langmuir* **2017**, *33*, 12171−12179.

(20) Steck, K.; Schmidt, C.; Stubenrauch, C. The Twofold Role of 12-Hydroxyoctadecanoic Acid (12-HOA) in a Ternary Water-Surfactant-12-HOA System: Gelator and Co-Surfactant. *Gels* **2018**, *4*, 78.

(21) Inoue, T.; Matsuda, M.; Nibu, Y.; Misono, Y.; Suzuki, M. Phase Behaviour of Heptaethylene Glycol Dodecyl Ether and Its Aqueous Mixture Revealed by DSC and FT-IR Spectroscopy. *Langmuir* **2001**, *17*, 1833−1840.

(22) Steck, K.; van Esch, J. H.; Smith, D. K.; Stubenrauch, C. Tuning gelled lyotropic liquid crystals (LLCs) − probing the influence of different low molecular weight gelators on the phase diagram of the system H_2O/NaCl − Genapol LA070. *Soft Matter* **2019**, *15*, 3111−3121.

(23) Dunmur, D., Toriyama, K. Elastic Properties. In *Handbook of Liquid Crystals*; Demus, D., Goodby, J., Gray, G. W., Spiess, H.-W., Vill, V., Eds.; Wiley-VCH Verlag GmbH: Weinheim1998; pp 253−280.

(24) Collings, P. J., Hird, M. *Introduction to Liquid Crystals: Chemistry and Physics*; Taylor & Francis Ltd.: United Kingdom, 1997.

(25) Flory, P. J. Introductory lecture. *Faraday Discuss. Chem. Soc.* **1974**, *57*, 7−18.

(26) Nishinari, K. Some Thoughts on The Definition of a Gel. *Prog. Colloid Polym. Sci.* **2009**, *136*, 87−94.

(27) Douglas, J. Weak and Strong Gels and the Emergence of the Amorphous Solid State. *Gels* **2018**, *4*, 19.

(28) Weiss, R. G. The Past, Present, and Future of Molecular Gels. What Is the Status of the Field, and Where Is It Going? *J. Am. Chem. Soc.* **2014**, *136*, 7519−7530.

(29) Mezzenga, R.; Meyer, C.; Servais, C.; Romoscanu, A. I.; Sagalowicz, L.; Hayward, R. C. Shear Rheology of Lyotropic Liquid Crystals: A Case Study. *Langmuir* **2005**, *21*, 3322−3333.

DOI: 10.1021/acs.langmuir.9b01688
Langmuir 2019, 35, 17132−17141

(30) Weiss, R. G., Terech, P. *Molecular Gels: Materials with Self-Assembled Fibrillar Networks*; Springer: The Netherlands, 2005.
(31) Terech, P.; Rossat, C.; Volino, F. On the Measurement of Phase Transition Temperatures in Physical Molecular Organogels. *J. Colloid Interface Sci.* **2000**, *227*, 363−370.
(32) Stegemeyer, H. *Liquid Crystals*; Steinkopff: Darmstadt, 1999.
(33) Rosevear, F. B. The Microscopy of the Liquid Crystalline Neat and Middle Phases of Soaps and Synthetic Detergents. *J. Am. Oil Chem. Soc.* **1954**, *31*, 628−639.
(34) Laughlin, R. G. *The Aqueous Phase Behaviour of Surfactants*; Academic Press Limited: London, 1994.
(35) Yamasaki, S.; Tsutsumi, H. Microscopic Studies of 1,3 : 2,4-Di-O-benzylidene-D-sorbitol in Ethylene Glycol. *Bull. Chem. Soc. Jpn.* **1994**, *67*, 906−911.

DOI: 10.1021/acs.langmuir.9b01688
Langmuir 2019, 35, 17132−17141

Paper IV

LANGMUIR Article
Cite This: Langmuir 2019, 35, 17142−17149
pubs.acs.org/Langmuir

Gelling Lyotropic Liquid Crystals with the Organogelator 1,3:2,4-Dibenzylidene-D-sorbitol Part II: Microstructure

Katja Steck, Natalie Preisig, and Cosima Stubenrauch*

Institute of Physical Chemistry, University of Stuttgart, Pfaffenwaldring 55, 70569 Stuttgart, Germany

Supporting Information

ABSTRACT: This study deals with the gelation of lyotropic liquid crystals (LLCs) of the binary system H_2O−heptaethylene glycol monododecyl ether ($C_{12}E_7$). The L_α and H_1 phases are gelled with the organogelator 1,3:2,4-dibenzylidene-D-sorbitol (DBS). The microstructure of the gelled LLCs is compared to those of the binary counterparts, i.e., the pure LLCs and the binary gel ethylene glycol−DBS. We present the first examples of gelled lyotropic liquid crystals (LLCs) formed by two different ways upon cooling: (1) At a DBS mass fraction of η = 0.015, the gel is formed first, followed by LLC formation. (2) At η = 0.0075, the LLC is formed first, followed by gel formation. Addressing LLC and gel formation in different orders, the influence of the LLC on the gel network and vice versa can be examined. Independent of which structure is formed first, the interlayer spacing d_{LLC} of the LLCs is only slightly larger in the presence of the gel network compared to the nongelled counterparts. Likewise, the influence of the LLCs on the gel fibers is independent of the chronology of the gel and LLC formation. For both ways, the gel fibers are twisted and arranged in bundles parallel to the bilayers of the L_α phase and the cylindrical micelles of the H_1 phase. Whereas the twisted structure of the gel fibers in ethylene glycol is retained in the presence of the LLCs, the arrangement in bundles is not observed in the binary gels. In the latter case, randomly distributed single fibers which are also slightly thinner are detected. However, we observed the fiber bundles independent of whether the gel network is formed in the isotropic phase or in the LLC and argue that the difference is caused by different interactions of organogelator DBS with the system H_2O−$C_{12}E_7$ than with ethylene glycol. In summary, we found that both the surfactant and the gelator molecules self-assemble in the presence of each other, leading to the coexistence of an LLC and a gel network. This is what is called orthogonal self-assembly.

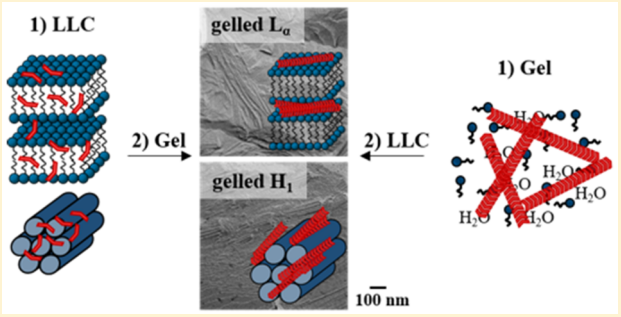

INTRODUCTION

Gelled lyotropic liquid crystals (gelled LLCs) combine two structures with different functions:[1] lyotropic liquid crystals can act as a template for nanostructured materials[2] or can be used to effectively solubilize drugs,[3] whereas gels are used as vehicles for topical drug delivery[4] or for cosmetic applications.[5] In our studies, the focus is always on gelled LLCs formed by two self-assembled supramolecular structures: (1) lyotropic liquid crystals formed by the self-assembly of surfactants in water and (2) self-assembled fibrillar gel networks (SAFiNs) formed by the self-assembly of low-molecular-weight gelators (LMWG).[6−10] Particular emphasis is placed on the question as to whether the LLC and the gel network influence each other's formation and/or arrangement and structure. In other words, can the final microstructure of gelled LLCs be influenced by the chronology of gel and LLC formation such as in the case of gelled thermotropic LCs? Kato et al. showed that the final microstructure of gelled thermotropic LCs is different if (a) the gel is formed first, followed by thermotropic LC formation while cooling or (b) the thermotropic LC is formed first, followed by gel formation at lower temperatures. Following pathway (a) leads to randomly distributed gelator fibers that coexist with thermotropic LC polydomains, which is referred to as a type I gel. In contrast, pathway (b), where the gelator fibers grow in an anisotropic thermotropic LC, leads to well-aligned gelator fibers. The latter is referred to as a type II gel.[11−18]

In part I,[10] we introduced the gelled LLCs (gelled lamellar L_α phase, gelled hexagonal H_1 phase, and gelled bicontinuous cubic V_1 phase) of the system H_2O−$C_{12}E_7$ (heptaethylene glycol monododecyl ether)[19] formed by adding organogelator DBS (1,3:2,4-dibenzylidene-D-sorbitol)[20] and showed that it is possible to form gelled LLCs following pathway (a) or pathway (b) by varying the DBS mass fraction (Figure 1). (a) At a DBS mass fraction of η = 0.015, the sol−gel transition temperature ($T_{sol-gel}$) is higher than the LLC-to-isotropic phase transition temperature ($T_{LLC-iso}$). (b) At a DBS mass fraction of η = 0.0075, $T_{sol-gel} < T_{LLC-iso}$ holds. Following pathway (a) hence allows us to study the influence of the gel network on the formation and structure of the LLCs. Here the gel network is

Received: October 27, 2019
Revised: November 28, 2019
Published: December 18, 2019

DOI: 10.1021/acs.langmuir.9b03346
Langmuir 2019, 35, 17142−17149

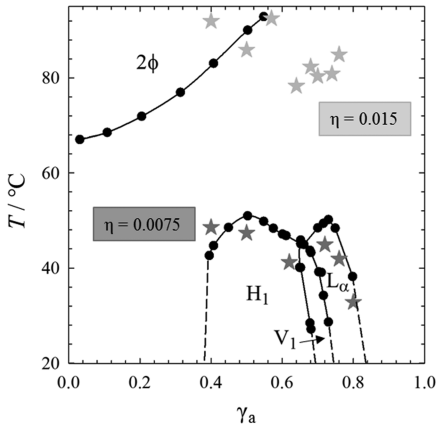

Figure 1. Temperature (T)−surfactant mass fraction (γ_a) phase diagram of the binary system $H_2O-C_{12}E_7$ (black symbols) with the sol−gel transition temperature lines of the gelled lyotropic liquid crystals (lamellar L_α phase, hexagonal H_1 phase, bicontinuous cubic V_1 phase) at DBS mass fractions of η = 0.0075 (dark-gray stars) and η = 0.015 (light-gray stars).

formed first in the isotropic phase which becomes an LLC while cooling down. In contrast, pathway (b) enables us to investigate how the LLC affects the formation and structure/arrangement of the gel fibers. Here the gel fibers are formed in an anisotropic LLC on cooling down.

Whereas the phase behavior and the viscoelastic behavior of the gelled L_α phase and the gelled H_1 phase were addressed in part I, part II focuses on the microstructure of the LLCs and the gel network. We present results from small-angle X-ray scattering (SAXS), dynamic light scattering light scattering (DLS), and freeze fracture electron microscopy (FFEM) of the gelled lamellar L_α and gelled H_1 phases at DBS mass fractions of η = 0.0075 and 0.015. For the sake of comparison, we also studied the binary counterparts, i.e., the pure LLCs and the binary gel consisting of ethylene glycol and DBS). The measurements were carried out to answer the following questions. (1) Does the chronology of gel and LLC formation influence the final microstructure of the gelled LLCs? (2) Are our gelled LLCs another example of an orthogonal self-assembled system where the LLC and the gel network form and coexist independently?

EXPERIMENTAL SECTION

Sample Preparation. We purchased heptaethylene glycol monododecyl ether ($C_{12}E_7$) from TCI and Nikkol and 1,3:2,4-dibenzylidene-D-sorbitol (DBS) as "Geniset D" from NJC Europe. The chemicals were used without further purification. The samples of the systems $H_2O-C_{12}E_7$ and $H_2O-C_{12}E_7$−DBS were prepared with the surfactant mass fraction

$$\gamma_a = \frac{m_{C_{12}E_7}}{m_{C_{12}E_7} + m_{H_2O}} \quad (1)$$

and the gelator mass fraction

$$\eta = \frac{m_{DBS}}{m_{C_{12}E_7} + m_{H_2O} + m_{DBS}} \quad (2)$$

using bidistilled water. We always used γ_a = 0.76 for the L_α phases and γ_a = 0.50 for the H_1 phases. For the binary gel ethylene glycol (EG)−DBS, the gelator mass fraction was calculated by

$$\eta = \frac{m_{DBS}}{m_{ethylene\ glycol} + m_{DBS}} \quad (3)$$

For gelator-containing samples, DBS mass fractions of η = 0.0075 and 0.015 were used. The components were weighed in glass tubes sealed with plugs and heated to T = 95 °C in water baths because the gelator had to be dissolved. For the binary gel EG-DBS at η = 0.015 and the gelled H_1 phase at γ_a = 0.50 and at η = 0.015, the samples were quickly heated with a heat gun in order to dissolve DBS. To ensure homogeneity, the samples were stirred at T = 95 °C for at least 15 min. Subsequently, the pure L_α and pure H_1 phases, the gelled L_α phase, and the gelled H_1 phase at η = 0.0075 as well as binary gel EG-DBS at η = 0.0075 and 0.015 were cooled to room temperature for gelation. The gelled L_α and gelled H_1 phases at η = 0.015 were cooled to $T \approx$ 50 °C for gelation. Room temperature was chosen as the gelation temperature for the gelled LLCs at the DBS mass fraction of η = 0.0075 because the LLCs are formed much quicker than the gel network, i.e., by gelling the LLCs at room temperature, we ensure that the LLC is formed first, followed by gel formation after a couple of hours. In the case of the gelled LLCs at η = 0.015, we chose a temperature ($T \approx$ 50 °C) that was as low as possible to allow gel formation in a reasonable time but still in the isotropic phase of system $H_2O-C_{12}E_7$. After the gels were formed, the samples were put

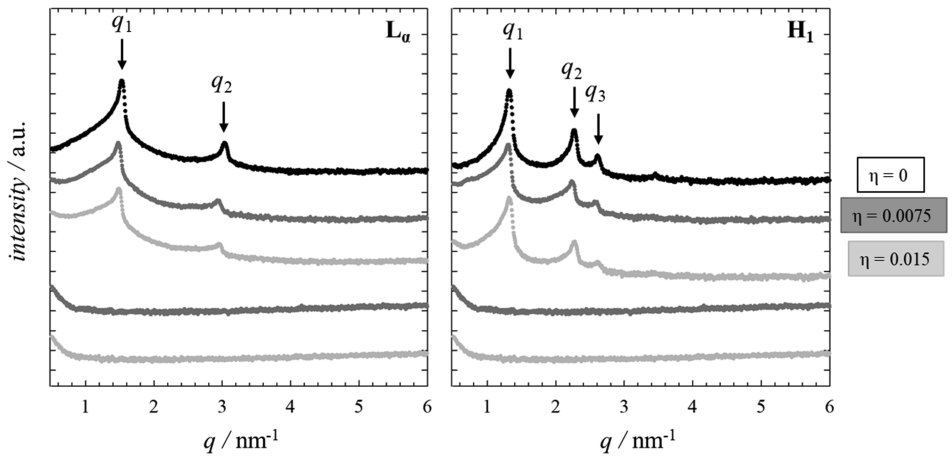

Figure 2. (Left, top) SAXS curves of the pure L_α phase (black symbols), the gelled L_α phases at DBS mass fractions of η = 0.0075 (dark-gray symbols) and η = 0.015 (light-gray symbols). (Right, top) SAXS curves of the pure H_1 phase (black symbols) and the gelled H_1 phases at DBS mass fractions. (bottom) SAXS curves of binary gel EG-DBS at η = 0.0075 (dark-gray symbols) and η = 0.015 (light-gray symbols). All curves were recorded at T = 22 °C and are shifted vertically with regard to the LLCs at η = 0.015 by factors of 100 for the pure LLCs, 10 for the gelled LLCs at η = 0.0075, 10^{-1} for the binary gel at η = 0.0075, and 10^{-2} for the binary gel at η = 0.015 to avoid overlap.

DOI: 10.1021/acs.langmuir.9b03346
Langmuir 2019, 35, 17142−17149

to room temperature for LLC formation. Gelation was indicated by either turbidity or increasing viscosity, i.e., the loss of flow ability. A more detailed description of how gelation is recognized is given in part I.[10]

Small-Angle X-ray Scattering (SAXS). SAXS measurements were carried out with a SAXSess system from Anton Paar. The X-ray radiation (Cu Kα, wavelength λ = 0.15418 nm) was generated by an ISO-DEBYEFLEX 3003 X-ray generator (GE Inspection Technologies GmbH), and the X-ray scattering was recorded using a CMOS detector (Dectris, Mythen 2 1K). The samples were placed in Mark capillary tubes (Hilgenberg, glass no. 14) with a wall thickness of 0.01 mm and an outer diameter of 0.7 mm. The samples were placed in a homemade rotating sample holder and irradiated for 30 min at constant temperature T = 22 °C, which was controlled by the TSC 120 sample holder unit.

Dynamic Light Scattering. Dynamic light scattering (DLS) measurements were carried out with a goniometer system (LS spectrometer) from LS Instruments AG. As the incident beam, a helium/neon laser with a wavelength of λ = 561 nm was used. During the measurements, the temperature was set to T = 22 °C and the scattering angle was varied from 30 to 130° in steps of 10° with a measuring time of 5 min for each scattering angle. The intensity was detected as the count rate of the photons with an avalanche photodiode (APD) detector. For LLC-containing samples, the apparent viscosities η_{app} and the refractive indices n of the pure L_α phase (η_{app} = 527 mPa·s, n = 1.438) and the pure H_1 phase (η_{app} = 13 000 mPa·s, n = 1.404) were determined (Figure S1).

Freeze Fracture Electron Microscopy (FFEM). Replicas of the samples were prepared using the EM BAF060 freeze-fracture and etching system from Leica. The samples were placed with a spatula onto two separate copper grids connected to two copper plates (4.5 mm × 3.0 mm), which were subsequently assembled into a so-called sandwich. The latter were quickly frozen in liquid ethane, fractured and shadowed with platinum−carbon (~2 nm) at 45°, and subsequently covered by a layer of pure carbon (~20 nm) at 90° in the vacuum chamber of BAF060, in which the sample stage was cooled to T = −150 °C. The samples were cleaned with ethanol, dried, and studied with the Tecnai G2 Sphera (gelled L_α and gelled H_1 phase at η = 0.0075) transmission electron microscope from FEI or the EM10 from Zeiss (pure LLCs, binary gels and gelled LLCs at η = 0.015). The replicas were studied at room temperature.

RESULTS

Small-Angle X-ray Scattering (SAXS). In Figure 2 (left), the SAXS curves of the gelled L_α phases at DBS mass fractions of η = 0.0075 and 0.015 as well as those of the binary counterparts (i.e., the pure L_α phase and the binary gels) are shown. For the pure L_α phase, two Bragg peaks with a characteristic peak ratio of $q_1/q_2 = 1/2$[21,22] are found, whereas the spectra of the binary gels do not show any peak pattern. In the case of the gelled L_α phases, the characteristic lamellar peak pattern is also observed (i.e., the L_α phase still forms in the presence of DBS at η = 0.0075 and 0.015). However, the Bragg peaks of the gelled L_α phases are broader and less intense. This results from a shorter correlation length compared to the pure L_α phase (i.e., the gel network slightly reduces the translational order of the L_α phase independent of the DBS mass fraction[21]). Comparing the first-order Bragg peak of the gelled L_α phases with that of the pure L_α phase, one sees that the peaks are marginally shifted to lower q values for the gelled phases (Table 1). Consequently, the interlayer spacing d_{LLC}, which is calculated from the first-order Bragg peak, is slightly larger for the gelled L_α phases than for the pure L_α phase, which might be due to a partial dissolution of a small fraction of DBS in the L_α phase and/or the general presence of the gel network. The observed effect is in accordance to the gelled L_α phase of the system H_2O−$2C_{12}$DAB−12-hydroxyoctadecanoic acid (12-HOA).[7] Looking at the values of the two gelled L_α phases, one sees that the interlayer spacing d_{LLC} is slightly larger for the gelled L_α phase at the lower DBS mass fraction.

Table 1. SAXS peak positions, ratios $q_1/q_2/q_3$, and interlayer spacing d_{LLC} of the pure L_α and H_1 Phases and of the gelled LLC phases at DBS mass fractions of η = 0.0075 and 0.015

	q_1/nm^{-1}	q_2/nm^{-1}	q_3/nm^{-1}	$q_1/q_2/q_3$	d_{LLC}/nm
L_α (η = 0)	1.53	3.03		1/2/−	4.11
gelled L_α (η = 0.0075)	1.48	2.94		1/2/−	4.25
gelled L_α (η = 0.015)	1.49	2.95		1/2/−	4.22
H_1 (η = 0)	1.33	2.27	2.61	$1/\sqrt{3}/\sqrt{4}$	5.45
gelled H_1 (η = 0.0075)	1.31	2.24	2.57	$1/\sqrt{3}/\sqrt{4}$	5.53
gelled H_1 (η = 0.015)	1.32	2.27	2.61	$1/\sqrt{3}/\sqrt{4}$	5.50

The SAXS curves of the gelled H_1 phases as well as those of the pure H_1 phase and the binary gels are shown in Figure 2 (right). For all H_1 phases, i.e., for the pure H_1 as well as for the gelled H_1 phases at DBS mass fractions of η = 0.0075 and 0.015, three Bragg peaks with a characteristic ratio of $q_1/q_2/q_3 = 1/\sqrt{3}/\sqrt{4}$[21,22] are detected, i.e., the H_1 phase still forms after the addition of DBS. As was the case for the gelled L_α phase, the Bragg peaks of the gelled H_1 phases are broader and less intense than those of the pure H_1 phase as a result of a shorter correlation length, i.e., reduced translational order of the H_1 phases due to the presence of the gel network. The interlayer spacings d_{LLC} of the pure H_1 and the gelled H_1 phases differ only slightly, again with marginally larger values for the gelled phases. In accordance with the gelled L_α phase at η = 0.0075, the gelled H_1 phase at the same DBS mass fraction has the largest interlayer spacing, though the difference is small compared to that of the gelled LLCs at η = 0.015.

Dynamic Light Scattering. Gels are known to be nonergodic systems with position-dependent fluctuations[23] and dynamic behavior which is often characterized by fast and slow relaxation modes.[24,25] It holds that the average relaxation time of the fast relaxation mode obtained from DLS measurements at various sample positions is related to the apparent diffusion coefficient, which, in turn, is related to the average mesh size of the gel network.[26] We thus performed dynamic light scattering (DLS) measurements at various scattering angles in order to gain additional information about the gel network, i.e., to learn something about the mesh size of the gel network.

In Figure 3, the time−intensity correlation functions $g^2(\tau) - 1$ (ICFs) of the binary gels, of the gelled LLCs, and of the pure LLCs as a function of the decay time τ at a scattering angle of θ = 70° are shown. The ICFs of the binary gels at DBS mass fractions of η = 0.0075 and 0.015 (Figure 3, left) saturate at a constant value after the initial decay, i.e., they remain τ-independent and no fast relaxation mode is detected. At longer decay times, however, the final relaxation occurs at both DBS mass fractions, i.e., there are indeed fluctuations within the network of the binary gels. In the case of the pure L_α phase, the data is highly scattered, i.e., no ICF is detected. The scattering of the data is suppressed for the gelled L_α phases at both DBS mass fractions and the ICFs remain τ-independent after the initial decay, as was the case for the binary gels. At the lower DBS mass fraction, the ICF has an abnormal shape, i.e., it increases at high decay times, which we cannot explain. For the

DOI: 10.1021/acs.langmuir.9b03346
Langmuir 2019, 35, 17142−17149

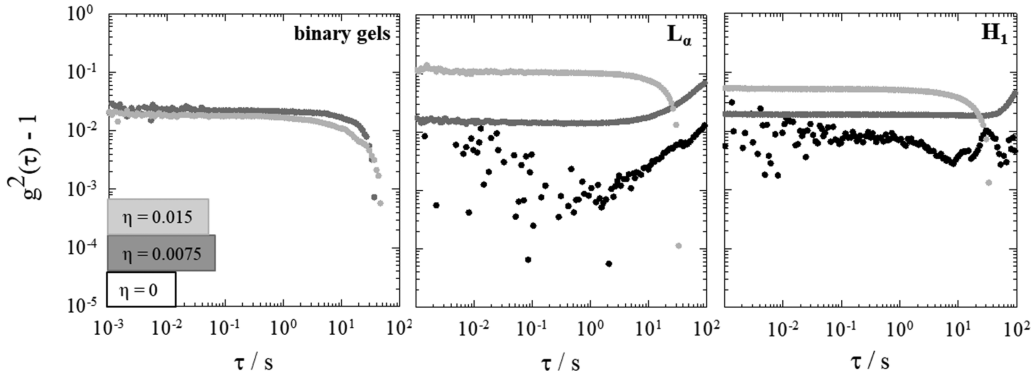

Figure 3. Time−intensity correlation functions $g^2(\tau) - 1$ as a function of the decay time τ for the binary gels, the gelled L_α phases, and the gelled H_1 phases at DBS mass fractions of $\eta = 0.0075$ (dark-gray circles) and $\eta = 0.015$ (light-gray circles) as well as of the pure LLCs (black circles, $\eta = 0$). The data were recorded at a scattering angle of $\theta = 70°$ and a temperature of $T = 22$ °C.

gelled L_α phase at $\eta = 0.015$, the ICF shows a final relaxation. Looking at the ICF of the pure H_1 phase, one observes that the data is less scattered than for the L_α phase, but again no clear ICF and relaxation can be detected. For the gelled H_1 phases, however, which is in line with the gelled L_α phases and the binary gels, the scattering of the data is lower and the ICFs are τ-independent, i.e., no fast relaxation mode occurs. In addition, the ICF of the gelled H_1 phase at $\eta = 0.0075$ shows the same abnormal behavior as that of the gelled L_α phase at $\eta = 0.0075$, while both ICFs of the gelled LLCs have a final relaxation at $\eta = 0.015$. Note that we show only the ICFs at a scattering angle of $\theta = 70°$ because they best describe the results obtained for all measured scattering angles. However, looking at different scattering angles (data not shown), one finds at some angles (a) ICFs with a final relaxation for gelled LLCs at $\eta = 0.0075$ and (b) ICFs with no relaxation whatsoever for gelled LLCs at $\eta = 0.015$ and the binary gels. Unfortunately, we have no explanation for the angle-dependent shape of the curves at high decay times.

To summarize, the dynamic behavior of the binary gels and the gelled LLCs is characterized by τ-independent ICFs followed by a final relaxation at long decay times τ. Okabe et al. reported on the dynamic behavior of various organogelators.[27,28] They distinguished between gelators with gel relaxation at short decay times and gelators with frozen mobility showing τ-independent ICFs such as the binary gels and the gelled LLCs in this article. Thus, the binary gels and the gelled LLCs possess frozen mobility, although the behavior at high decay times indicates some fluctuations within the gel networks. However, because of the absence of a fast relaxation mode for the binary gels and the gelled LLCs, it is not possible to determine an average mesh size of the gel networks via DLS as reported by Meister et al.[26]

Freeze Fracture Electron Microscopy (FFEM). To visualize the microstructure of the gelled LLCs, we used freeze fracture electron microscopy. As a starting point, FFEM pictures of the pure L_α and pure H_1 phases as well as of the binary gels at DBS mass fractions of $\eta = 0.0075$ and 0.015 are shown in Figure 4. For the pure L_α phase (top left), one observes the characteristic layered microstructure representing the lamellar bilayers which appear as flat areas if one looks perpendicular to the bilayers.[29] A layer-to-layer distance of $d_{LLC} \approx 4$ nm (Table 2) is estimated for L_α, which is in good agreement with the interlayer spacing calculated from SAXS. Looking at the FFEM picture of the pure H_1 phase (top right), one sees a layered, and in some areas a rather steplike,

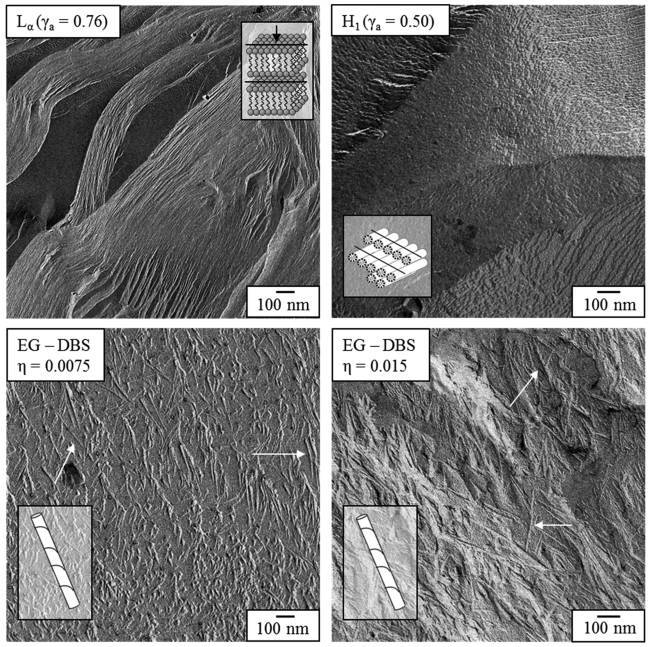

Figure 4. FFEM pictures of the pure L_α phase at a surfactant mass fraction of $\gamma_a = 0.76$ (top left), the pure H_1 phase ($\gamma_a = 0.50$, top right) of the system $H_2O-C_{12}E_7$, and the binary gel ethylene glycol (EG)−DBS at DBS mass fractions of $\eta = 0.0075$ (bottom left) and 0.015 (bottom right). The white arrows in the pictures of the binary gels point to gel fibers. Note that the scale bars are slightly different.

structure similar to (FFEM) pictures reported in the literature.[29] The layers indicate a plane of cylindrical micelles which appears flat if one looks perpendicular to it (Figure 4, inset). In some areas, though, the layers seem to be striated (bottom right corner), i.e., if one looks diagonal with respect to the plane of cylindrical micelles. In line with SAXS, the repeat distance of the cylindrical micelles is approximately $d_{LLC} \approx 5$ nm. For the binary gels at DBS mass fractions of $\eta = 0.0075$ and 0.015 (Figure 4, bottom), single gel fibers as well as bundles of a small number of fibers with no preferred direction are detected. In both cases, the fibers are twisted and very thin with diameters of $d_{fibril} \approx 5-8$ nm at both DBS mass fractions, though even thinner fibers ($d_{fibril} < 5$ nm) are detected occasionally. Thus, the microstructure of the gel fibers is independent of the DBS mass fraction. However, as expected, the fibers are more concentrated at the higher DBS mass fraction, i.e., the gel network is denser. Note that only a small

DOI: 10.1021/acs.langmuir.9b03346
Langmuir 2019, 35, 17142−17149

Table 2. Interlayer Spacing d_{LLC} and Diameters of the Gel Fibers d_{fibril} of the Gelled L_α and the Gelled H_1 Phases of the System $H_2O-C_{12}E_7$ at Surfactant Mass Fraction γ_a and at Two DBS Mass Fractions η[a]

	η = 0		η = 0.0075			η = 0.015		
	d_{LLC}/nm		d_{LLC}/nm		d_{fibril}/ nm	d_{LLC}/nm		d_{fibril}/nm
	SAXS	FFEM	SAXS	FFEM	FFEM	SAXS	FFEM	FFEM
L_α (γ_a = 0.76)	4.11	4	4.25	4	8−18	4.22	4	6−18
H_1 (γ_a = 0.50)	5.45	5	5.53	5	8−15	5.50	5	8−25
binary gel					5−8			5−8

[a]For the sake of comparison, the respective FFEM data of the binary counterparts as well as the SAXS data are also shown.

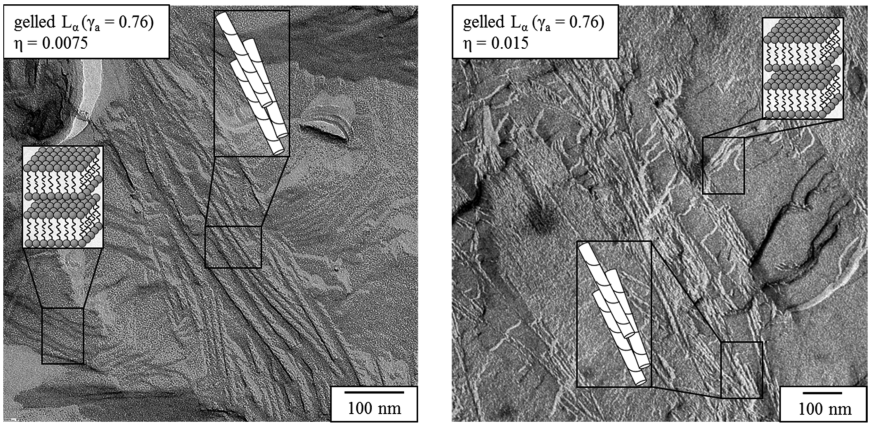

Figure 5. FFEM pictures of the gelled L_α phases of the system $H_2O-C_{12}E_7$ in the presence of DBS at a surfactant mass fraction of γ_a = 0.76 and at DBS mass fractions of η = 0.0075 (left) and η = 0.015 (right). Note that the scale bars are slightly different.

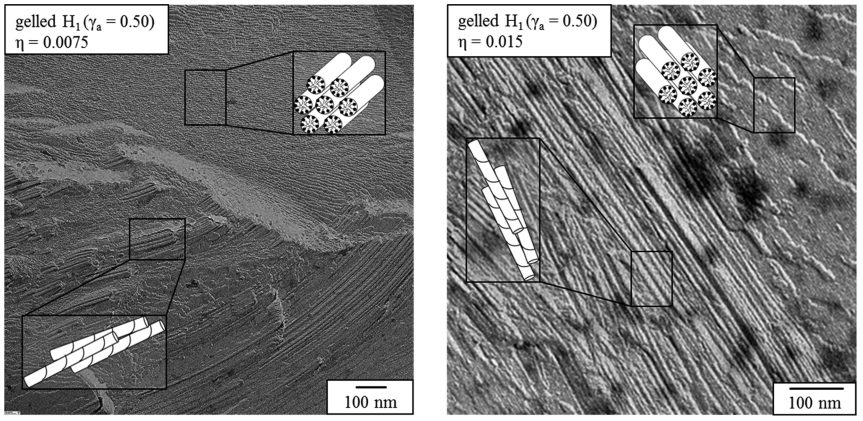

Figure 6. FFEM pictures of the gelled H_1 phases of the system $H_2O-C_{12}E_7$ in the presence of DBS at a surfactant mass fraction of γ_a = 0.50 and at DBS mass fractions of η = 0.0075 (left) and 0.015 (right). Note that the scale bars are slightly different.

area of the sample is imaged by FFEM, which might not be representative of the whole sample. Therefore, we provide further FFEM pictures on different areas of the samples in the Supporting Information (Figure S2), which support our findings.

In Figure 5, FFEM pictures of the gelled L_α phases at η = 0.0075 and at η = 0.015 are shown. One sees that the two self-assembled structures, i.e., the lamellar bilayers and the gel fibers, indeed coexist. At both DBS mass fractions, the order and the distance of the lamellar bilayers is not noticeably influenced by the presence of the gel fibers in line with the SAXS data. The layer-to-layer distance of the lamellar bilayers is $d_{LLC} \approx 4$ nm, like that of the pure L_α phase. Looking at the gel fibers at both DBS mass fractions, one sees that the general appearance of the gel fibers, i.e., the twisted structure, is not affected by the presence of the L_α phase. However, the fibers are slightly thicker ($d_{fibril} \approx 6-18$ nm) compared to the binary gels ($d_{fibril} \approx 5-8$ nm). Moreover, again independent of the DBS mass fraction, the gel fibers preferably occur in bundles which are arranged and are aligned parallel to the lamellar bilayers as opposed to the binary gels, for which single fibers as well as bundles of a small number of fibers with no preferred orientation were observed. As mentioned before, the pictures show only a small area of the whole sample, which is why additional FFEM pictures of the gelled L_α phases at η = 0.0075 and 0.015 are shown in the Supporting Information (Figure S3). For both gelled L_α phases, one sees that the bundles of gel fibers are heterogeneously distributed, i.e., in some areas, the gel fibers are very dense, and in other areas, the lamellar bilayers predominate (Figure S3), which is in line with the pictures seen in Figure 6.

DOI: 10.1021/acs.langmuir.9b03346
Langmuir 2019, 35, 17142−17149

In the case of the gelled H_1 phases at DBS mass fractions of η = 0.0075 and 0.015 (Figure 6), one sees that the H_1 phase and the gel network coexist at both DBS mass fractions as well. As was the case for the gelled L_α phases, the gel fibers do not affect the order or the repeat distance of the cylindrical micelles (i.e., independent of the DBS mass fraction, the interlayer spacing of the gelled H_1 phases is $d_{LLC} \approx 5$ nm, like that of the pure H_1 phase and in good agreement with SAXS). The gel fibers are again twisted but slightly thicker, $d_{fibril} \approx 8-25$ nm, in the presence of the H_1 phase as compared to the gel fibers of the binary gels ($d_{fibril} \approx 5-8$ nm). However, unlike for the gelled L_α phases, for which an equal range of fiber diameters was detected at both DBS mass fractions, the gel fibers are thicker at the higher DBS mass fraction (Table 2). Moreover, again in contrast to the binary gel, the gel fibers are preferably bundled and aligned in one direction in the presence of the H_1 phase at both DBS mass fractions. For both gelled H_1 phases, one observes that the fiber bundles are located in between the layers of cylindrical micelles. In the case of the gelled H_1 phase at η = 0.015 (Figure 6, right), however, the FFEM picture shows that the gel fibers are aligned in the direction of the cylindrical micelles. For the gelled H_1 phase at η = 0.0075, the FFEM pictures do not allow a clear statement of the direction of the fiber bundles relative to the cylindrical micelles. However, most likely, the gel fibers are also aligned in the direction of the cylindrical micelles. In addition, independent of the DBS mass fraction, the bundles of gel fibers are again heterogeneously distributed (Figure S4), as was the case for the gelled L_α phases.

DISCUSSION

In this article, we studied the microstructure of the gelled L_α phases and the gelled H_1 phases of the system $H_2O-C_{12}E_7-$DBS at DBS mass fractions of η = 0.0075 and 0.015 via small-angle X-ray scattering, dynamic light scattering, and freeze fracture electron microscopy. We recall the following: (a) At η = 0.015, on cooling, the gel is formed in the isotropic phase, which becomes an LLC at lower temperatures. (b) At η = 0.0075, the LLC is formed first on cooling, followed by gel formation. We will discuss the results with a focus on the following issues: (1) whether the chronology of gel and LLC formation influences the final microstructure of the gelled LLCs and (2) whether gelled L_α phases and gelled H_1 phases are orthogonal self-assembled systems.

Gelled L_α Phases. *Does the Chronology of Gel and L_α Phase Formation Play a Role?* For the gelled L_α phases, it was found that the interlayer spacings d_{LLC} and the dynamic properties of the gelled L_α phases are independent of which structure is formed first. The structure of the gel network is also independent of whether the gel is formed in the isotropic or in the L_α phase: the gel fibers are twisted in both cases, have the same diameter, and are preferably bundled and aligned parallel to the bilayers. Thus, the chronology of gel and L_α phase formation has no influence on the final microstructure of gelled L_α phases.

Are Gelled L_α Phases Orthogonal Self-Assembled Systems? We recall that the gelator and the surfactant self-assemble in the presence of each other, resulting in the coexistence of a gel network and an L_α phase. The interlayer spacings d_{LLC} of the gelled L_α phases are slightly larger than that of the pure L_α phase. Moreover, the gel fibers retain their twisted structure but are slightly thicker and more oriented in the presence of the L_α phase, i.e., they occur in bundles and are aligned parallel to the lamellar bilayers. This arrangement is different from the one in ethylene glycol where the gel fibers are randomly distributed. However, the gel fibers are bundled independently of whether they are formed in the L_α or the isotropic phase, i.e., the gel fibers are bundled as a result of less favorable interactions of the organogelator DBS with the system $H_2O-C_{12}E_7$ than with ethylene glycol and not due to presence of the L_α phase. Thus, the gelled L_α phases of the system under study are indeed orthogonal self-assembled systems.

Gelled H_1 Phases. *Does the Chronology of Gel and H_1 Phase Formation Play a Role?* As was the case for the gelled L_α phase, the interlayer spacings d_{LLC} and the dynamic properties of the gelled H_1 phases are independent of whether the H_1 phase or the gel is formed first. This is also the case for the structure of the gel network. The gel fibers are twisted and arranged in bundles parallel to the cylindrical micelles independent of whether the gel network is formed in the isotropic or the H_1 phase. For the fiber diameter, though, it was found that the gel fibers are slightly thicker at the higher DBS mass fraction, i.e., if the gel network is formed in the isotropic phase. Most likely, this is rather caused by the higher DBS mass fraction in general than being an effect of the chronology of gel and H_1 phase formation. Therefore, in accordance with the gelled L_α phases, the final microstructure of gelled H_1 phases is also not influenced by addressing the gel and the H_1 phase formation in different orders.

Are Gelled H_1 Phases Orthogonal Self-Assembled Systems? In the case of the gelled H_1 phases, the gelator and the surfactant also self-assemble in the presence of each other, i.e., the gel network and the H_1 phase coexist. In accordance with the gelled L_α phases, the interlayer spacings d_{LLC} of the gelled H_1 phases are slightly increased compared to that of the pure H_1 phase. In addition, we found still twisted but thicker and bundled gel fibers in the gelled H_1 phases, with the gel fibers aligned parallel to the cylindrical micelles as opposed to the arrangement in the binary gels. However, following our discussion of the gelled L_α phases, the fiber bundles are a result of less favorable interactions of the organogelator with the system $H_2O-C_{12}E_7$ because the structure of the gelled H_1 phases is independent of whether the gel network is formed in the isotropic or the H_1 phase. Therefore, the gelled H_1 phases of the system under study are also examples of orthogonal self-assembled systems.

To summarize, the LLC and the gel network coexist in the presence of each other, and the final microstructure is independent of the chronology of gel and LLC formation. Thus, both the gelled L_α phases and the gelled H_1 phases of the system under study are examples of orthogonal self-assembled systems. Whereas no literature is available on gelled H_1 phases, the microstructure of two different L_α phases gelled with the organogelator 12-hydroxyoctadecanoic acid (12-HOA) have been studied by FFEM, namely, the gelled L_α phases of the systems (a) H_2O-n-decane/12-HOA–tetraethylene monodecylether ($C_{10}E_4$)[6] and (b) H_2O-didodecyl dimethylammonium bromide ($2C_{12}$DAB)–12-HOA.[7] The retention of the twisted structure of the gel fibers is in accordance with the observation made for H_2O-2C_{12}DAB–12-HOA but opposed to that made for H_2O-n-decane/12-HOA–$C_{10}E_4$. In the latter case, the gel fibers changed their structure from being twisted in *n*-decane or in the bicontinuous microemulsion to not being twisted if formed in the L_α phase of the very same system but at different surfactant mass fractions.

DOI: 10.1021/acs.langmuir.9b03346
Langmuir 2019, 35, 17142–17149

This raised the question of whether the structure of the gel fibers might be influenced by the surfactant mass fraction. We did not observe such an effect for the gelled LLCs of the system $H_2O-C_{12}E_7$–DBS for which the structure of the gel fibers is the same for the gelled L_α and the gelled H_1 phase, i.e., independent of the surfactant mass fraction. However, the formation of thicker and bundled gel fibers in the gelled L_a phases (compared to the binary gels) is in line with the observations made for the gelled L_α phase of the system H_2O–*n*-decane/12-HOA–$C_{10}E_4$. On the basis of our experimental results, we can argue that the formation of thicker and bundled gel fibers is caused by the fact that the respective organogelators (DBS and 12-HOA) interact differently in the aqueous surfactant solutions ($H_2O-C_{12}E_7$ and H_2O–*n*-decane/12-HOA–$C_{10}E_4$) than in the organic solvents (ethylene glycol and *n*-decane). In a nutshell, the slightly thicker and bundled gel fibers are formed to avoid unfavorable interactions of the organogelators with the aqueous surfactant solutions.

CONCLUSIONS AND OUTLOOK

In the L_α and H_1 phases of the system $H_2O-C_{12}E_7$ gelled with the gelator DBS, the surfactant and the gelator self-assemble in the presence of each other. In other words, in the gelled L_α and gelled H_1 phases an LLC and a gel network coexist. In contrast to thermotropic LCs, however, the microstructure of both gelled LLCs cannot be triggered by inducing gel and LLC formation in different orders. Independent on whether the gel network is formed in the LLC or in the isotropic phase, the gel fibers are arranged in bundles parallel to the lamellar bilayers of the L_α phase and to the cylindrical micelles of the H_1 phase, but they do not form bundles in the binary gel. We argue that the fibers are bundled because of different interactions of the organolator DBS with $H_2O-C_{12}E_7$ than with ethylene glycol, and we conclude that gelled L_α and gelled H_1 phases of the system $H_2O-C_{12}E_7$–DBS are indeed orthogonal self-assembled systems.

What comes next? In future studies, we will address two topics. (1) First, we want to answer fundamental questions about the interactions of the gel network and the LLCs. We found that the thickness of the gel fibers in gelled LLCs is different for various organogelators. For example, the gel fibers in the gelled LLCs in this article are 8–25 nm thick, whereas fibers of organogelator 12-HOA in gelled L_α phases are much thicker (35–70 nm).[6] This raises the question of whether there is a critical fiber thickness up to which the gel network and the LLC self-assemble independently, i.e., orthogonally. To answer this question, we need to study LLCs gelled by a selection of low-molecular-weight gelators whose gel fibers have different thicknesses in the presence of the LLC. (2) Second, we are aiming at formulating gelled LLCs for transdermal drug delivery applications. Note that photo-responsive hydrogels[30] in which the sol–gel transition can be triggered by UV irradiation were reported as drug delivery systems because they allow a controlled drug release rate. Compared to hydrogels, our gelled LLCs have the advantage of being able to dissolve both hydrophilic and hydrophobic drugs. What we need to do is (a) replace $C_{12}E_7$ with a biologically and dermatologically suitable surfactant, (b) find an appropriate photosensitive gelator, (c) load our system with both hydrophobic and hydrophilic model drugs, and (d) carry out skin permeability and penetration tests.

ASSOCIATED CONTENT

Supporting Information

The Supporting Information is available free of charge at https://pubs.acs.org/doi/10.1021/acs.langmuir.9b03346.

Flow curves of the pure H_1 and pure L_α phases; additional FFEM pictures of the pure LLCs and the binary gels; additional FFEM pictures of the gelled L_α phases at DBS mass fractions of η = 0.0075 and 0.015; and additional FFEM pictures of the gelled H_1 phases at DBS mass fractions of η = 0.0075 and 0.015 (PDF)

AUTHOR INFORMATION

Corresponding Author

*E-mail. cosima.stubenrauch@ipc.uni-stuttgart.de. Phone: +49-711-685 64470.

ORCID

Cosima Stubenrauch: 0000-0002-1247-4006

Notes

The authors declare no competing financial interest.

ACKNOWLEDGMENTS

We thank Thomas Sottmann for his help and advice with the manuscript and David K. Smith for the provision of DBS. Financial support by the Deutsche Forschungsgemeinschaft (grant no. STU287/6-1) is gratefully acknowledged.

REFERENCES

(1) Stubenrauch, C.; Gießelmann, F. Gelled Complex Fluids: Combining Unique Structures with Mechanical Stability. *Angew. Chem., Int. Ed.* **2016**, *55*, 3268–3275.

(2) Wang, C.; Chen, D.; Jiao, X. Lyotropic liquid crystal directed synthesis of nanostructured materials. *Sci. Technol. Adv. Mater.* **2009**, *10*, 023001.

(3) Kim, D.-H.; Jahn, A.; Cho, S.-J.; Kim, J. S.; Ki, M.-H.; Kim, D.-D. Lyotropic Liquid Crystal systems in drug delivery: a review. *J. Pharm. Invest.* **2015**, *45*, 1–45.

(4) Kumar, R.; Katare, O. P. Lecithin Organogels as a Potential Phopsholipid-Structured System for Topcial Drug Delivery: A Review. *AAPS PharmSciTech* **2005**, *6*, E298–E310.

(5) (a) Kirilov, P.; Cong, A. K. L.; Denis, A.; Rabehi, H.; Rum, S.; Villa, C.; Haftek, M.; Pirot, F. Organogels for cosmetic and dermo-cosmetic applications – classification, preparation and characterization of organogel formulations – PART 1. *Household and Personal Care Today* **2015**, *10* (3), 15–19. (b) Kirilov, P.; Cong, A. K. L.; Denis, A.; Rabehi, H.; Rum, S.; Villa, C.; Haftek, M.; Pirot, F. Organogels for cosmetic and dermo-cosmetic applications – classification, preparation and characterization of organogel formulations – PART 2. *Household and Personal Care Today* **2015**, *10* (4), 16–21.

(6) Xu, Y.; Laupheimer, M.; Preisig, N.; Sottmann, T.; Schmidt, C.; Stubenrauch, C. Gelled Lyotropic Liquid Crystals. *Langmuir* **2015**, *31*, 8589–8598.

(7) Koitani, S.; Dieterich, S.; Preisig, N.; Aramaki, K.; Stubenrauch, C. Gelling Lamellar Phases of the Binary System Water-Didodecyldimethylammonium Bromide with an Organogelator. *Langmuir* **2017**, *33*, 12171–12179.

(8) Steck, K.; Schmidt, C.; Stubenrauch, C. The Twofold Role of 12-Hydroxyoctadecanoic Acid (12-HOA) in a Ternary Water – Surfactant – 12-HOA System: Gelator and Co-surfactant. *Gels* **2018**, *4*, 78.

(9) Steck, K.; van Esch, J. H.; Smith, D. K.; Stubenrauch, C. Tuning gelled lyotropic liquid crystals (LLCs) – probing the influence of different low molecular weight gelators on the phase diagram of the system H_2O/NaCl – Genapol LA070. *Soft Matter* **2019**, *15*, 3111–3121.

DOI: 10.1021/acs.langmuir.9b03346
Langmuir 2019, 35, 17142–17149

(10) Steck, K.; Stubenrauch, C. Gelling Lyotropic Liquid Crystals with the Organogelator 1,3:2,4-Dibenzylidene-D-sorbitol Part I: Phase Studies and Sol-Gel Transitions. *Langmuir* **2019**.
(11) Kato, T.; Kutsuna, T.; Hanabusa, K.; Ukon, M. Gelation of Room-Temperature Liquid Crystals by the Association of a *trans*-(1,2)-Bis(amino)cyclohexane Derivative. *Adv. Mater.* **1998**, *10*, 606−608.
(12) Kato, T.; Kondo, G.; Hanabusa, K. Thermoreversible Self-Organized Gels of a Liquid Crystal Formed by Aggregation of *trans*-1,2-Bis(acylamino)cyclohexane Containing a Mesogenic Moiety. *Chem. Lett.* **1998**, *27*, 193−194.
(13) Mizoshita, N.; Kutsuna, T.; Hanabusa, K.; Kato, T. Smectic liquid-crystalline physical gels. Anisotropic self-aggregation of hydrogen-bonded molecules in layered structures. *Chem. Commun.* **1999**, *0*, 781−782.
(14) Kato, T.; Kutsuna, T.; Yabuuchi, K.; Mizoshita, N. Anisotropic Self-Aggregation of an Anthracene Derivative: Formation of Liquid-Crystalline Physical Gels in Oriented States. *Langmuir* **2002**, *18*, 7086−7088.
(15) Mizoshita, K.; Hanabusa, K.; Kato, T. Fast and High-Contrast Electro-optical Switching of Liquid-Crystalline Physical Gels: Formation of Oriented Microphase-Separated Structures. *Adv. Funct. Mater.* **2003**, *13*, 313−317.
(16) Moriyama, M.; Mizoshita, N.; Yokota, T.; Kishimoto, K.; Kato, T. Photoresponsive Anisotropic Soft Solids: Liquid-Crystalline Physical Gels Based on a Chiral Photochromic Gelator. *Adv. Mater.* **2003**, *15*, 1335−1337.
(17) Kato, T.; Mizoshita, N.; Kishimoto, K. Functional Liquid-Crystalline Assemblies: Self-Organized Soft Materials. *Angew. Chem., Int. Ed.* **2006**, *45*, 38−68.
(18) Kato, T.; Hirai, Y.; Nakaso, S.; Moriyama, M. Liquid-crystalline physical gels. *Chem. Soc. Rev.* **2007**, *36*, 1857−1867.
(19) Inoue, T.; Matsuda, M.; Nibu, Y.; Misono, Y.; Suzuki, M. Phase Behaviour of Heptaethylene Glycol Dodecyl Ether and Its Aqueous Mixture Revealed by DSC and FT-IR Spectroscopy. *Langmuir* **2001**, *17*, 1833−1840.
(20) Okesola, B. O.; Vieira, V. M. P.; Cornwell, D. J.; Whitelaw, N. K.; Smith, D. K. 1,3:2,4-Dibenzylidene-D-sorbitol (DBS) and its derivatives − efficient, versatile and industrially-relevant low molecular weight gelators with over 100 years of history and bright future. *Soft Matter* **2015**, *11*, 4768−4787.
(21) Seddon, J. M. Structural Studies of Liquid Crystals by X-ray Diffraction. *Handbook of Liquid Crystals*; Wiley-VHC, Weinheim, 1998; Vol. *1*, pp 635−679.
(22) Hiltrop, K. Lyotropic Liquid Crystals. *Liquid Crystals*; Steinkopff: Darmstadt, 1994; pp 143−171.
(23) Pusey, P. N.; Van Megen, W. Dynamic Light Scattering By Non-Ergodic Media. *Phys. A* **1989**, *157*, 705−741.
(24) Martin, J. E.; Wilcoxon, J. P. Critical Dynamics of the Sol-Gel Transition. *Phys. Rev. Lett.* **1988**, *61*, 373−376.
(25) Shibayama, M.; Tsujimoto, M.; Ikkai, F. Statig Inhomogeneities in Physical Gels: Comparison of Temperature-Induced and Concentration-Induced Sol-Gel Transition. *Macromolecules* **2000**, *33*, 7868−7876.
(26) Meister, A.; Bastrop, M.; Koschorek, S.; Garamus, V. M.; Sinemus, T.; Hempel, G.; Drescher, S.; Dobner, B.; Richtering, W.; Huber, K.; Blume, A. Structure-Property Relationship in Stimulus-Responsive Bolaamphiphile Hydrogels. *Langmuir* **2007**, *23*, 7715−7723.
(27) Okabe, S.; Ando, K.; Hanabusa, K.; Shibayama, M. Dynamic Light Scattering and Small-Angle Neutron Studies on Organogels Formed with a Gelator. *J. Polym. Sci., Part B: Polym. Phys.* **2004**, *42*, 1841−1848.
(28) Okabe, S.; Hanabusa, K.; Shibayama, M. Gelation Mechanism and Microstructure of Organogels Formed with Various Types of Gelators. *J. Polym. Sci., Part B: Polym. Phys.* **2005**, *43*, 3567−3574.
(29) Müller-Goymann, C. C. Anwendung lyotroper Flüssigkristalle in Pharmazie und Medizin. *Lyotrope Flüssigkristalle*; Steinkopff, Darmstadt, 1999; pp 141−167.
(30) Tomatsu, I.; Peng, K.; Kros, A. Photoresponsive hydrogels for biomedical applications. *Adv. Drug Delivery Rev.* **2011**, *63*, 1257−1266.

DOI: 10.1021/acs.langmuir.9b03346
Langmuir 2019, 35, 17142−17149

Eigenständigkeitserklärung

Ich erkläre mit meiner Unterschrift, dass ich diese Arbeit selbstständig verfasst habe und keine anderen als die angegebenen Quellen benutzt habe. Alle Stellen dieser Arbeit, die dem Wortlaut, dem Sinn oder der Argumentation nach anderen Werken entnommen sind (einschließlich des *World Wide Web* und anderer elektronischer Text- und Datensammlungen), habe ich unter Angabe der Quellen vollständig kenntlich gemacht. Die Arbeit wurde bisher weder in dieser noch in ähnlicher Form einer anderen Prüfungsbehörde vorgelegt.

Stuttgart, den 18.12.2019

Katja Steck

(Katja Steck)